NIST GCR 95-667

FILE COPY
DO NOT TAKE

Assessment of Site Response Analysis Procedures

I.M. Idriss

A Report to:

U.S. DEPARTMENT OF COMMERCE
Technology Administration
National Institute of Standards
and Technology
Building and Fire Research Laboratory
Gaithersburg, MD 20899

Center for Geotechnical Modeling
Department of Civil & Environmental Engineering
University of California
David, California

NIST

NIST GCR 95-667

Assessment of Site Response Analysis Procedures

I.M. Idriss

A Report to:

U.S. DEPARTMENT OF COMMERCE
Technology Administration
National Institute of Standards
and Technology
Building and Fire Research Laboratory
Gaithersburg, MD 20899

Center for Geotechnical Modeling
Department of Civil & Environmental Engineering
University of California
David, California

July 1993

U.S. DEPARTMENT OF COMMERCE
Ronald H. Brown, Secretary

TECHNOLOGY ADMINISTRATION
Mary L. Good, Under Secretary for Technology

NATIONAL INSTITUTE OF STANDARDS
AND TECHNOLOGY
Arati Prabhakar, Director

TABLE OF CONTENTS

Page Number

1.0 INTRODUCTION 1

2.0 SITE RESPONSE ANALYSES 3

3.0 TREASURE ISLAND SITE 4

3.1 Subsurface Conditions at The Treasure Island Site 4
3.2 Dynamic Soil Properties 4
3.3 Equivalent Linear Analyses 5
3.3.1 Response at Treasure Island Using the Stronger Component of the Recording at YBI as Input Rock Outcrop Motion 5
3.3.1.1 Results Using Best Estimate Shear Wave Velocity Profile 5
3.3.1.2 Results Using Various Shear Wave Velocity Profiles 7
3.3.2 Response at Treasure Island Using the Weaker Component of the Recording at YBI as Input Rock Outcrop Motion 7
3.3.2.1 Results Using Best Estimate Shear Wave Velocity Profile 7
3.3.2.2 Results Using Various Shear Wave Velocity Profiles 8
3.3.3 Response at Treasure Island Using the Recorded Motions at All the Rock Sites in San Francisco Bay Area as Input Rock Outcrop Motions 8
3.3.3.1 Results Using the Stronger Components 8
3.3.3.2 Results Using the Weaker Components 9
3.3.3.3 Discussion of Results 9
3.4 Nonlinear Analyses 10

4.0 SAN FRANCISCO AIRPORT SITE 11

4.1 Subsurface Conditions at The San Francisco Airport Site 11
4.2 Dynamic Soil Properties 11
4.3 Equivalent Linear Analyses 12
4.3.1 Response at San Francisco Airport Using the Stronger Component of the Recording at Sierra Point as Input Rock Outcrop Motion 12

4.3.1.1 Results Using Best Estimate Shear Wave Velocity Profile 12
4.3.1.2 Results Using Various Shear Wave Velocity Profiles 13
4.3.2 Response at San Francisco Airport Using the Weaker Component of the Recording at Sierra Point as Input Rock Outcrop Motion 14
4.3.3 Response at San Francisco Airport Using the Recorded Motions at All the Rock Sites in San Francisco Bay Area as Input Rock Outcrop Motions 14

5.0 SUMMARY AND CONCLUSIONS 16

6.0 ACKNOWLEDGMENTS 18

7.0 REFERENCES 18

APPENDIX A EARTHQUAKE GROUND MOTIONS RECORDED DURING THE 1989 LOMA PRIETA EARTHQUAKE

APPENDIX B CHARACTERISTICS OF THE HORIZONTAL EARTHQUAKE GROUND MOTIONS RECORDED AT ROCK SITES DURING THE 1989 LOMA PRIETA EARTHQUAKE

APPENDIX C CHARACTERISTICS OF THE HORIZONTAL EARTHQUAKE GROUND MOTIONS RECORDED AT SOFT SOIL SITES DURING THE 1989 LOMA PRIETA EARTHQUAKE

APPENDIX D INPUT DATA FOR EQUIVALENT LINEAR ANALYSES AT THE TREASURE ISLAND SITE AND AT THE SAN FRANCISCO AIRPORT SITE BASED ON BEST ESTIMATE SHEAR WAVE VELOCITIES

LIST OF TABLES

Table A-1 Volume I Peak Accelerations of Earthquake Ground Motions Recorded By USGS And By CSMIP at Rock Sites During the Loma Prieta Earthquake

Table A-2 Volume I Peak Accelerations of Earthquake Ground Motions Recorded By USGS And By CSMIP at Soft Soil Sites During the Loma Prieta Earthquake

Table A-3 Volume I Peak Accelerations of Earthquake Ground Motions Recorded By USGS And By CSMIP at Soil Sites (Other Than Soft Soil Sites) During the Loma Prieta Earthquake

Table B-1 Peak Accelerations, Velocities And Displacements of Horizontal Earthquake Ground Motions Recorded at Rock Sites Within a Distance of About 20 Km From the Source During the Loma Prieta Earthquake

Table B-2 Values of v/a and ad/v^2 of Horizontal Earthquake Ground Motions Recorded at Rock Sites Within a Distance of About 20 Km From the Source During the Loma Prieta Earthquake

Table B-3 Effective Duration Derived from Husid Plots of Horizontal Earthquake Ground Motions Recorded at Rock Sites Within a Distance of About 20 Km From the Source During the Loma Prieta Earthquake

Table B-4 Peak Accelerations, Velocities and Displacements of Horizontal Earthquake Ground Motions Recorded at Rock Sites In San Francisco-Bay Area During the Loma Prieta Earthquake

Table B-5 Values of v/a and ad/v^2 of Horizontal Earthquake Ground Motions Recorded at Rock Sites In San Francisco-Bay Area During the Loma Prieta Earthquake

Table B-6 Effective Duration Derived from Husid Plots of Horizontal Earthquake Ground Motions Recorded at Rock Sites In San Francisco-Bay Area During the Loma Prieta Earthquake

Table C-1 Peak Accelerations, Velocities and Displacements of Horizontal Earthquake Ground Motions Recorded at Soft Soil Sites During the Loma Prieta Earthquake

Table C-2 Values of v/a and ad/v^2 of Horizontal Earthquake Ground Motions Recorded at Soft Soil Sites During the Loma Prieta Earthquake

Table C-3 Effective Duration Determined from Husid Plots of Horizontal Earthquake Ground Motions Recorded at Soft Soil Sites During the Loma Prieta Earthquake

LIST OF FIGURES

Fig. 1-1 Locations of CSMIP Recording Stations in the San Francisco-Bay Area used in Present Studies

Fig. 3-1 Locations of Recording Stations at Treasure Island and at Yerba Buena Island

Fig. 3-2 Spectra for Surface Motions Recorded at Treasure Island (TI) and at Yerba Buena Island (YBI)

Fig. 3-3 Log of Boring and Shear Wave Velocities Measured at Treasure Island by USGS

Fig. 3-4 Shear Wave Velocities Measured at Treasure Island and Best Estimate Values of Velocities Used in the Analyses

Fig. 3-5 Modulus Reduction and Damping Relationships Used in All Analyses

Fig. 3-6 Maximum Shear Strains and Stresses at TI Calculated Using Best Estimate Shear Wave Velocities and Stronger Component of YBI Record as Input Motion

Fig. 3-7 Strain-Compatible Damping Ratios and Shear Wave Velocities at TI Calculated Using Best Estimate Shear Wave Velocities and Stronger Component of YBI Record as Input Motion

Fig. 3-8 Peak Horizontal Accelerations at TI Calculated Using Best Estimate Shear Wave Velocities and Stronger Component of YBI Record as Input Motion

Fig. 3-9 Spectrum for Recorded Surface Motion and Spectrum for Surface Motion at TI Calculated Using Best Estimate Shear Wave Velocities and Stronger Component of YBI Record as Input Motion

Fig. 3-10 Accelerogram of Recorded Surface Motion and Accelerograms of Surface Motions at TI Calculated Using Various Shear Wave Velocity Profiles and Stronger Component of YBI Record as Input Motion

Fig. 3-11 Spectrum for Recorded Surface Motion and Spectra for Surface Motions at TI Calculated Using Various Shear Wave Velocity Profiles and Stronger Component of YBI Record as Input Motion

Fig. 3-12 Spectrum for Recorded Surface Motion, Spectrum for Surface Motion Calculated Using Best Estimate Shear Wave Velocities and Median Spectrum for all Cases Considered at Treasure Island Using Stronger Component of YBI Record as Input Motion

Fig. 3-13 Spectrum for Recorded Surface Motion and Spectrum for Surface Motion at TI Calculated Using Best Estimate Shear Wave Velocities and Weaker Component of YBI Record as Input Motion

Fig. 3-14 Spectrum for Recorded Surface Motion and Spectra for Surface Motions at TI Calculated Using Various Shear Wave Velocity Profiles and Weaker Component of YBI Record as Input Motion

Fig. 3-15 Spectrum for Recorded Surface Motion, Spectrum for Surface Motion Calculated Using Best Estimate Shear Wave Velocities and Median Spectrum for all Cases Considered at Treasure Island Using Weaker Component of YBI Record as Input Motion

Fig. 3-16a Spectrum for Recorded Surface Motion and Spectra for Surface Motions at TI Calculated Using Best Estimate Shear Wave Velocities and Stronger Component of Motions Recorded at Yerba Buena, LBL, Piedmont and Rincon as Input Motions

Fig. 3-16b Spectrum for Recorded Surface Motion and Spectra for Surface Motions at TI Calculated Using Best Estimate Shear Wave Velocities and Stronger Component of Motions Recorded at Diamond Heights, Telegraph Hill, Pacific Heights and Presidio as Input Motions

Fig. 3-16c Spectrum for recorded Surface Motion and Spectra for Surface Motions at TI Calculated Using Best Estimate Shear Wave Velocities and Stronger Component of Motions Recorded at Golden Gate, Cliff House and Sierra Point as Input Motions

Fig. 3-17 Spectrum for recorded Surface Motion and Spectra for Surface Motions at TI Calculated Using Best Estimate Shear Wave Velocities and Stronger Component of Motions recorded at Yerba Buena and Other Rock Sites as Input Motions

Fig. 3-18 Spectrum for Recorded Surface Motion and Spectra for Surface Motions at TI Calculated Using Best Estimate Shear Wave Velocities and Weaker Component of Motions recorded at Yerba Buena and Other Rock Sites as Input Motions

Fig. 3-19 Spectra for Recorded Surface Motions and Median and 84th Percentile Spectra for Surface Motions at Treasure Island Calculated Using Motions Recorded at All Rock Sites in San Francisco Bay area as Input Motions

Fig. 3-20 Comparison of the Average Spectrum for the Two Components of Recorded Surface Motions with Median and 84th Percentile Spectral Values for All Calculated Surface Motions at Treasure Island

Fig. 3-21 Comparison of Spectral Ordinates at Ground Surface at TI Calculated Using Equivalent Linear and Nonlinear Response Analyses

Fig. 4-1 Locations of Recording Stations at The San Francisco Airport

Fig. 4-2 Spectra for Surface Motions Recorded at the San Francisco Airport (SFO) and at Sierra Point (SP)

Fig. 4-3 Log of Boring and Shear Wave Velocities Measured at the San Francisco Airport by USGS

Fig. 4-4 Shear Wave Velocities Measured at the San Francisco Airport and Best Estimate Values of Velocities Used in the Analyses

Fig. 4-5 Maximum Shear Strains and Stresses at SFO Calculated Using Best Estimate Shear Wave Velocities and Stronger Component of SP Record as Input Motion

Fig. 4-6 Strain-Compatible Damping Ratios and Shear Wave Velocities at SFO Calculated Using Best Estimate Shear Wave Velocities and Stronger Component of SP Record as Input Motion

Fig. 4-7 Peak Horizontal Accelerations at SFO Calculated Using Best Estimate Shear Wave Velocities and Stronger Component of SP Record as Input Motion

Fig. 4-8 Spectrum for Recorded Surface Motion and Spectrum for Surface Motion at SFO Calculated Using Best Estimate Shear Wave Velocities and Stronger Component of SP Record as Input Motion

Fig. 4-9 Spectrum for Recorded Surface Motion and Spectra for Surface Motions at SFO Calculated Using Various Shear Wave Velocity Profiles and Stronger Component of Sierra Point Record as Input Motion

Fig. 4-10 Spectrum for Recorded Surface Motion and Spectra for Surface Motions at SFO Calculated Using Various Shear Wave Velocity Profiles and Weaker Component of Sierra Point Record as Input Motion

Fig. 4-11 Spectrum for recorded Surface Motion and Spectra for Surface Motions at SFO Calculated Using Best Estimate Shear Wave Velocities and Stronger Component of Motions recorded at Sierra Point and Other Rock Sites as Input Motions

Fig. 4-12 Spectrum for Recorded Surface Motion and Spectra for Surface Motions at SFO Calculated Using Best Estimate Shear Wave Velocities and Weaker Component of Motions recorded at Sierra Point and Other Rock Sites as Input Motions

Fig. 4-13 Spectra for Recorded Surface Motions and Median and 84th Percentile Spectra for Surface Motions at San Francisco Airport Calculated Using Motions Recorded at All Rock Sites in San Francisco Bay area as Input Motions

Fig. 4-14 Comparison of the Average Spectrum for the Two Components of Recorded Surface Motions with Median and 84th Percentile Spectral Values for All Calculated Surface Motions at the San Francisco Airport

Fig. 5-1 Comparison of Median Normalized Spectral Shapes for Horizontal Rock Motions Recorded During the Loma Prieta Earthquake With Those Calculated Using Attenuation Relationship for Rock Sites Derived by Idriss (1991b)

Fig. A-1 Location of the Main Shock of the Loma Prieta Earthquake, Area of aftershocks and Inferred Extent of Fault Rupture

Fig. A-2 Transverse Section Showing Distribution of Aftershocks and Dip of Fault Plane

Fig. A-3 Locations of USGS Stations Which Recorded the Loma Prieta Earthquake

Fig. A-4 Locations of CSMIP Stations Which Recorded the Loma Prieta Earthquake

Fig. A-5 Horizontal Accelerations Recorded During the 1989 Loma Prieta Earthquake

Fig. A-6 Vertical Accelerations Recorded During the 1989 Loma Prieta Earthquake and Ratio of Vertical Acceleration to Horizontal Acceleration

Fig. B-1 Accelerograms and Spectral Ordinates of the Horizontal Components of Earthquake Ground Motions Recorded at Corralitos during the Loma Prieta Earthquake

Fig. B-2 Accelerograms and Spectral Ordinates of the Horizontal Components of Earthquake Ground Motions Recorded at Abutment of Lexington Dam During the Loma Prieta Earthquake

Fig. B-3 Accelerograms and Spectral Ordinates of the Horizontal Components of Earthquake Ground Motions Recorded at Gilroy No. 1 During the Loma Prieta Earthquake

Fig. B-4 Accelerograms and Spectral Ordinates of the Horizontal Components of Earthquake Ground Motions Recorded at Gilroy No. 6 During the Loma Prieta Earthquake

Fig. B-5 Accelerograms and Spectral Ordinates of the Horizontal Components of Earthquake Ground Motions Recorded at Abutment of Coyote Dam During the Loma Prieta Earthquake

Fig. B-6 Accelerograms and Spectral Ordinates of the Horizontal Components of Earthquake Ground Motions Recorded at Santa Cruz During the Loma Prieta Earthquake

Fig. B-7 Normalized Spectra for Motions Recorded at Rock Sites within 20 km from Source During the Loma Prieta Earthquake

Fig. B-8 Husid Plots of Horizontal Components of Earthquake Ground Motions Recorded at Corralitos During the Loma Prieta Earthquake

Fig. B-9 Husid Plots of Horizontal Components of Earthquake Ground Motions Recorded at Abutment of Lexington Dam During the Loma Prieta Earthquake

Fig. B-10 Husid Plots of Horizontal Components of Earthquake Ground Motions Recorded at Gilroy No. 1 During the Loma Prieta Earthquake

Fig. B-11 Husid Plots of Horizontal Components of Earthquake Ground Motions Recorded at Gilroy No. 6 During the Loma Prieta Earthquake

Fig. B-12 Husid Plots of Horizontal Components of Earthquake Ground Motions Recorded at Abutment of Coyote Dam During the Loma Prieta Earthquake

Fig. B-13 Husid Plots of Horizontal Components of Earthquake Ground Motions Recorded at Santa Cruz During the Loma Prieta Earthquake

Fig. B-14 Husid Plots of Horizontal Components of Earthquake Ground Motions Recorded at Rock Sites Within a Distance of About 20 Km From the Source During the Loma Prieta Earthquake

Fig. B-15 Accelerograms and Spectral Ordinates of the Horizontal Components of Earthquake Ground Motions Recorded at Sierra Point During the Loma Prieta Earthquake

Fig. B-16 Accelerograms and Spectral Ordinates of the Horizontal Components of Earthquake Ground Motions Recorded at Diamond Heights During the Loma Prieta Earthquake

Fig. B-17 Accelerograms and Spectral Ordinates of the Horizontal Components of Earthquake Ground Motions Recorded at Rincon Hill During the Loma Prieta Earthquake

Fig. B-18 Accelerograms and Spectral Ordinates of the Horizontal Components of Earthquake Ground Motions Recorded at Pacific Heights During the Loma Prieta Earthquake

Fig. B-19 Accelerograms and Spectral Ordinates of the Horizontal Components of Earthquake Ground Motions Recorded at Telegraph Hill During the Loma Prieta Earthquake

Fig. B-20 Accelerograms and Spectral Ordinates of the Horizontal Components of Earthquake Ground Motions Recorded at Golden Gate During the Loma Prieta Earthquake

Fig. B-21 Accelerograms and Spectral Ordinates of the Horizontal Components of Earthquake Ground Motions Recorded at the Presidio During the Loma Prieta Earthquake

Fig. B-22 Accelerograms and Spectral Ordinates of the Horizontal Components of Earthquake Ground Motions Recorded at the Cliff House During the Loma Prieta Earthquake

Fig. B-23 Accelerograms and Spectral Ordinates of the Horizontal Components of Earthquake Ground Motions Recorded at Yerba Buena Island During the Loma Prieta Earthquake

Fig. B-24 Accelerograms and Spectral Ordinates of the Horizontal Components of Earthquake Ground Motions Recorded at Piedmont During the Loma Prieta Earthquake

Fig. B-25 Accelerograms and Spectral Ordinates of the Horizontal Components of Earthquake Ground Motions Recorded at Lawrence Berkeley Lab During the Loma Prieta Earthquake

Fig. B-26 Normalized Spectra for Motions Recorded at Rock Sites in the San Francisco Bay Area During the Loma Prieta Earthquake

Fig. B-27 Husid Plots of Horizontal Components of Earthquake Ground Motions Recorded at Sierra Point During the Loma Prieta Earthquake

Fig. B-28 Husid Plots of Horizontal Components of Earthquake Ground Motions Recorded at Diamond Heights During the Loma Prieta Earthquake

Fig. B-29 Husid Plots of Horizontal Components of Earthquake Ground Motions Recorded at Rincon Hill During the Loma Prieta Earthquake

Fig. B-30 Husid Plots of Horizontal Components of Earthquake Ground Motions Recorded at Pacific Heights During the Loma Prieta Earthquake

Fig. B-31 Husid Plots of Horizontal Components of Earthquake Ground Motions Recorded at Telegraph Hill During the Loma Prieta Earthquake

Fig. B-32 Husid Plots of Horizontal Components of Earthquake Ground Motions Recorded at Golden Gate During the Loma Prieta Earthquake

Fig. B-33 Husid Plots of Horizontal Components of Earthquake Ground Motions Recorded at the Presidio During the Loma Prieta Earthquake

Fig. B-34 Husid Plots of Horizontal Components of Earthquake Ground Motions Recorded at the Cliff House During the Loma Prieta Earthquake

Fig. B-35 Husid Plots of Horizontal Components of Earthquake Ground Motions Recorded at Yerba Buena Island During the Loma Prieta Earthquake

Fig. B-36 Husid Plots of Horizontal Components of Earthquake Ground Motions Recorded at Piedmont During the Loma Prieta Earthquake

Fig. B-37 Husid Plots of Horizontal Components of Earthquake Ground Motions Recorded at Lawrence Berkeley Laboratory During the Loma Prieta Earthquake

Fig. B-38 Husid Plots of Horizontal Components of Earthquake Ground Motions Recorded at Rock Sites in the San Francisco Bay Area During the Loma Prieta Earthquake

Fig. B-39 Median Normalized Spectral Shapes for Rock Motions Recorded During the Loma Prieta Earthquake

Fig. B-40 Effective Duration Obtained for Motions Recorded at Rock Sites During the Loma Prieta Earthquake

Fig. C-1 Accelerograms and Spectral Ordinates of the Horizontal Components of Earthquake Ground Motions Recorded at APEEL No. 2 During the Loma Prieta Earthquake

Fig. C-2 Accelerograms and Spectral Ordinates of the Horizontal Components of Earthquake Ground Motions Recorded at Foster City During the Loma Prieta Earthquake

Fig. C-3 Accelerograms and Spectral Ordinates of the Horizontal Components of Earthquake Ground Motions Recorded at San Francisco Airport During the Loma Prieta Earthquake

Fig. C-4 Accelerograms and Spectral Ordinates of the Horizontal Components of Earthquake Ground Motions Recorded at Alameda Naval Station During the Loma Prieta Earthquake

Fig. C-5 Accelerograms and Spectral Ordinates of the Horizontal Components of Earthquake Ground Motions Recorded at Outer Harbor Wharf During the Loma Prieta Earthquake

Fig. C-6 Accelerograms and Spectral Ordinates of the Horizontal Components of Earthquake Ground Motions Recorded at Emeryville During the Loma Prieta Earthquake

Fig. C-7 Accelerograms and Spectral Ordinates of the Horizontal Components of Earthquake Ground Motions Recorded at Treasure Island During the Loma Prieta Earthquake

Fig. C-8 Accelerograms and Spectral Ordinates of the Horizontal Components of Earthquake Ground Motions Recorded at Richmond During the Loma Prieta Earthquake

Fig. C-9 Accelerograms and Spectral Ordinates of the Horizontal Components of Earthquake Ground Motions Recorded at Larkspur During the Loma Prieta Earthquake

Fig. C-10 Normalized Spectra of Horizontal Motions Recorded at Soft Soil Sites in San Francisco-Bay Area During the Loma Prieta Earthquake

Fig. C-11 Accelerograms and Husid Plots of the Horizontal Components of Earthquake Ground Motions Recorded at APEEL No. 2 During the Loma Prieta Earthquake

Fig. C-12 Accelerograms and Husid Plots of the Horizontal Components of Earthquake Ground Motions Recorded at Foster City During the Loma Prieta Earthquake

Fig. C-13 Accelerograms and Husid Plots of the Horizontal Components of Earthquake Ground Motions Recorded at San Francisco Airport During the Loma Prieta Earthquake

Fig. C-14 Accelerograms and Husid Plots of the Horizontal Components of Earthquake Ground Motions Recorded at Alameda Naval Station During the Loma Prieta Earthquake

Fig. C-15 Accelerograms and Husid Plots of the Horizontal Components of Earthquake Ground Motions Recorded at Outer Harbor Wharf During the Loma Prieta Earthquake

Fig. C-16 Accelerograms and Husid Plots of the Horizontal Components of Earthquake Ground Motions Recorded at Emeryville During the Loma Prieta Earthquake

Fig. C-17 Accelerograms and Husid Plots of the Horizontal Components of Earthquake Ground Motions Recorded at Treasure Island During the Loma Prieta Earthquake

Fig. C-18 Accelerograms and Husid Plots of the Horizontal Components of Earthquake Ground Motions Recorded at Richmond During the Loma Prieta Earthquake

Fig. C-19 Accelerograms and Husid Plots of the Horizontal Components of Earthquake Ground Motions Recorded at Larkspur During the Loma Prieta Earthquake

Fig. C-20 Husid Plots of Horizontal Components of Earthquake Ground Motions Recorded at Soft Soil Sites in the San Francisco Bay Area During the Loma Prieta Earthquake

Fig. C-21 Effective Duration for Horizontal Motions Recorded at Soft Soil Sites and at Rock Sites During the Loma Prieta Earthquake

ASSESSMENT OF SITE RESPONSE ANALYSIS PROCEDURES

by
I. M. Idriss

1.0 INTRODUCTION

The Loma Prieta earthquake occurred on October 17, 1989 at 5:04 pm Pacific daylight time along a 45-km long segment of the San Andreas fault in the Santa Cruz Mountains. The earthquake was assigned a surface wave magnitude, $M_S = 7.1$, and a moment magnitude, $M_W = 7$ making it the largest earthquake to occur in Northern California since the 1906 earthquake.

The earthquake triggered by far the largest number of instruments ever triggered by an earthquake and recordings were obtained at well over 200 locations, including free-field stations, small buildings, high rise structures and dams. Of these, 88 stations were at locations that can be considered to represent free-field conditions, i.e., the instrument had been placed in a small instrument shack or is at the ground floor of a small structure (three stories or less) with no basement.

The records obtained from the free-field stations are summarized in Appendix A of this report. These include 31 stations at rock sites, nine stations at soft soil sites and 48 stations at other soils sites. The recordings at the soft soil sites are the largest set of recordings ever obtained at such site conditions at these levels of shaking.

The records obtained at the soft soil sites offered an excellent opportunity to assess the procedures used for calculating the response of soil sites during earthquakes. This was particularly the case because rock outcrop motions were also available from nearby locations and subsurface information was gathered at most of these soft soil sites. In particular, six soft soil sites and the rock site at Yerba Buena Island were investigated by the Electric Power Research Institute (EPRI) with technical support from USGS and partial financial support from the University of California at Davis (through a grant from the four companies listed in Section 6.0) and from the San Francisco International Airport Authority. The investigation at each soft soil site consisted of drilling through the soil profile and into bedrock, some sampling and measurement of shear wave and compression wave velocities

The results of these subsurface investigations at Treasure Island site and at the San Francisco Airport site were used in this study to calculate the horizontal components of site response at these two sites and to assess the procedures used for conducting such response calculations.

The locations of these two sites and other recording stations pertinent to this study are shown in Fig. 1-1. The three-digit numbers shown in the figure identify the recording stations operated by the California Strong Motion Instrumentation Program (CSMIP); the stations pertinent to this study are the following:

Station Number	Station Name	Site Condition
117	Treasure Island	Soft Soil Site
223	San Francisco Airport	Soft Soil Site
539	Sierra Point	Rock Site
130	Diamond Heights	Rock Site
131	Pacific Heights	Rock Site
132	Cliff House	Rock Site
133	Telegraph Hill	Rock Site
151	Rincon Hill	Rock Site
163	Yerba Buena Island	Rock Site
222	Presidio	Rock Site
not shown in Fig. 1-1	Golden Gate	Rock Site
not shown in Fig. 1-1	Piedmont	Rock Site
not shown in Fig. 1-1	Lawrence Berkeley Lab	Rock Site

The horizontal components of motion recorded at Yerba Buena Island (Station No. 163 in Fig. 1-1) were used as rock outcrop motion in the analysis of the horizontal response of the Treasure Island site (Station No. 117 in Fig. 1-1) and those recorded at Sierra Point (Station No. 539 in Fig. 1-1) were used as rock outcrop motion in the analysis of the horizontal response of the San Francisco Airport site (Station No. 223 in Fig. 1-1). The horizontal components recorded at the other rock sites listed above were also used as rock outcrop in the response calculations for both sites. The locations of the three stations not shown in Fig. 1-1 are as follows: the Golden Gate station is just northwest of the Presidio station; the Piedmont station is about 7 km northeast and the Lawrence Berkeley Laboratory is about 14 km north of downtown Oakland, respectively.

The characteristics of the horizontal components of the recordings obtained at these rock sites are summarized in Appendix B and those obtained at soft soil sites, which include the sites at Treasure Island and at the San Francisco Airport and seven other stations, are summarized in Appendix C.

The results of the analyses completed for the Treasure Island and the San Francisco Airport are presented in the following sections of this report.

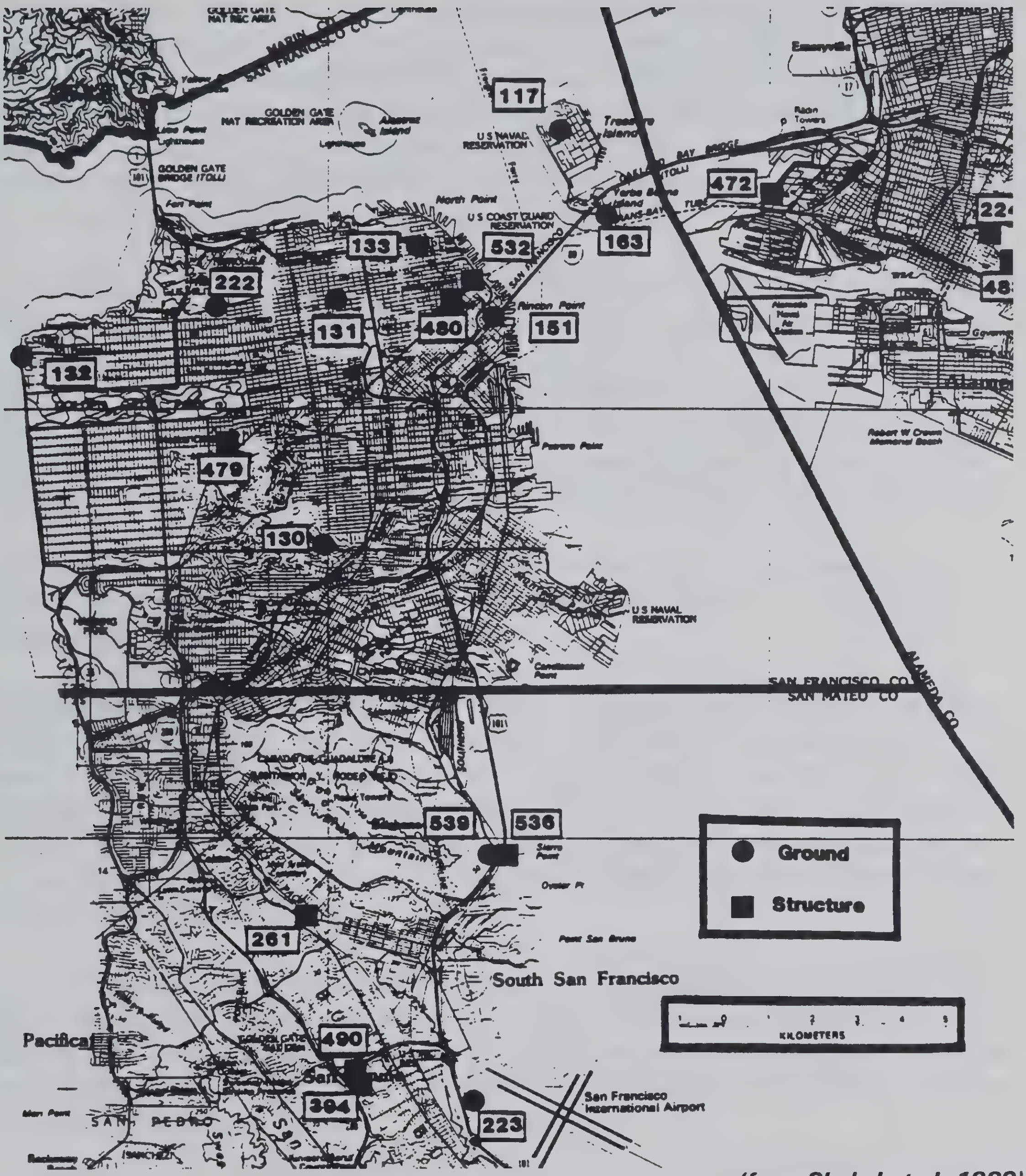

(from Shakal et al, 1989)

Fig. 1-1 Locations of CSMIP Recording Stations in the San Francisco-Bay Area used in Present Studies

2.0 SITE RESPONSE ANALYSES

Procedures for calculating the response of soil profile to earthquake shaking have been available for a long time. The currently available procedures use either an equivalent linear or a nonlinear representation for the stress-strain behavior of the various soil layers comprising the soil profile. While other formulations are available, many situations are reasonably approximated by a horizontal multi-layered system of semi-infinite extent. The latter is most conveniently represented by a one dimensional system consisting of a series of soil sublayers over a half-space.

The equivalent linear procedure was introduced by Idriss and Seed (1968) and has been implemented in several computer programs. Currently, the most widely used computer program for a multi-layered system over a half-space, which also incorporates the equivalent linear formulation, is program SHAKE (Schnabel et al, 1972). Another computer program that is also used in many applications is program RASCALS; the original program (which was designated RASCAL) was developed and coded by Silva and Lee (1987) has been considerably updated by Silva (personal communication, 1992).

The program SHAKE91 (Idriss and Sun, 1992) was used in the present study. The program SHAKE91 is a modification and an update of the original SHAKE program (Schnabel et al, 1972).

There are many nonlinear procedures available for calculating the response of a multi-layered system overlying a half-space. For the present study, only two of these procedures were examined. One procedure is that incorporated in the program DESRA-2 (Lee and Finn, 1978) which was developed by Finn and his colleagues at the University of British Columbia. The other procedure used in this study is that incorporated in the program SUMDES (Li et al, 1992) which was developed by Li and his colleagues at the University of California at Davis.

As part of this study, detailed response analyses were conducted for the Treasure Island Site and for the San Francisco Airport Site. Equivalent linear as well as nonlinear analyses were completed for the Treasure Island Site and only equivalent linear analyses were completed for the San Francisco Airport Site. The results are presented in Sections 3.0 and 4.0 of this report.

3.0 TREASURE ISLAND SITE

The location of the recording station at Treasure Island is shown in Fig. 1-1 and in more detail in Fig. 3-1. Also shown in Fig. 3-1 is the location of the recording station at Yerba Buena Island which is the closest rock site to the Treasure Island recording station. The spectra of the horizontal motions recorded at Treasure Island and at Yerba Buena Island are presented in Fig. 3-2. The upper part of Fig. 3-2 shows the spectra for the stronger components (EW components) of the recorded motions and the lower part of the figure shows the spectra for the weaker components (NS components). More details regarding the characteristics of the recordings at Yerba Buena Island are given in Appendix B and those for Treasure Island are summarized in Appendix C.

3.1 Subsurface Conditions at The Treasure Island Site

The subsurface conditions at the Treasure Island site were obtained by drilling a boring nearby the station to a depth of 338 feet (103 meters). The shear wave velocities were measured in the same boring by USGS (Gibbs et al, 1992) and by Redpath (1991) using down-hole measuring techniques and by Rollins et al (1992) at other, but nearby, locations using a seismic cone (SCPT).

The log of boring and the shear wave velocities measured by USGS are shown in Fig. 3-3 and the shear wave velocities measured by USGS, by Redpath (both the originally reported as well the revised velocities) and by Rollins et al are shown in Fig. 3-4. Also shown in Fig. 3-4 are the values of the "best estimate" shear wave velocities used in the analyses; these values are listed below in Section 3.2.

The log of boring indicates that the subsurface conditions at the Treasure Island site consist of sandy fill overlying a natural deposit of loose sand to a depth of about 40 ft (12.2 m), which in turn is underlain by a 55-ft (16.8 m) layer of Young Bay Mud. Alternating layers of dense sand and Old Bay Mud are encountered below a depth of 95 ft (29 m) to a depth of about 290 ft (88.4 m). Weathered shale extends from this depth to a depth of 320 ft (97.5 m), where a more competent sandstone is encountered.

3.2 Dynamic Soil Properties

The dynamic soil properties needed for an equivalent linear analysis include the maximum shear wave velocity (or maximum shear modulus), modulus-reduction as a function of strain and damping ratio as a function of strain. The maximum shear wave velocities are based on the velocities measured at the site and the values selected to represent the best estimate shear wave velocities are shown in Fig. 3-4. The best estimate input properties used in the equivalent linear analyses are listed in Appendix D.

The modulus reduction curves shown in the upper part of Fig. 3-5 were used in this study. The upper curve was used for all the clay layers at the site; it is approximately equal to modulus reduction curve published by Sun et al (1988) and by Vucetic and Dobry (1991) for a plasticity index (PI) of about 30. The curve used for sand is approximately equal to the upper range for sand published by Seed and Idriss (1970).

The damping ratio versus strain curve shown in the lower part of Fig. 3-5 was used for both the clay as well as the sand layers; it corresponds approximately to the lower range damping curve for sand published by Seed and Idriss (1970).

3.3 Equivalent Linear Analyses

The response of the Treasure Island site was calculated incorporating equivalent linear modulus and damping representation for the following conditions:

- using the stronger component of the recording at Yerba Buena Island (YBI) as input rock outcrop motion, and
    - best estimate of the shear wave velocity profile
    - various estimates of the shear wave velocity profile

- using the weaker component of the recording at Yerba Buena Island (YBI) as input rock outcrop motion, and
    - best estimate of the shear wave velocity profile
    - various estimates of the shear wave velocity profile

- using the best estimate of the shear wave velocity profile and the stronger and the weaker components of all the rock motions recorded in the San Francisco Bay Area (see Table B-3) as input outcrop motions

The results of these analyses are presented below.

3.3.1 Response at Treasure Island Using the Stronger Component of Recording at YBI as Input Rock Outcrop Motion

3.3.1.1 Results Using Best Estimate Shear Wave Velocity Profile

The best estimate shear wave velocities for the Treasure Island site are based on the measured shear wave velocities shown in Fig. 3-4 and are summarized below:

Depth Below Ground Surface - ft		Total Unit Weight - pcf	Maximum Shear Wave Velocity - ft/sec
From	To		
0	10	120	800
10	20	125	500
20	30	125	525
30	40	125	550
40	50	100	600

50	70	100	700
70	95	100	600
95	135	130	1000
135	240	130	900
240	290	130	1250
290	half-space	140	4000

The corresponding values in SI units are listed below:

Approximate Depth Below Ground Surface - meter		Total Unit Weight kN/m^3	Maximum Shear Wave Velocity m/sec
From	To		
0	3.05	18.9	243.9
3.05	6.10	19.7	152.4
6.10	9.15	19.7	160.1
9.15	12.2	19.7	167.7
12.20	15.24	15.7	182.9
15.24	21.34	15.7	213.4
21.34	28.96	15.7	213.4
28.96	41.16	20.4	304.9
41.16	73.17	20.4	274.4
73.17	88.41	20.4	381.1
88.41	half-space	22.0	1,220

The response of this soil profile was calculated using the computer program SHAKE91. The results of the response calculations are presented in Figs. 3-6 through 3-9. Figure 3-6 shows the calculated maximum shear strains and stresses and Fig. 3-7 shows the calculated strain-compatible damping ratios and shear wave velocities as well as the best estimate maximum shear wave velocities. As can be noted in these figures, the largest strain values are induced in the lower parts of the sandy fill and natural loose sand and in the Young Bay Mud layer. The maximum strains are quite small, however. Accordingly, the damping ratios are below 10% and the strain-compatible shear wave velocities are not much smaller than the maximum shear wave velocities as illustrated in Fig. 3-7.

Figure 3-8 shows the variations of peak horizontal accelerations with depth. It is interesting that a significant part of the peak acceleration amplification occurs in the upper 40 feet (12.2 m) of the soil profile.

The spectrum for the surface motion at Treasure Island, calculated using the best estimate shear wave velocities and the stronger component of the Yerba Buena Island record as input motion, is compared to the spectrum for the recorded surface motion in Fig. 3-9. As can be seen in this figure, the spectrum for the calculated surface motion provides a reasonable approximation of the spectrum for the recorded surface motion for almost the entire period range.

Accordingly, the use of best estimate shear wave velocities and the recorded motion from a nearby rock site as input motion in an equivalent linear analysis provides a reasonable approximation for the recorded motions.

The effects of using different shear wave velocities are considered in the next section.

3.3.1.2 Results Using Various Shear Wave Velocity Profiles

Several shear wave velocity profiles were considered for assessing the effects of varying shear wave velocities on the response calculations. These variations included using a lower bound and an upper bound shear wave velocity profiles and the addition of a 50-ft (15.2 m) layer of weathered shale at the bottom of the soil profile. They also included varying the shear wave velocity of the half-space from 3,000 to 5,000 ft/sec (914 to 1,524 m/sec) and using two different values of the ratio of equivalent uniform strain to maximum strain. For most cases, a value of 0.5 was adopted for the this ratio, but for two of the cases a value of 0.35 was used; the latter value is similar to that used by Dickenson et al (1991) for similar calculations.

The results of the response calculations, using various shear wave velocity profiles and the stronger component of the recording at Yerba Buena Island as input motion, are presented in Figs. 3-10, 3-11 and 3-12. Figure 3-10 shows the accelerograms calculated at the ground surface at the Treasure Island site for four of the cases considered. Also shown in the figure is the accelerogram of the stronger component of the recorded surface motion. As can be noted in the figure, the calculated motions are not significantly affected by the variations in the shear wave velocity profile. This is further illustrated in Fig. 3-11 which shows a comparison of the spectrum for the recorded motion and those for the calculated motions. Figure 3-12 indicates that the use of the best estimate shear wave velocities results in calculating a surface motion whose spectrum is very close to the median spectrum for all the cases considered.

3.3.2 Response at Treasure Island Using the Weaker Component of the Recording at YBI as Input Rock Outcrop Motion

3.3.2.1 Results Using Best Estimate Shear Wave Velocity Profile

The same best estimate shear wave velocities which were used in conjunction with the stronger component of input motion were also used in conjunction with the weaker component of the input motion.

The spectrum for the surface motion at Treasure Island, calculated using the best estimate shear wave velocities and the weaker component of the Yerba Buena Island record as input motion, is compared to the spectrum for the recorded surface motion in Fig. 3-13. The spectrum for the calculated surface motion is similar in shape to the spectrum for the recorded surface motion, but is considerably lower in amplitude over a significant range of periods.

Accordingly, the use of best estimate shear wave velocities and the recorded motion from a nearby rock site as input motion in an equivalent linear analysis provides a reasonable approximation for the recorded motions only in one direction for the Treasure Island site.

The effects of using different shear wave velocities are considered in the next section.

3.3.2.2 Results using Various Shear Wave Velocity Profiles

The same shear wave velocity profiles described in Section 3.3.1.2 were also considered for assessing the effects of varying shear wave velocities on the response calculations using the weaker component of the input motion. Figure 3-14 shows a comparison of the spectrum for the recorded motion and those for the calculated motions considering various shear wave velocity profiles and the weaker component of the Yerba Buena Island as input motion. Figure 3-15 shows the spectrum for the calculated surface motion using the best estimate shear wave velocities and the median spectrum for all the other cases considered together with the spectrum for the weaker component of the recorded surface motion. Use of the various shear wave velocity profiles appears to somewhat improve the comparison between the spectrum for the recorded motion and those for the calculated motions.

3.3.3 Response at Treasure Island Using the Recorded Motions at All the Rock Sites in San Francisco Bay Area as Input Rock Outcrop Motions

It is seldom that a soil site has an immediately adjacent rock site (such as was the case at Treasure Island and at Yerba Buena Island) both of which had instruments that recorded the motions generated by the same earthquake. Many times, recording stations at rock sites are several, if not tens, of kilometers away from the soil site under consideration.

Several rock sites in the San Francisco Bay Area had strong motion instruments which were triggered during the Loma Prieta earthquake. Recordings at eleven such sites were obtained as summarized in Appendix B. These rock motions were then used as input rock outcrop motions for evaluating the response at the Treasure Island site. The best estimate shear wave velocities were used in all the response calculations.

3.3.3.1 Results Using the Stronger Components

The stronger component of each record obtained at the eleven rock sites was first scaled to a peak acceleration of 0.07g (i.e., its peak acceleration was made equal to that of the stronger component recorded at Yerba Buena Island). The response was then calculated using this scaled accelerogram as rock outcrop input motion using the best estimate shear wave velocities for the soil profile. Strain-compatible damping ratios and shear wave velocities were obtained for each response calculation.

Figures 3-16a, 3-16b and 3-16c show a direct comparison of the spectrum for the recorded surface motion and the spectrum for the surface motion at Treasure Island calculated using the stronger component of motions recorded at each rock site. As can be seen from these figures, the results using the record at Yerba Buena Island provide the best estimate to the recorded values. The results using some of the other records (e.g., Piedmont and Sierra Point) provide reasonable estimates in some period ranges. The remaining records provide results that are significantly different from the recorded values.

It may be noted that peak acceleration is estimated quite well using any of the rock records. Therefore, it is not sufficient to rely on making estimates of the peak acceleration in checking the accuracy of an analytical procedure.

Figure 3-17 shows the spectrum for the recorded surface motion and the spectra for surface motions at Treasure Island calculated using the stronger component of motions recorded at Yerba Buena and at the other rock sites. This figure highlights the fact that using various rock input motions has a far greater effect on the calculated results than any other parameter.

3.3.3.2 Results Using the Weaker Components

The results using the weaker components are presented in Fig. 3-18. These results indicate a small improvement in the accuracy of estimating the spectrum of the recorded motion when the other rock records are used as input motions.

3.3.3.3 Discussion of Results

The material presented in this section of the report indicate that the results of a response analysis can be significantly affected by the input motion used in the response calculations. In fact, the input motion appears to have the most dominant effect on the results. Consequently, it would seem inappropriate to rely on the results of any one single analysis and that response calculations should always include variations in the input motion.

In practice, it is quite often the case that the input motion is not known and may have to be generated using synthetically generated accelerograms or to rely on accelerograms recorded during prior earthquakes. The results shown in Figs. 3-16a, 3-16b, 3-16c, 3-17 and 3-18 show the range of possible variations in computed spectral ordinates. Often, similar results are obtained for a particular site and then the median or the 84th percentile values of the ensemble of calculated spectra is used. This process is tested using the results for the Treasure Island site as summarized in Figs. 3-19 and 3-20. These figures show that:

1. The median of the calculated spectra underestimates the spectrum for the recorded motion for either component or for the average of the two components.

2. The 84th percentile spectrum for the calculated motions provides a reasonable estimate of the spectrum for the weaker component of the recorded motion, but does not do so for the stronger component as illustrated in Fig. 3-19.

3. The 84th percentile spectrum for all the calculated motions (i.e., considering both components) appears to provide a reasonable estimate for the average spectrum for the two components of the recorded motions as shown in Fig. 3-20.

3.4 Nonlinear Analyses

The results using the program DESRA-2 are presented in Fig. 3-21 together with those obtained using the results of an equivalent linear analysis. These results indicate that the DESRA-2 nonlinear analyses provide a somewhat reasonable estimate of the spectrum for the stronger component of motion at Treasure Island. They also show that the results of the equivalent linear analyses and those using this nonlinear procedure are comparable, although in this case the equivalent linear analysis provides an improved estimation of the spectrum of the recorded motion. Similar results were obtained using the nonlinear procedure incorporated in the program SUMDES.

Similar comparisons have been made by Dickenson et al (1992) and by Chin and Aki (1993), who also concluded that at the levels of shaking experienced during the Loma Prieta earthquake, the two methods of analyses provide comparable results.

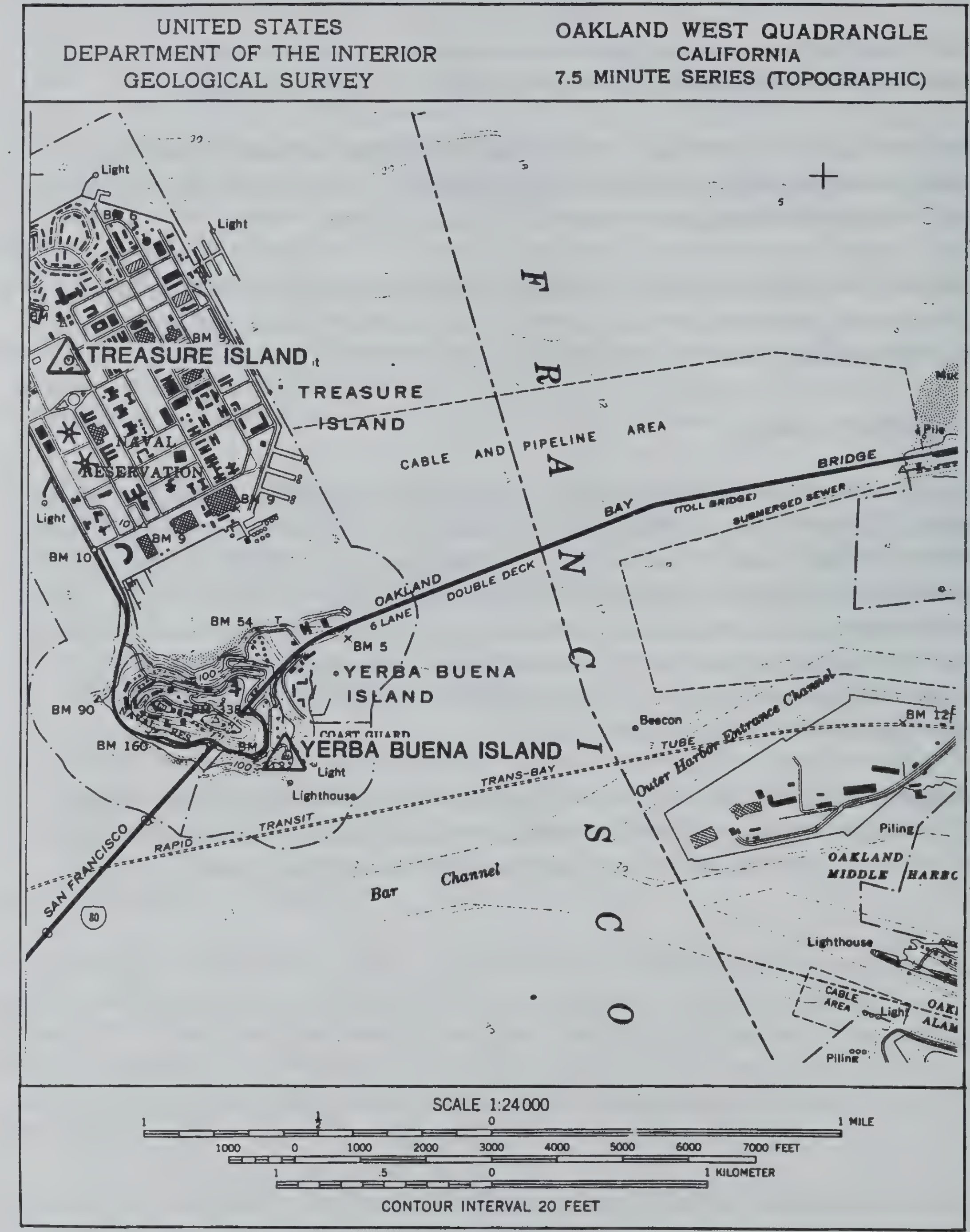

(from Gibbs et al, 1992)

Fig. 3-1 Locations of Recording Stations at Treasure Island and at Yerba Buena Island

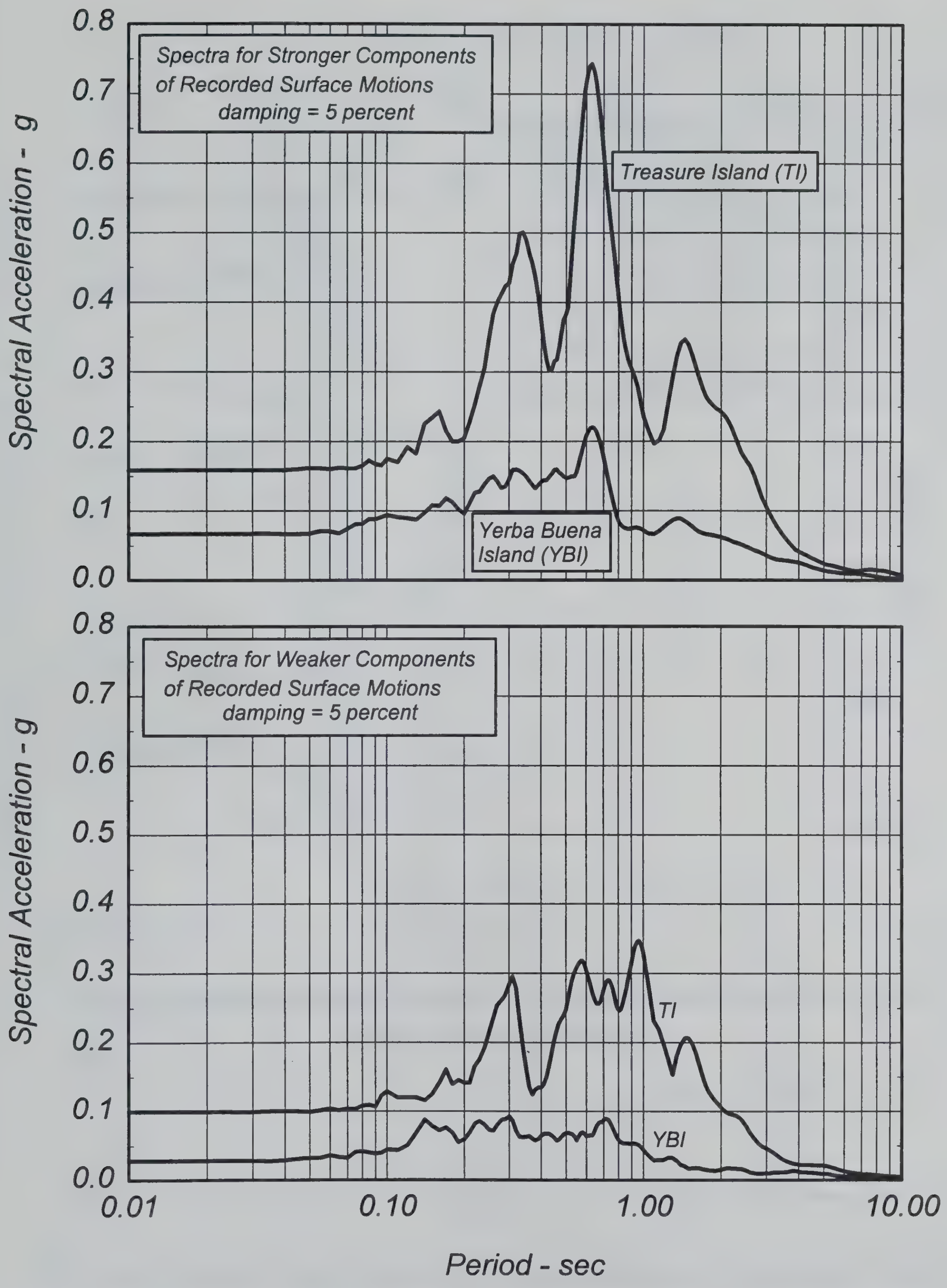

Fig. 3-2 Spectra for Surface Motions Recorded at Treasure Island (TI) and at Yerba Buena Island (YBI)

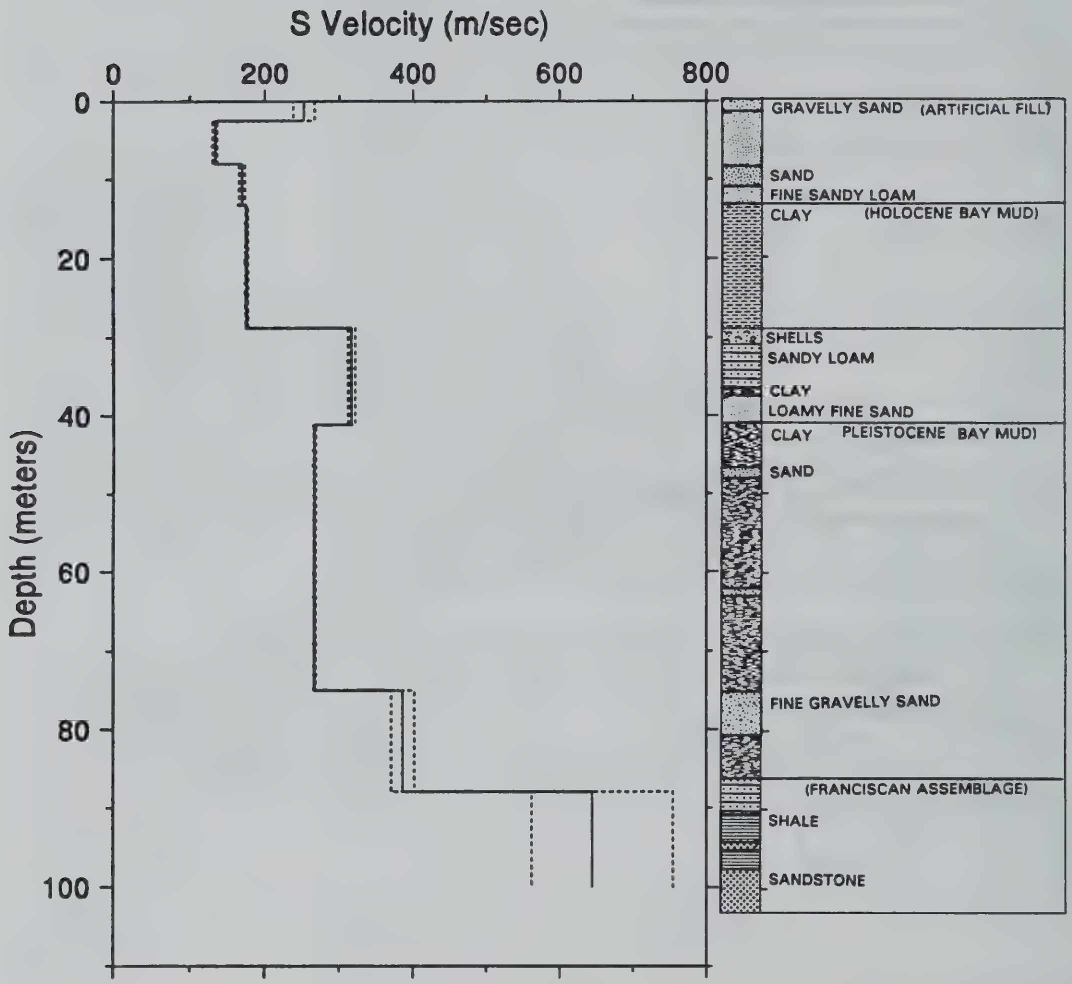

(from Gibbs et al, 1992)

Fig. 3-3 Log of Boring and Shear Wave Velocities Measured at Treasure Island by USGS

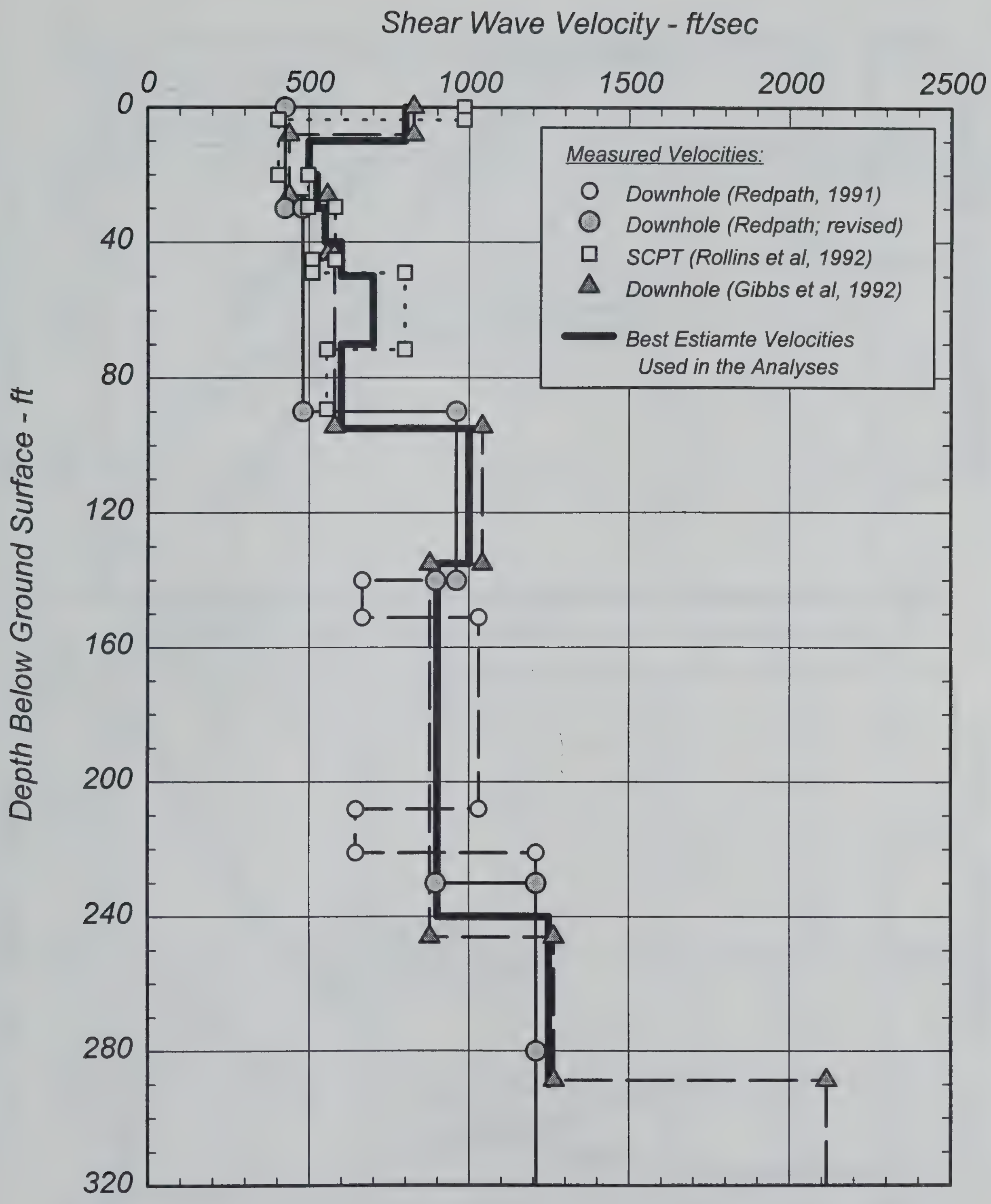

Fig. 3-4 Shear Wave Velocities Measured at Treasure Island and Best Estimate Values of Velocities Used in the Analyses

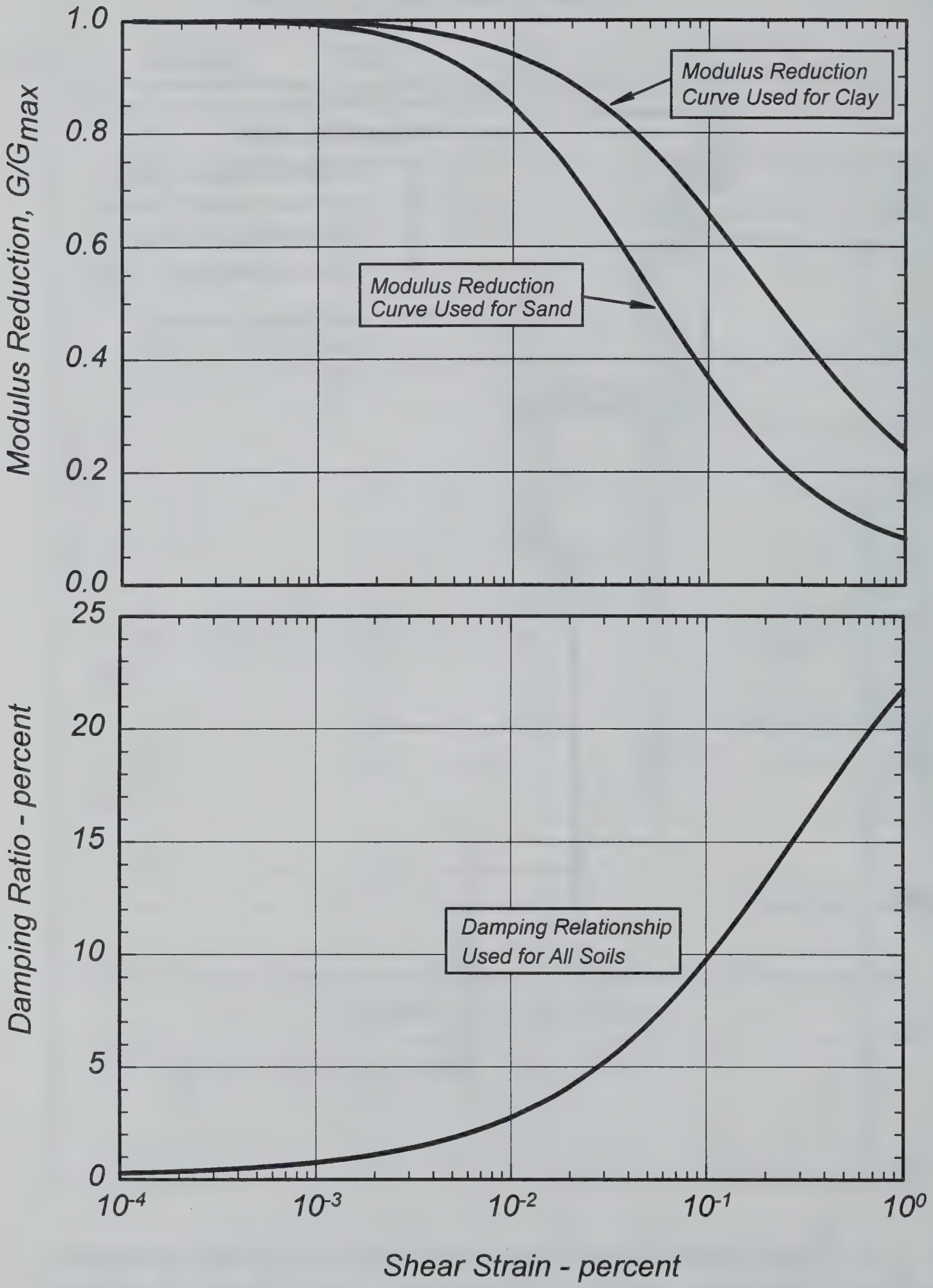

Fig. 3-5 Modulus Reduction and Damping Relationships Used in All Analyses

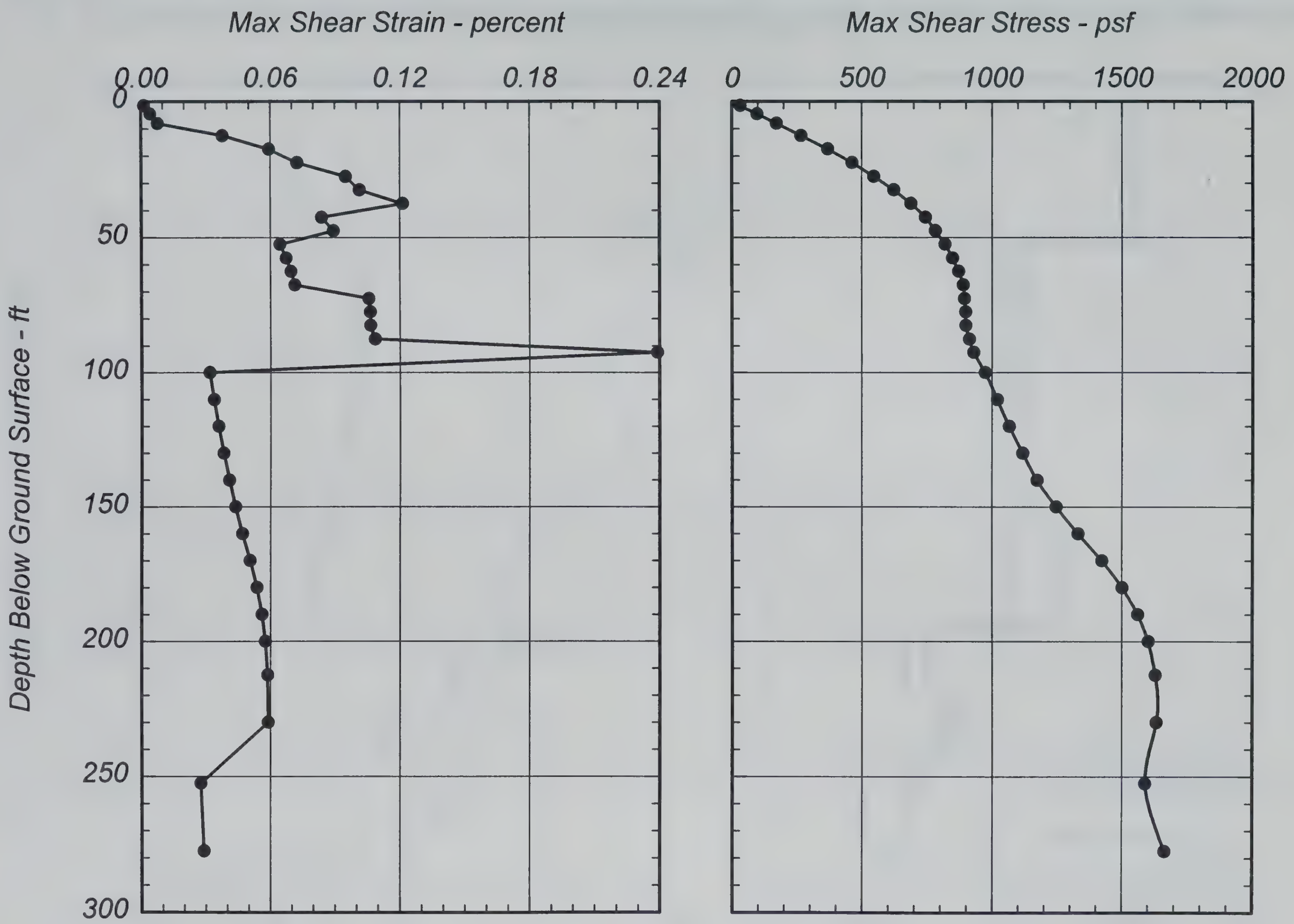

Fig. 3-6 Maximum Shear Strains and Stresses at TI Calculated Using Best Estimate Shear Wave Velocities and Stronger Component of YBI Record as Input Motion

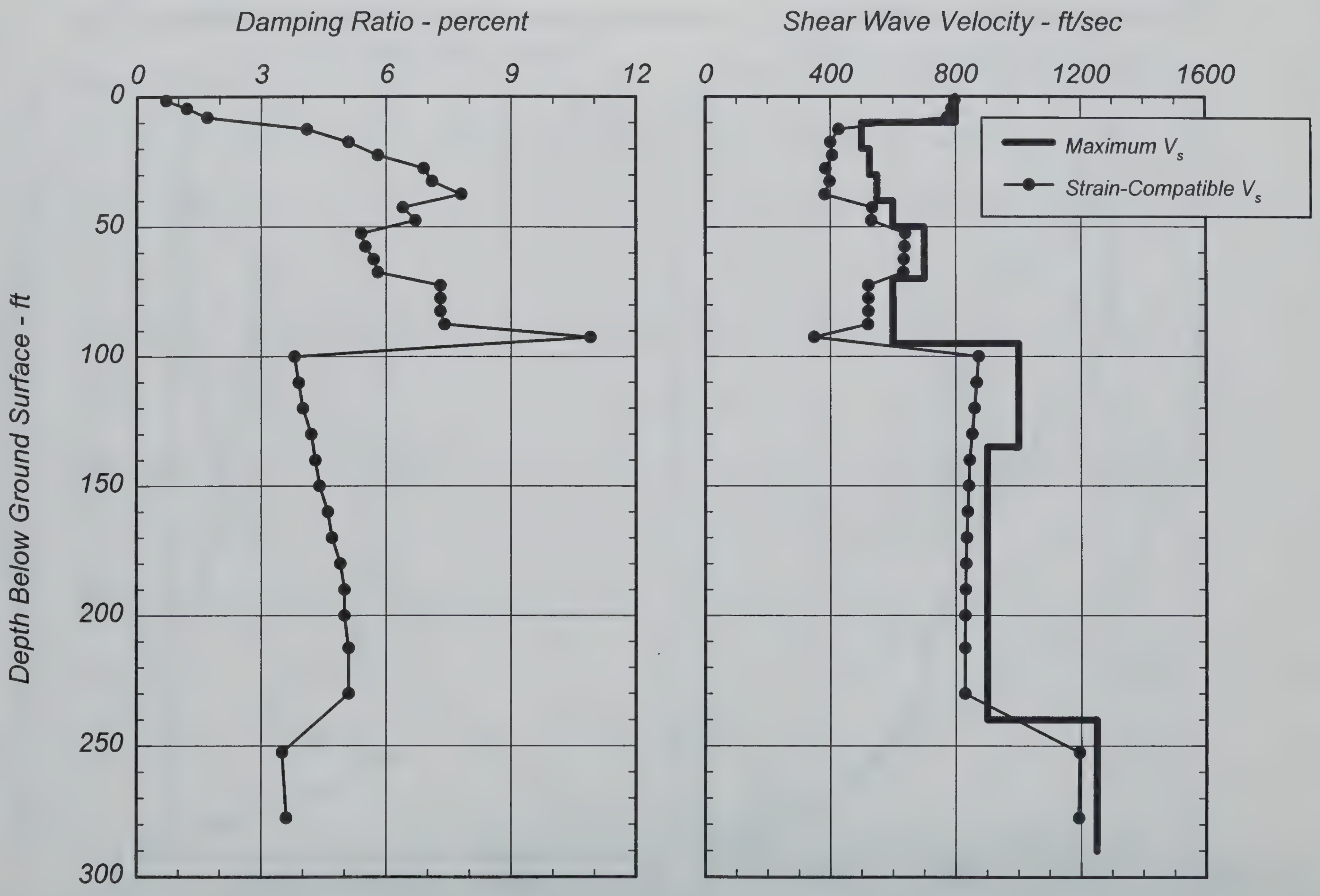

Fig. 3-7 Strain-Compatible Damping Ratios and Shear Wave Velocities at TI Calculated Using Best Estimate Shear Wave Velocities and Stronger Component of YBI Record as Input Motion

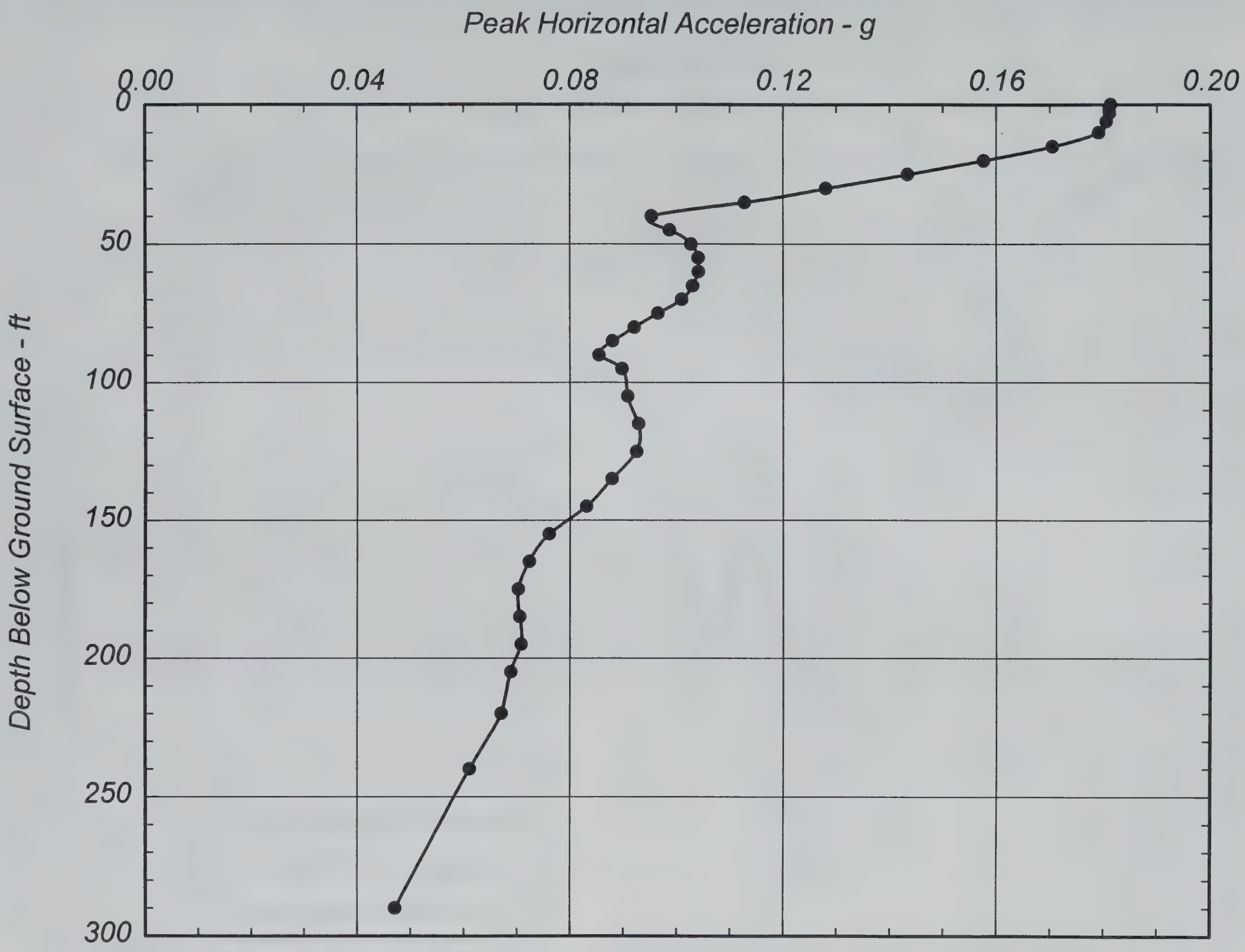

Fig. 3-8 Peak Horizontal Accelerations at TI Calculated Using Best Estimate Shear Wave Velocities and Stronger Component of YBI Record as Input Motion

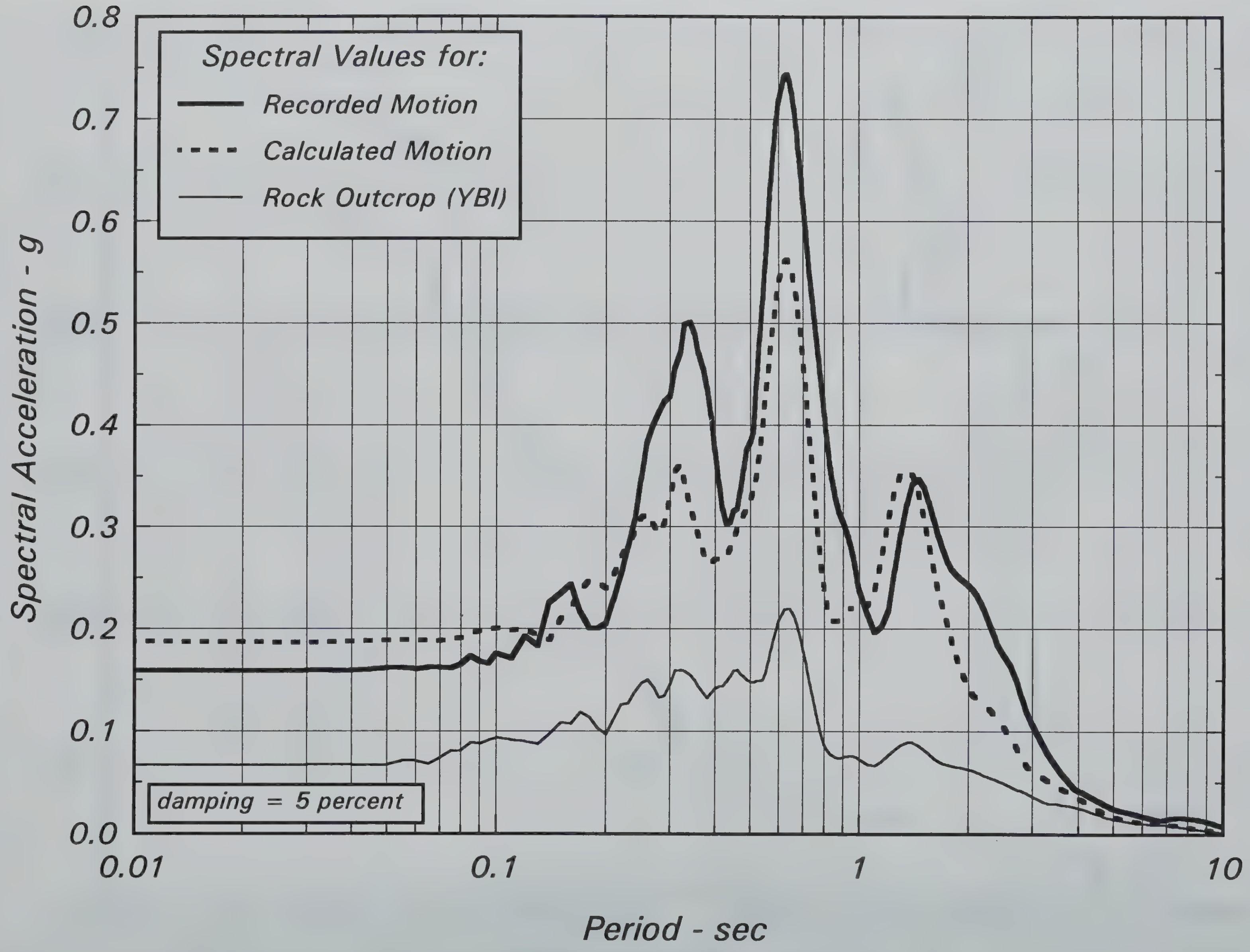

Fig. 3-9 Spectrum for Recorded Surface Motion and Spectrum for Surface Motion at TI Calculated Using Best Estimate Shear Wave Velocities and Stronger Component of YBI Record as Input Motion

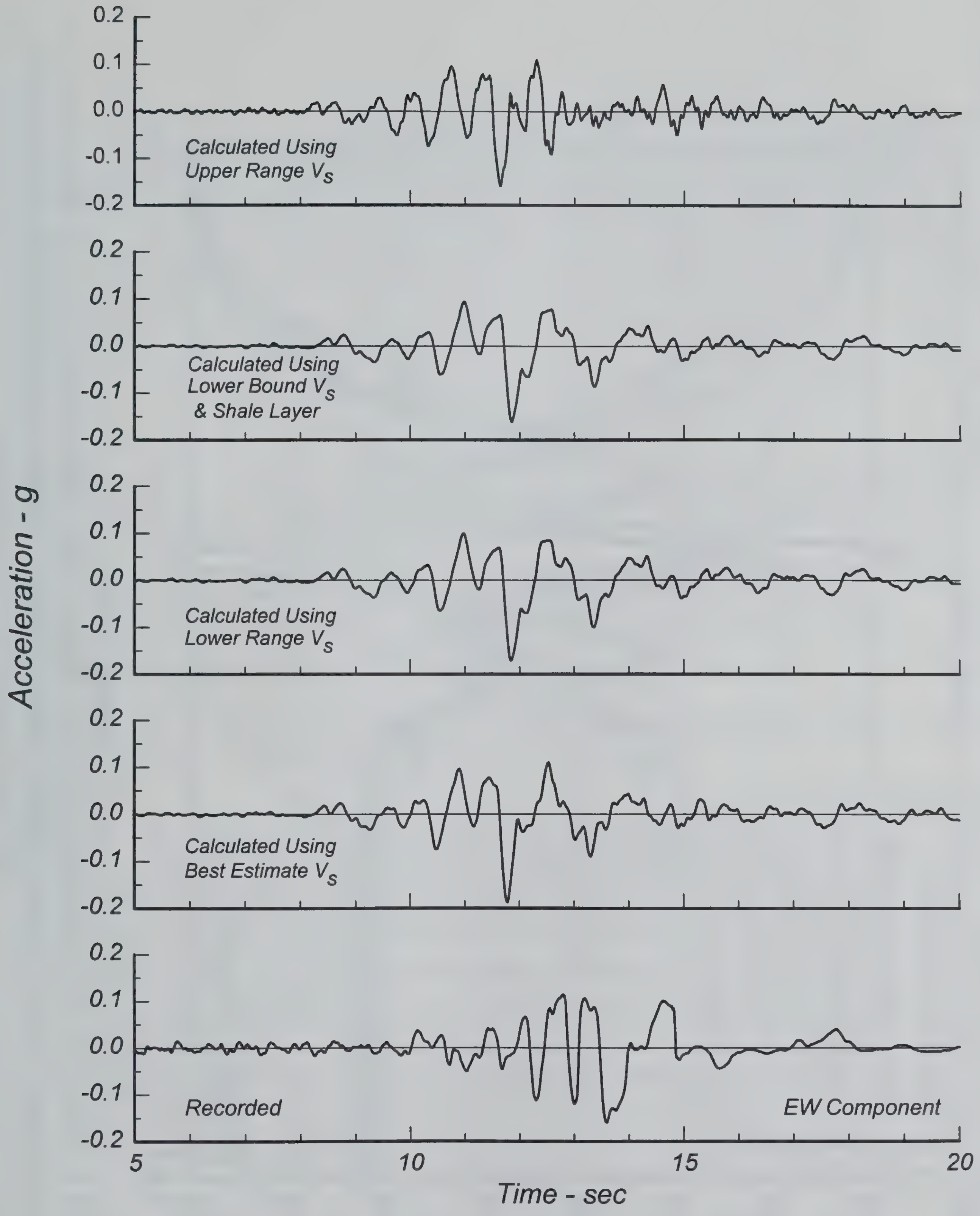

Fig. 3-10 Accelerogram of Recorded Surface Motion and Accelerograms of Surface Motions at TI Calculated Using Various Shear Wave Velocity Profiles and Stronger Component of YBI Record as Input Motion

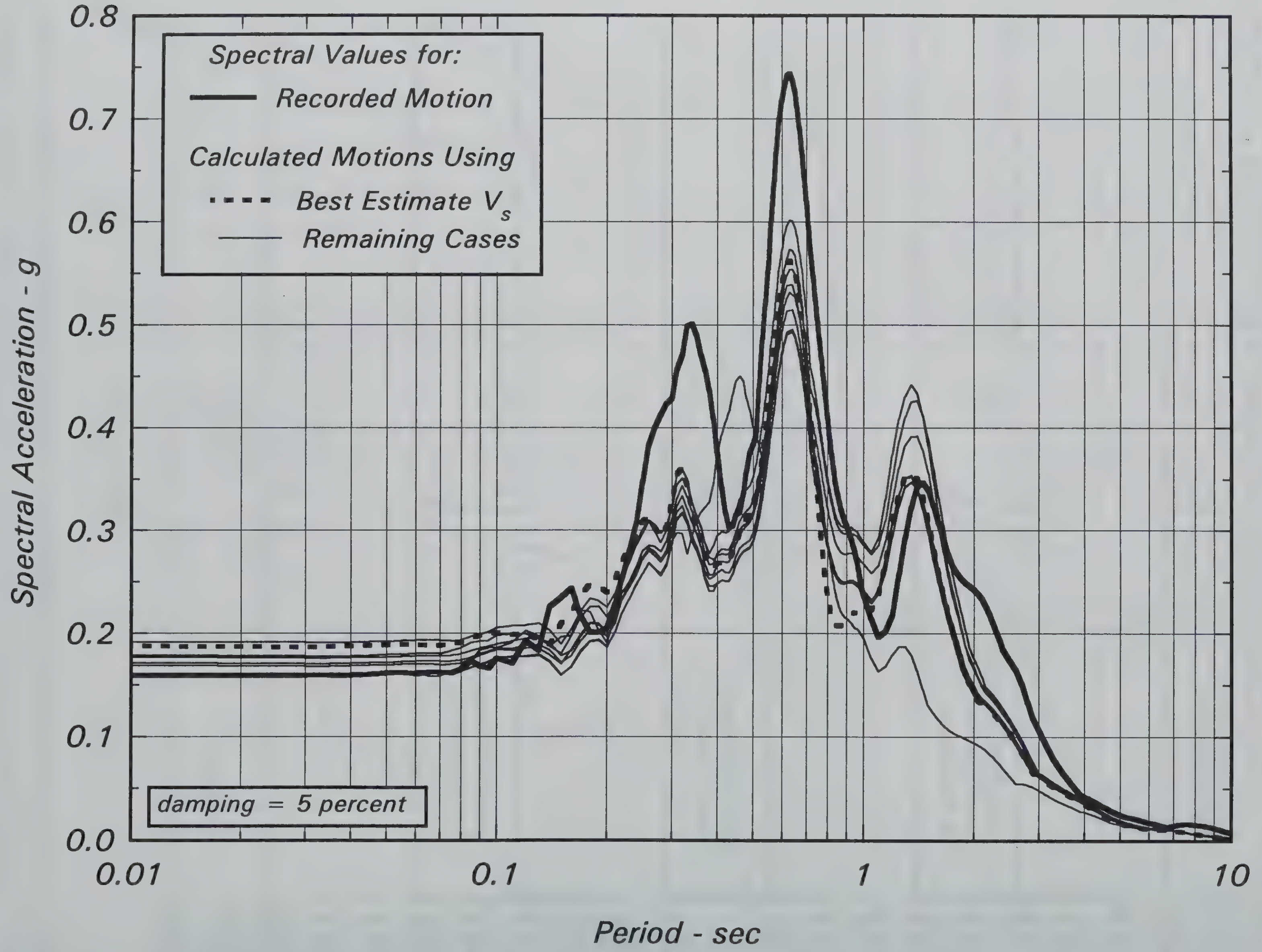

Fig. 3-11 Spectrum for Recorded Surface Motion and Spectra for Surface Motions at TI Calculated Using Various Shear Wave Velocity Profiles and Stronger Component of YBI Record as Input Motion

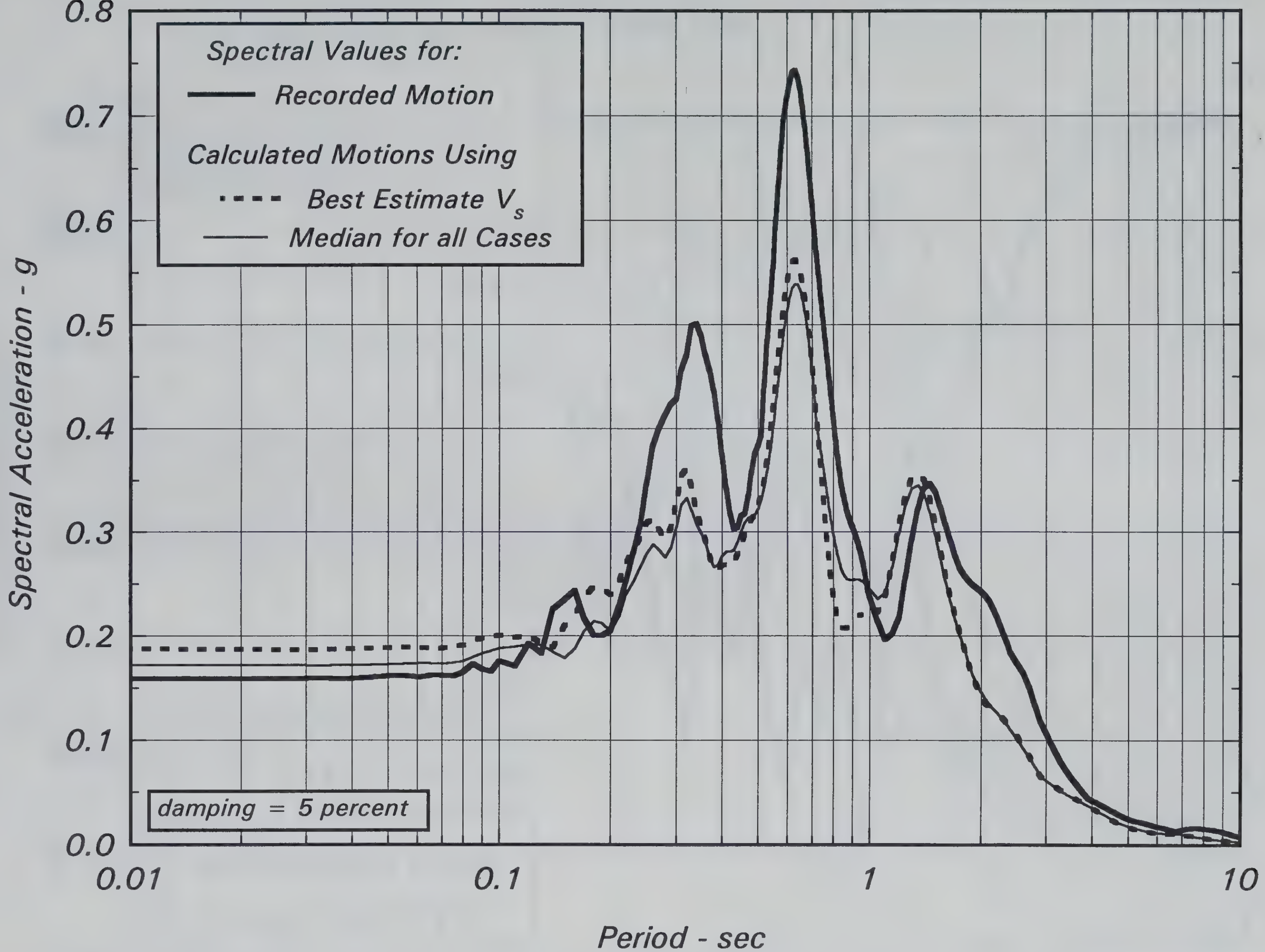

Fig. 3-12 Spectrum for Recorded Surface Motion, Spectrum for Surface Motion Calculated Using Best Estimate Shear Wave Velocities and Median Spectrum for Cases Considered at Treasure Island Using Stronger Component of YBI Record as Input Motion

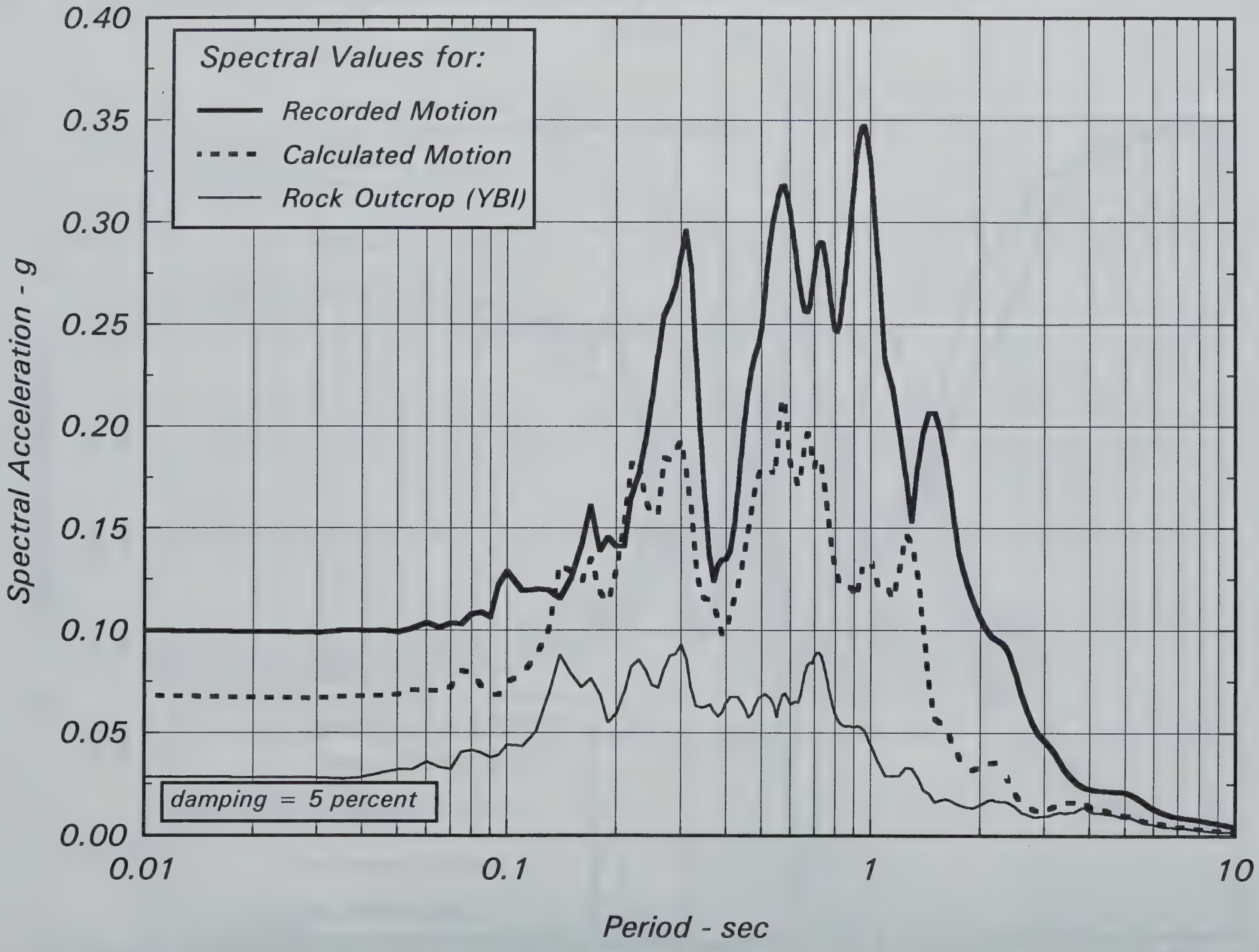

Fig. 3-13 Spectrum for Recorded Surface Motion and Spectrum for Surface Motion at TI Calculated Using Best Estimate Shear Wave Velocities and Weaker Component of YBI Record as Input Motion

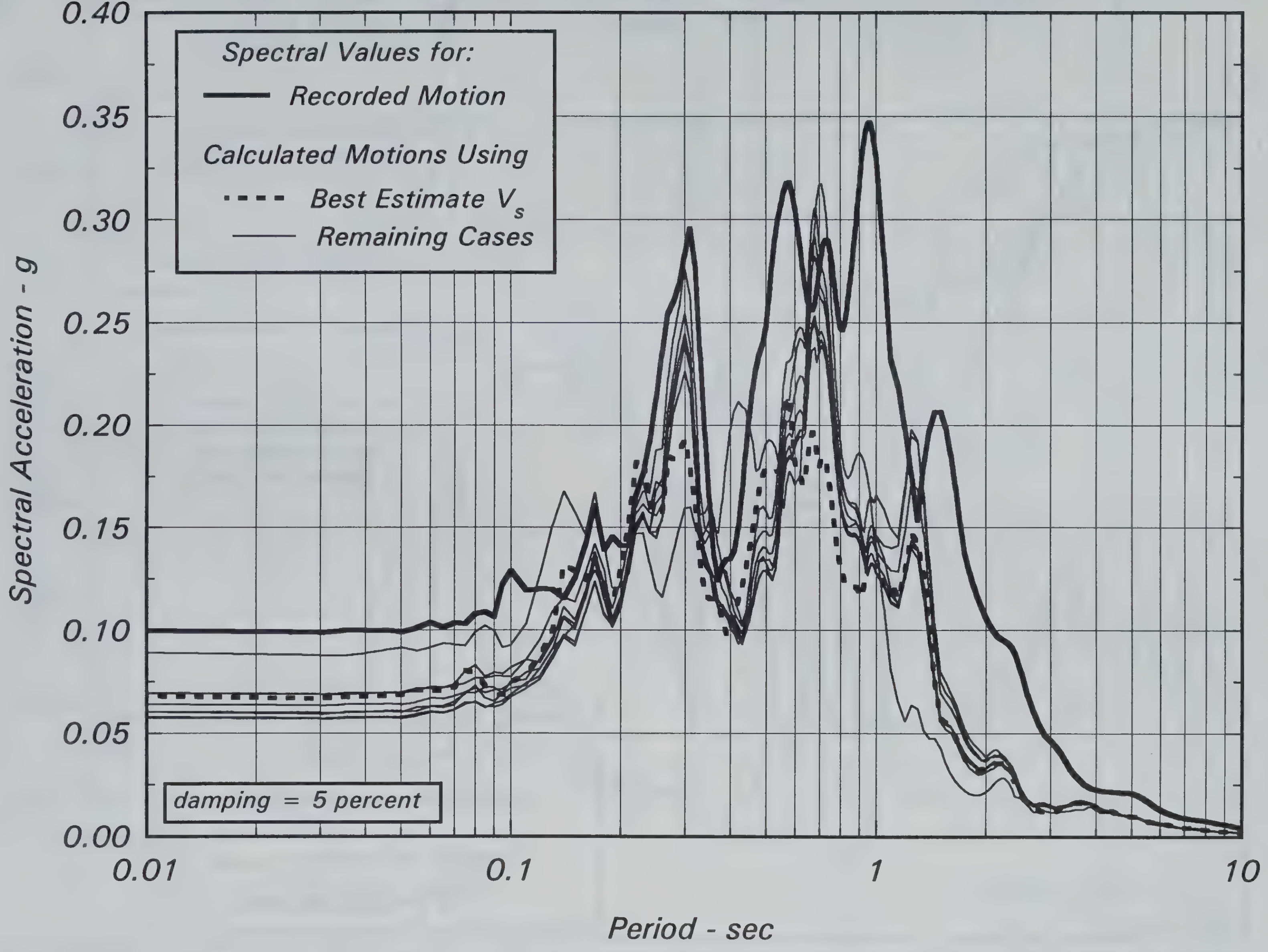

Fig. 3-14 Spectrum for Recorded Surface Motion and Spectra for Surface Motions at TI Calculated Using Various Shear Wave Velocity Profiles and Weaker Component of YBI Record as Input Motion

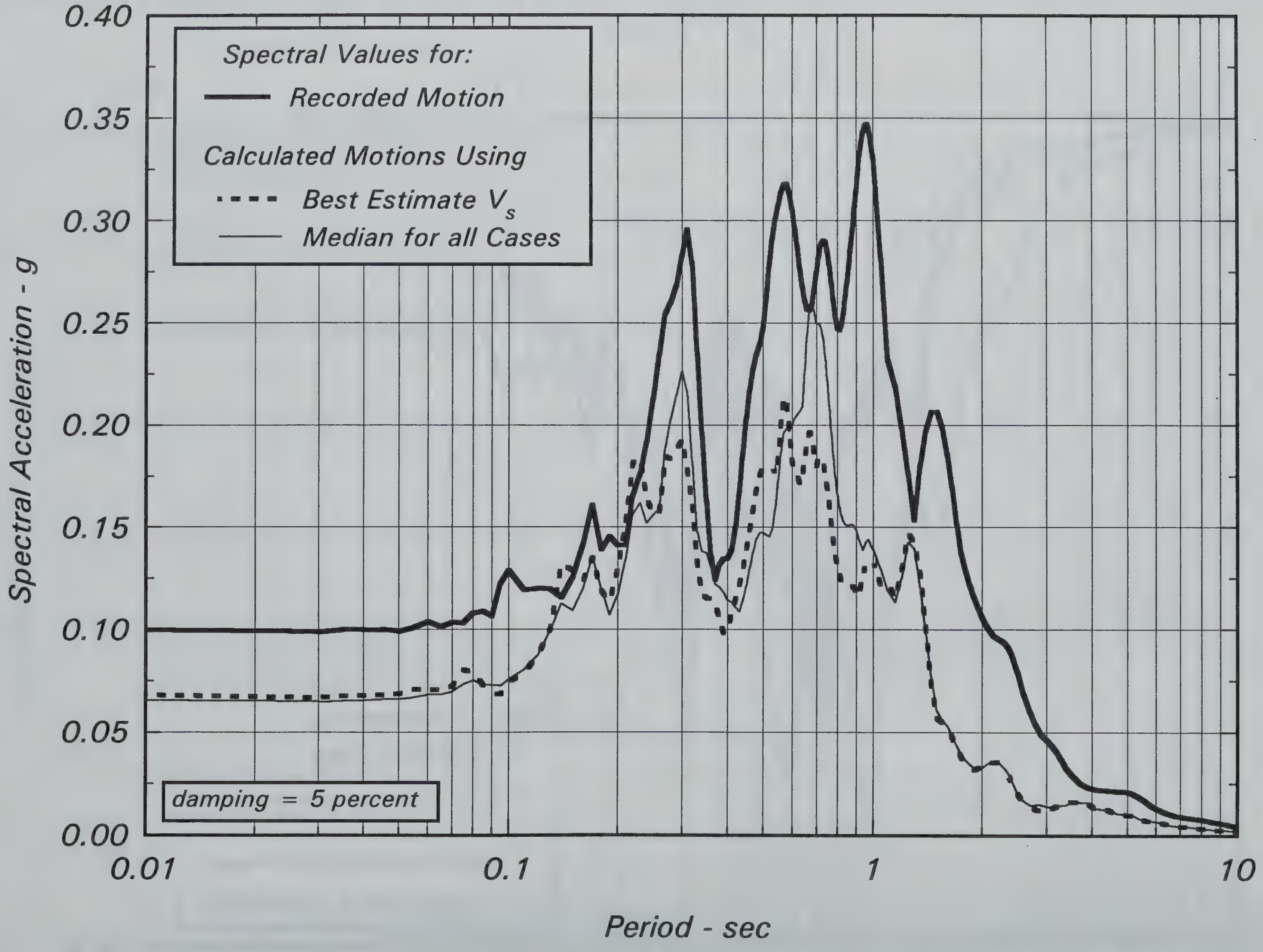

Fig. 3-15 Spectrum for Recorded Surface Motion, Spectrum for Surface Motion Calculated Using Best Estimate Shear Wave Velocities and Median Spectrum for Cases Considered at Treasure Island Using Weaker Component of YBI Record as Input Motion

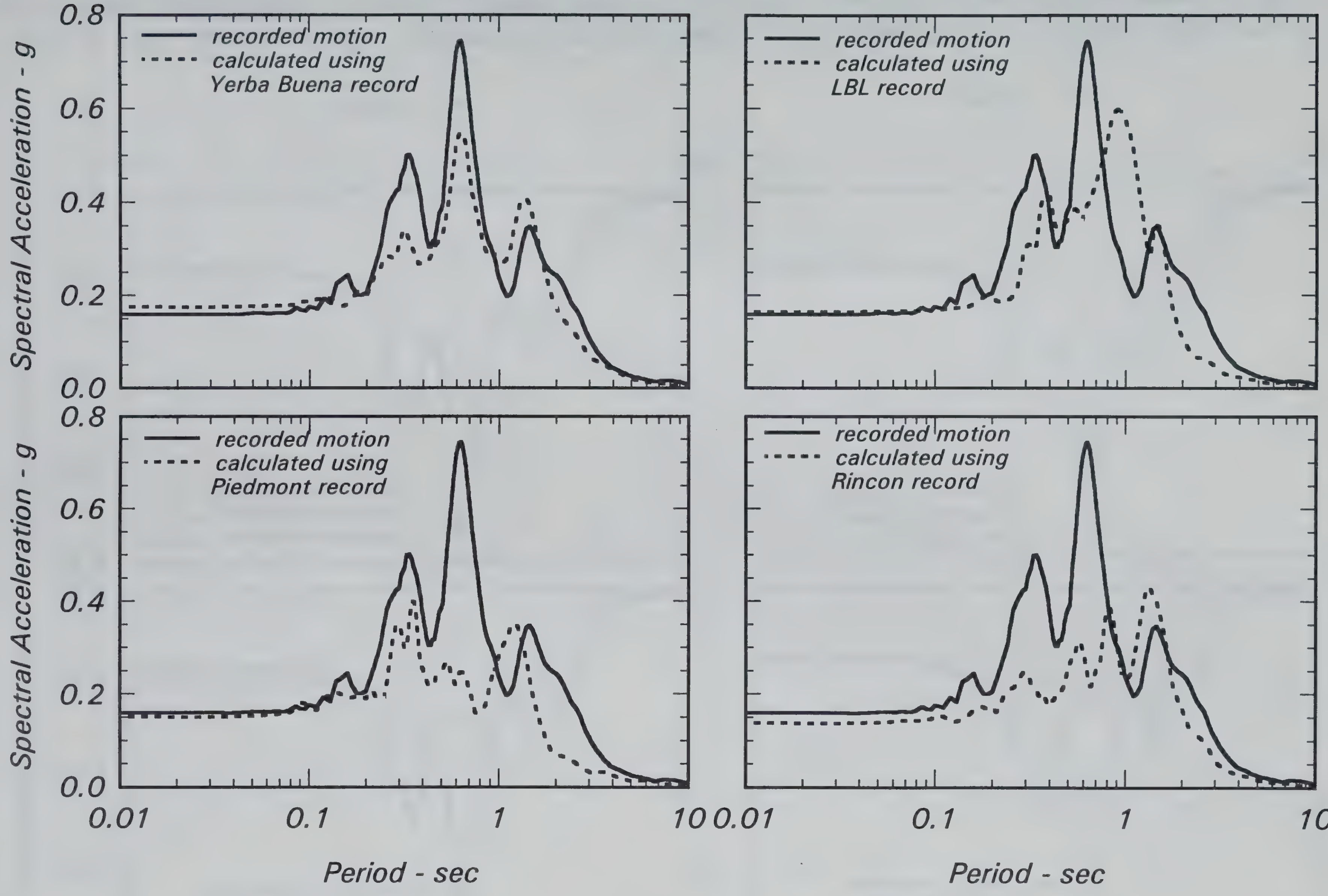

Fig. 3-16a Spectrum for Recorded Surface Motion and Spectra for Surface Motions at TI Calculated Using Best Estimate Shear Wave Velocities and Stronger Component of Motions Recorded at Yerba Buena, LBL, Piedmont and Rincon as Input Motions

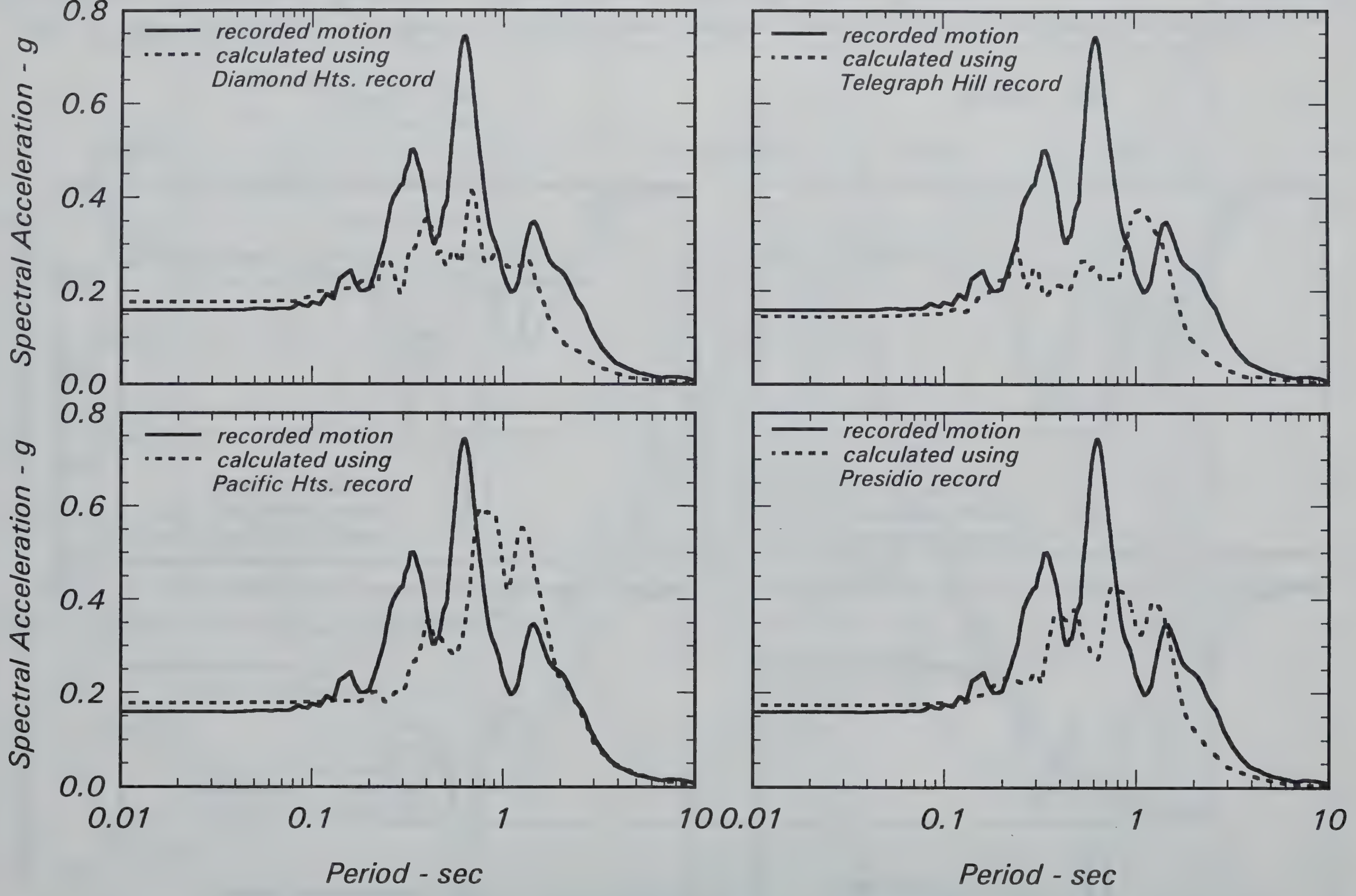

Fig. 3-16b Spectrum for Recorded Surface Motion and Spectra for Surface Motions at TI Calculated Using Best Estimate Shear Wave Velocities and Stronger Component of Motions Recorded at Diamond Heights, Telegraph Hill, Pacific Heights and Presidio as Input Motions

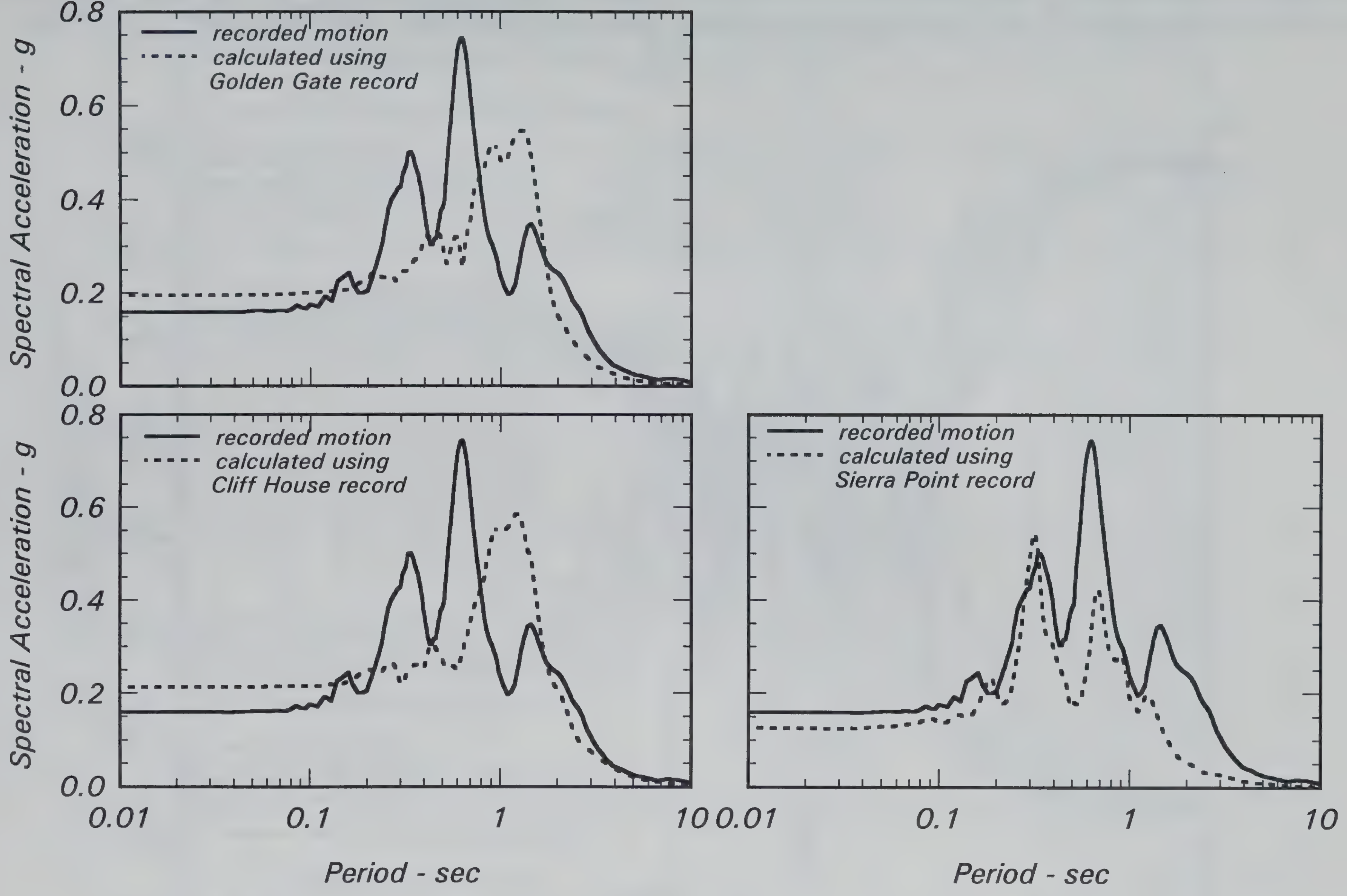

Fig. 3-16c Spectrum for Recorded Surface Motion and Spectra for Surface Motions at TI Calculated Using Best Estimate Shear Wave Velocities and Stronger Component of Motions Recorded at Golden Gate, Cliff House and Sierra Point as Input Motions

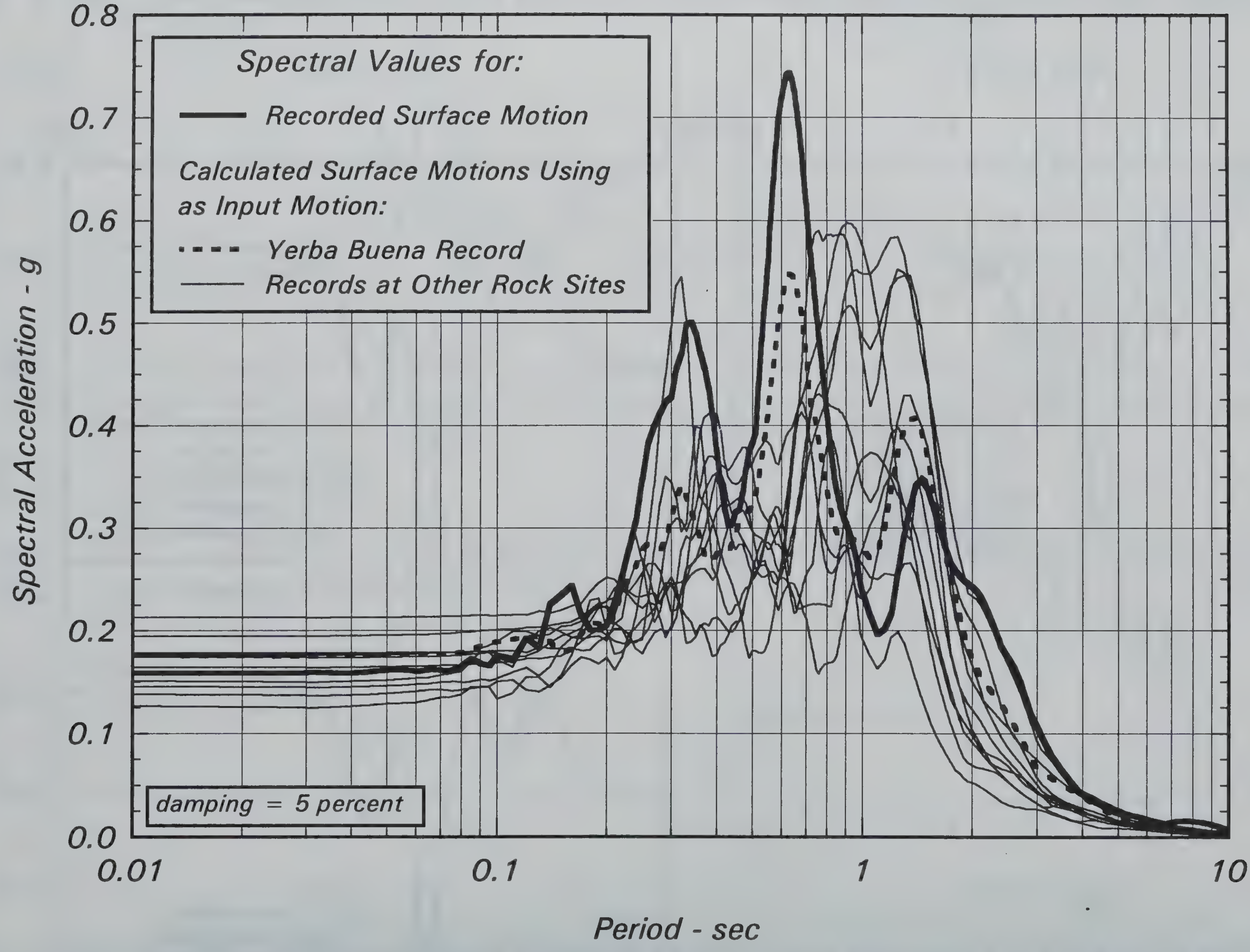

Fig. 3-17 Spectrum for Recorded Surface Motion and Spectra for Surface Motions at TI Calculated Using Best Estimate Shear Wave Velocities and Stronger Component of Motions Recorded at Yerba Buena and Other Rock Sites as Input Motions

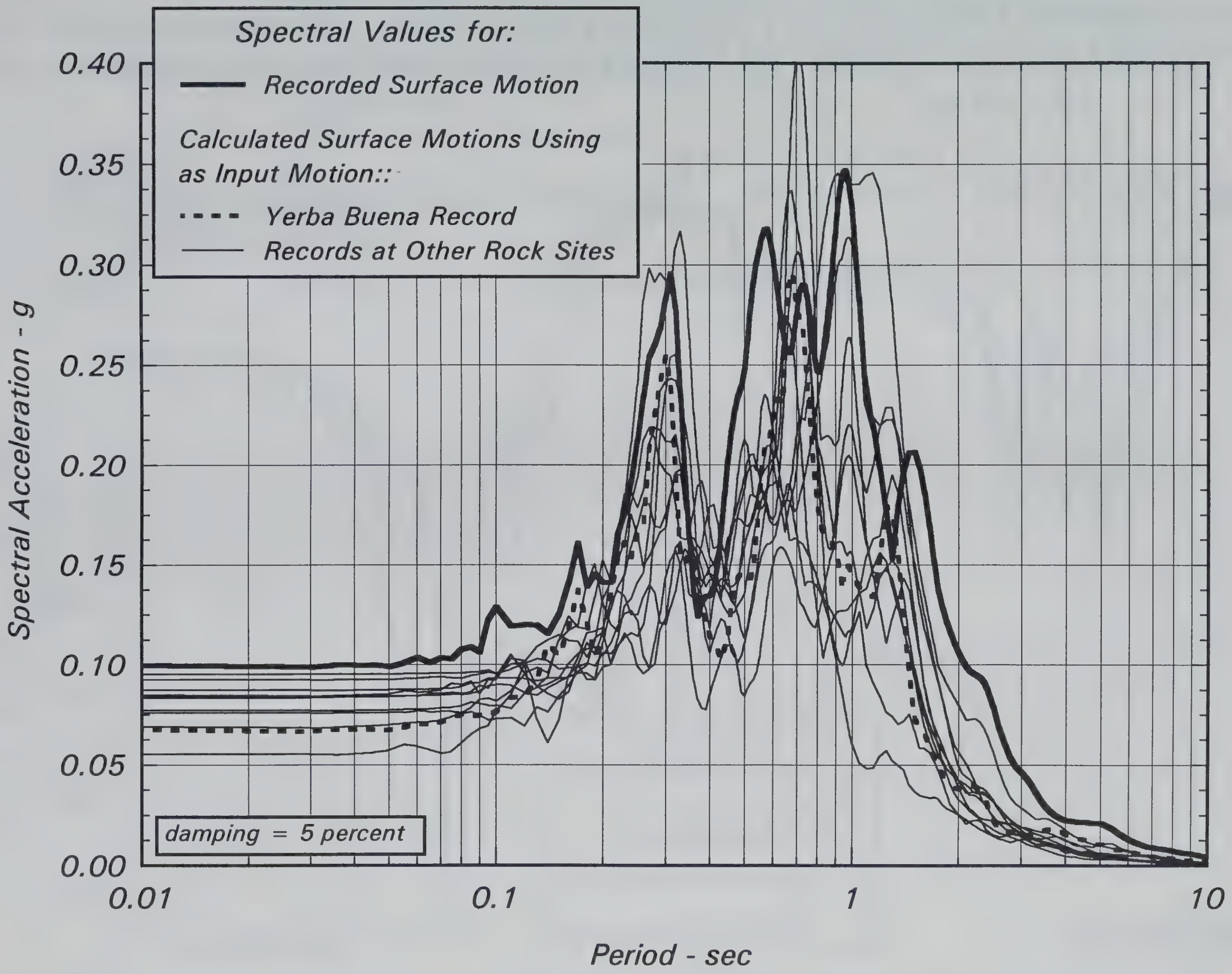

Fig. 3-18 Spectrum for Recorded Surface Motion and Spectra for Surface Motions at TI Calculated Using Best Estimate Shear Wave Velocities and Weaker Component of Motions Recorded at Yerba Buena and Other Rock Sites as Input Motions

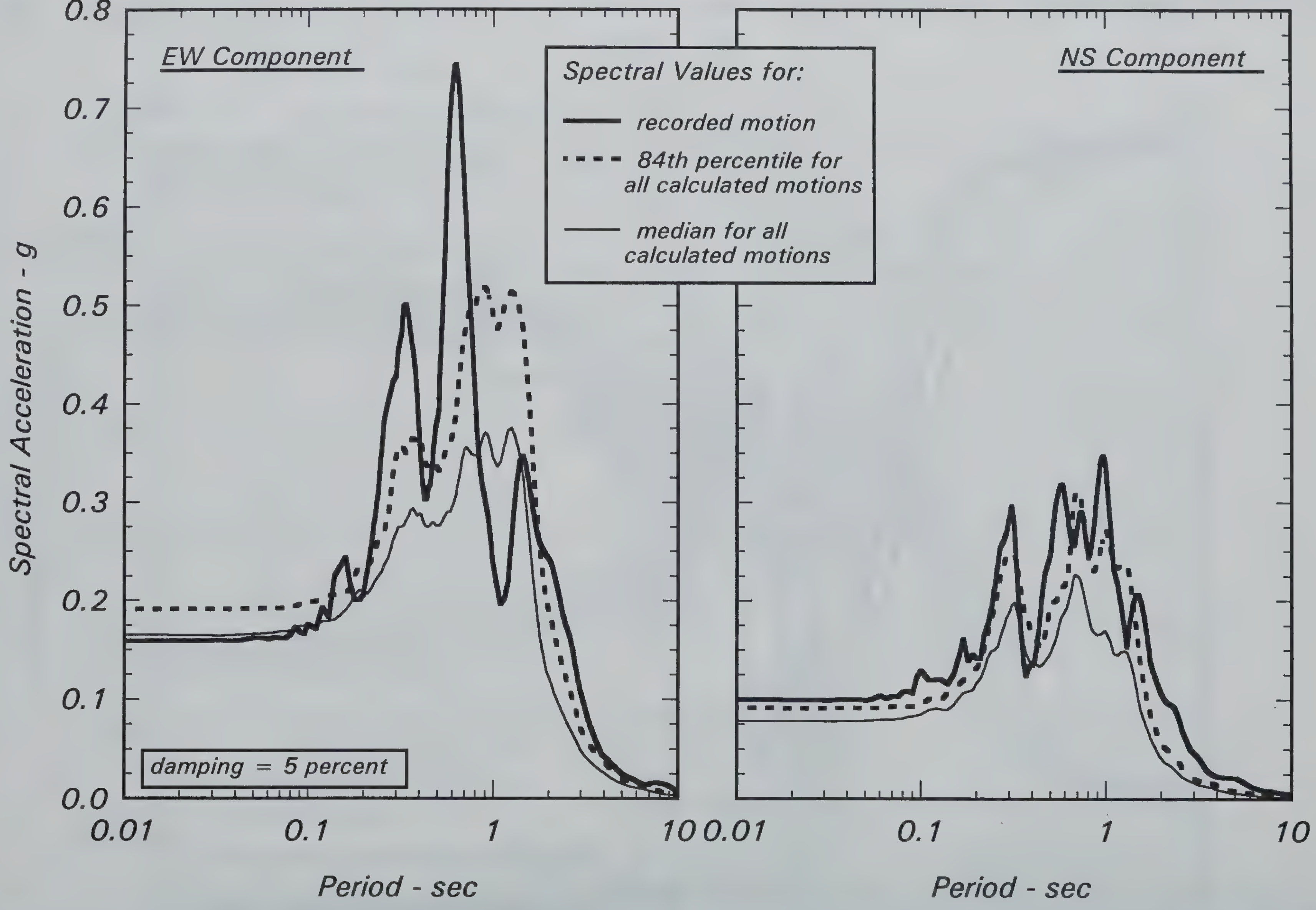

Fig. 3-19 Spectra for Recorded Surface Motions and Median and 84th Percentile Spectra for Surface Motions at Treasure Island Calculated Using Motions Recorded at All Rock Sites in San Francisco Bay Area as Input Motions

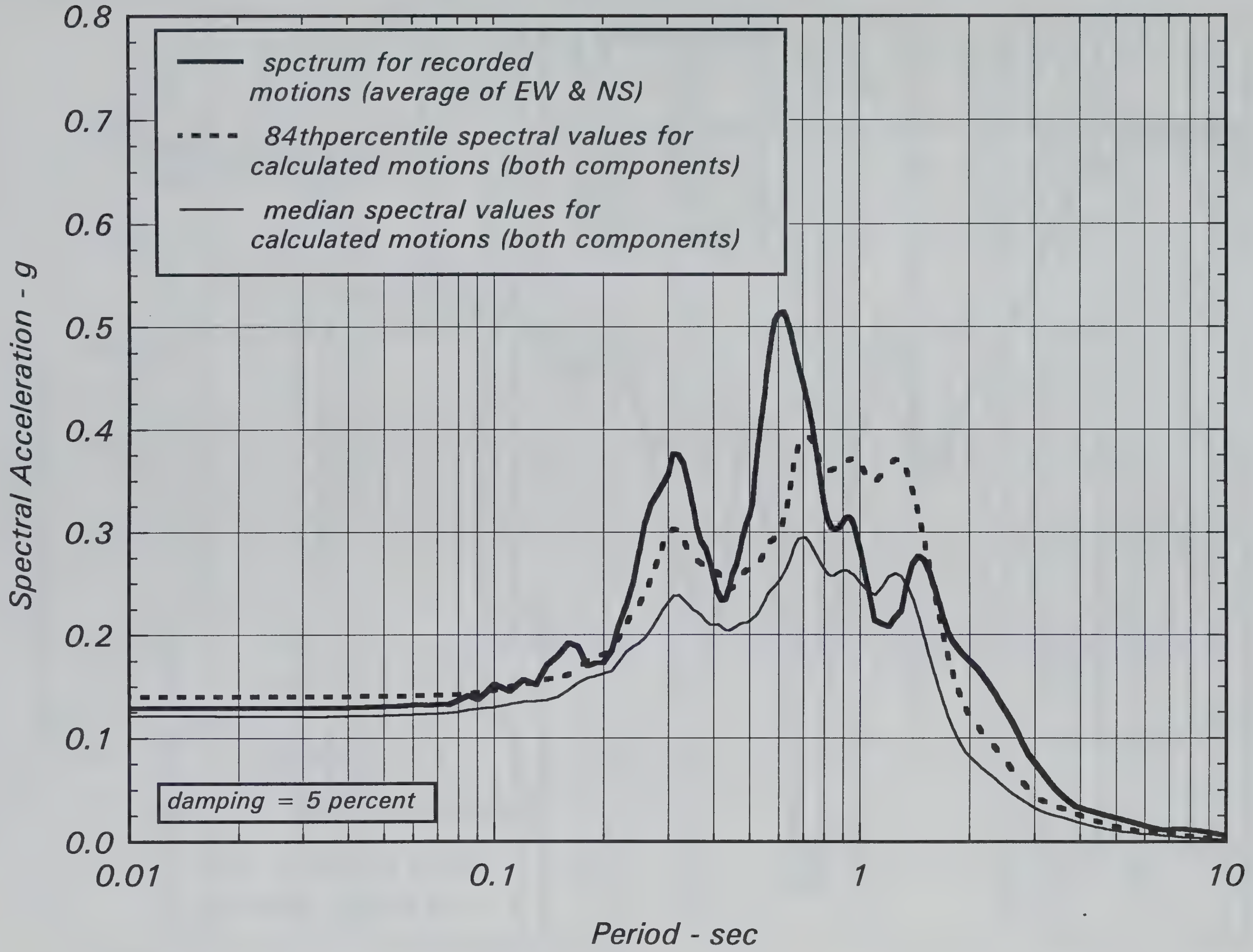

Fig. 3-20 Comparison of the Average Spectrum for the Two Components of Recorded Surface Motions with Median and 84th Percentile Spectral Values for All Calculated Surface Motions at Treasure Island

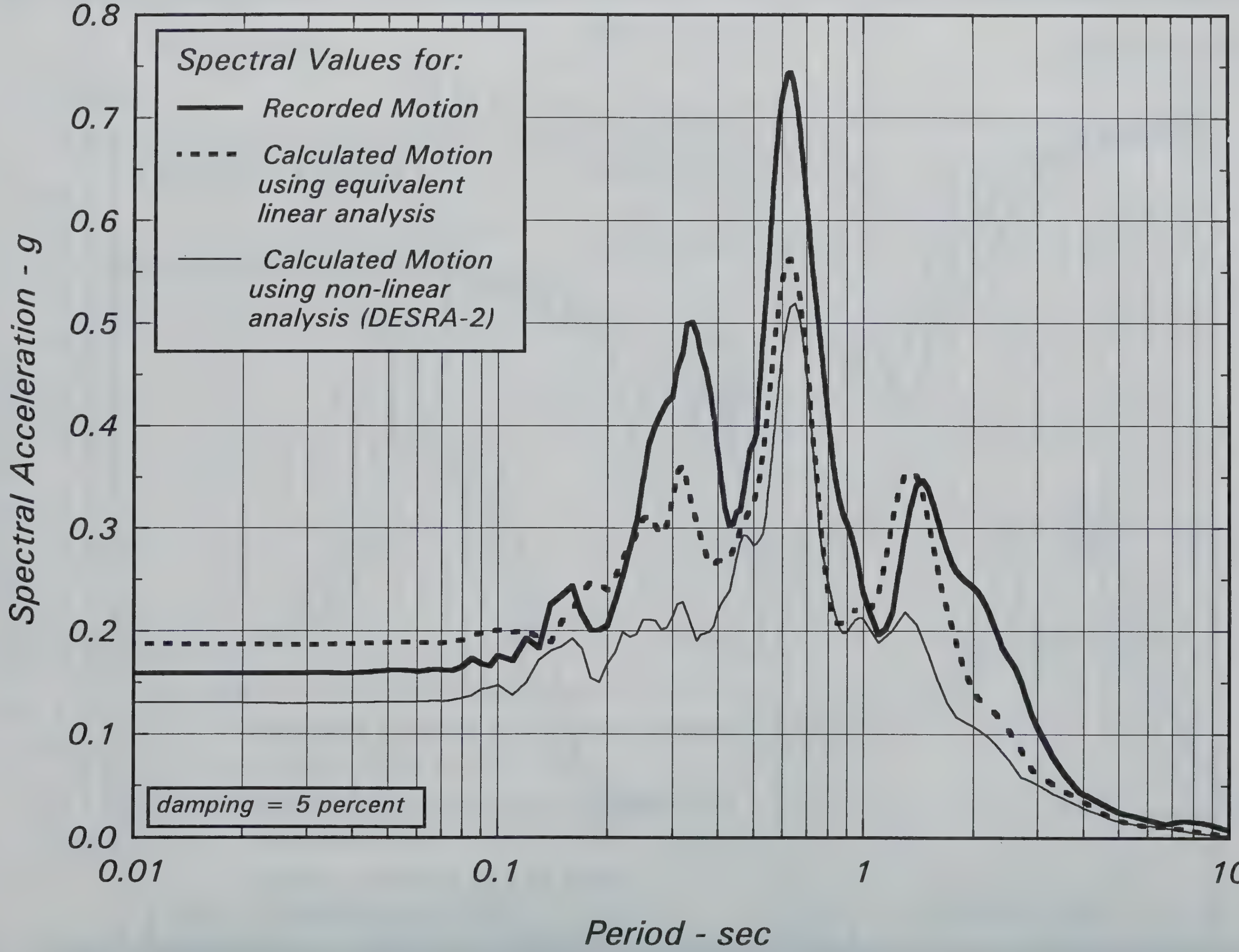

Fig. 3-21 Comparison of Spectral Ordinates at Ground Surface at TI Calculated Using Equivalent Linear and Nonlinear Response Analyses

4.0 SAN FRANCISCO AIRPORT SITE

The recording station at San Francisco Airport is shown in Fig. 1-1 (Station No. 223) and in more detail in Fig. 4-1. The closest rock recording to the San Francisco Airport is that obtained at Sierra Point (Station No. 539 in Fig. 1-1). The recording station at Sierra Point is about 5 km north of the recording station at the San Francisco Airport.

The spectra of the motions recorded at San Francisco Airport and at Sierra Point are presented in Fig. 4-2. The upper part of Fig. 4-2 shows the spectra for the stronger components of the recorded motions and the lower part of the figure shows the spectra for the weaker components. More details regarding the characteristics of the recordings at Sierra Point are given in Appendix B and those for San Francisco Airport are summarized in Appendix C.

4.1 Subsurface Conditions at The San Francisco Airport Site

The subsurface conditions at the San Francisco Airport site were obtained by drilling a boring nearby the station to a depth of 507 feet (154.5 m). The shear wave velocities were measured by USGS (Gibbs et al, 1992) and by Redpath (1991) using down-hole measuring techniques.

The log of boring and the shear wave velocities measured by USGS are shown in Fig. 4-3 and the shear wave velocities measured by USGS and by Redpath are shown in Fig. 4-4.

The log of boring indicates that the subsurface conditions consist mostly of dense sands and Old Bay Mud to a depth of about 440 ft (134.1 m), except that there is a 15-ft (4.6 m) layer of Young Bay Mud at a depth of about 5 ft (1.5 m) below the ground surface. A 55-ft (16.8 m) layer of weathered mudstone exists below the soils and is underlain by a more component sandstone of the Franciscan formation as shown in Fig. 4-3.

4.2 Dynamic Soil Properties

The maximum shear wave velocities are based on the velocities measured at the site and the values selected to represent the best estimate shear wave velocities are shown in Fig. 4-4. The best estimate input properties used in the equivalent linear analyses are listed in Subsection 4.3.1.1 below.

The modulus reduction curves shown in the upper part of Fig. 3-4 and the damping ratio versus strain curve shown in the lower part of Fig. 3-4 were used in all the analyses conducted at the San Francisco Airport Site.

4.3 Equivalent Linear Analyses

The response of the San Francisco Airport site was calculated incorporating equivalent linear modulus and damping representation for the following conditions:

- using the stronger component of the recording at Sierra Point (SP) as input rock outcrop motion, and
    - best estimate of the shear wave velocity profile
    - an upper and a lower range estimates of the shear wave velocity profile

- using the weaker component of the recording at Sierra Point (SP) as input rock outcrop motion, and
    - best estimate of the shear wave velocity profile
    - an upper and a lower range estimates of the shear wave velocity profile

- using the best estimate of the shear wave velocity profile and the stronger and the weaker components of all the rock motions recorded in the San Francisco Bay Area (see Table B-3) as input outcrop motions

The results of these analyses are presented below.

4.3.1 Response at San Francisco Airport Using the Stronger Component of Recording at Sierra Point as Input Rock Outcrop Motion

4.3.1.1 Results Using Best Estimate Shear Wave Velocity Profile

The best estimate shear wave velocities for the San Francisco Airport site are based on the measured shear wave velocities shown in Fig. 4-4 and are summarized below:

Depth Below Ground Surface - ft		Total Unit Weight - pcf	Maximum Shear Wave Velocity - ft/sec
From	To		
0	5	130	1260
5	20	105	290
20	32	120	500
32	56	120	1080
56	62	105	500
62	130	125	1215
130	160	130	1680
160	190	130	1450
190	250	130	1950
250	470	130	2040
470	half-space	140	4000

The corresponding values in SI units are listed below:

Approximate Depth Below Ground Surface - meter		Total Unit Weight kN/m^3	Maximum Shear Wave Velocity m/sec
From	To		
0	1.52	20.4	384.1
1.52	6.10	16.5	88.4
6.10	9.76	18.9	152.4
9.76	17.07	18.9	329.3
17.07	18.90	16.5	152.4
18.90	39.63	19.7	370.4
39.63	48.78	20.4	512.2
48.78	57.93	20.4	442.1
57.93	76.22	20.4	594.5
76.22	143.29	20.4	622.0
143.29	half-space	22.0	1,220

The response of this soil profile was calculated using the computer program SHAKE91. The results of the response calculations are presented in Figs. 4-5 through 4-8. Figure 4-5 shows the calculated maximum shear strains and stresses and Fig. 4-6 shows the calculated strain-compatible damping ratios and shear wave velocities. As can be noted in these figures, the largest strain values are induced in the Young Bay Mud layer. The maximum strains are quite small, however. Accordingly, the damping ratios are not very high and except for the Young Bay Mud layer the strain-compatible shear wave velocities are only slightly lower than the maximum shear wave velocities listed above.

Figure 4-7 shows the variations of peak horizontal accelerations with depth. It is interesting that a significant part of the peak acceleration amplification occurs in the upper 20 ft (6.1 m) of the soil profile.

The spectrum for the surface motion at San Francisco Airport, calculated using the best estimate shear wave velocities and the stronger component of the Sierra Point record as input motion, is compared to the spectrum for the recorded surface motion in Fig. 4-8. The spectrum for the calculated surface motion provides a very good approximation of the spectrum for the recorded surface motion for almost the entire period range.

The effects of using different shear wave velocities are considered in the next section.

4.3.1.2 Results using Various Shear Wave Velocity Profiles

In addition to the best estimate shear wave velocities, an upper range and a lower range shear wave velocity profiles were considered for assessing the effects of varying shear wave velocities on the response calculations at the San Francisco Airport site.

The results of the response calculations, using these three shear wave velocity profiles and the stronger component of the recording at Sierra Point as input motion, are presented in Fig. 4-9. Figure 4-9 shows a comparison of the spectrum for the recorded motion and those for the calculated motions. These results indicate that the use of the lower range values of shear wave velocities appear to underestimate the spectral ordinates for the recorded motion for periods shorter than about 0.4 sec. The use of the upper range values of shear wave velocities appears to overestimate these spectral ordinates in the period range of about 0.3 to 0.5 sec. The use of all three sets of shear wave velocities, however, appears to underestimate the peak acceleration.

4.3.2 Response at San Francisco Airport Using the Weaker Component of the Recording at Sierra Point as Input Rock Outcrop Motion

The same three sets of shear wave velocities (i.e., lower range, best estimate and upper range shear wave velocities) that were used in conjunction with the stronger component of input motion were also used in conjunction with the weaker component of the input motion.

The results of the response calculations are presented in Fig. 4-10. The spectra for the calculated surface motions are similar in shape to the spectrum for the recorded surface motion, but are considerably lower in amplitude over a significant range of periods.

Accordingly, the use of best estimate shear wave velocities and the recorded motion from a nearby rock site as input motion in an equivalent linear analysis appears to provide a reasonable approximation for the recorded motions only in one direction for the San Francisco Airport site. This finding is similar to that obtained for the Treasure Island site (Section 3.3.2.1)

4.3.3 Response at San Francisco Airport Using the Recorded Motions at All the Rock Sites in San Francisco Bay Area as Input Rock Outcrop Motions

The stronger component of each record obtained at the eleven rock sites was first scaled to have a peak acceleration of 0.1g (i.e., its peak acceleration was made equal to that of the stronger component recorded at Sierra Point). The response was then calculated using this scaled accelerogram as rock outcrop input motion using the best estimate shear wave velocities for the soil profile. Strain-compatible damping ratios and shear wave velocities were obtained for each response calculation.

Figure 4-11 shows the spectrum for the recorded surface motion and the spectra for surface motions at San Francisco Airport calculated using the stronger component of motions recorded at Sierra Point and at the other rock sites. This figure highlights the fact that using various rock input motions has a far greater effect on the calculated results than any other parameter.

Similar calculations were completed using the weaker components of the records obtained at all the rock sites in the San Francisco Bay Area. The weaker component of each record obtained at the eleven rock sites was first scaled to have a peak acceleration of 0.06g (i.e., its peak acceleration was made equal to that of the weaker component recorded at Sierra Point).

The results using the weaker components are presented in Fig. 4-12. These results indicate an improvement in the accuracy of estimating the spectrum of the recorded motion when the other rock records are used as input motions.

As was the case for the Treasure Island site, the results of a response analysis can be significantly affected by the input motion used in the response calculations. In fact, the input motion appears to have the most dominant effect on the results. Consequently, it would seem inappropriate to rely on the results of any one single analysis and that response calculations should always include variations in the input motion.

Again the use of the median or the 84th percentile values of the ensemble of calculated spectra is tested using the results for the San Francisco Airport site as summarized in Figs. 4-13 and 4-14. These figures show that:

1. The median of the calculated spectra underestimates the spectrum for the recorded motion for either component or for the average of the two components.

2. The 84th percentile spectrum for the calculated motions provides a reasonable estimate of the spectrum for both components of the recorded motion, except at a narrow period range as illustrated in Fig. 4-13.

3. The 84th percentile spectrum for all the calculated motions (i.e., considering both components) appears to provide a reasonable estimate for the average spectrum for the two components of the recorded motions except over a very narrow period range as shown in Fig. 4-14.

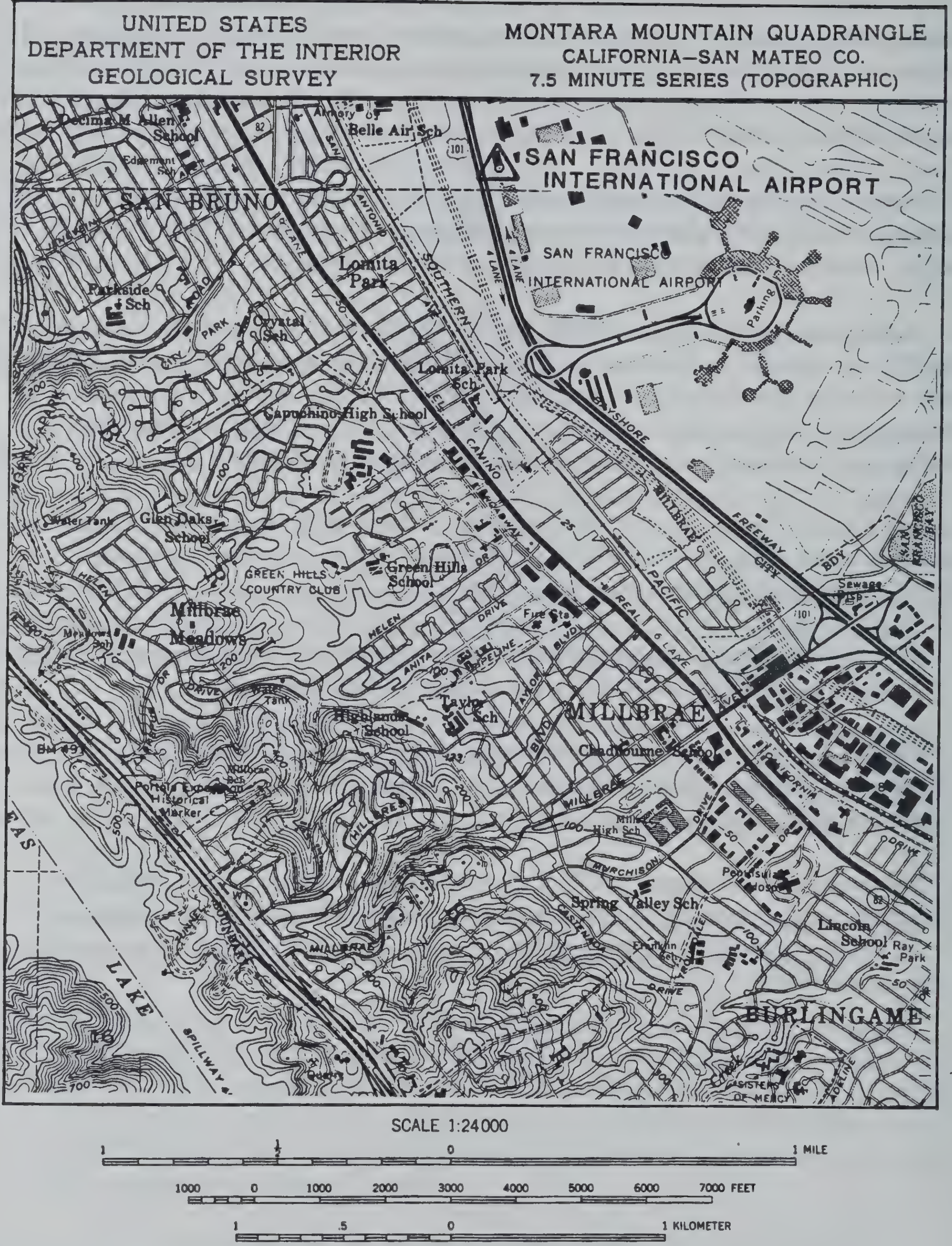

(from Gibbs et al, 1992)

Fig. 4-1 Location of Recording Station at The San Francisco Airport

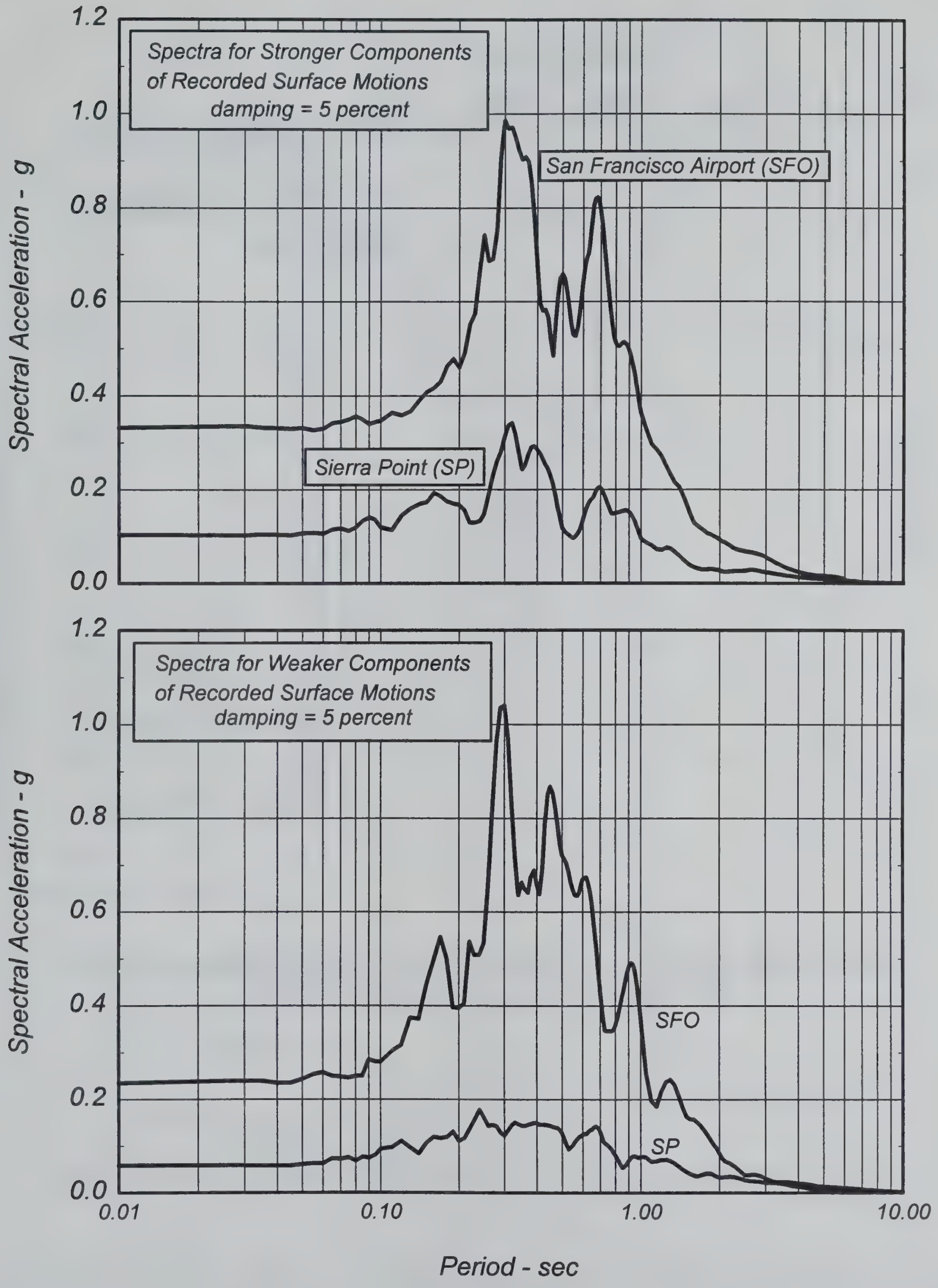

Fig. 4-2 Spectra for Surface Motions Recorded
at the San Francisco Airport (SFO) and at Sierra Point (SP)

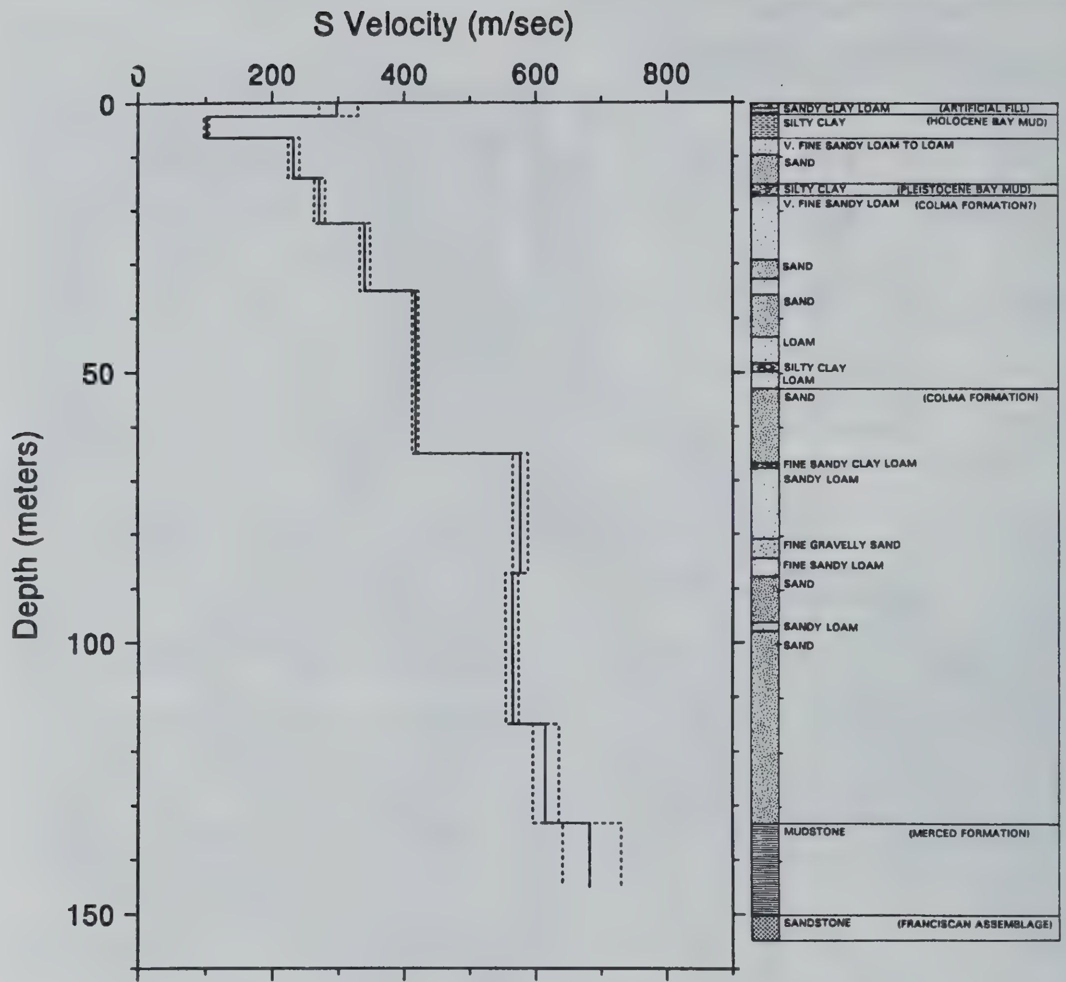

(from Gibbs et al, 1992)

Fig. 4-3 Log of Boring and Shear Wave Velocities Measured at the San Francisco Airport by USGS

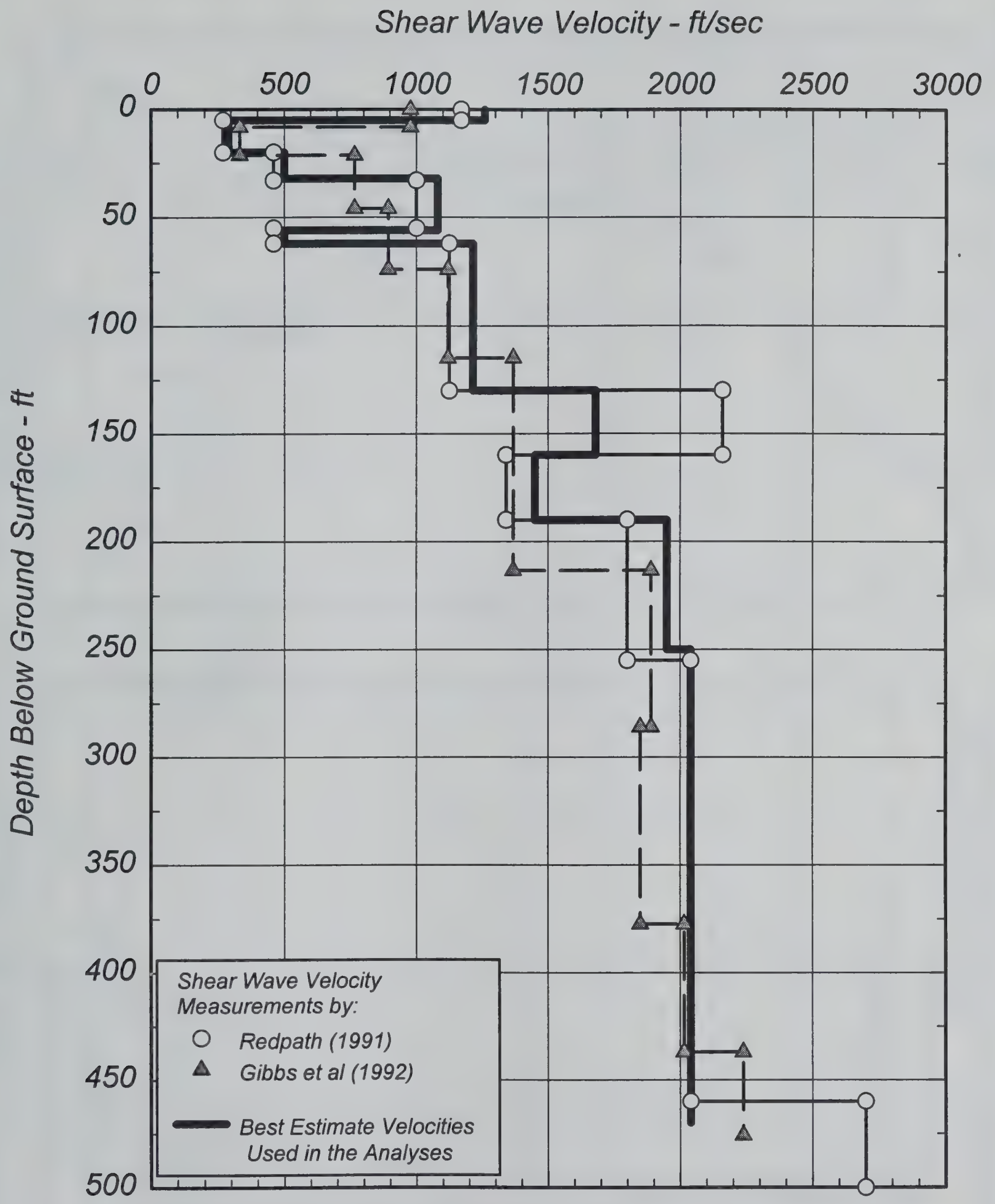

Fig. 4-4 Shear Wave Velocities Measured at The San Francisco Airport and Best Estimate Values of Velocities Used in the Analyses

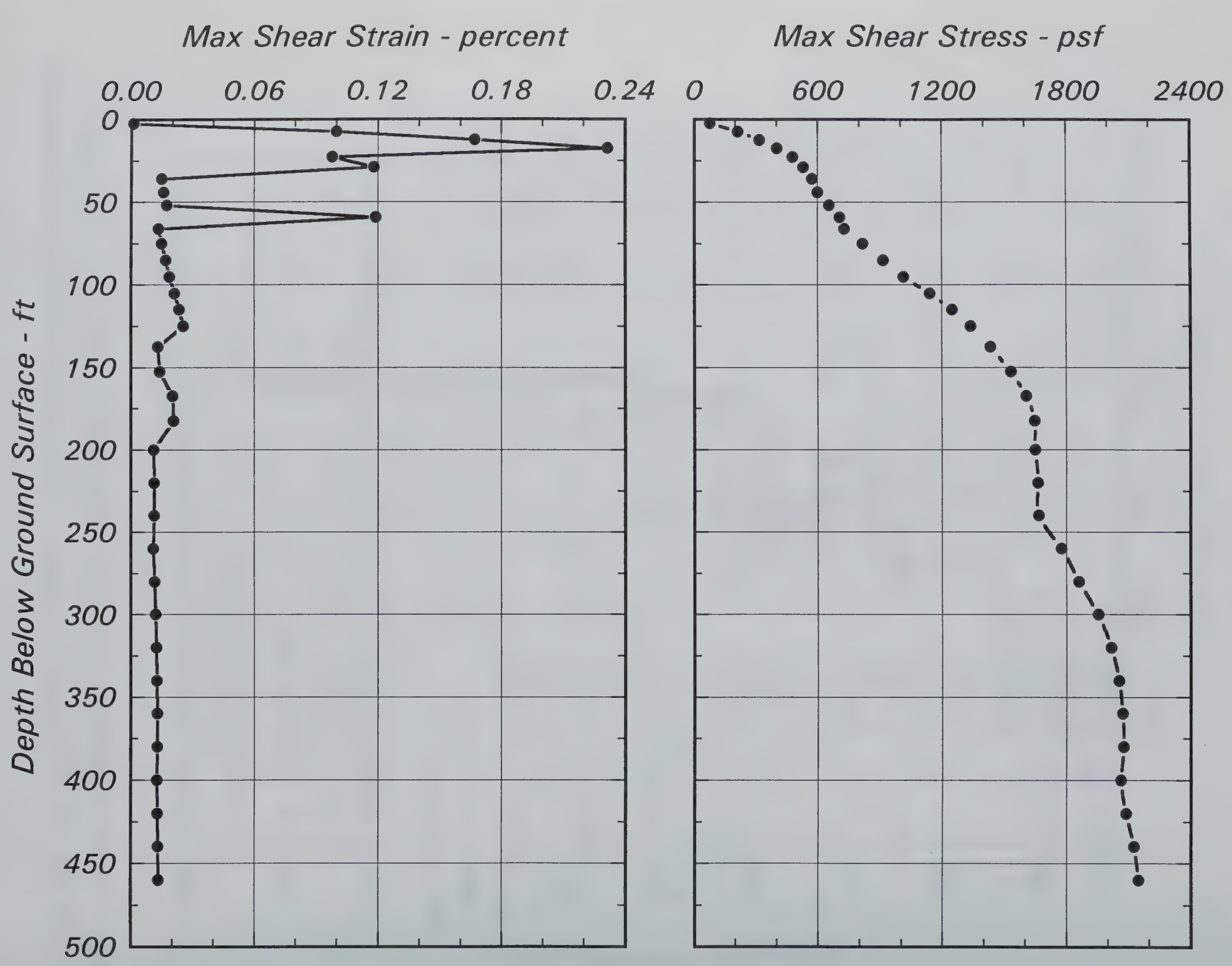

Fig. 4-5 Maximum Shear Strains and Stresses at SFO Calculated Using Best Estimate Shear Wave Velocities and Stronger Component of SP Record as Input Motion

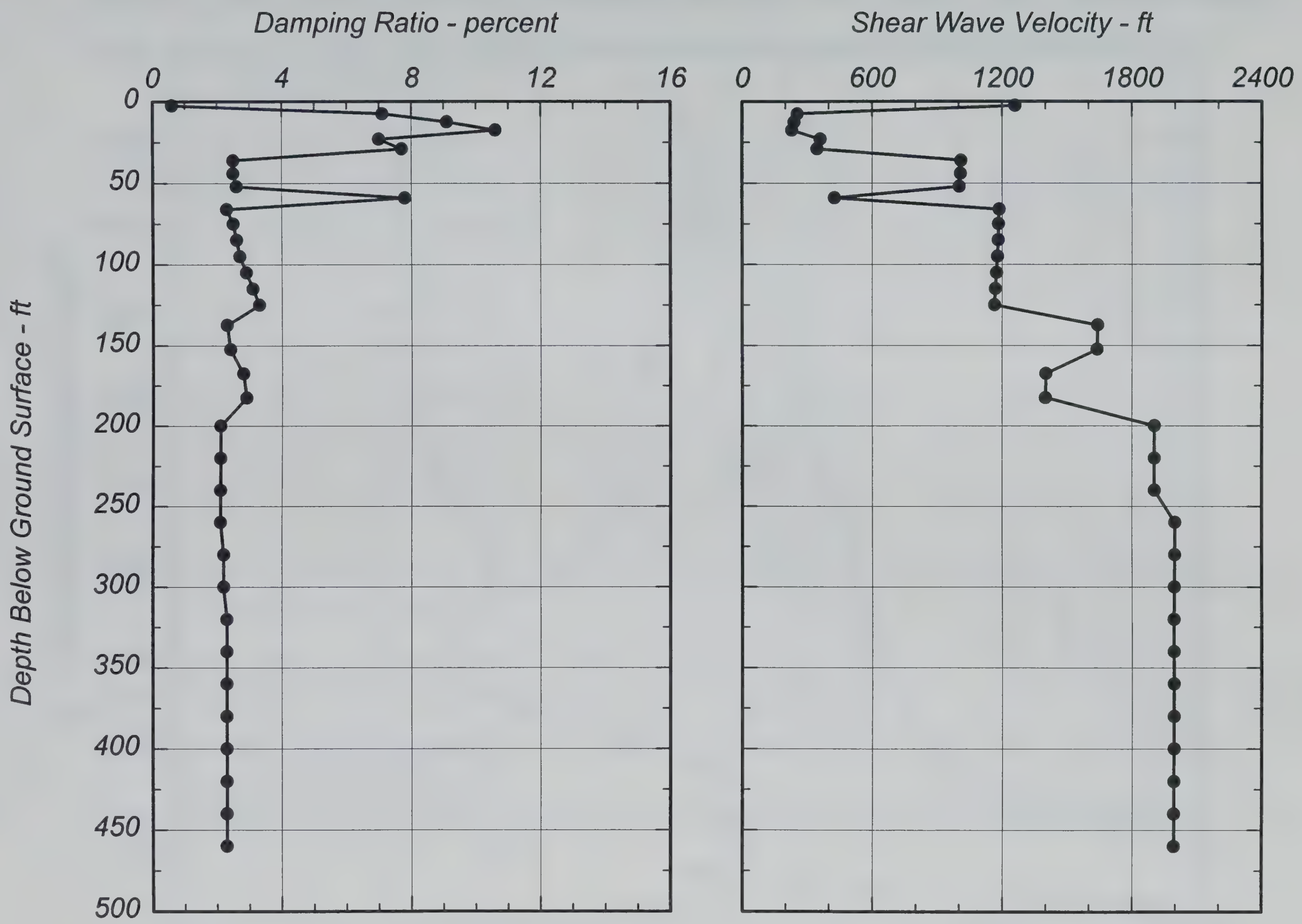

Fig. 4-6 Strain-Compatible Damping Ratios and Shear Wave Velocities at SFO Calculated Using Best Estimate Shear Wave Velocities and Stronger Component of SP Record as Input Motion

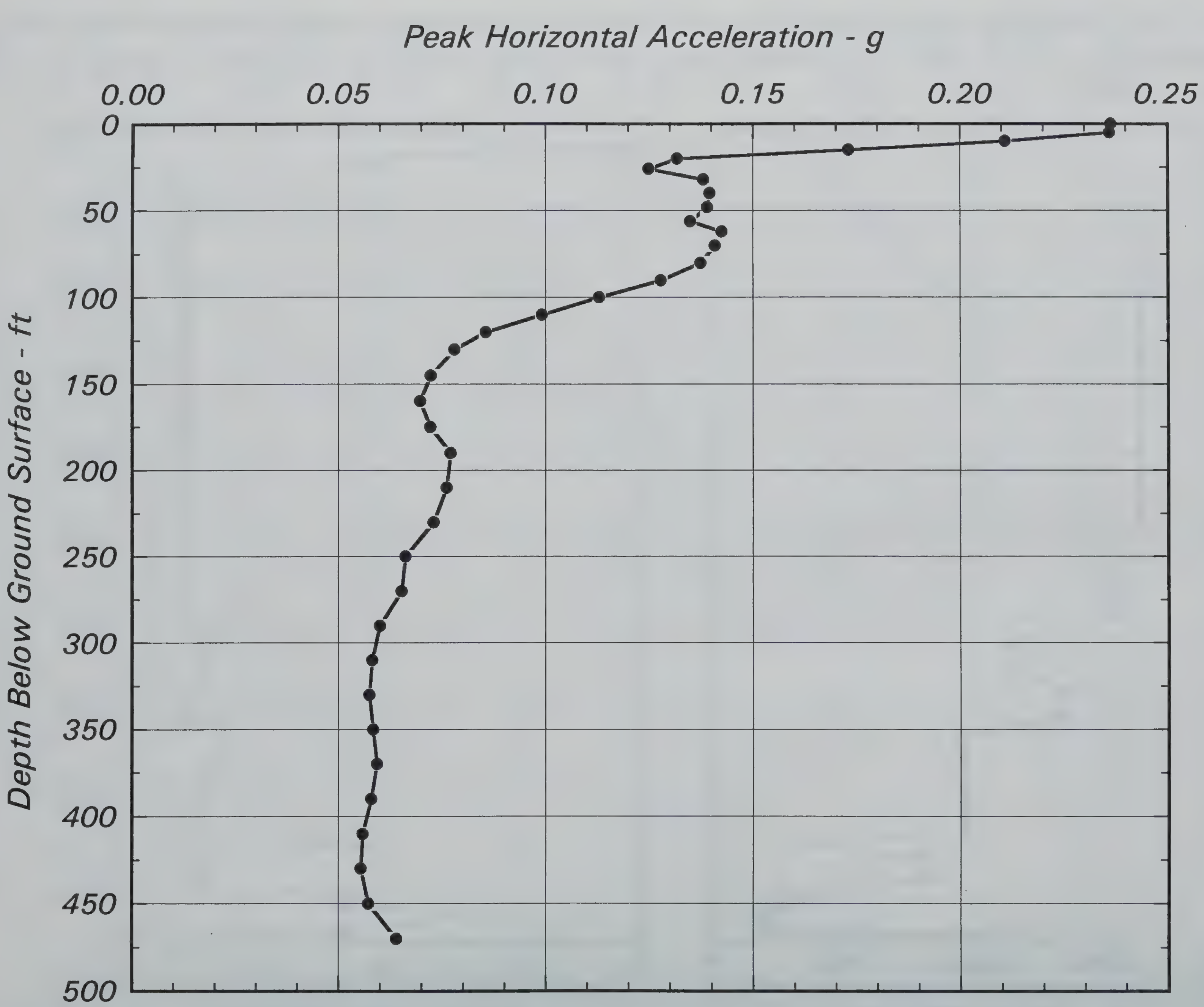

Fig. 4-7 Peak Horizontal Accelerations at SFO Calculated Using Best Estimate Shear Wave Velocities and Stronger Component of SP Record as Input Motion

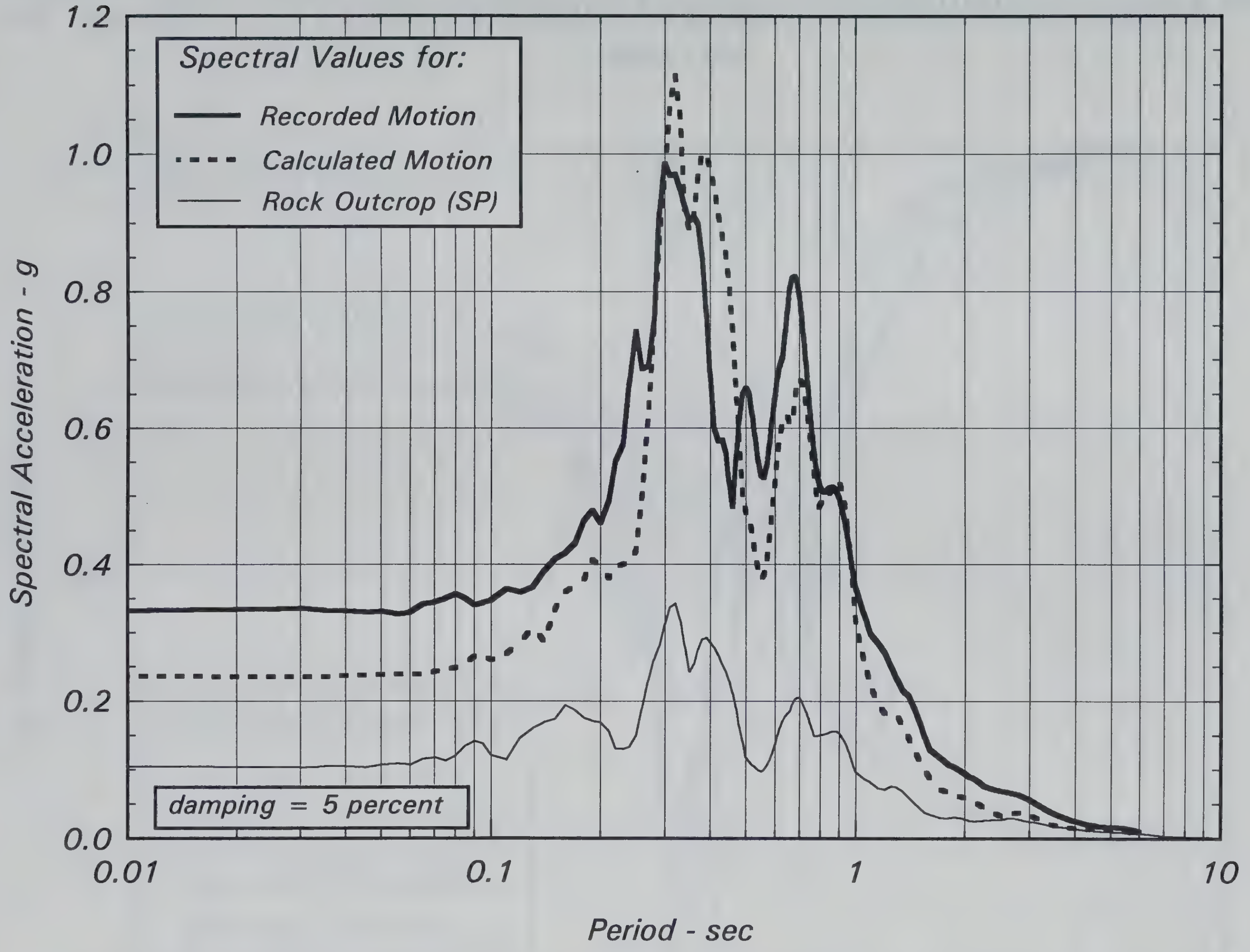

Fig. 4-8 Spectrum for Recorded Surface Motion and Spectrum for Surface Motion at SFO Calculated Using Best Estimate Shear Wave Velocities and Stronger Component of Sierra Point Record as Input Motion

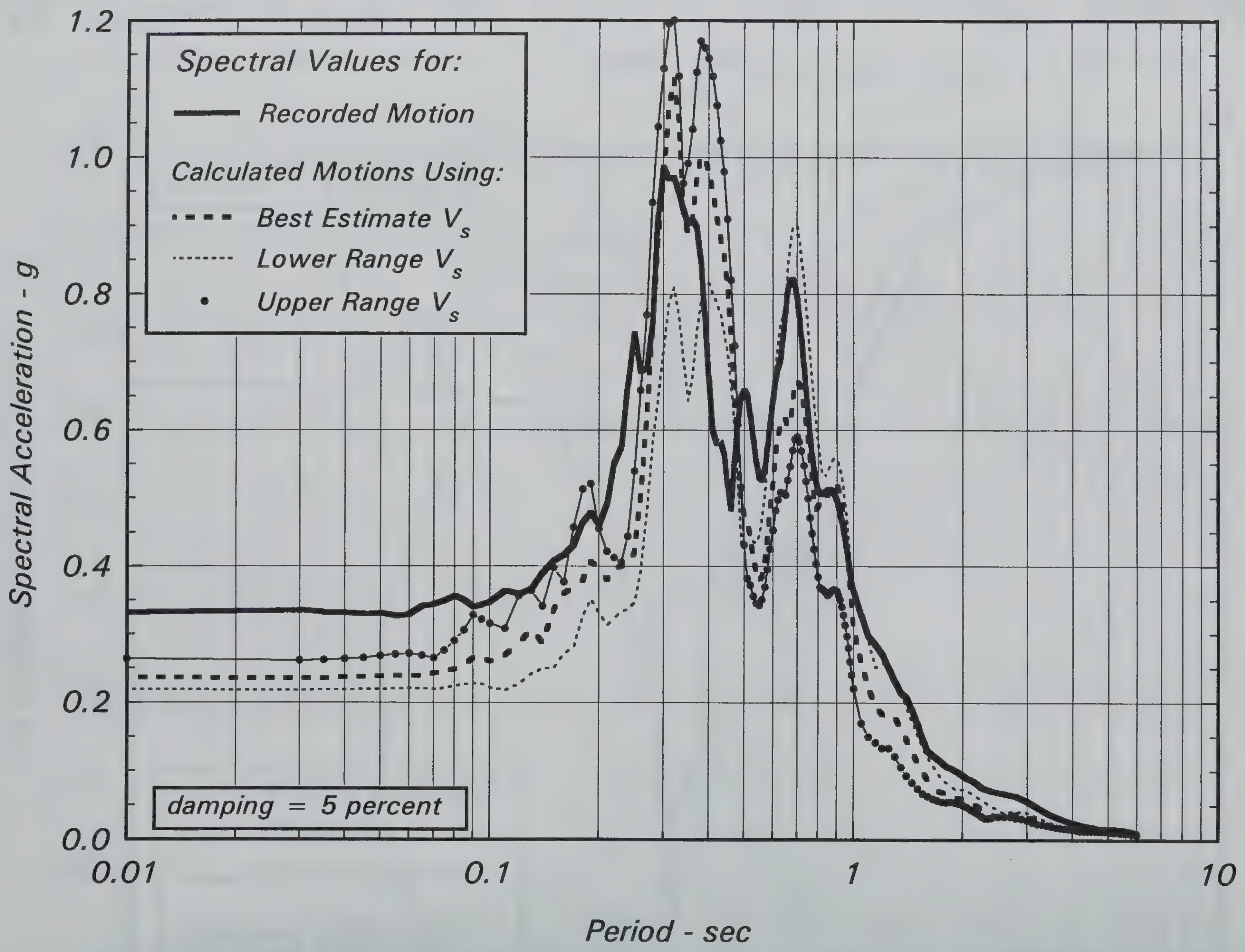

Fig. 4-9 Spectrum for Recorded Surface Motion and Spectrum for Surface Motion at SFO Calculated Using Various Shear Wave Velocity Profiles and Stronger Component of Sierra Point Record as Input Motion

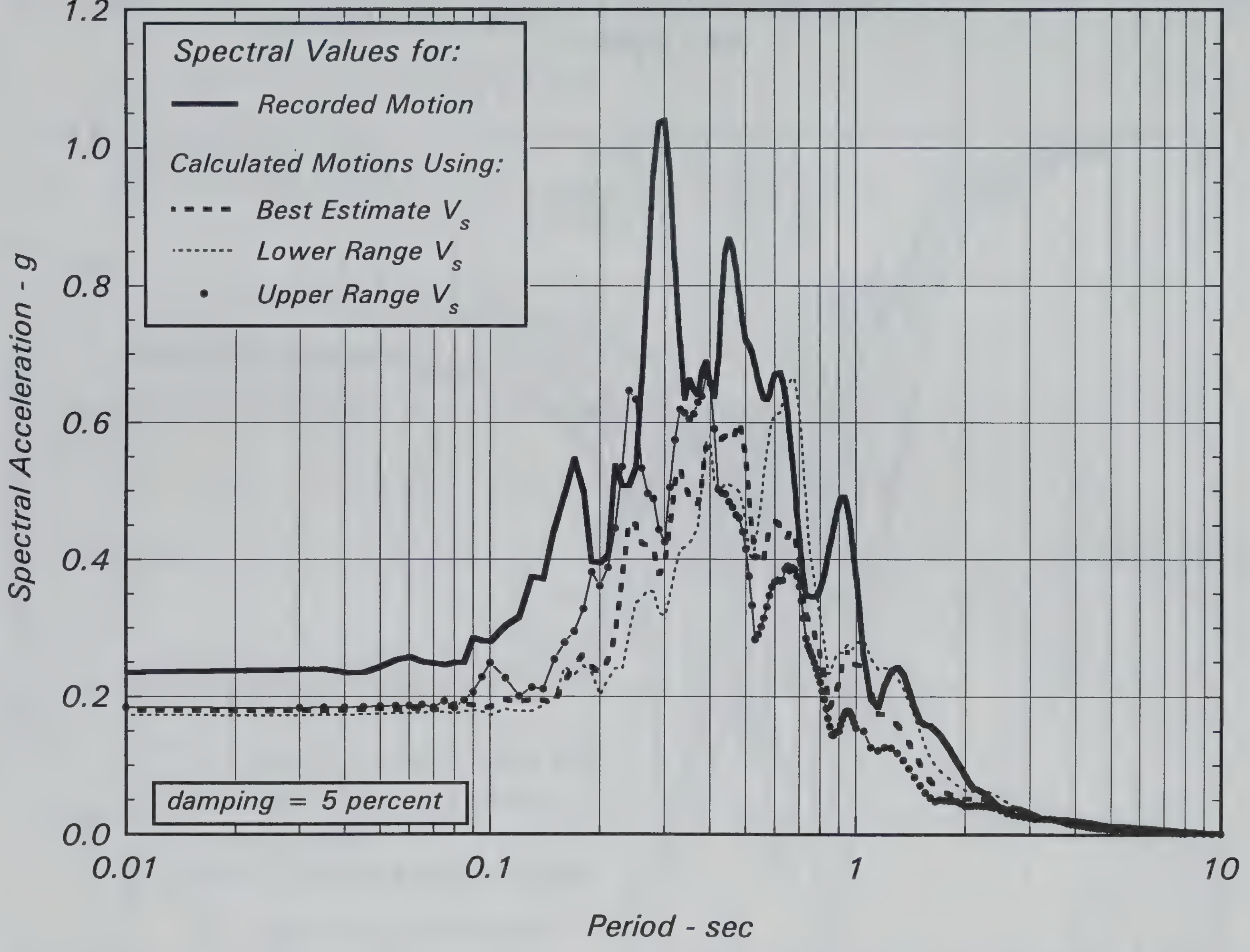

Fig. 4-10 Spectrum for Recorded Surface Motion and Spectrum for Surface Motion at SFO Calculated Using Various Shear Wave Velocity Profiles and Weaker Component of Sierra Point Record as Input Motion

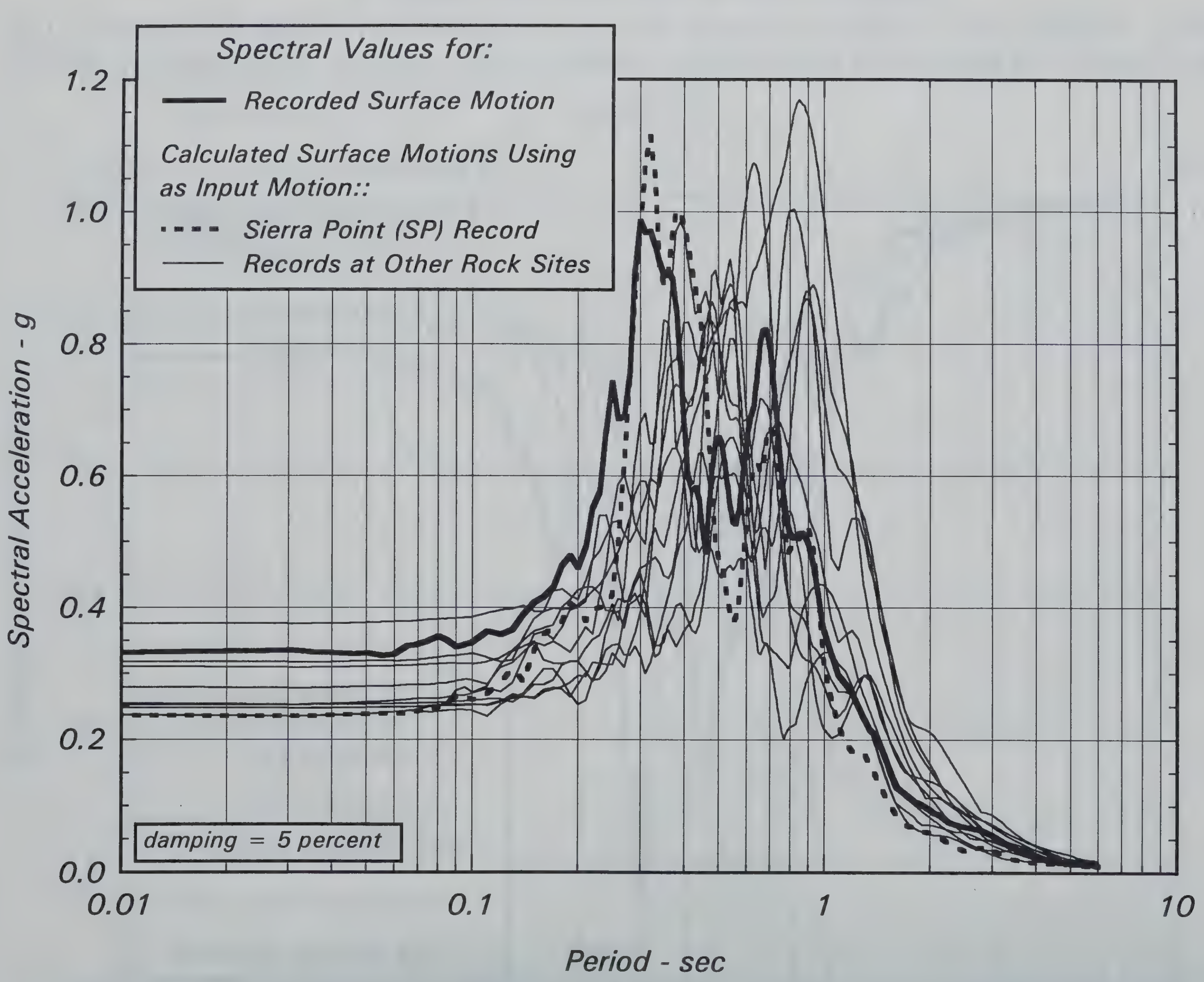

Fig. 4-11 Spectrum for Recorded Surface Motion and Spectra for Surface Motions at SFO Calculated Using Best Estimate Shear Wave Velocities and Stronger Component of Motions Recorded at Sierra Point and Other Rock Sites as Input Motions

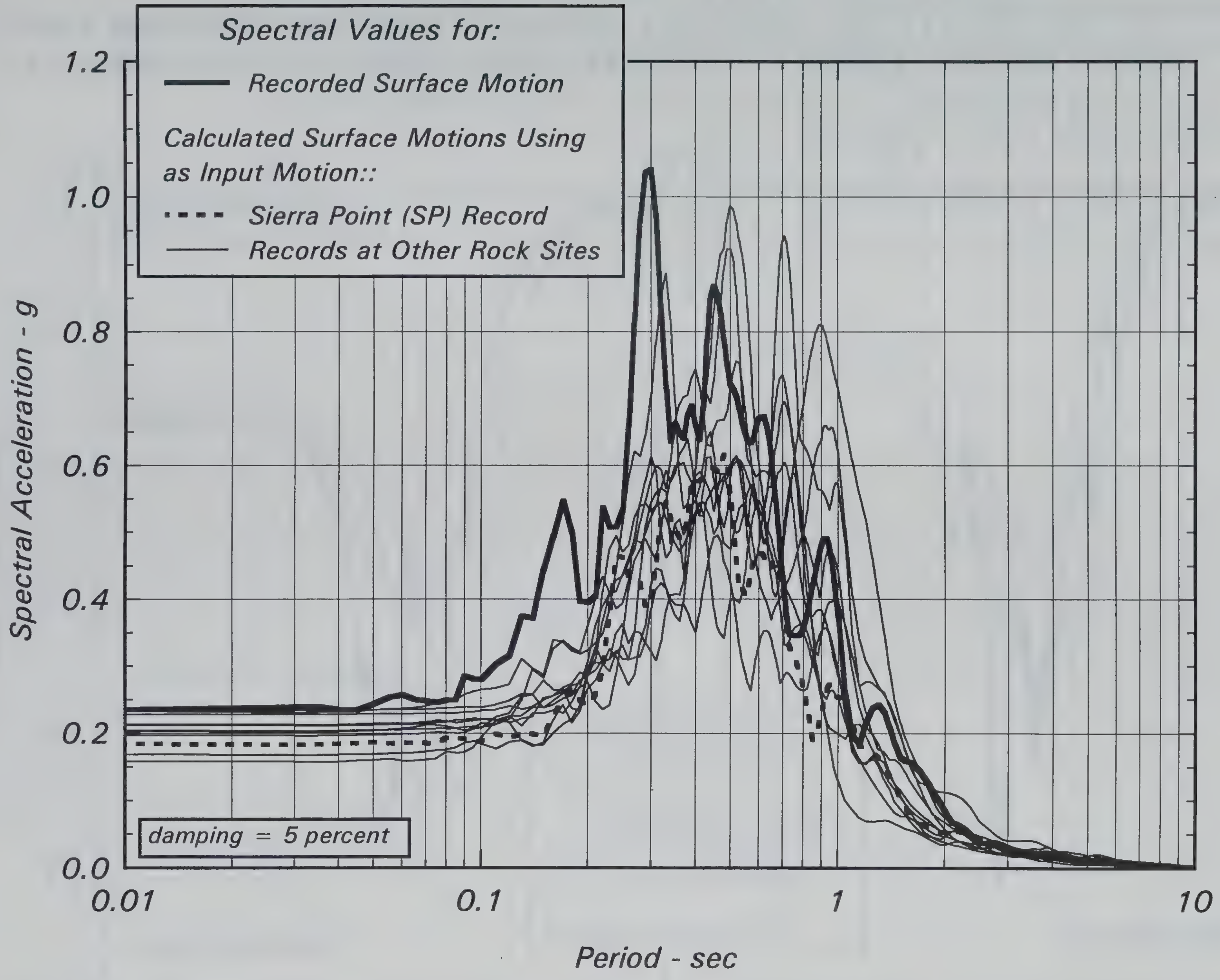

Fig. 4-12 Spectrum for Recorded Surface Motion and Spectra for Surface Motions at SFO Calculated Using Best Estimate Shear Wave Velocities and Weaker Component of Motions Recorded at Sierra Point and Other Rock Sites as Input Motions

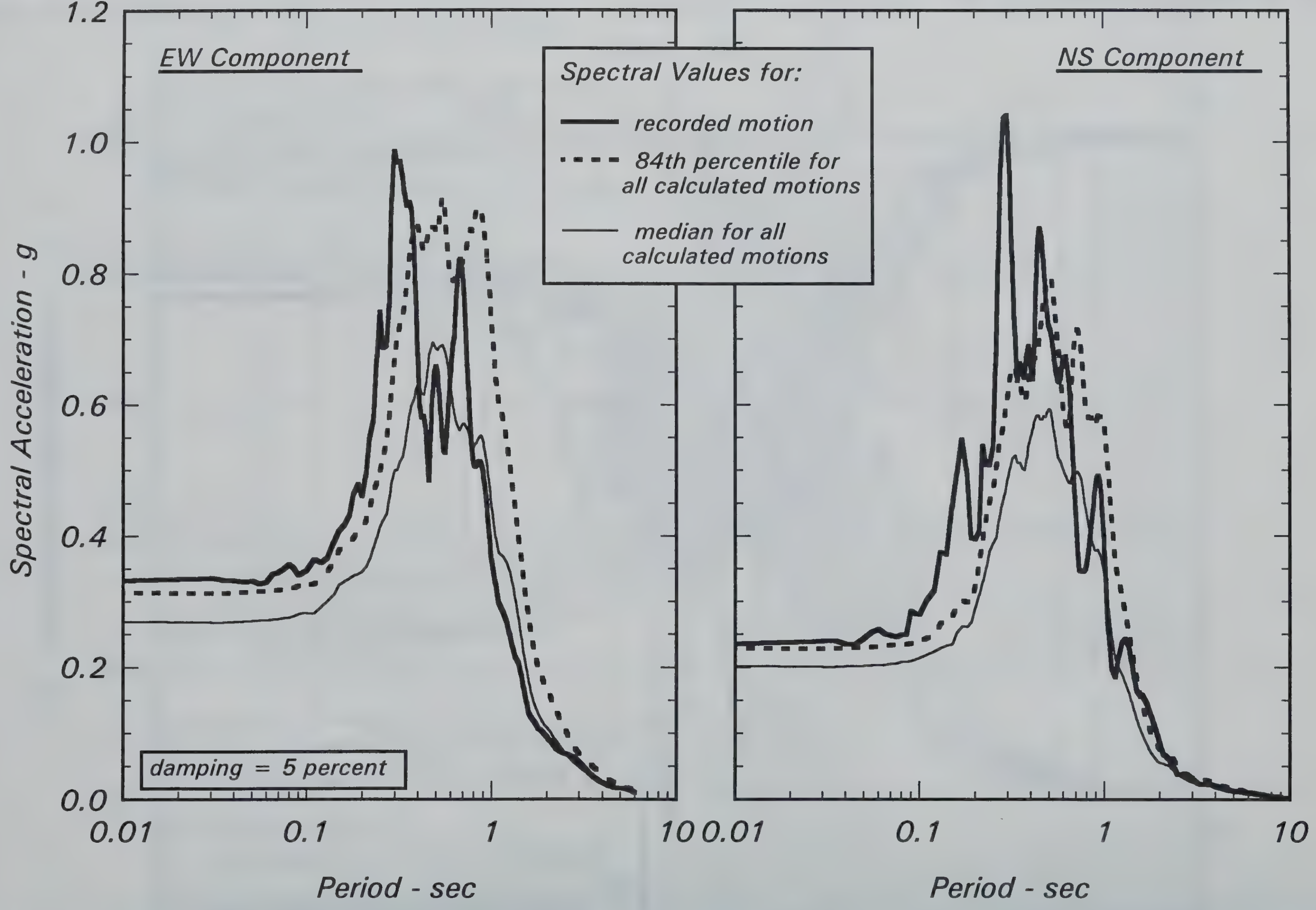

Fig. 4-13 Spectra for Recorded Surface Motions and Median and 84th Percentile Spectra for Surface Motions at San Francisco Airport Calculated Using Motions Recorded at All Rock Sites in San Francisco Bay Area as Input Motions

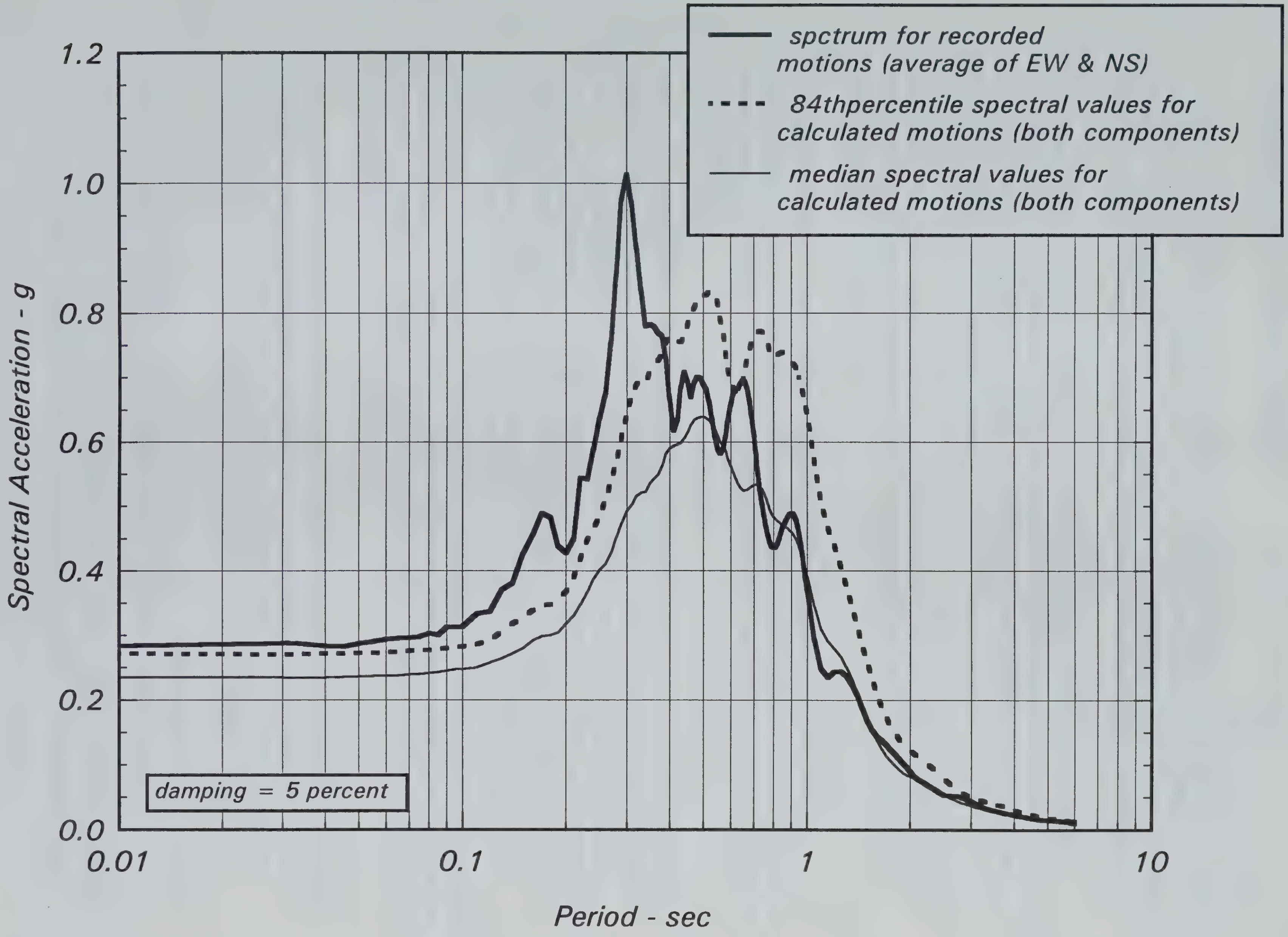

Fig. 4-14 Comparison of the Average Spectrum for the Two Components of Recorded Surface Motions with Median and 84th Percentile Spectral Values for All Calculated Surface Motions at the San Francisco Airport

5.0 SUMMARY AND CONCLUSIONS

The Loma Prieta earthquake was the largest earthquake to affect the San Francisco Bay Area since the 1906 San Francisco earthquake. It triggered by far the largest number of strong motion recording stations ever triggered by an earthquake. It provided earthquake ground motions at many free field stations underlain by various subsurface conditions.

The peak accelerations recorded at all these free field stations are summarized in Appendix A. The characteristics of the horizontal earthquake ground motions recorded at rock sites are summarized in Appendix B and those related to the horizontal motions recorded at soft soil sites are summarized in Appendix C.

The characteristics summarized in these appendices provide a significant insight into the nature of earthquake ground motions and the potential effects of site conditions and distance on these characteristics.

For example, the data indicate that peak horizontal accelerations at rock sites are comparable to those recorded at soil sites (other than soft soil sites). The peak horizontal accelerations at soft soil sites, however, are significantly larger than those at the other two site conditions.

The spectral shapes for horizontal motions recorded at rock sites show a strong distance dependence as shown in Fig. B-39. Typically, most available attenuation relationships assume a distance-independent shape or a shape that is weakly dependent on distance. This trend is illustrated in Fig. 5-1 which provides a comparison of the median spectral shapes for horizontal rock motions recorded during the Loma Prieta earthquake (Fig. B-39) with spectral shapes calculated using the attenuation relationship for rock sites derived by Idriss (1991b). This attenuation relationship incorporates distance-dependence of spectral shapes, but apparently not sufficiently to account for the measured effects obtained from Loma Prieta. Incorporation of the distance dependence of spectral shapes is essential for developing appropriate target rock spectra for a specific application and for conducting ground response analyses.

The records obtained at the soft soil sites offered an excellent opportunity to assess the procedures used for calculating response of soil sites during earthquakes. This was particularly the case because rock outcrop motions were also available from nearby locations and subsurface information was gathered at most of these soft soil sites.

Examination and studies of the response at these soft soil sites have been completed by several investigators since the occurrence of the Loma Prieta earthquake. These investigators include Borcherdt and Glassmoyer (1991), Chin and Aki (1993), Dickenson et al (1991), EPRI (1993), Hryciw et al (1991), Idriss (1990, 1991a), Jarpe et al (1989), Rollins et al (1992), Schneider et al (1991) and Yokel (1992). These investigations included examination of the recorded values at the soft soil sites in comparison to those recorded at the rock sites.

The results of the studies included in this report provide the following observations:

1. The equivalent linear procedure for calculating response of soil sites can provide reasonable estimates of the recorded motions if dynamic soil properties are reasonably well defined and if the rock outcrop input motion is reasonably well defined.

2. The estimation of earthquake ground motions using ground response analyses is affected greatly by the input motion. Therefore, it is important that variations in this input motion be incorporated in estimating earthquake ground motions for future events.

3. It is recommended that the 84th percentile of the results of site response analyses be used as an estimate of future shaking levels for the earthquake magnitude and distance under consideration.

4. It is important that response calculations take into account the difference in frequency content of rock motions recorded at close distances to the source compared to the frequency content of rock motions recorded at larger distances. This is particularly important when conducting site response analyses for sites located close to the potential source of future earthquakes.

Future studies need to address the response of deep soil sites (other than soft soil sites) and to make a systematic examination of the factors that affect the response of such sites. Subsurface data at many of these sites have been recently collected and can be used in studies similar to those presented in this report.

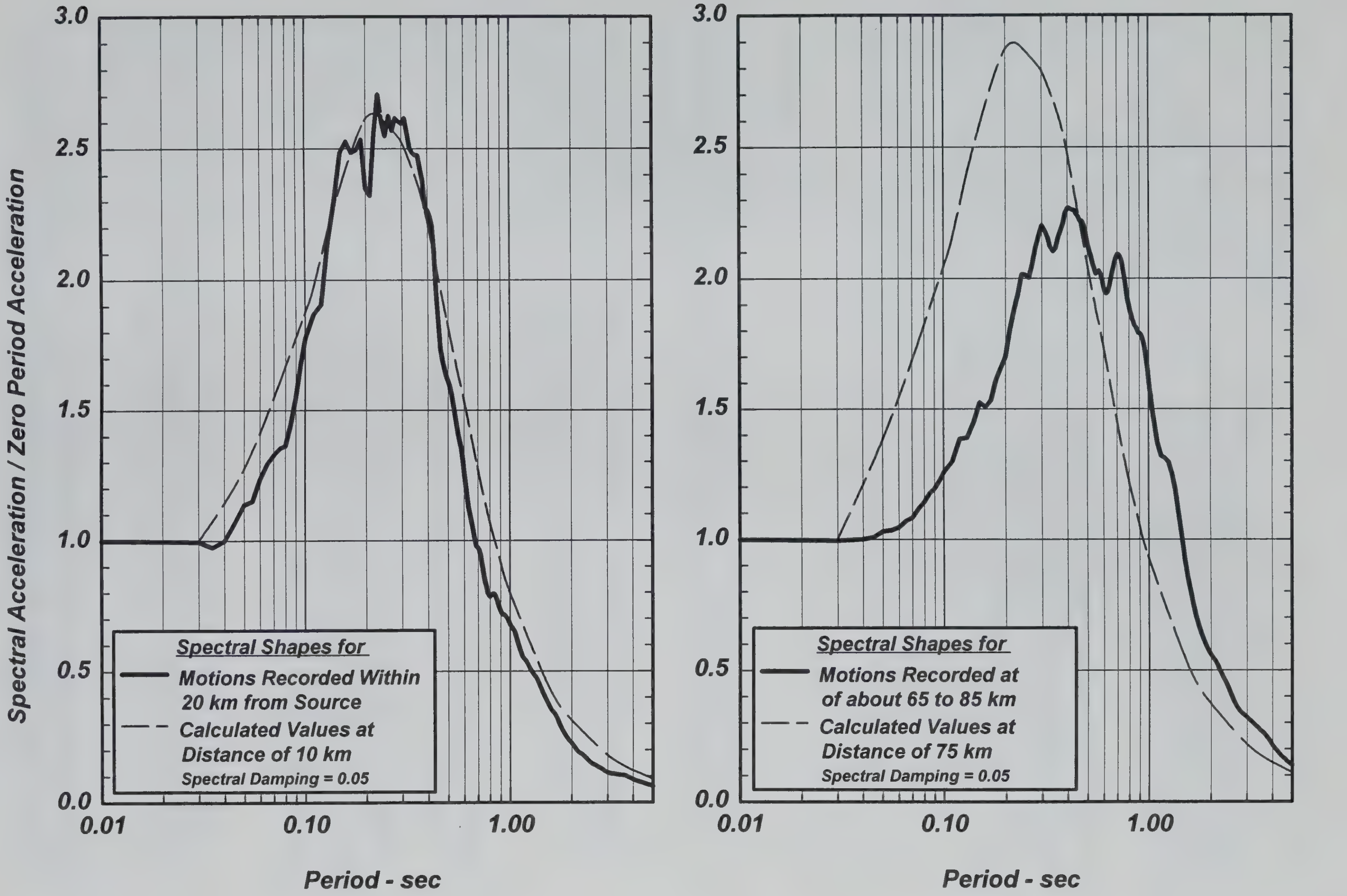

Fig. 5-1 Comparison of Median Normalized Spectral Shapes for Horizontal Rock Motions Recorded During the Loma Prieta Earthquake With Those Calculated Using Attenuation Relationship for Rock Sites Derived by Idriss (1991)

6.0 ACKNOWLEDGMENTS

The study has been supported by a research grant from the National Institute of Standards and Technology (NIST); Dr. Felix Y. Yokel of NIST is the Contract monitor. The writer gratefully acknowledges the support of NIST and thanks Dr. Yokel for his timely input and support during this study.

The subsurface information at the Treasure Island and the San Francisco Airport sites were investigated by the Electric Power Research Institute (EPRI) with technical support from USGS and partial financial support from the University of California at Davis and from the San Francisco International Airport Authority. The support by the University of California at Davis was provided through a grant to the writer from the following companies in Japan: Kiso-Jiban Consultants Co., Ltd.; Mitsui Construction Co., Ltd; NKK Corporation; and Sato Kogyo Co., Ltd. The writer gratefully acknowledges the contributions from these companies and the technical input from EPRI and USGS.

7.0 REFERENCES

Arias, A. (1969), “A Measurer of earthquake Intensity”, *Seismic Design for Nuclear Power Plants, Robert Hansen, Editor*, Massachusetts Institute of Technology Press, Cambridge, Massachusetts.

Borcherdt, R. D. and Glassmoyer, G. (1991), "On the Characteristics of Local Geology and its Influence on Ground Motions Generated by the Loma Prieta Earthquake in the San Francisco Bay Region, California", Bulletin of the Seismological Society of America, Vol. 81, No. 5, October, pp 1213-1232.

Chin, B-H. and Aki, Keiiti (1993), "Nonlinear Site response Study during the 1989 Loma Prieta Earthquake", Submitted to the Bulletin of the Seismological Society of America.

CSMIP (1989), "Plots of the Processed Data for the Interim Set of 14 Records from the Santa Cruz Mountains (Loma Prieta), California Earthquake of 17 October 1989", Report No. OSMS 89-08, California Strong Motion Instrumentation Program, Division of Mines and Geology, California Department of Conservation, Sacramento, California, December, 142p.

Dickenson, S. E. and Seed, R. B. (1991), "Correlations of Shear Wave Velocity and Engineering Properties for Soft Soil Deposits in the San Francisco Bay Region", Report No. UCB/EERC - 91, Earthquake Engineering Research Center, University of California, Berkeley, 110p.

Dickenson, S. E., Seed, R. B., Lysmer, J and Mok, C. M. (1991), "Response of Soft Soils during the 1989 Loma Prieta Earthquake and Implications for Seismic Design Criteria", Proceedings, Pacific Conference on Earthquake Engineering, Auckland, New Zealand, November.

Dobry, R., Idriss, I. M. and Ng, E. (1978), "Duration Characteristics of Horizontal Components of Strong-Motion Earthquake Records", Bulletin of the Seismological Society of America, Vol. 68, No. 5, October, pp 1487-1520.

Electric Power Research Institute (1993), "Guidelines for Determining Design Basis Ground Motions", Project Number RP3302, Palo Alto, California, March.

Gibbs, J. F., Fumal, T. E. and Borcherdt, R. D. (1975), "In-Situ Measurements of Seismic Velocities at Twelve Locations in the San Francisco Bay Region", USGS Open-File Report No. 75-564, USGS, Menlo Park, California, 87p.

Gibbs, J. F., Fumal, T. E., Boore, D. M. and Joyner, W. B. (1992), "Seismic Velocity and Geologic Logs from Borehole Measurements at Seven Strong-Motion Stations that Recorded the Loma Prieta Earthquake", USGS Open-File Report No. 92-287, USGS, Menlo Park, California, 139p.

Hardin, B. O. and Drnevich, V. P. (1970), "Shear Modulus and Damping in Soils: I. Measurement and Parameter Effects, II. Design Equations and Curves", Technical Reports UKY 27-70-CE 2 and 3, College of Engineering, University of Kentucky, Lexington, Kentucky, July. [These reports were later published in the Journal of Soil Mechanics and Foundation Division, ASCE, Vol. 98, No. 6, pp 603-624 and No. 7, pp 667-691, in June and July, 1972].

Hryciw, R. D., Rollins, K. M., Homolka, M., Shewbridge, S. E., and McHood, M. (1991), "Soil Amplification at Treasure Island During the Loma Prieta Earthquake", Proceedings, Second International Conference on Recent Advances in Geotechnical Earthquake Engineering and Soil Dynamics, St. Louis, Missouri, Vol. 2, pp 1679-1685.

Huang, M. J. et al (1989), "Second Interim Set of CSMIP Processed Strong-Motion Records from the Santa Cruz Mountains (Loma Prieta), California Earthquake of 17 October 1989", Report No. OSMS 90-01, California Strong Motion Instrumentation Program, Division of Mines and Geology, California Department of Conservation, Sacramento, California, February.

Hudson, D. E. (1976), “Strong Motion Earthquake Accelerograms - Index Volume”, Report No. EERL 76-02, Earthquake Engineering Research laboratory, California institute of Technology, Pasadena, August.

Husid, R. (1967), "Gravity Effects on the Earthquake Response of Yielding Structures", Research Report, Earthquake Engineering Research Laboratory, California Institute of Technology, Pasadena.

Idriss, I. M. (1990), "Response of Soft Soil Sites during Earthquakes", Proceedings, Memorial Symposium to honor Professor Harry Bolton Seed, Berkeley, California, Vol. II, May.

Idriss, I. M. (1991a), "Earthquake Ground Motions at Soft Soil Sites", Proceedings, Second International Conference on Recent Advances in Geotechnical Earthquake Engineering and Soil Dynamics, Vol. 3, St. Louis, Missouri, March.

Idriss, I. M. (1991b), "Procedures for Selecting Earthquake Ground Motions", a Report to the National Institute of Standards & Technology, US Department of Commerce, Gaithersburg, MD, Center for Geotechnical Modeling, Department of Civil & Environmental Engineering, University of California, Davis, September, 1991. The report was revised in March 1993 to include estimation of spectral ordinates at various damping ratios and was re-issued by NIST as Report No. NIST GCR 93-625.

Idriss, I. M. and Seed, H. Bolton (1968), "Seismic Response of Horizontal Soil Layers", Journal of the Soil Mechanics and Foundations Division, ASCE, Vol. 94, No. SM4, July.

Idriss, I. M. and Sun, Joseph I. (1992), "User's Manual for SHAKE91, a Computer Program for Conducting Equivalent Linear Seismic Response Analyses of Horizontally Layered Soil Deposits, Program Modified based on the original SHAKE program published in December 1972 by Schnabel, Lysmer & Seed", Report, Center for Geotechnical Modeling, Department of Civil & Environmental Engineering, University of California, Davis, November.

Jarpe, S., Hutchings, L, Hauk, T. and Shakal, A. (1989), "Selected Strong- and Weak-Motion Data from the Loma Prieta Earthquake Sequence", Seismological research Letters, 60, pp 167-176.

Joyner, W. B. and Boore, D. M. (1988), "Measurement, Characteristics and Prediction of Strong Ground Motion", State-of-the-Art Report, Proceedings, Specialty Conference on Earthquake Engineering and Soil Dynamics II -- Recent Advances in Ground Motion Evaluation, ASCE, Park City, Utah, June, pp 43-102.

Kanai, K. (1951), "Relation Between the Nature of Surface Layer and the Amplitude of Earthquake Motions", Bulletin, Tokyo Earthquake Research Institute.

Lee, M. K. W. and Finn, W. D. L. (1978), "DESRA-2, Dynamic Effective Stress Response Analysis of Soil Deposits with Energy Transmitting Boundary Including Assessment of Liquefaction Potential", Soil Mechanics Series No. 38, Department of Civil Engineering, University of British Columbia, Vancouver, B. C.

Li, X. S., Wang, Z. L. and Shen, C. K. (1992), "SUMDES A Nonlinear Procedure for Response Analysis of Horizontally-Layered Sites Subjected to Multi-Directional

Earthquake Loading", Report, Department of Civil Engineering, University of California, Davis, March.

Lysmer, J., Seed, H. Bolton and Schnabel, P. B. (1971), "Influence of Base -Rock Characteristics on Ground Response", Bulletin of the Seismological Society of America, Vol. 61, No. 5, October, pp 1213-1232.

Maley, R. et al (1989), "U. S. Geological Survey Strong Motion Records from the Northern California (Loma Prieta) Earthquake of October 17, 1989", Geological Survey Open-File Report 89-568, USGS, Menlo Park, California, October, 85p.

McNutt, S. (1990), "Loma Prieta Earthquake, October 17, 1989, Santa Cruz County, California", California Geology, Department of Conservation, Division of Mines and Geology, Vol. 43, No. 1, January, pp 3-7.

Redpath, Bruce B. (1991), "Seismic Velocity Logging in the San Francisco Bay Area", Report to the Electric Power Research Institute, by Redpath Geophysics, Murphys, California.

Rollins, K. M., Hryciw, R. D., McHood, M., Homolka, M. and Shewbridge, S. E. (1992), "Soil Amplification at San Francisco Airport During the Loma Prieta Earthquake", Paper prepared for Inclusion in the NEHRP Report to Congress on the Loma Prieta Earthquake.

Schnabel, P. B., Lysmer, J. and Seed, H. B. (1972), "SHAKE: A Computer Program for Earthquake Response Analysis of Horizontally Layered Sites", Report No. UCB/EERC-72/12, Earthquake Engineering Research Center, University of California, Berkeley, December, 102p.

Schneider, John F., Silva, Walter J. and Stark, Cathy (1991), "Ground Motion Model for the M 6.9 Loma Prieta Earthquake Including Effects of Source, Path and Site", Proceedings, Symposium on "New Horizons in Strong Motion: Seismic Studies and Engineering Practice", Santiago, Chile, June 4-7

Seed, H. B. and Idriss, I. M. (1970), "Soil Moduli and Damping Factors for Dynamic Response Analysis", Report No. UCB/EERC-70/10, Earthquake Engineering Research Center, University of California, Berkeley, December, 48p.

Seed, H. B. and Idriss, I. M. (1982), "Ground Motions and Soil Liquefaction during Earthquakes", Monograph No. 5, Earthquake Engineering Research Institute, Berkeley, California, December 1982.

Shakal, A. et al (1989), "CSMIP Strong-Motion Records from the Santa Cruz Mountains (Loma Prieta), California Earthquake of 17 October 1989", Report No. OSMS 89-06, California Strong Motion Instrumentation Program, Division of Mines and Geology, California Department of Conservation, Sacramento, California, November, 184p.

Silva, Walter J. and Lee, Kin (1987), "WES RASCAL Code for Synthesizing Earthquake Ground Motions", Miscellaneous Paper S-73-1, Report No. 24 in the Series "State-of-the-Art for Assessing Earthquake Hazards in the United States", US Army Engineer Waterways Experiment Station, Vicksburg, Mississippi.

Sun, J. I., Golesorkhi, R. and Seed, H. Bolton (1988), "Dynamic Moduli and Damping Ratios for Cohesive Soils", Report No. UCB/EERC-88/15, Earthquake Engineering Research Center, University of California, Berkeley, 42p.

Trifunac, M. D. and Brady, A. G. (1975), "A Study of the Duration of Strong Earthquake Ground Motion", Bulletin of the Seismological Society of America, Vol. 65, pp 581-626.

Vucetic, M. and Dobry, R. (1991), "Effect of Soil Plasticity on Cyclic Response", Journal of the Geotechnical Engineering Division, ASCE, Vol. 111, No. 1, January, pp 89-107.

Yokel, F. Y. (1992), " Effects of Subsurface Conditions on Earthquake Ground Motions", Report No. NISTIR 4769, Building and Fire Research Laboratory, National Institute of Standards and Technology, Gaithersburg, Maryland, 85p .

APPENDIX A

EARTHQUAKE GROUND MOTIONS RECORDED DURING THE 1989 LOMA PRIETA EARTHQUAKE

To Report on:

ASSESSMENT OF SITE RESPONSE ANALYSIS PROCEDURES

APPENDIX A

EARTHQUAKE GROUND MOTIONS RECORDED DURING THE 1989 LOMA PRIETA EARTHQUAKE

A.1 INTRODUCTION

The Loma Prieta earthquake occurred on October 17, 1989 at 5:04 pm Pacific daylight time along a 45-km long segment of the San Andreas fault in the Santa Cruz Mountains as shown in Fig. A-1. The earthquake was named after the highest topographic point (3791 ft or approximately 1155 m)) adjacent to the fault zone. The hypocenter of the earthquake was at a depth of about 18 km. The rupture plane dips to the southwest at about 70 degrees, as shown in Fig. A-2; thus the epicenter is several kilometers west of the San Andreas fault trace. The earthquake was assigned a surface wave magnitude, M_S = 7.1, and a moment magnitude, M_W = 7. The rupture was bilateral, i.e., the rupture was initiated at the hypocenter and propagated both northward and southward simultaneously.

Strong motion instruments had been installed by the United States Geological Survey (USGS) and by the California Strong Motion Instrumentation Program (CSMIP) at numerous locations and on various site conditions. These included: 33 stations at rock sites (of these two stations were at abutments of earth dams); nine stations at soft soil sites; and 47 stations at other soil sites (other than soft soil sites). The locations of the USGS stations that recorded the Loma Prieta earthquake are shown in Fig. A-3 and the locations of the CSMIP stations are shown in Fig. A-4.

The peak horizontal accelerations and the peak vertical accelerations recorded during this earthquake at free-field sites are summarized below.

The characteristics of the horizontal motions recorded at rock sites are summarized in Appendix B and the characteristics of the horizontal motions recorded at the soft soil sites are summarized in Appendix C.

A.2 PEAK ACCELERATIONS OF RECORDED MOTIONS

The Volume I[**] peak accelerations (two horizontal and one vertical components) of the motions recorded by the USGS and by CSMIP at rock sites are listed in Table A-1. The Volume I peak accelerations of the motions recorded at soft soil sites are listed in Table

---

[**] Volume I values are digitized at an unequal time basis, aimed at defining all significant features of the record (Hudson, 1976), and hence contain all the peak values of the original record. Volume II values, however, are digitized at an equal time increment and can result in peak accelerations that are somewhat smaller than the peak values in the original record. Volume II records (i.e., those digitized at an equal time increment) are usually used to calculate velocities, displacements, response spectra, Fourier amplitudes ... etc.

A-2 and those recorded at other soil sites are listed in Table A-3. The data listed in these tables are for stations considered to represent free-field conditions (except possibly for those at the abutments of earth dams and at the Emeryville site).

Included in each table are the name of the station, the distance to the source and the volume I peak horizontal and vertical accelerations. Note that the distance given in these tables pertains to the distance from the recording station to the closest point along the rupture surface (as defined by aftershocks) at a depth of three kilometers below the ground surface.

The horizontal peak accelerations are shown in Fig. A-5. The upper part of the figure shows the peak horizontal accelerations of both the strong and the weak components and the lower part of the figure shows the geometric average of the two horizontal components. As can be noted in both parts of the figure, the peak horizontal accelerations at rock and at soil sites (other than soft soil sites) are very similar and little distinction can be made between the two sets of peak horizontal accelerations. The peak horizontal accelerations at the soft soil sites, however, are significantly greater than those at the other two site conditions.

The vertical accelerations are shown in the upper part of Fig. A-6. The lower part of the figure shows the ratio of the peak vertical acceleration, a_v, divided by the geometric average, a_h, of the two horizontal components. The peak vertical accelerations at rock sites appear to be smaller than those recorded at soil sites during this earthquake. The variations of the ratio a_v / a_h with distance for the data recorded during this earthquake are typical of such variations. The ratio for soft soil sites is quite low (because of the high horizontal accelerations) and the data points in Fig. A-6 are among the few available for this ratio at soft soil sites.

Table A-1
Volume I Peak Accelerations of Earthquake Ground Motions Recorded by USGS and by CSMIP at Rock Sites During the Loma Prieta Earthquake

Site	Distance	H1	H2	V
Corralitos	5.2	0.640	0.500	0.470
Abutment - Lexington Dam	5.8	0.450	0.410	0.150
Gilroy #1	10.0	0.500	0.430	0.220
Gilroy #6	18.1	0.170	0.130	0.100
Abutment - Coyote Lake Dam	19.5	0.490	0.150	0.080
Santa Cruz	20.2	0.470	0.440	0.400
Hollister (S St. & Pine Drive)	31.3	0.060	0.040	0.050
Monterey - City Hall	31.5	0.070	0.070	0.030
Sago South (Cienega Road)	35.2	0.070	0.070	0.080
Woodside Fire Station	39.2	0.080	0.080	0.050
Redwood City	40.3	0.090	0.050	0.040
APEEL # 9	46.2	0.120	0.110	0.060
Upper Crystal Spring (APEEL 7)	46.9	0.160	0.090	0.060
Upper Crystal Spring (APEEL 10)	47.2	0.100	0.090	0.040
Hayward - CSUH FF	52.0	0.080	0.080	0.050
Lower Crystal - 58233	53.5	0.090	0.060	0.030
Sierra Point	68.0	0.110	0.060	0.050
Bear Valley St. 7	70.1	0.060	0.040	0.030
Diamond Heights	76.0	0.120	0.100	0.050
Rincon Hill	78.5	0.090	0.080	0.030
Yerba Buena Island	79.3	0.060	0.030	0.030
Piedmont Junior High	80.0	0.080	0.070	0.030
Pacific Heights	80.5	0.060	0.050	0.030
Telegraph Hills	80.8	0.080	0.060	0.030
Big Sur	81.0	0.060	0.050	0.030
Berkeley - Strawberry Canyon	81.8	0.080	0.040	0.020
Presidio	82.0	0.210	0.100	0.060
Golden Gate Bridge	82.2	0.240	0.120	0.060
Lawrence Berkeley Laboratory	82.8	0.120	0.050	0.040
Cliff House	83.4	0.110	0.080	0.060
Pleasant Hill	85.0	0.130	0.080	0.030
Point Bonita	87.0	0.070	0.070	0.030
San Rafael	107.0	0.040	0.030	0.030

Table A-2
Volume I Peak Accelerations of Earthquake Ground Motions Recorded by USGS and by CSMIP at Soft Soil Sites During the Loma Prieta Earthquake

Site	Distance	H1	H2	V
Redwood City (APEEL No. 2)	46.8	0.280	0.230	0.080
Foster City	48.3	0.290	0.260	0.110
San Francisco Airport	63.5	0.330	0.240	0.050
Alameda Naval Station❖	76.0	0.268	0.209	0.061
Outer Harbor Wharf	76.4	0.290	0.270	0.070
Emeryville	81.0	0.260	0.220	0.060
Treasure Island	81.6	0.160	0.110	0.020
Richmond City hall - Parking Lot	85.0	0.130	0.110	0.040
Larkspur Ferry Terminal	99.0	0.140	0.100	0.060

❖ Peak accelerations for this site are Volume II values.

Table A-3
Volume I Peak Accelerations of Earthquake Ground Motions Recorded by USGS and by CSMIP at Soil Sites (other than Soft Soil Sites) During the Loma Prieta Earthquake

Site	Distance	H1	H2	V
Gilroy (Gavilan; Physical Bldg.)	10.4	0.370	0.330	0.200
Gilroy (Firehouse)	10.9	0.280	0.250	0.150
Gilroy #2	11.3	0.370	0.330	0.310
Saratoga (Aloha Ave.)	11.9	0.530	0.340	0.410
Saratoga Gymnasium	12.3	0.330	0.260	0.270
Gilroy #3	13.0	0.550	0.370	0.380
Gilroy #4	14.4	0.420	0.220	0.170
Capitola	16.7	0.540	0.470	0.600
Anderson Dam - downstream	19.1	0.260	0.250	0.170
Coyote Lake Dam - downstream	20.0	0.190	0.170	0.100
San Jose (Santa Teresa Hills)	20.9	0.280	0.270	0.220
San Jose (Station No. 57562)	22.0	0.200	0.200	0.140
Gilroy #7	22.4	0.330	0.100	0.120
Hollister Airport	25.4	0.290	0.270	0.160
Agnews State Hospital	26.2	0.170	0.160	0.100
Sunnyvale - Colton Ave.	27.1	0.220	0.190	0.100
Hollister City Hall	28.1	0.250	0.230	0.220
Hollister - FF	28.6	0.380	0.180	0.200
Halls Valley - Grant Park	30.2	0.130	0.060	0.110
Milpitas	30.3	0.140	0.090	0.080
Hollister - Warehouse	31.0	0.380	0.180	0.200
Calaveras Array - L Abut	32.0	0.090	0.070	0.060
Salinas	34.5	0.120	0.090	0.110
Palo Alto	34.6	0.210	0.200	0.090
Calaveras Array - ground	35.1	0.130	0.080	0.070
Stanford - SLAC	35.4	0.290	0.190	0.100
Menlo Park VA	37.8	0.270	0.120	0.110
Fremont	40.9	0.130	0.110	0.090
Calaveras Array - Fremont	41.4	0.200	0.150	0.070
California Array - Sunol FS	48.7	0.100	0.070	0.030
Bear Valley St. 12	51.8	0.170	0.160	0.100
Hayward - Muir School	52.0	0.180	0.140	0.100
Hayward Bart FF	54.0	0.160	0.160	0.080
Bear Valley St. 5	54.4	0.070	0.070	0.040
APEEL #2E, Muir School	55.6	0.160	0.130	0.060
California Array, Dublin FS	60.5	0.090	0.080	0.030
Livermore	67.6	0.040	0.020	0.020

Table A-3 (Cont'd)

Volume I Peak Accelerations of Earthquake Ground Motions Recorded by USGS and by CSMIP at Soil Sites (other than Soft Soil Sites) During the Loma Prieta Earthquake

Site	Distance	H1	H2	V
Bear Valley St. 10	68.4	0.130	0.100	0.050
San Francisco (1295 Shafer St.)	72.6	0.110	0.070	0.050
San Benito	73.1	0.050	0.050	0.020
Oakland - 2 story	76.0	0.260	0.200	0.160
Los Banos	76.5	0.050	0.050	0.010
SF State U - Thornton	76.6	0.140	0.110	0.040
Tracy	82.3	0.060	0.060	0.020
Greenfield	82.4	0.080	0.080	0.060
UCB Stadium	82.8	0.130	0.070	0.030
Bitterwater	93.0	0.070	0.060	0.030

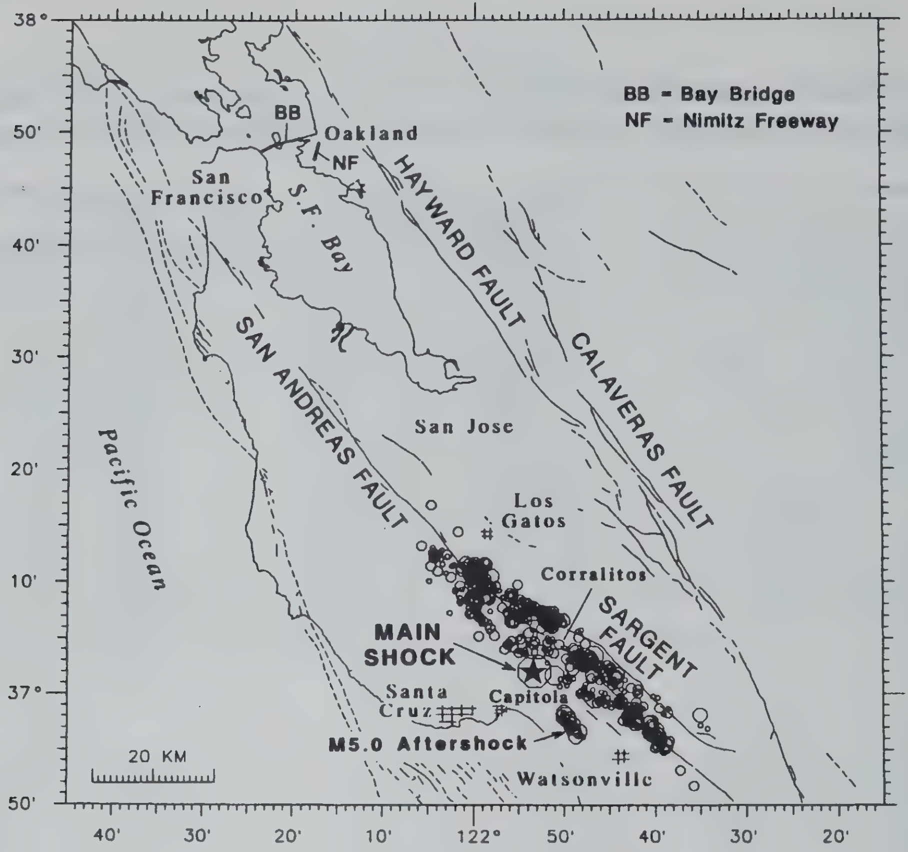

Fig. A-1 Location of the Main Shock of the Loma Prieta Earthquake, Area of Aftershocks and Inferred Extent of Fault Rupture (from McNutt, 1990)

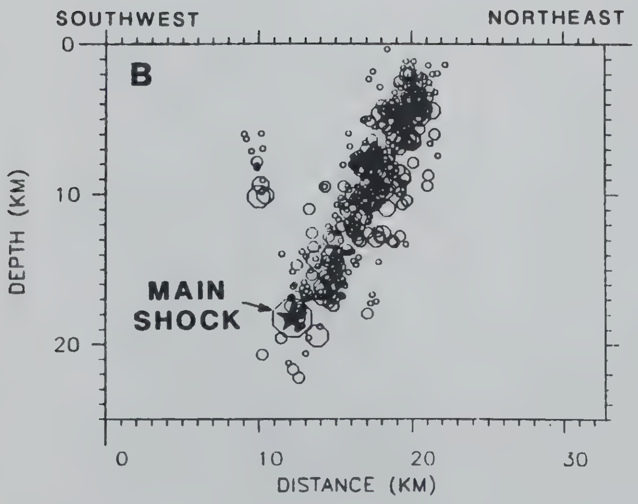

Fig. A-2 Transverse Section Showing Distribution of Aftershocks and Dip of Fault Plane (from McNutt, 1990)

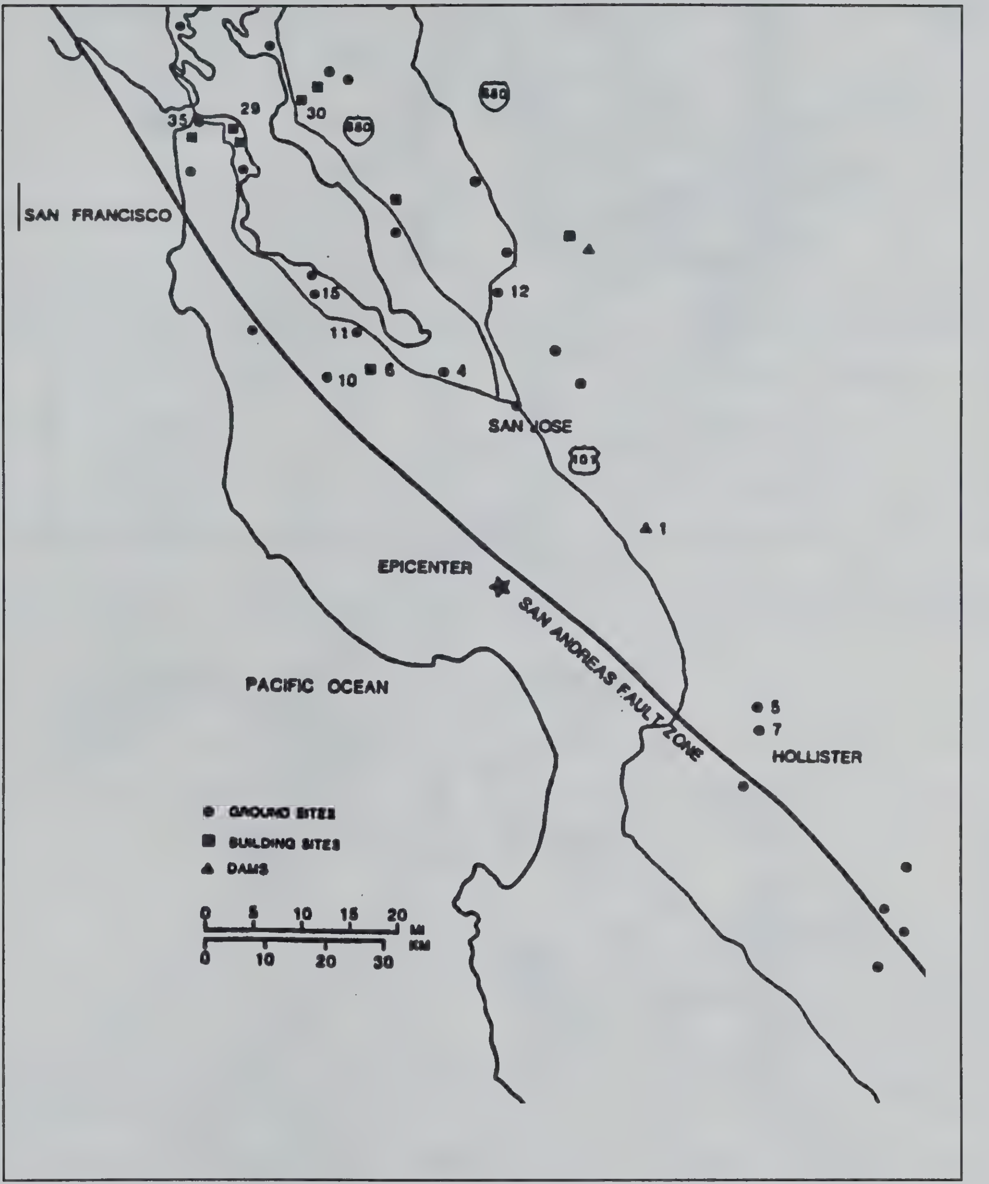

Fig. A-3 Locations of USGS Stations Which Recorded the Loma Prieta Earthquake

(from Maley et al, 1989)

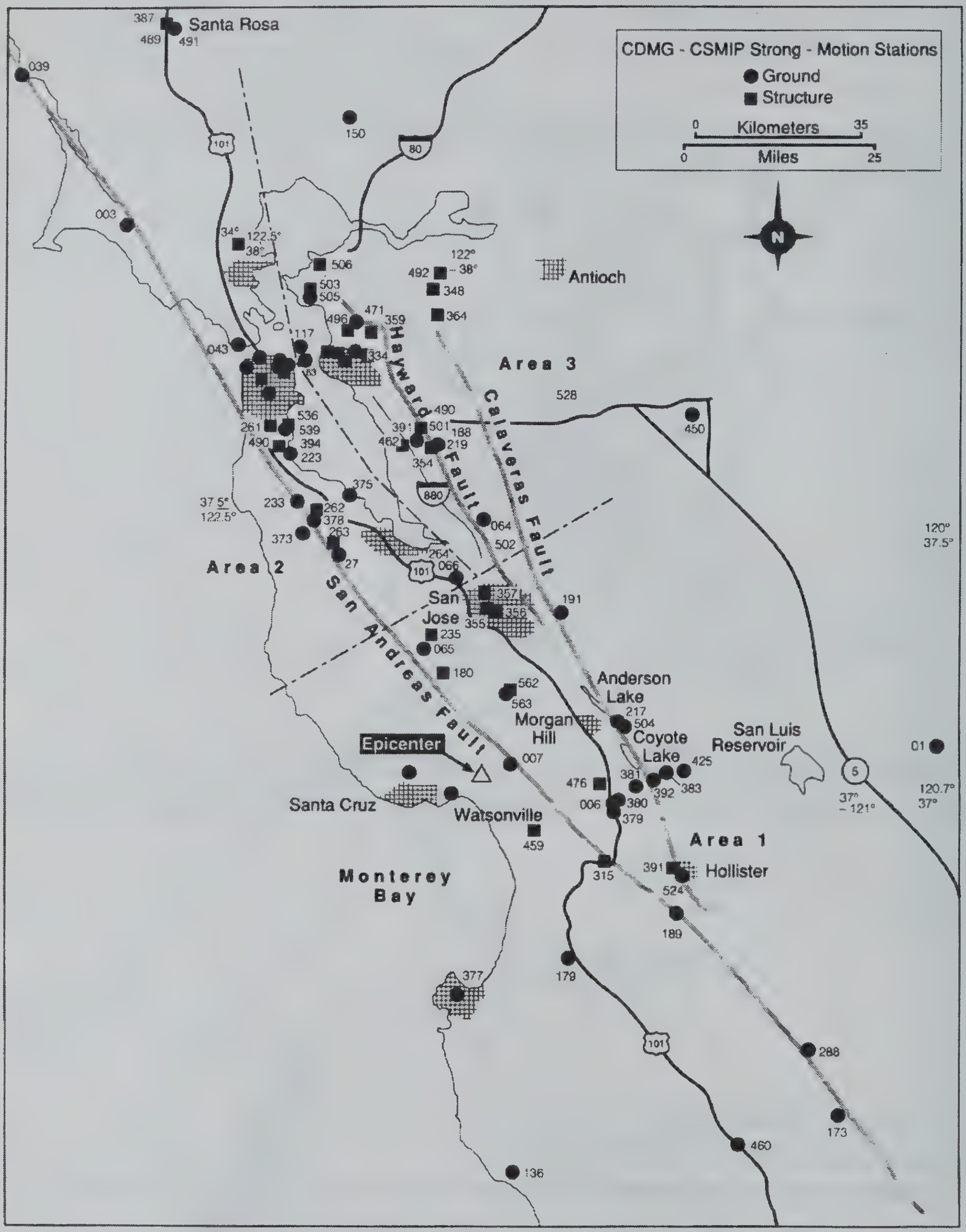

Fig. A-4 Locations of CSMIP Stations Which Recorded the Loma Prieta Earthquake
(from Shakal et al, 1989)

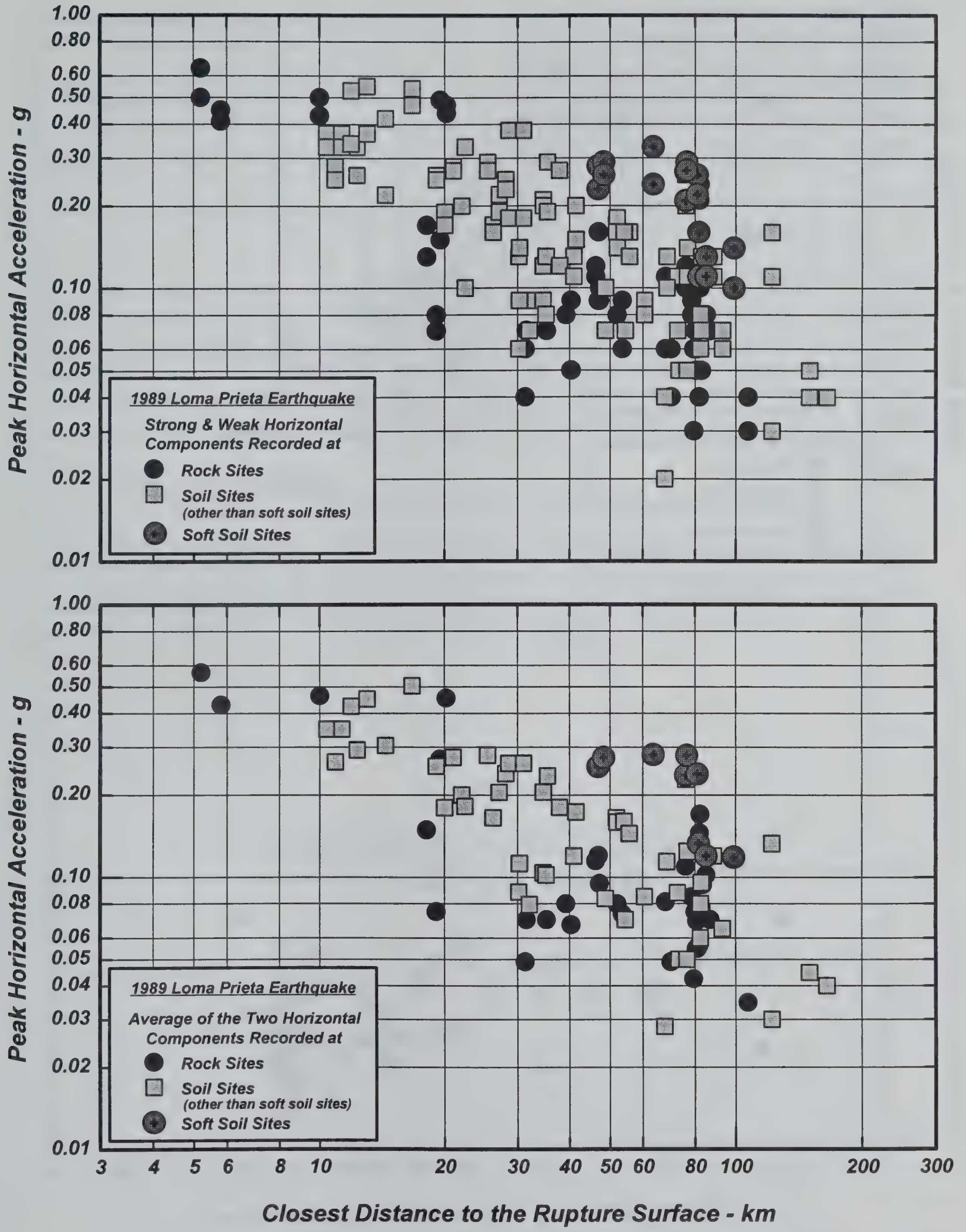

Fig. A-5 Horizontal Accelerations Recorded During the 1989 Loma Prieta Earthquake

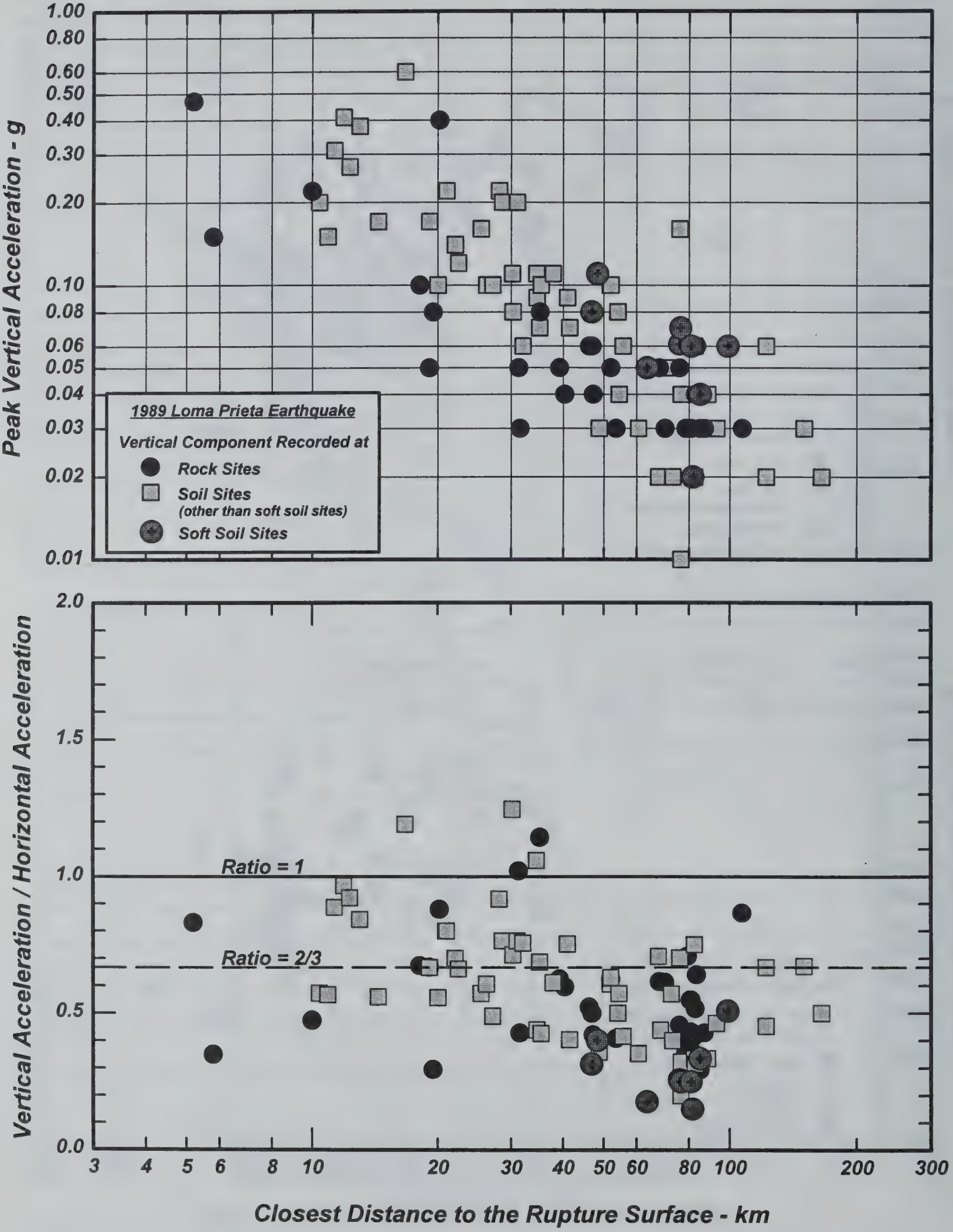

Fig. A-6 Vertical Accelerations Recorded During the 1989 Loma Prieta Earthquake and Ratio of Vertical Acceleration to Horizontal Acceleration

APPENDIX B

CHARACTERISTICS OF THE HORIZONTAL EARTHQUAKE GROUND MOTIONS RECORDED AT ROCK SITES DURING THE 1989 LOMA PRIETA EARTHQUAKE

To Report on:

ASSESSMENT OF SITE RESPONSE
ANALYSIS PROCEDURES

APPENDIX B

CHARACTERISTICS OF THE HORIZONTAL EARTHQUAKE GROUND MOTIONS RECORDED AT ROCK SITES DURING THE 1989 LOMA PRIETA EARTHQUAKE

B.1 INTRODUCTION

As described in Appendix A, 33 of the 89 free field recordings obtained during Loma Prieta earthquake were at rock sites. Of particular interest to this study are the recordings obtained in the vicinity of the source (say, within 20 ± km) and those obtained in the San Francisco-Bay Area. The peak accelerations, peak velocities, peak displacements, spectral ordinates and effective duration (as defined from a Husid plot) of these rock motions are summarized in this Appendix.

B.2 ROCK MOTIONS WITHIN 20 KM FROM THE SOURCE

Six recording stations located on rock were within 20 km from the source of the Loma Prieta earthquake. Two of these recording stations were at abutments of earth dams; the characteristics of the ground motions obtained from these two stations are presented in this Appendix but are not used in evaluating the characteristics of rock motions within 20 km of the source.

The characteristics of the horizontal earthquake ground motions recorded at these rock sites during the Loma Prieta earthquake are listed in Tables B-1 through B-3 and in Figs. B-1 through B-14 and are summarized below.

B.2.1 Peak Horizontal Accelerations, a, Velocities, v, and Displacements, d

The peak accelerations (Volume II), velocities and displacements of the earthquake ground motions recorded at these rock sites are listed in Table B-1.

B.2.2 Ratios v/a and ad/v^2

The ratios v/a and ad/v^2 for the twelve horizontal components listed in Table B-1 are listed in Table B-2. The average value of the ratio v/a for all the records listed in Table B-1 is about 110 cm/sec/g if the records obtained at the dam abutments are included. If these two records are not included the average value of the ratio v/a is about 79. The corresponding average values of the ratio ad/v^2 are about 2.9 and 3.5, respectively.

B.2.3 Accelerograms and Spectral Accelerations

The accelerograms and the spectral accelerations (5 percent spectral damping) for these ground motions are presented in Figs. B-1 through B-6. The normalized spectra for the horizontal accelerograms recorded at Corralitos, Gilroy No. 1, Gilroy No. 6 and Santa Cruz (i.e., normalized spectra for all components listed in Table B-1 except for the four components recorded at abutments of earth dams) are shown in Fig. B-7. Also shown in Fig. B-7 is the median normalized spectrum for these eight accelerograms.

B.2.4 Husid Plots and Effective Duration

Effective duration of a given accelerogram is assessed using the procedure originally proposed by Trifunac and Brady (1975). This procedure is based on the time required for the buildup of the integral

$$\int_0^t a^2(t)dt$$

in which *a(t)* is the acceleration time history. Arias (1969) showed that this integral is a measure of the energy of the accelerogram, and defined the intensity of the entire record by the following expression:

$$I_A(t_f) = \frac{\pi}{2g}\int_0^{t_f} a^2(t)dt$$

in which I_A is the Arias' intensity and t_f is the total duration. Husid (1969) proposed the use of the normalized variable *h(t):*

$$h(t) = \frac{I_A(t)}{I_A(t_f)} = \frac{\int_0^t a^2(t)dt}{\int_0^{t_f} a^2(t)dt} \qquad \text{Equation B-1}$$

Thus, *h(t)* = 0 at the beginning of the record and = 1 (or 100 percent) at the end of the record. The plot of *h(t)* versus *t* is designated the Husid plot.

Effective duration as defined by Trifunac and Brady (1975) is the time interval needed for *h(t)* to build up from 5 to 95 percent.

The Husid plots for the twelve horizontal components listed in Table B-1 are presented in Figs. B-8 through B-13. The Husid plots for all the motions considered are shown in Fig.

B-14. The time at which *h(t)* = 5 percent and the time at which *h(t)* = 95 percent are listed in Table B-3 for each component included in Figs. B-8 through B-13. Also listed in Table B-3 are the values of effective duration as defined above. The effective duration varies from about 3.7 to 8 seconds within distances of about 10 km from the source and from about 9.5 to 13 seconds at distances of 18 to 20 km (the range is from 9.5 to about 16 seconds if the recordings at the abutment of the Coyote dam are included).

B.3 ROCK MOTIONS IN THE SAN FRANCISCO BAY AREA

The recording stations located on rock sites in the San Francisco Bay Area are listed in Table B-4. The characteristics of the horizontal earthquake ground motions recorded at these eleven rock sites during the Loma Prieta earthquake are listed in Tables B-4 through B-6 and in Figs. B-15 through B-38 and are summarized below.

B.3.1 Peak Horizontal Accelerations, a, Velocities, v, and Displacements, d

The peak accelerations (Volume II), velocities and displacements of the earthquake ground motions recorded at these rock sites are listed in Table B-4.

B.3.2 Ratios v/a and ad/v^2

The ratios *v/a* and ad/v^2 for the twelve records listed in Table B-4 are listed in Table B-5. The average value of the ratio *v/a* for all the records listed in Table B-4 is about 147 cm/sec/g and the average value of ad/v^2 is about 2.1.

B.3.3 Accelerograms and Spectral Accelerations

The accelerograms and the spectral accelerations (5 percent spectral damping) for these ground motions are presented in Figs. B-15 through B-25. The normalized spectra for all these horizontal accelerograms are shown in Fig. B-26. Also shown in Fig. B-26 is the median normalized spectrum for these 22 accelerograms.

B.3.4 Husid Plots and Effective Duration

The Husid plots (using Eq. B-1) for the horizontal accelerograms obtained at these rock sites in the San Francisco Bay Area are presented in Figs. B-27 through B-37. The Husid plots for the motions considered are shown in Fig. B-38; note that the Husid plots for the two horizontal components at Telegraph Hill are not included in Fig. B-38 because several seconds of the early part of these two components had been eliminated in the digitizing process. The time at which *h(t)* = 5 percent and the time at which *h(t)* = 95 percent are listed in Table B-6 for each component included in Figs. B-27 through B-37. Also listed in Table B-6 are the values of effective duration as defined above; the values of effective duration range from about 6 to 20 seconds.

B.4 DISCUSSION

The material presented in this Appendix provides information regarding the general characteristics of rock motions recorded at close distance from the source and those recorded at considerably larger distances from the source. The median frequency content of each set of recordings is shown in Fig. B-39 in terms of normalized spectral shapes. As can be noted in the figure, the median normalized spectrum for the records obtained at close distances from the source has a peak at a period of about 0.22 sec (or a frequency of about 4.5 Hz) while the median normalized spectrum for the more distant records has a peak at about a period of about 0.42 sec (or a frequency of about 2.4 Hz). These frequency characteristics are very important to take into account when selecting input motions for response calculations, especially for softer soil sites (Idriss, 1991).

The effective duration values obtained for all the recordings on rock presented in this Appendix are shown in Fig. B-40. Also shown in the figure is the line representing the least square fit for the data shown in the figure; the equation of this line is as follows:

$$Ln(D_e) = 1.695 + 0.151 Ln(R) \qquad \text{Equation B-2}$$

in which D_e is the effective duration in seconds and R is distance (as defined in Appendix A) in km. The standard error term is 0.31 (natural logarithm basis). The trend represented by the data and the results of the least square fit suggest a weak dependence of effective duration on distance.

Table B-1
Peak Accelerations, Velocities and Displacements of Horizontal Earthquake Ground Motions Recorded at Rock Sites Within a Distance of about 20 km from the Source during the Loma Prieta Earthquake

Station	Distance km	Component	Peak Acceleration g	Peak Velocity cm/sec	Peak Displacement cm
Corralitos	5.2	EW	0.478	47.5	11.5
		NS	0.629	55.2	9.50
Abutment - Lexington Dam	5.8	EW	0.413	95.0	25.8
		NS	0.444	84.4	14.7
Gilroy #1	10	EW	0.442	33.8	6.32
		NS	0.435	31.9	6.49
Gilroy # 6	18.1	EW	0.114	13.1	4.95
		NS	0.171	13.9	3.35
Abutment - Coyote Lake Dam	19.5	N75E	0.480	37.5	11.1
		S15E	0.152	15.1	5.20
Santa Cruz	20.2	EW	0.409	21.2	6.81
		NS	0.441	21.2	6.61

Notes:
1. Peak accelerations listed in this table are "Volume II" accelerations.

Table B-2

Values of v/a and ad/v^2 of Horizontal Earthquake Ground Motions Recorded at Rock Sites Within a Distance of about 20 km from the Source during the Loma Prieta Earthquake

Station	Distance km	Component	v/a cm/sec/g	ad/v^2
Corralitos	5.2	EW	99.4	2.39
		NS	87.8	1.92
Abutment - Lexington Dam	5.8	EW	230	1.16
		NS	190	0.90
Gilroy #1	10	EW	76.5	2.40
		NS	73.3	2.72
Gilroy # 6	18.1	EW	115	3.23
		NS	81.3	2.91
Abutment - Coyote Lake Dam	19.5	N75E	78.1	3.72
		S15E	99.3	3.40
Santa Cruz	20.2	EW	51.8	6.08
		NS	48.1	6.37

Table B-3

Effective Duration Determined from Husid Plots of Horizontal Earthquake Ground Motions Recorded at Rock Sites Within a Distance of about 20 km from the Source during the Loma Prieta Earthquake

Station	Distance km	Component	Time at 5% seconds	Time at 95% seconds	Effective Duration seconds
Corralitos	5.2	EW	2.25	10.22	7.97
		NS	2.33	9.16	6.83
Abutment - Lexington Dam	5.8	EW	3.77	7.89	4.12
		NS	3.97	8.31	4.34
Gilroy #1	10	EW	2.86	6.54	3.68
		NS	2.7	9.32	6.62
Gilroy # 6	18.1	EW	3.46	16.12	12.66
		NS	3.38	16.36	12.98
Abutment - Coyote Lake Dam	19.5	N75E	3.69	15.92	12.23
		S15E	3.98	19.74	15.76
Santa Cruz	20.2	EW	4.25	13.95	9.7
		NS	3.9	13.4	9.5

Table B-4
Peak Accelerations, Velocities and Displacements of Horizontal Earthquake Ground Motions Recorded at Rock Sites in San Francisco-Bay Area during the Loma Prieta Earthquake

Station	Distance km	Component	Peak Acceleration g	Peak Velocity cm/sec	Peak Displacement cm
Sierra Point	68	S25E	0.105	8.19	2.03
		S65W	0.058	6.13	2.46
Diamond Heights	76	EW	0.113	14.3	4.31
		NS	0.098	10.5	2.83
Rincon Hill	79	EW	0.090	11.6	4.88
		NS	0.080	7.34	2.62
Pacific Heights	80	EW	0.061	14.3	4.88
		NS	0.047	9.88	3.08
Telegraph Hill	81	EW	0.092	9.59	2.76
		NS	0.052	6.50	1.43
Golden Gate	82	EW	0.243	35.5	7.42
		NS	0.126	18.0	3.86
Presidio	82	EW	0.199	33.5	6.35
		NS	0.100	13.3	4.13
Cliff House	83	EW	0.108	21.0	6.40
		NS	0.075	11.2	3.70
Yerba Buena	79	EW	0.067	14.7	4.12
		NS	0.29	4.61	1.39
Piedmont	80	N45W	0.083	9.17	2.76
		N45E	0.071	9.67	2.20
Lawrence Berkeley Laboratory	83	EW	0.117	22.0	3.50
		NS	0.049	8.70	2.06

Note: peak accelerations listed in this table are "Volume II" accelerations.

Table B-5
Values of v/a and ad/v^2 of Horizontal Earthquake Ground Motions Recorded at Rock Sites in San Francisco-Bay Area during the Loma Prieta Earthquake

Station	Distance km	Component	v/a cm/sec/g	ad/v^2
Sierra Point	68	S25E	78.0	3.12
		S65W	106	3.73
Diamond Heights	76	EW	127	2.34
		NS	107	2.47
Rincon Hill	79	EW	129	3.20
		NS	91.8	3.82
Pacific Heights	80	EW	234	1.43
		NS	210	1.46
Telegraph Hill	81	EW	104	2.71
		NS	125	1.73
Golden Gate	82	EW	146	1.40
		NS	143	1.47
Presidio	82	EW	168	1.11
		NS	133	2.29
Cliff House	83	EW	194	1.54
		NS	149	2.17
Yerba Buena	79	EW	219	1.25
		NS	159	1.86
Piedmont	80	N45W	110	2.67
		N45E	136	1.64
Lawrence Berkeley Laboratory	83	EW	188	0.83
		NS	178	1.31

Table B-6
Effective Duration Determined from Husid Plots of Horizontal Earthquake Ground Motions Recorded at Rock Sites in San Francisco-Bay Area during the Loma Prieta Earthquake

Station	Distance km	Component	Time at 5% seconds	Time at 95% seconds	Effective Duration seconds
Sierra Point	68	S25E	7.42	16.89	9.47
		S65W	7.08	18.74	11.66
Diamond Heights	76	EW	8.14	17.44	9.30
		NS	8.94	17.72	8.78
Rincon Hill	79	EW	8.32	19.74	11.42
		NS	5.97	19.84	13.87
Pacific Heights	80	EW	8.91	19.56	10.65
		NS	8.77	20.84	12.07
Telegraph Hill	81	EW	0.25	9.33	9.08
		NS	0.51	11.16	10.65
Golden Gate	82	EW	9.76	15.85	6.09
		NS	9.22	16.68	7.46
Presidio	82	EW	9.44	17.99	8.55
		NS	8.99	19.42	10.43
Cliff House	83	EW	9.84	17.08	7.24
		NS	8.50	18.74	10.24
Yerba Buena	79	EW	9.43	17.46	8.03
		NS	3.71	23.66	19.95
Piedmont	80	N45W	7.20	18.96	11.76
		N45E	7.41	19.11	11.70
Lawrence Berkeley Laboratory	83	EW	9.01	17.14	8.13
		NS	8.18	25.62	17.44

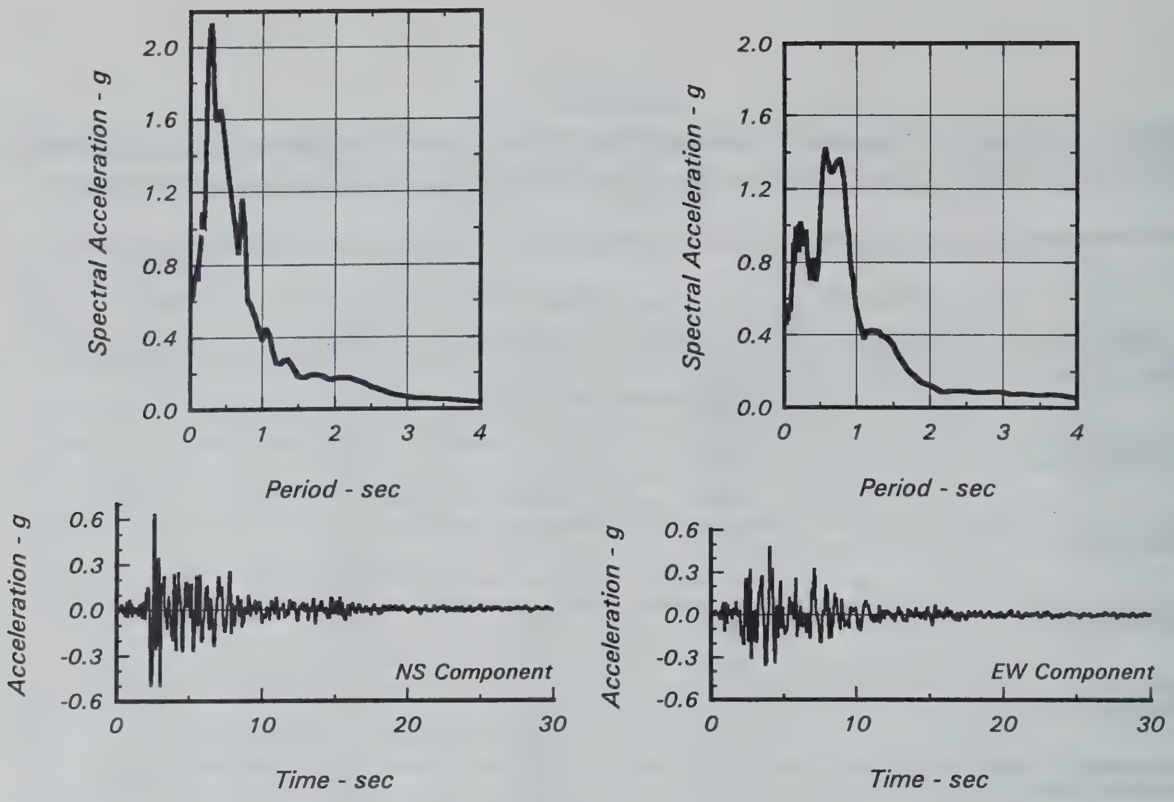

Fig. B-1 Accelerograms and Spectral Ordinates of the Horizontal Components of Earthquake Ground Motions Recorded at Corralitos during the Loma Prieta Earthquake

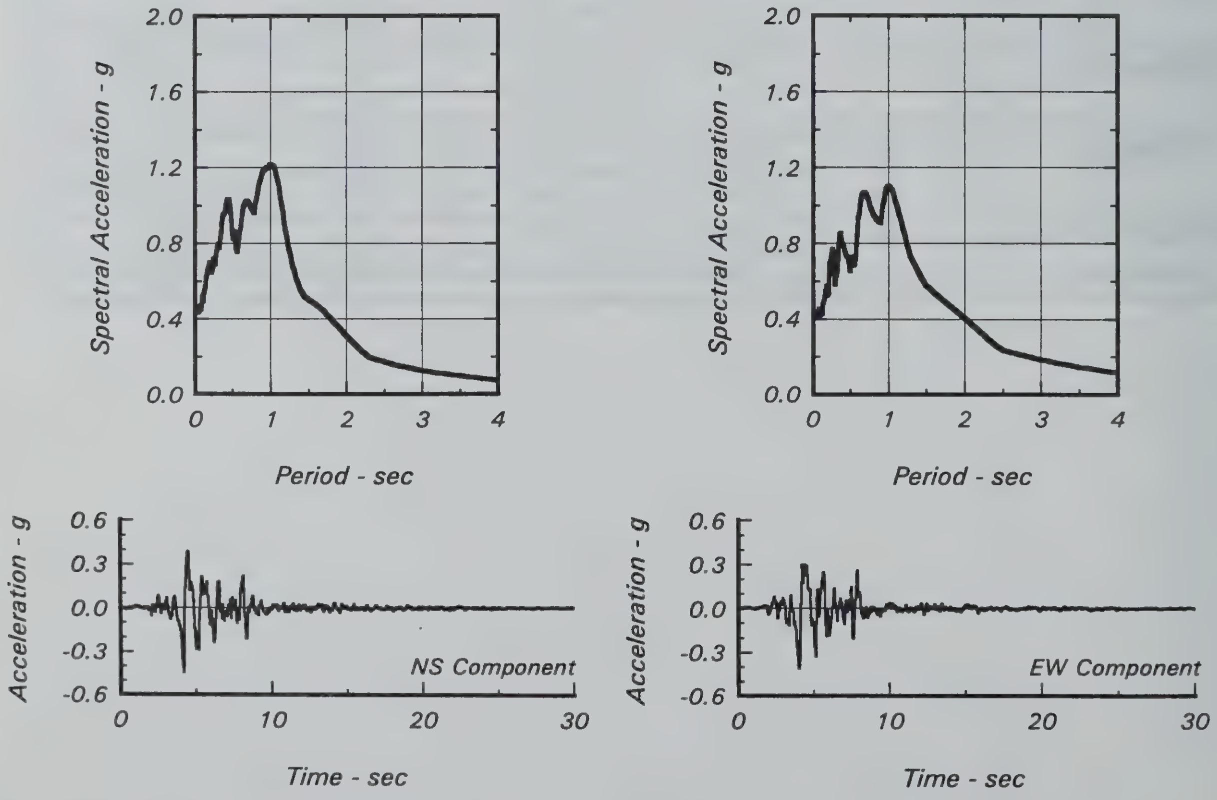

Fig. B-2 Accelerograms and Spectral Ordinates of the Horizontal Components of Earthquake Ground Motions Recorded at Abutment of Lexington Dam during the Loma Prieta Earthquake

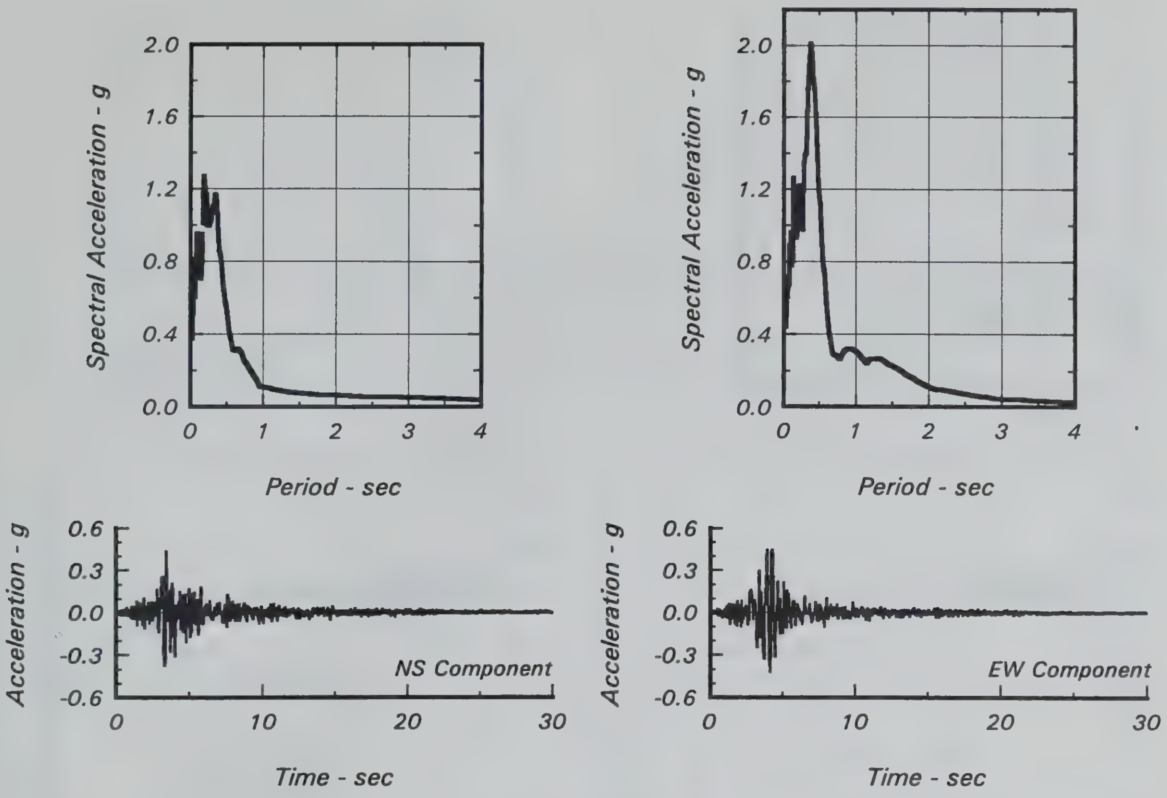

Fig. B-3 Accelerograms and Spectral Ordinates of the Horizontal Components of Earthquake Ground Motions Recorded at Gilroy No.1 during the Loma Prieta Earthquake

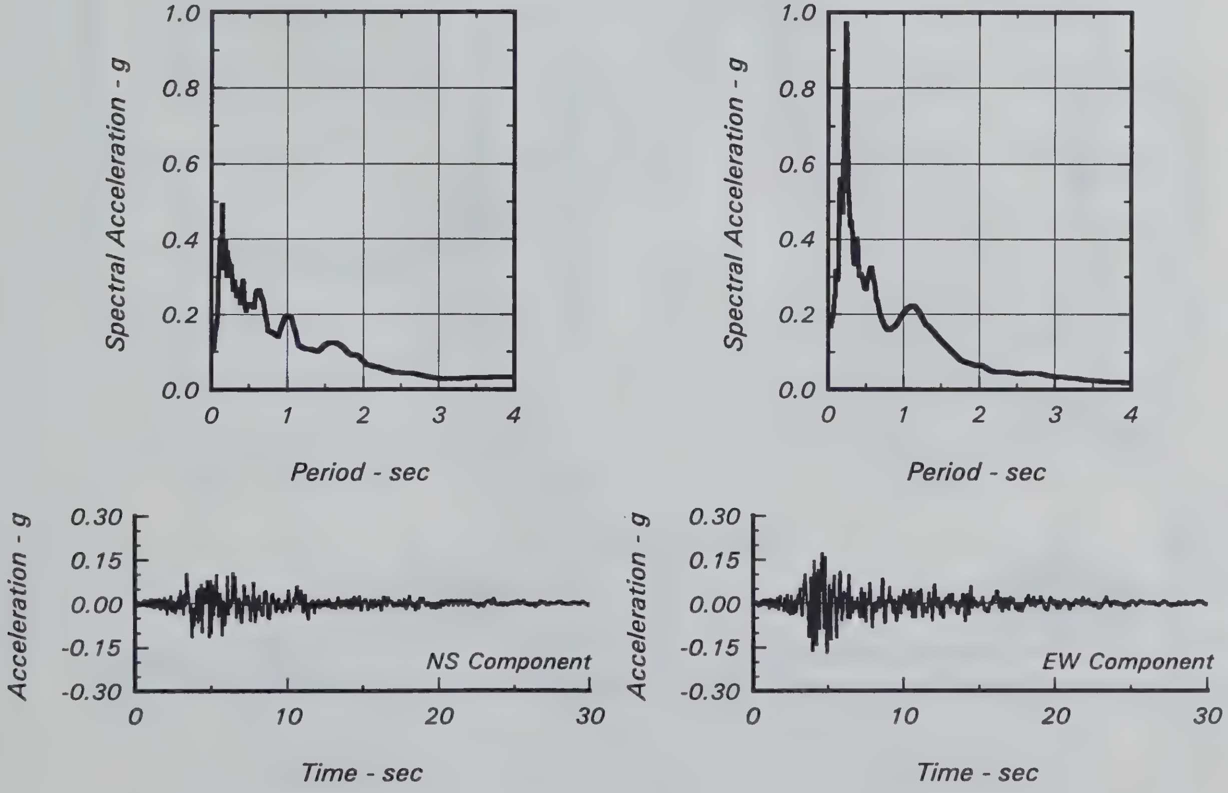

Fig. B-4 Accelerograms and Spectral Ordinates of the Horizontal Components of Earthquake Ground Motions Recorded at Gilroy No. 6 during the Loma Prieta Earthquake

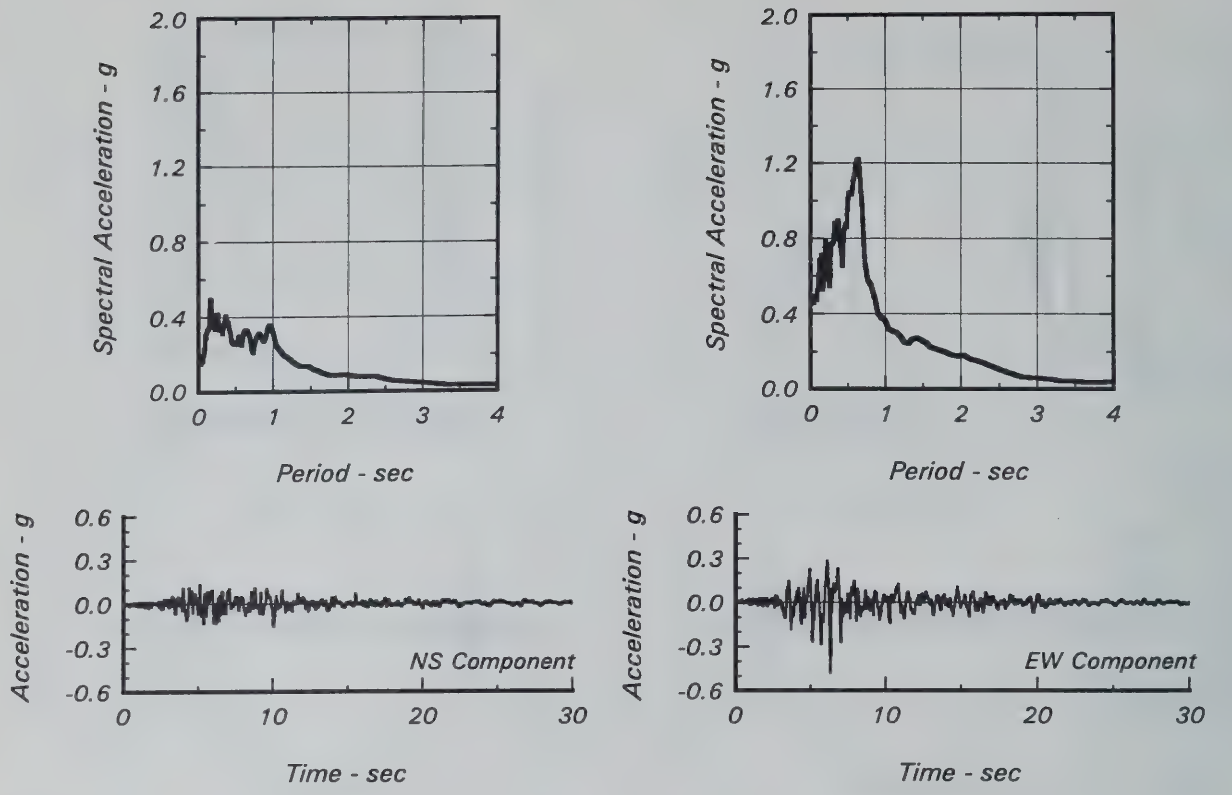

Fig. B-5 Accelerograms and Spectral Ordinates of the Horizontal Components of Earthquake Ground Motions Recorded at Abutment of Coyote Dam during the Loma Prieta Earthquake

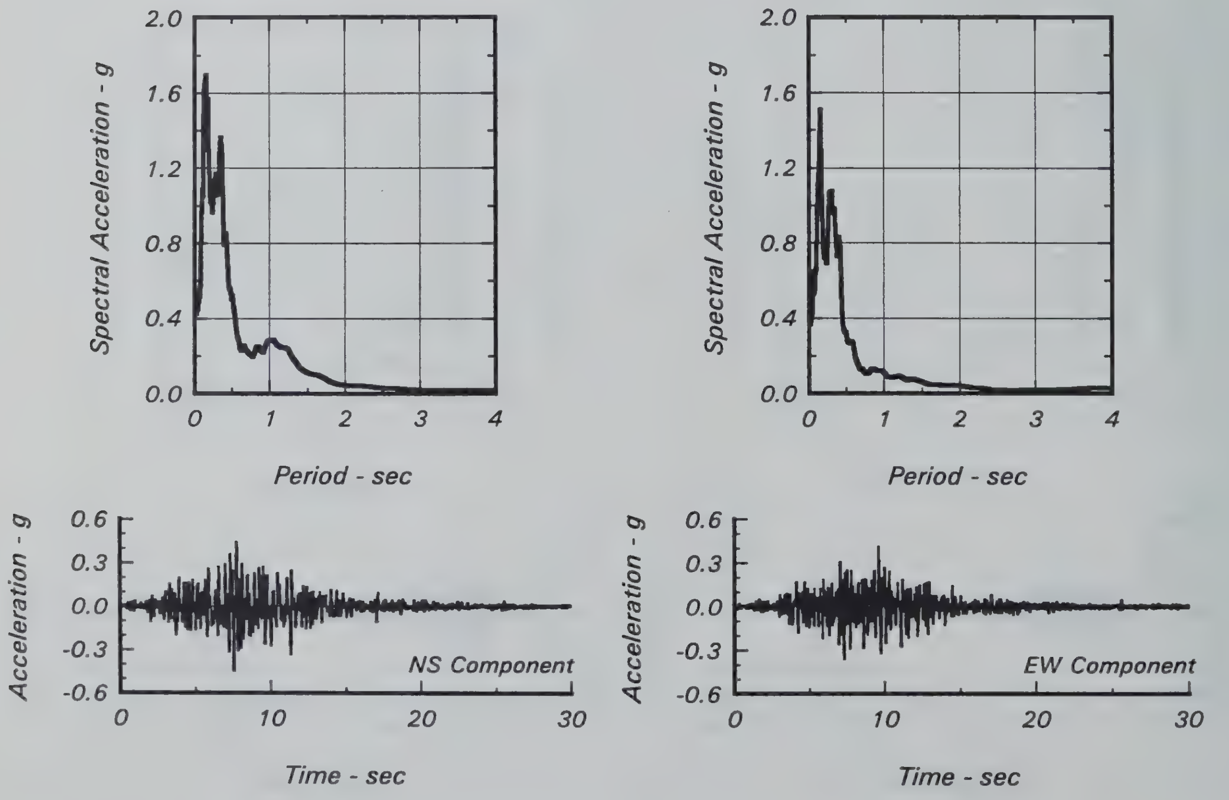

Fig. B-6 Accelerograms and Spectral Ordinates of the Horizontal Components of Earthquake Ground Motions Recorded at Santa Cruz during the Loma Prieta Earthquake

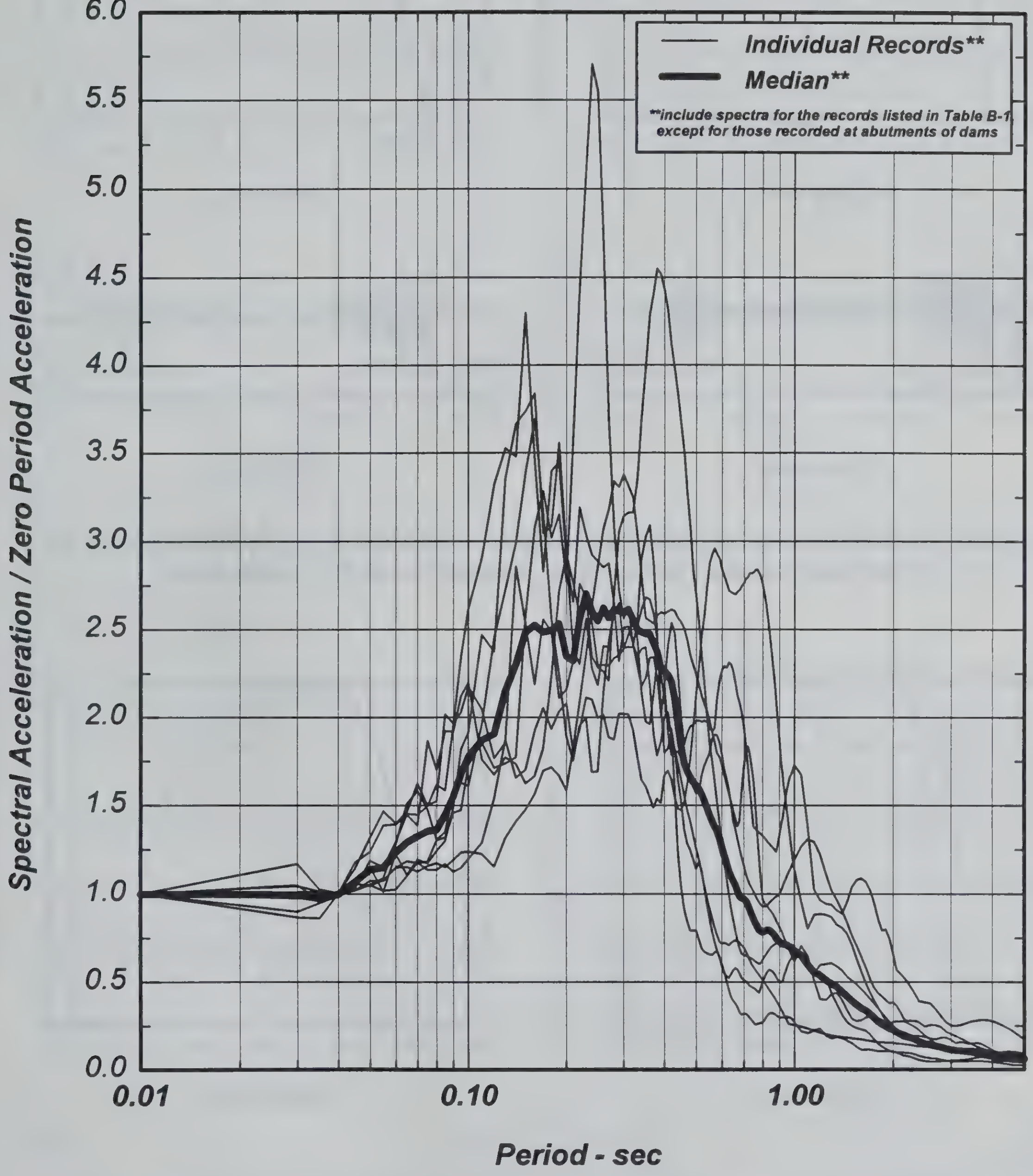

Fig. B-7 Normalized Spectra for Motions Recorded at Rock Sites within 20 km from Source During the Loma Prieta Earthquake

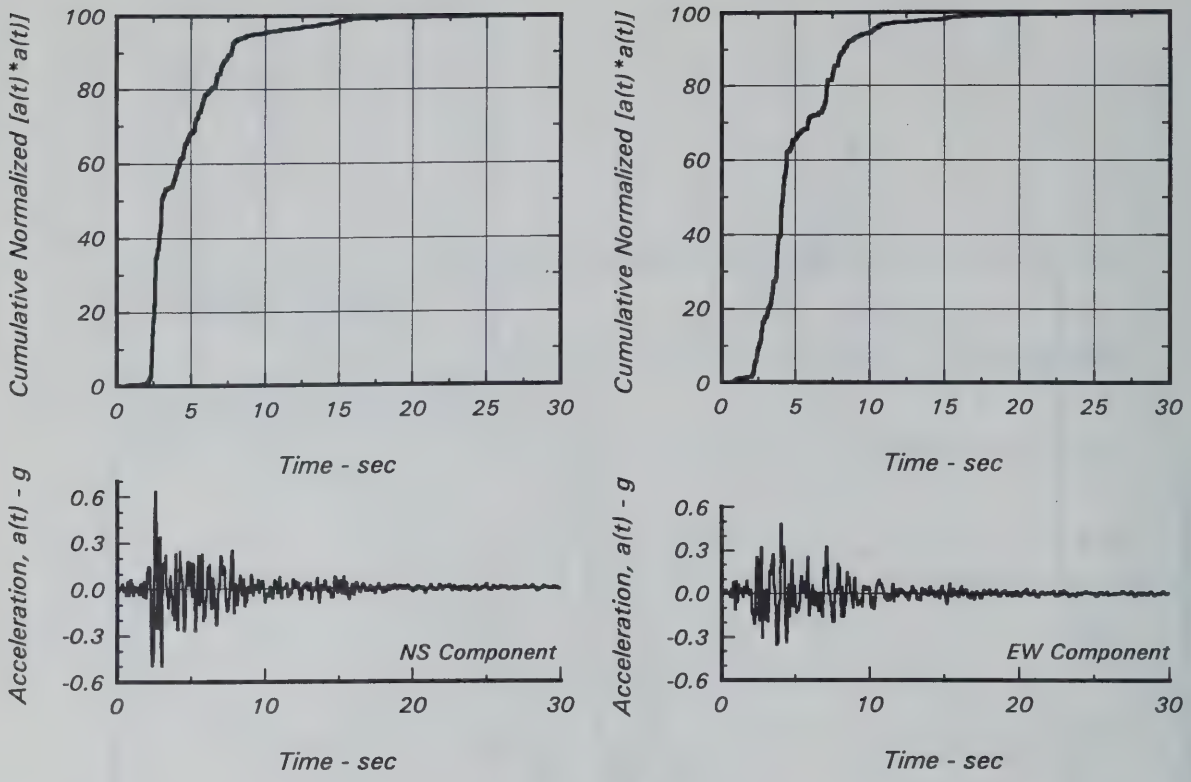

Fig. B-8 Husid Plots of Horizontal Components of Earthquake Ground Motions Recorded at Corralitos during the Loma Prieta Earthquake

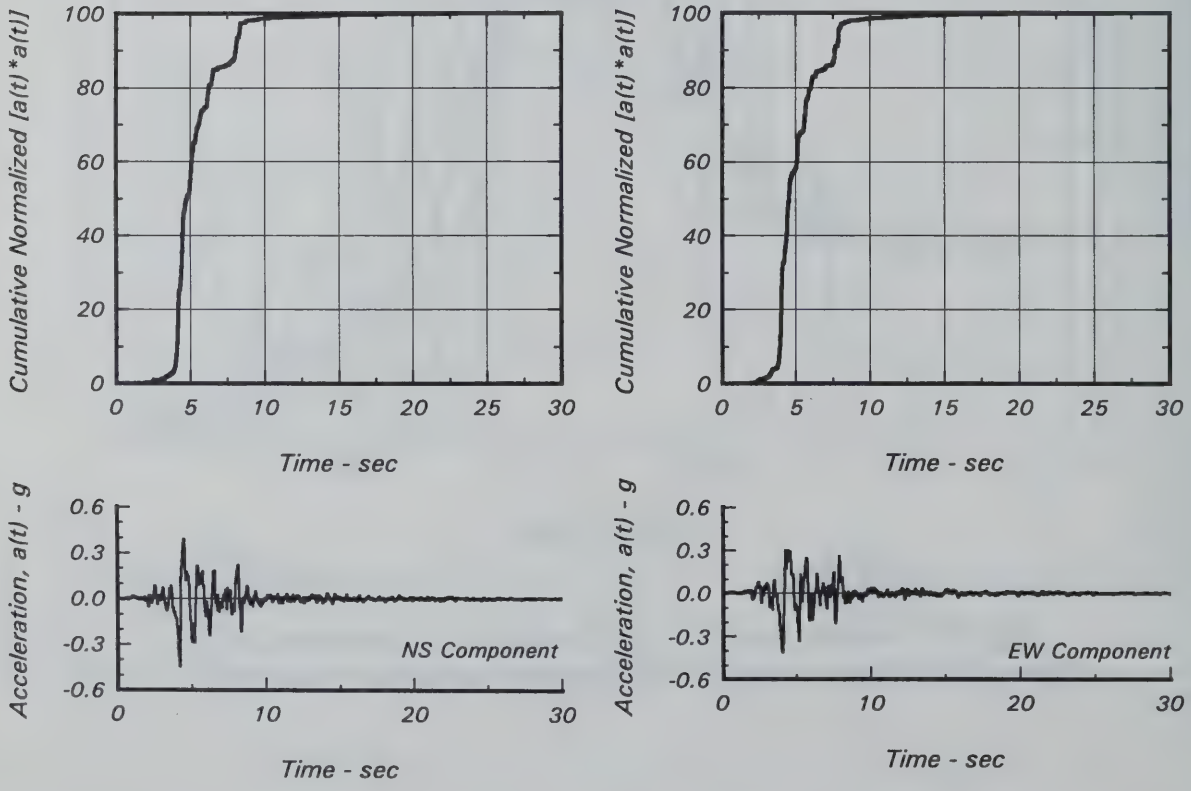

Fig. B-9 Husid Plots of Horizontal Components of Earthquake Ground Motions Recorded at Abutment of Lexington Damduring the Loma Prieta Earthquake

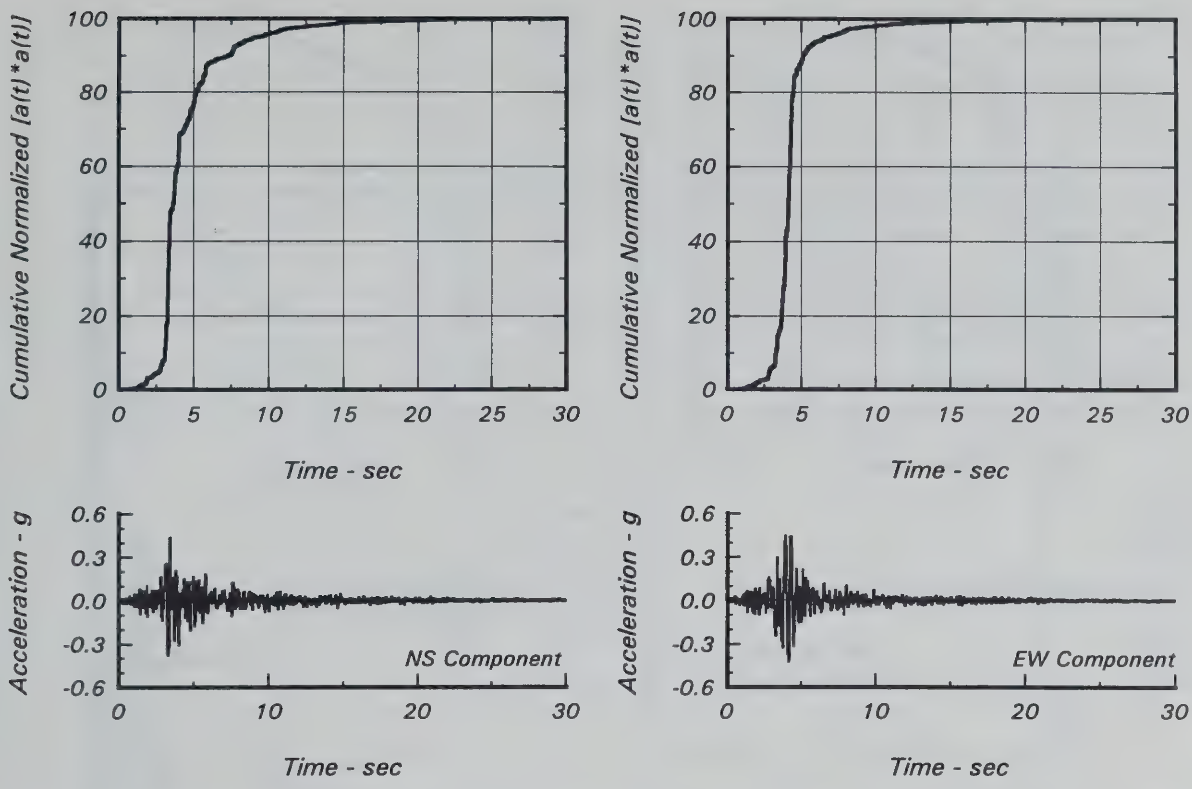

Fig. B-10 Husid Plots of Horizontal Components of Earthquake Ground Motions Recorded at Gilroy No.1 during the Loma Prieta Earthquake

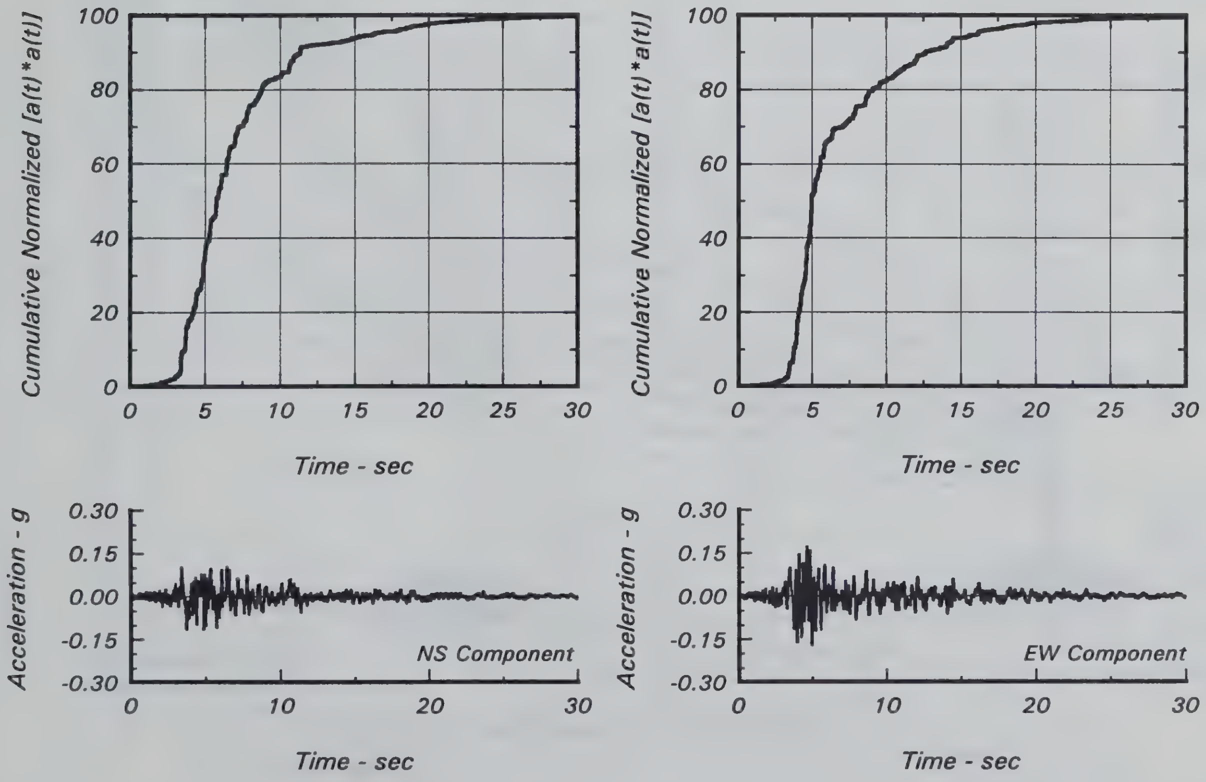

Fig. B-11 Husid Plots of Horizontal Components of Earthquake Ground Motions Recorded at Gilroy No. 6 during the Loma Prieta Earthquake

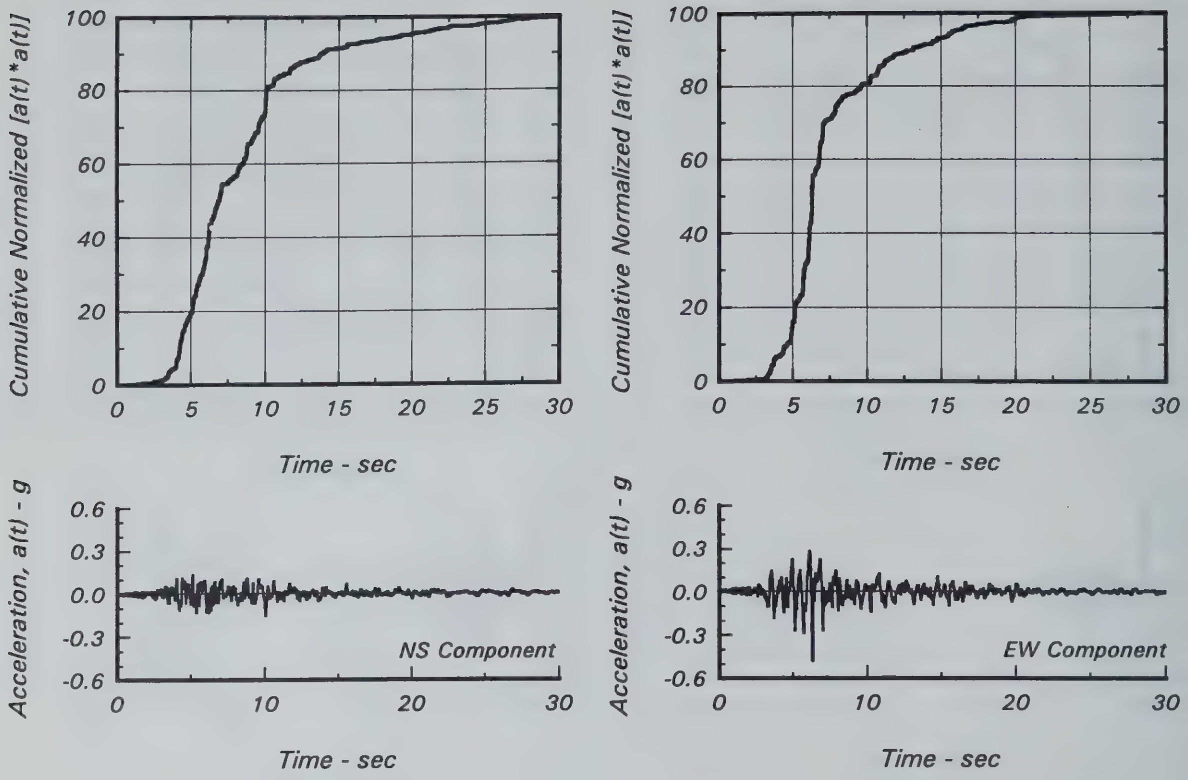

Fig. B-12 Husid Plots of Horizontal Components of Earthquake Ground Motions Recorded at Abutment of Coyote Dam during the Loma Prieta Earthquake

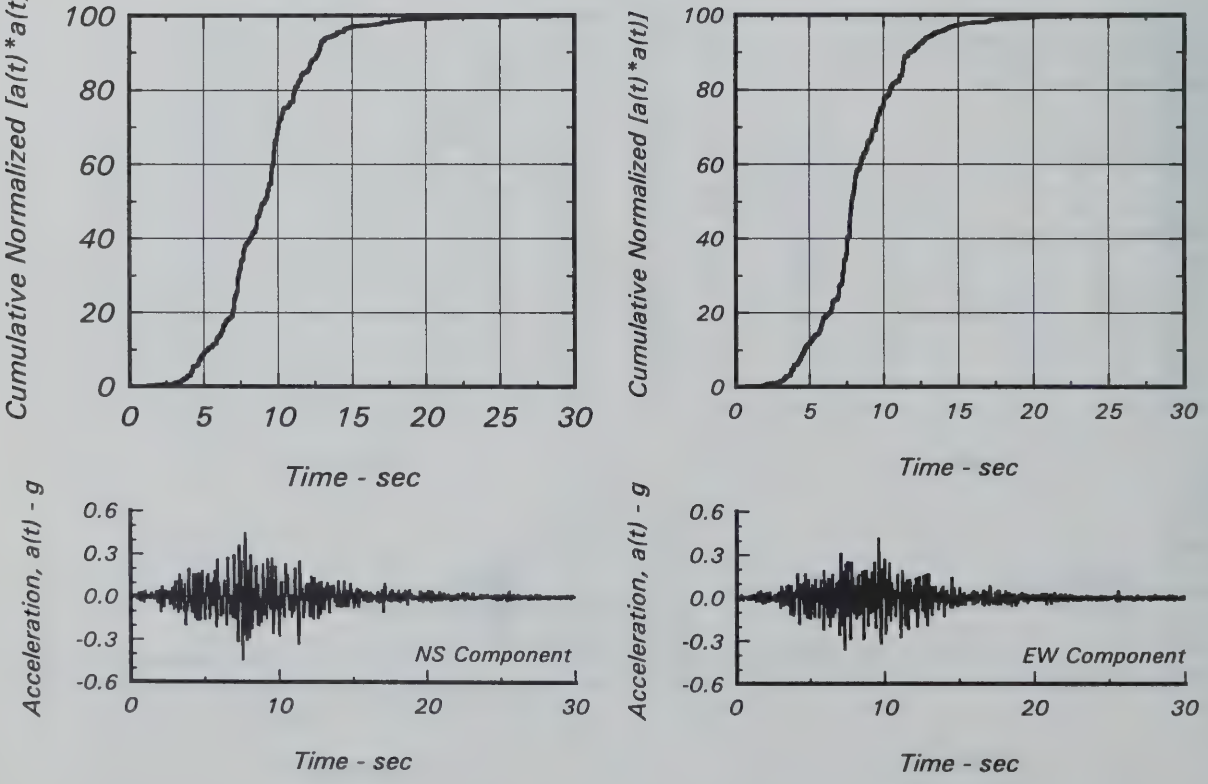

Fig. B-13 Husid Plots of Horizontal Components of Earthquake Ground Motions Recorded at Santa Cruz during the Loma Prieta Earthquake

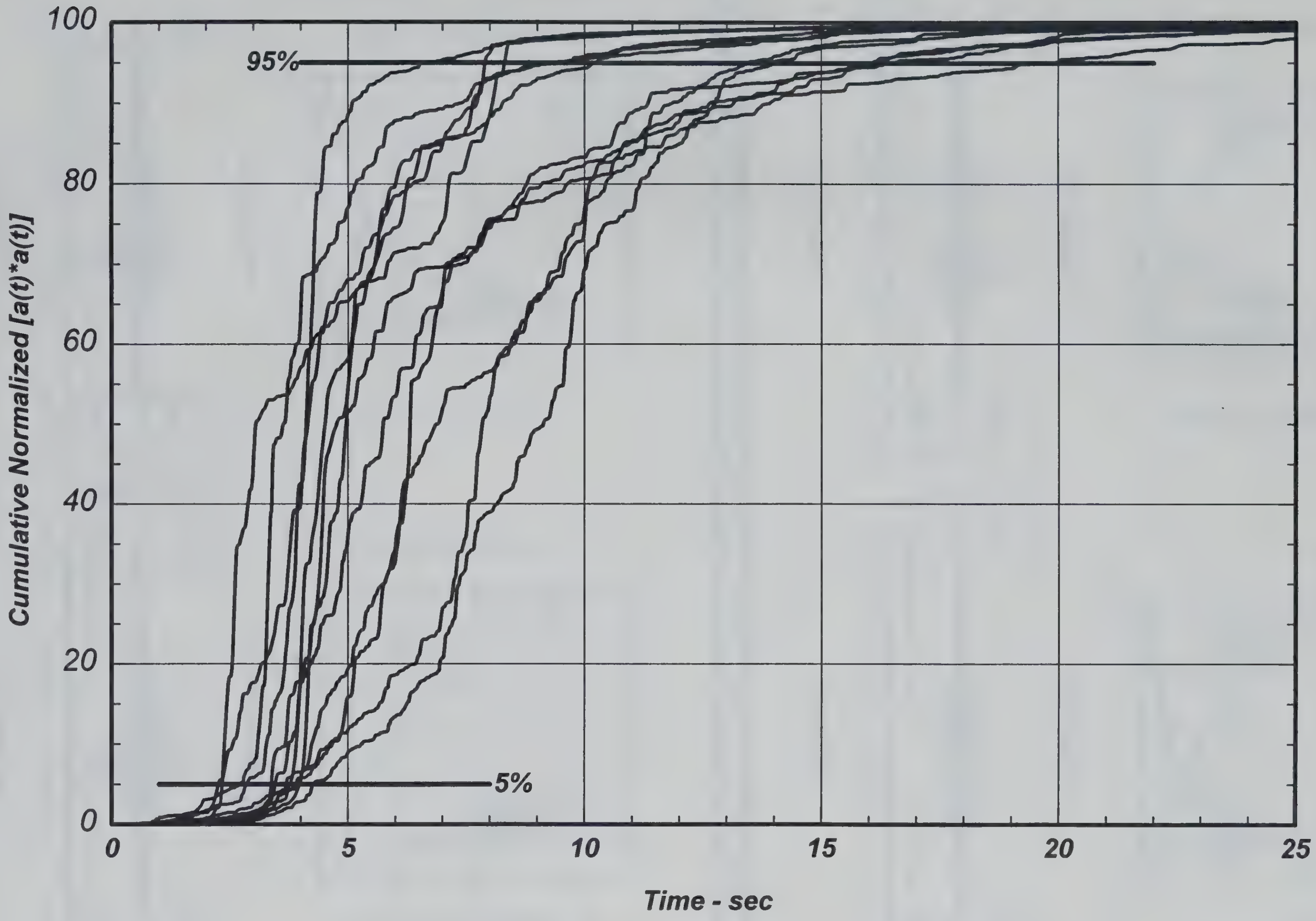

Fig. B-14 Husid Plots of Horizontal Components of Earthquake Ground Motions Recorded at Rock Sites Within a Distance of About 20 km During the Loma Prieta Earthquake

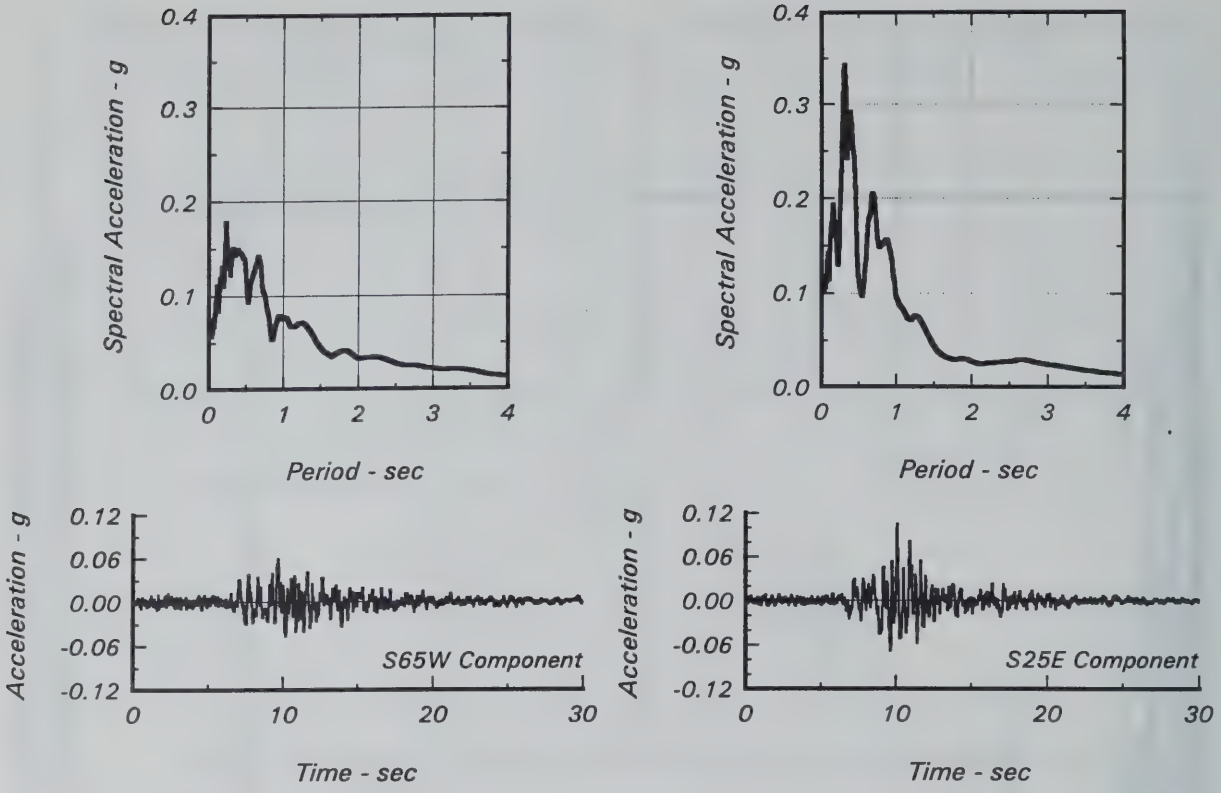

Fig. B-15 Accelerograms and Spectral Ordinates of the Horizontal Components of Earthquake Ground Motions Recorded at Sierra Point during the Loma Prieta Earthquake

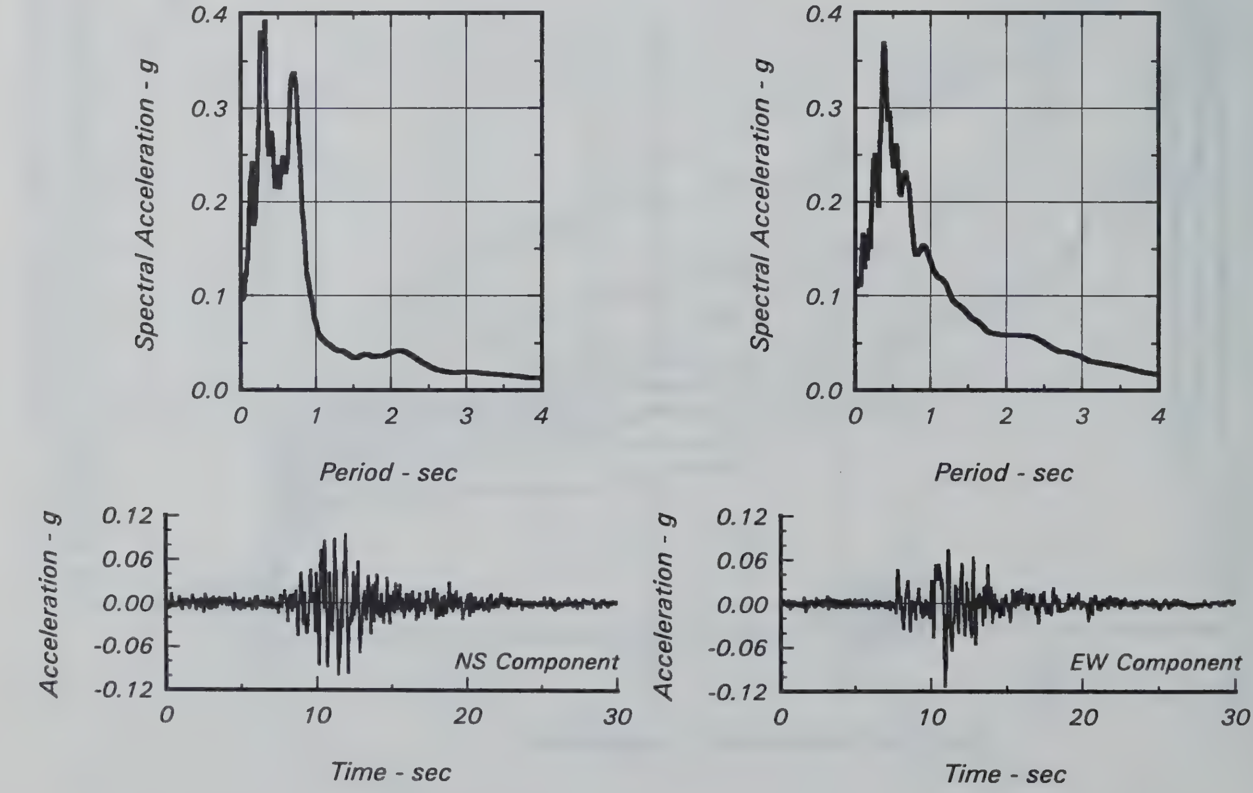

Fig. B-16 Accelerograms and Spectral Ordinates of the Horizontal Components of Earthquake Ground Motions Recorded at Diamond Heights during the Loma Prieta Earthquake

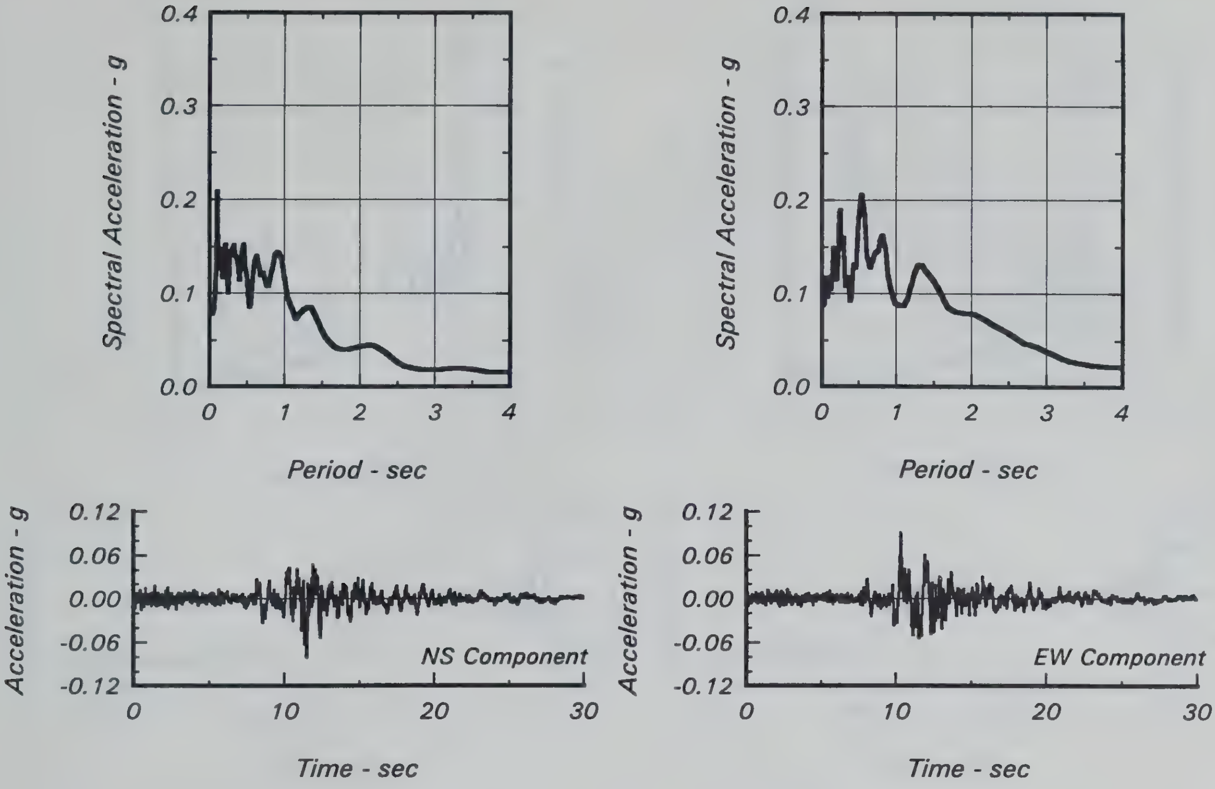

Fig. B-17 Accelerograms and Spectral Ordinates of the Horizontal Components of Earthquake Ground Motions Recorded at Rincon Hill during the Loma Prieta Earthquake

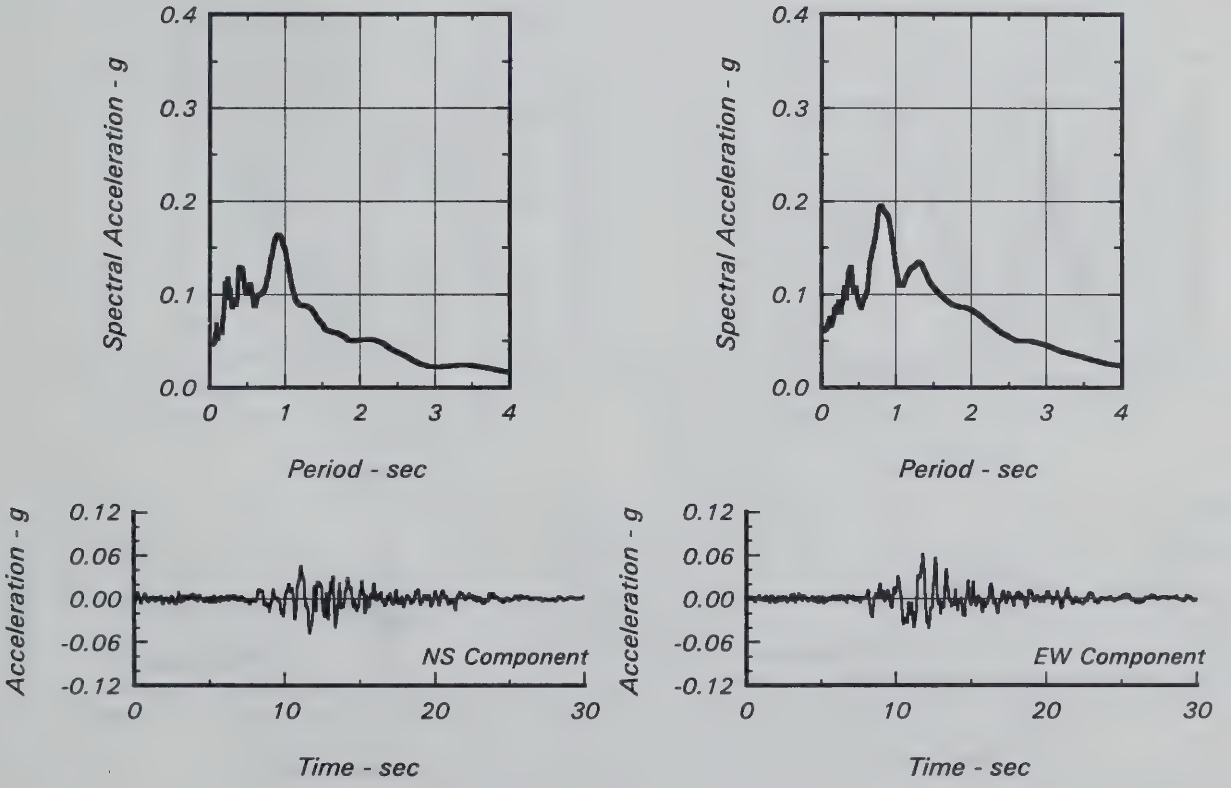

Fig. B-18 Accelerograms and Spectral Ordinates of the Horizontal Components of Earthquake Ground Motions Recorded at Pacific Heights during the Loma Prieta Earthquake

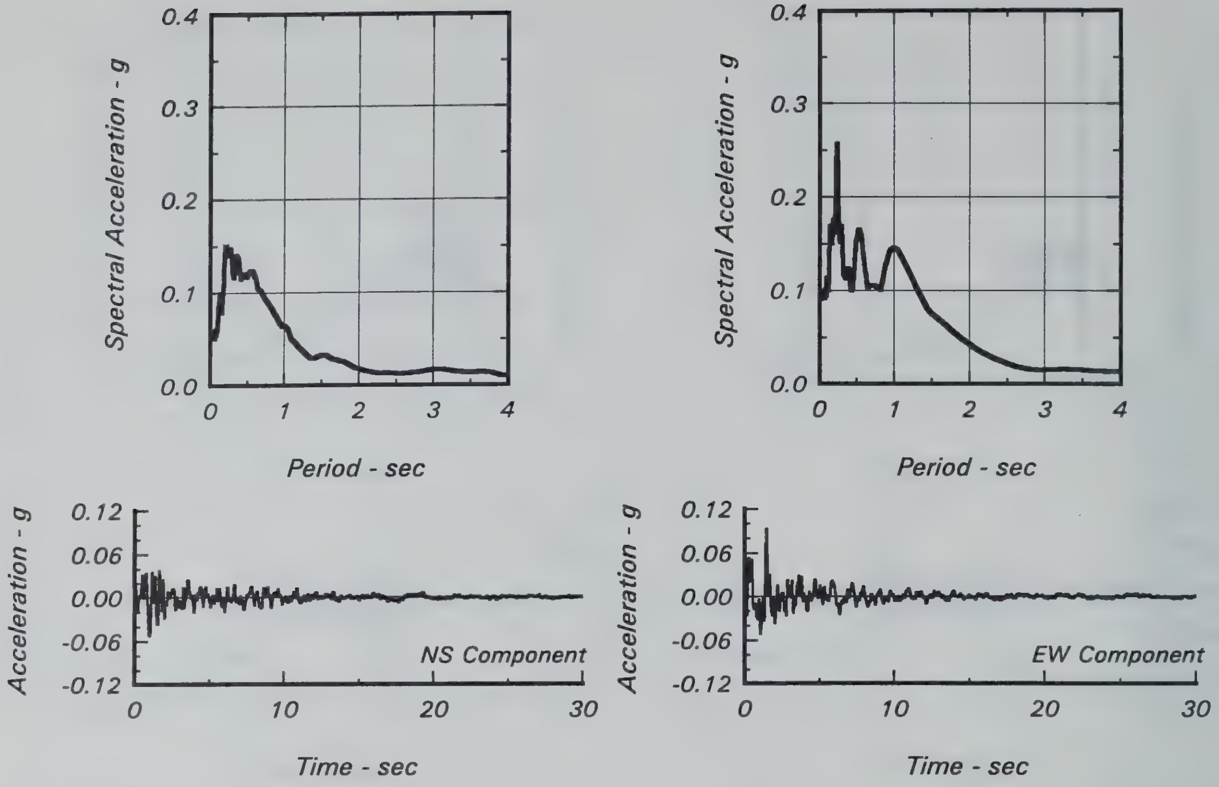

Fig. B-19 Accelerograms and Spectral Ordinates of the Horizontal Components of Earthquake Ground Motions Recorded at Telegraph Hill during the Loma Prieta Earthquake

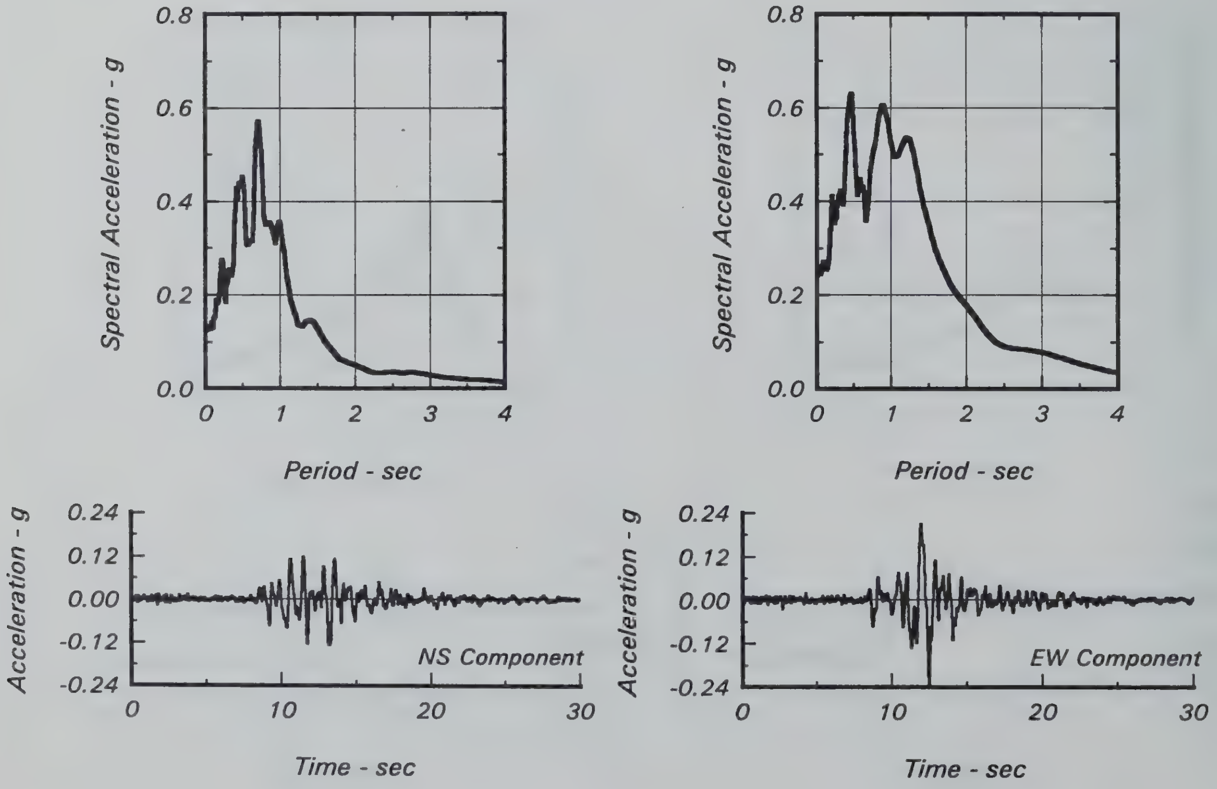

Fig. B-20 Accelerograms and Spectral Ordinates of the Horizontal Components of Earthquake Ground Motions Recorded at Golden Gate during the Loma Prieta Earthquake

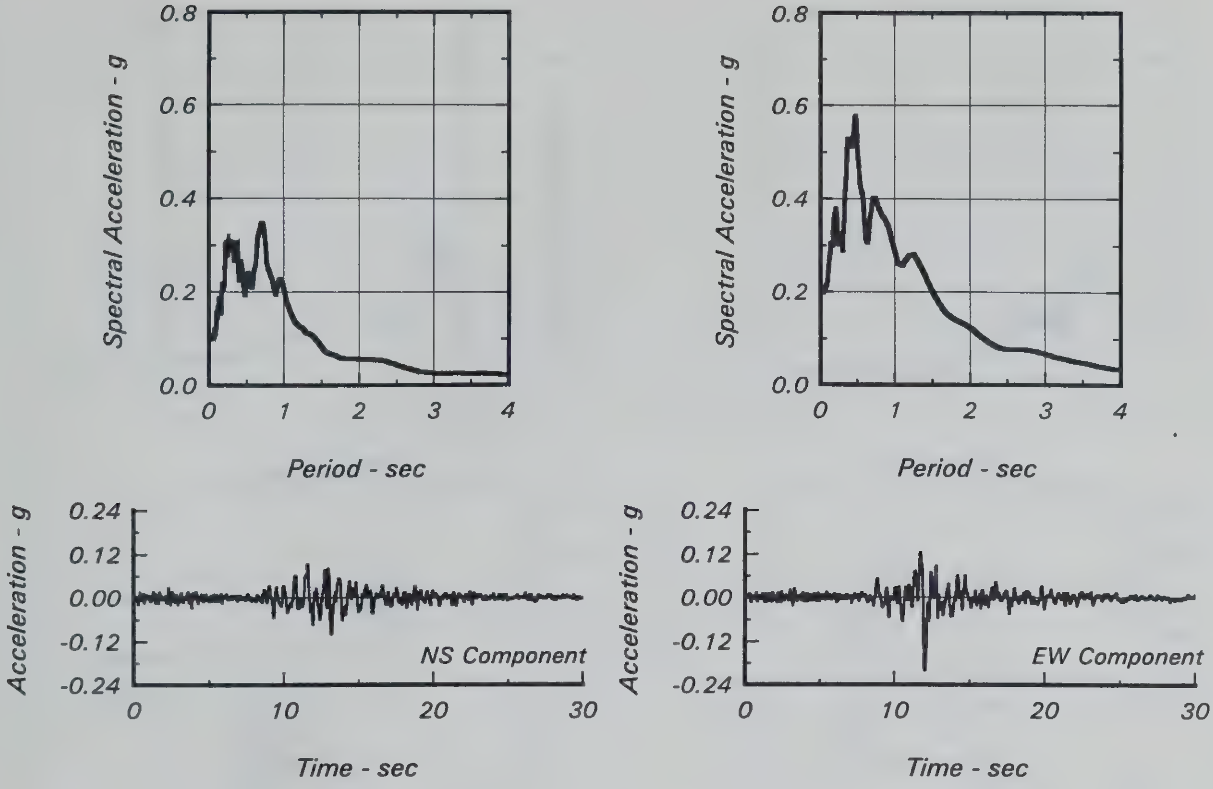

Fig. B-21 Accelerograms and Spectral Ordinates of the Horizontal Components of Earthquake Ground Motions Recorded at the Presidio during the Loma Prieta Earthquake

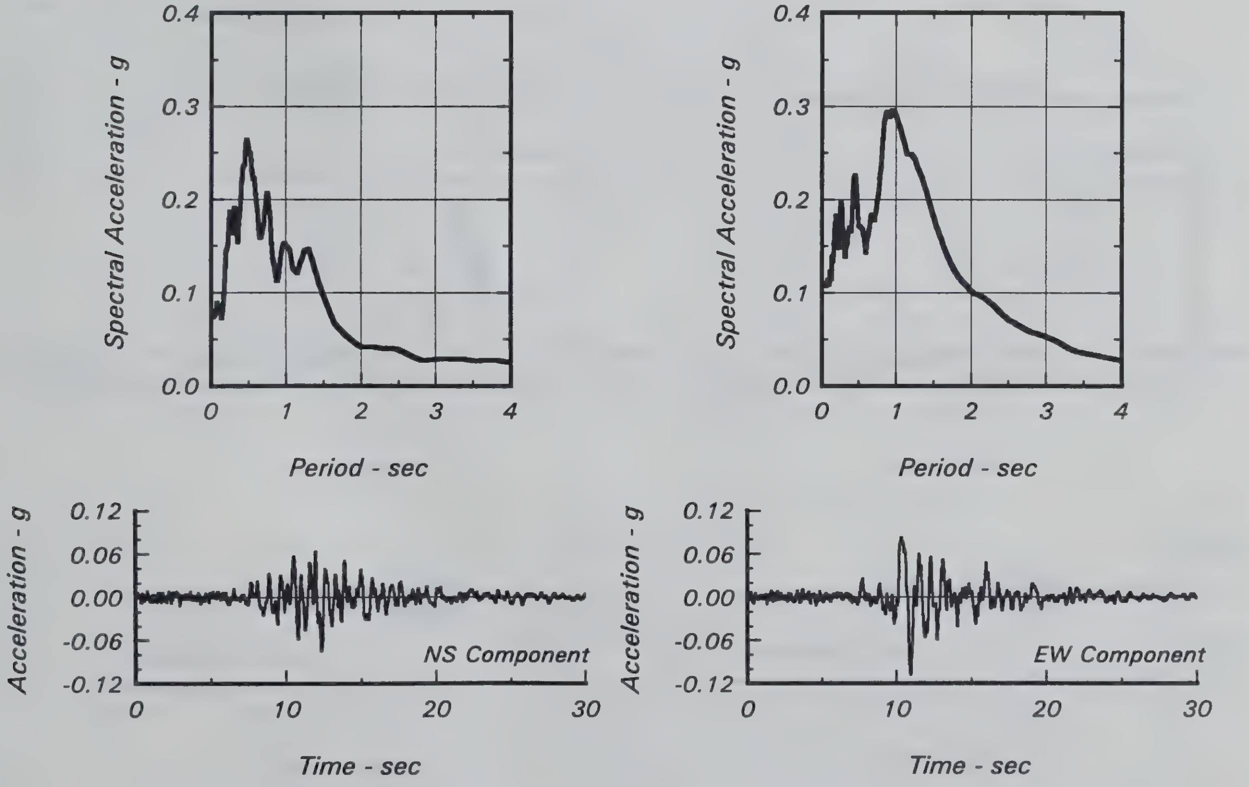

Fig. B-22 Accelerograms and Spectral Ordinates of the Horizontal Components of Earthquake Ground Motions Recorded at the Cliff House during the Loma Prieta Earthquake

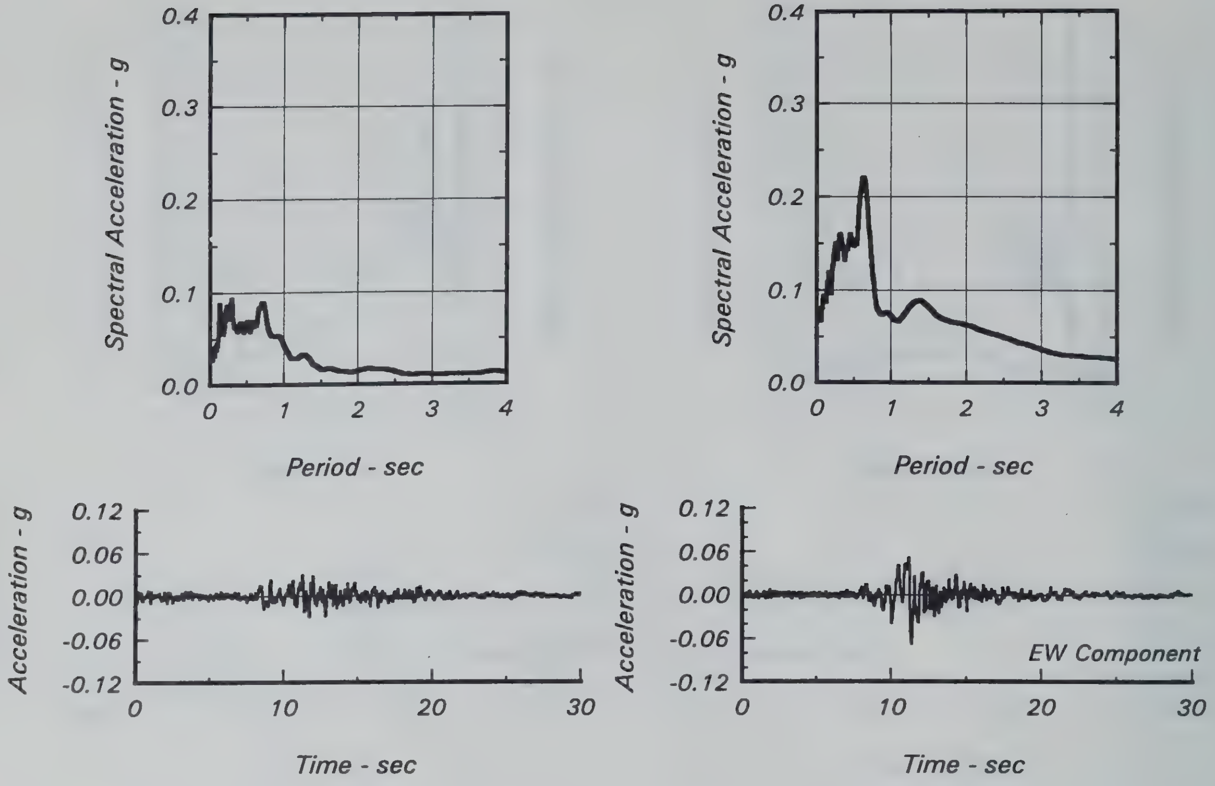

Fig. B-23 Accelerograms and Spectral Ordinates of the Horizontal Components of Earthquake Ground Motions Recorded at Yerba Buena Island during the Loma Prieta Earthquake

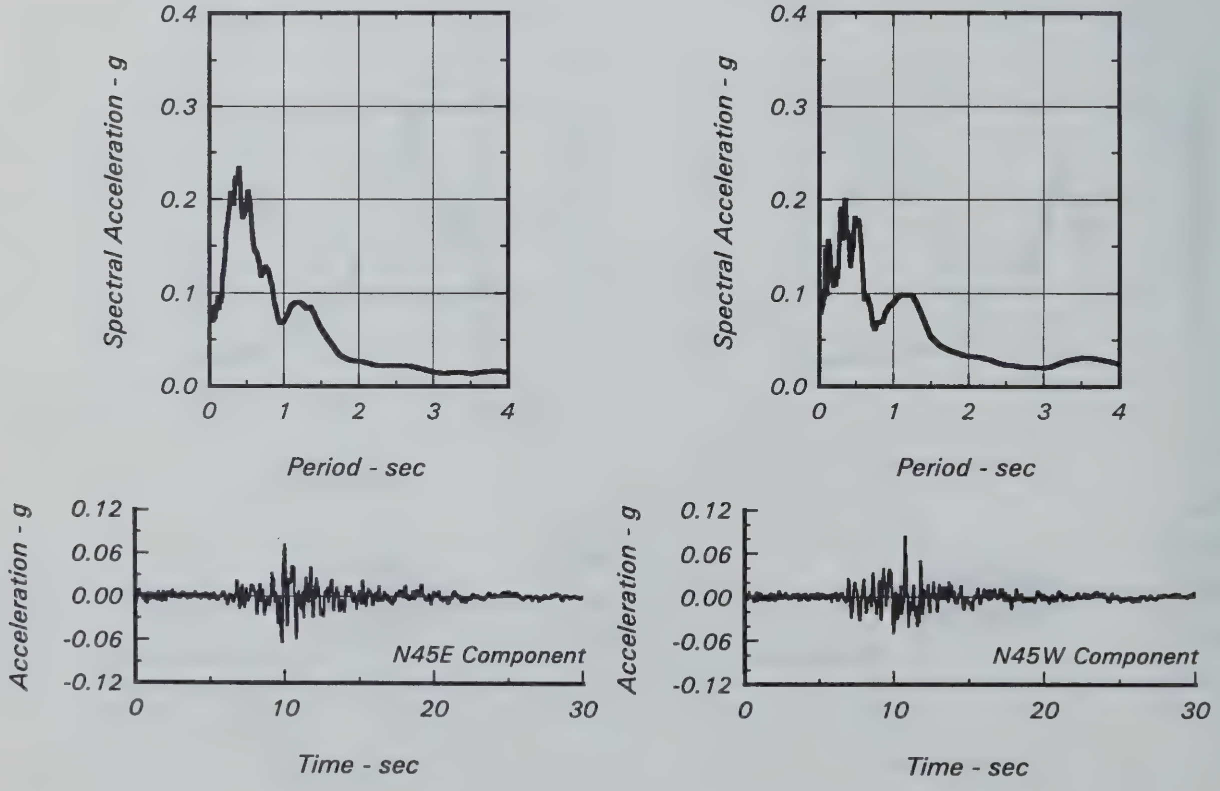

Fig. B-24 Accelerograms and Spectral Ordinates of the Horizontal Components of Earthquake Ground Motions Recorded at Piedmontd during the Loma Prieta Earthquake

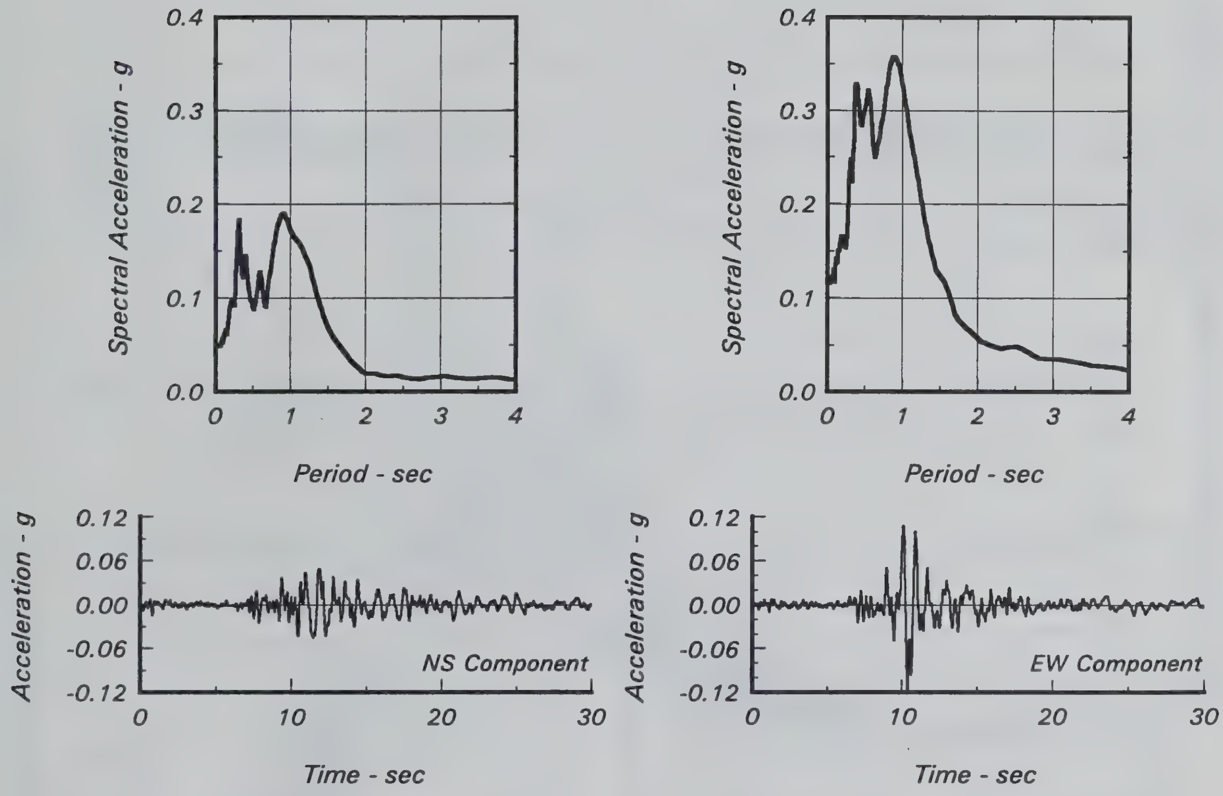

Fig. B-25 Accelerograms and Spectral Ordinates of the Horizontal Components of Earthquake Ground Motions Recorded at Lawrence Berkeley Lab during the Loma Prieta Earthquake

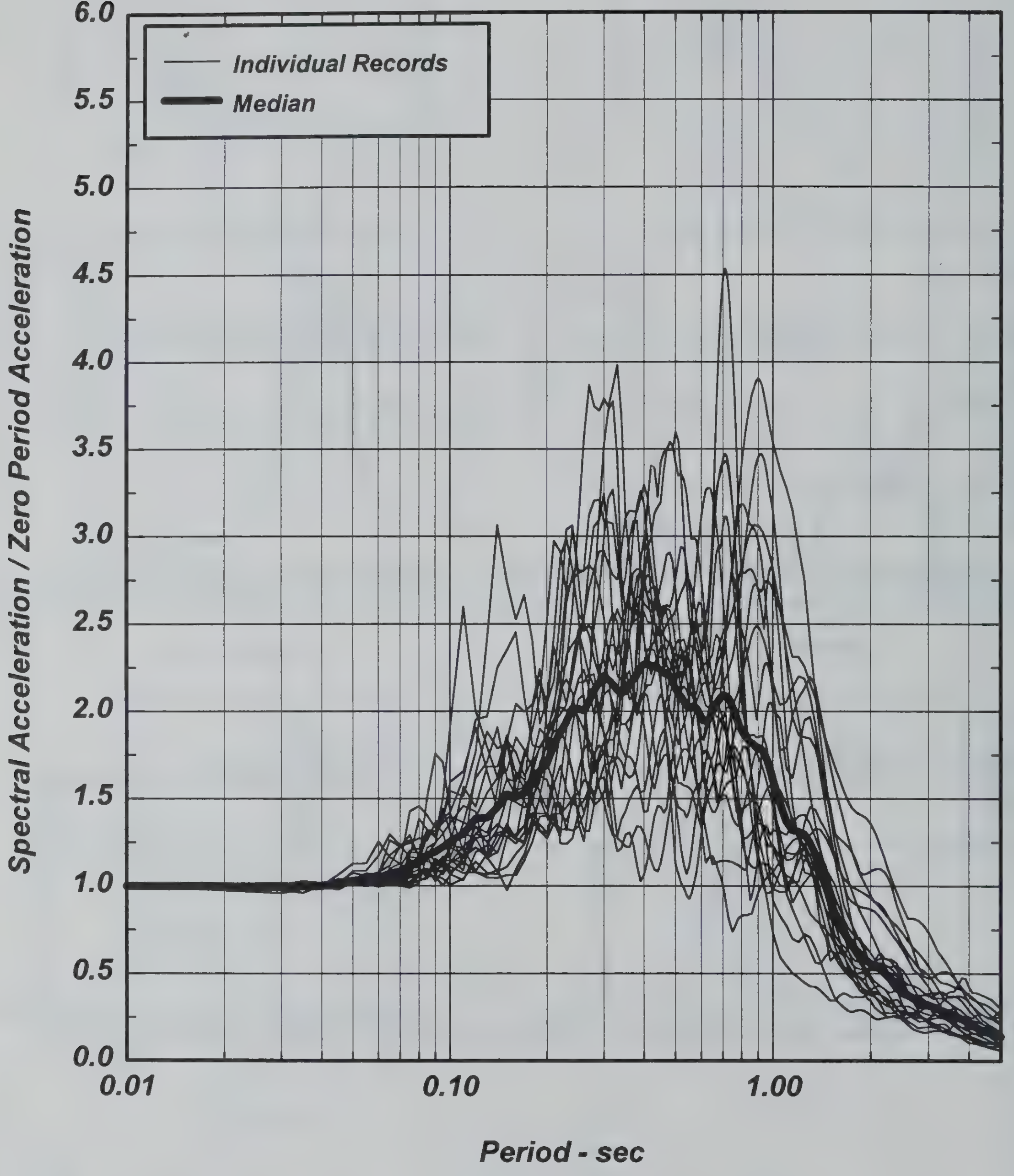

Fig. B-26 Normalized Spectra for Motions Recorded at Rock Sites in the San Francisco Bay Area during the Loma Prieta Earthquake

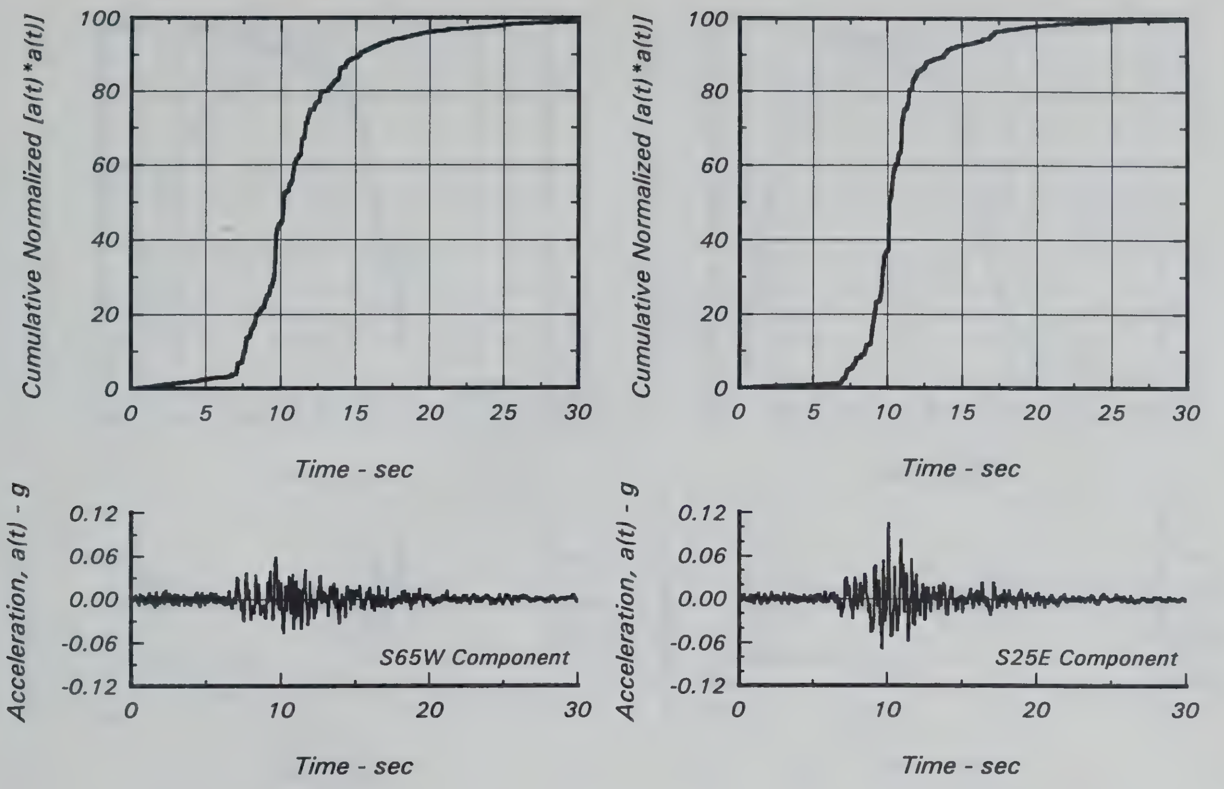

Fig. B-27 Husid Plots of Horizontal Components of Earthquake Ground Motions Recorded at Sierra Point during the Loma Prieta Earthquake

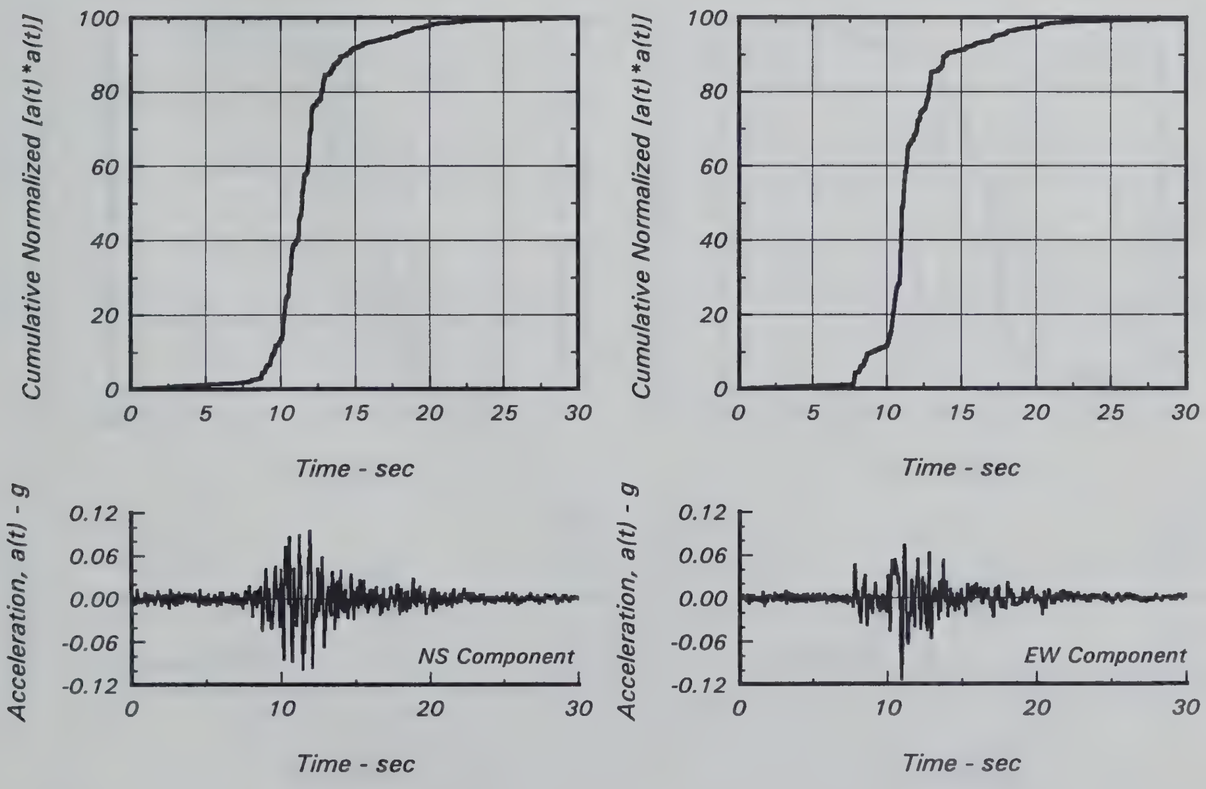

Fig. B-28 Husid Plots of Horizontal Components of Earthquake Ground Motions Recorded at Diamond Heights during the Loma Prieta Earthquake

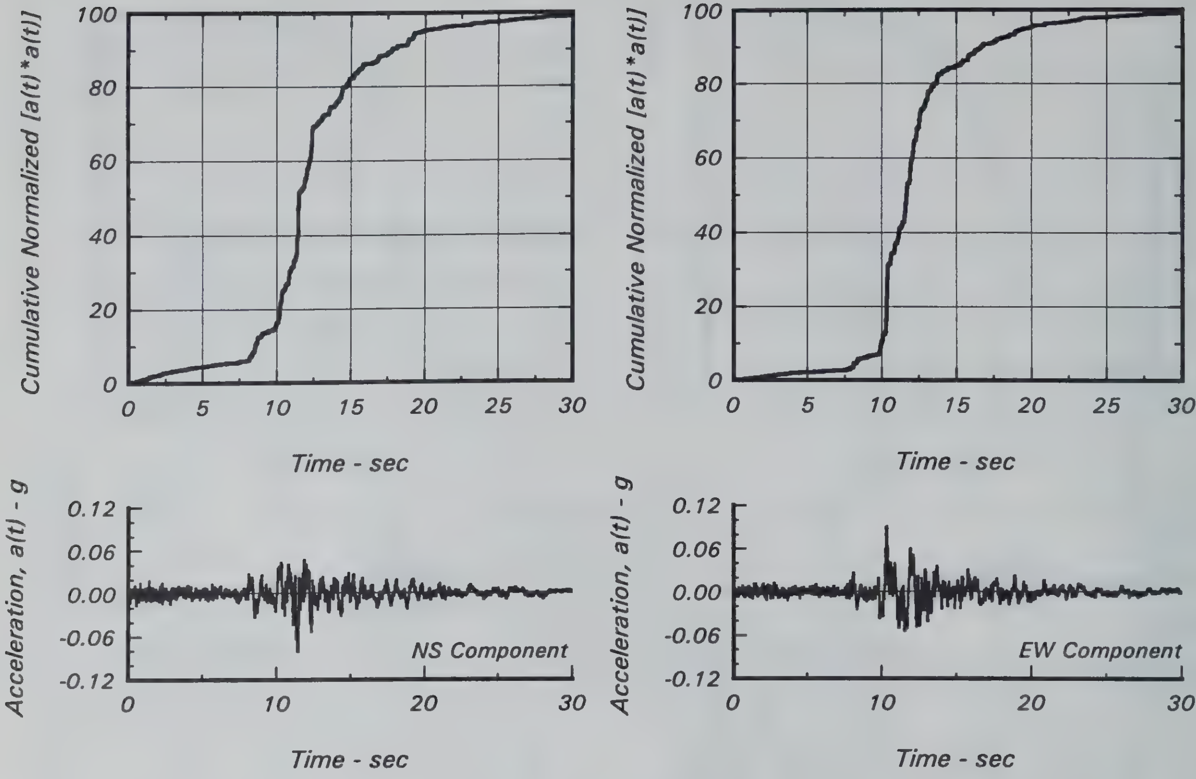

Fig. B-29 Husid Plots of Horizontal Components of Earthquake Ground Motions Recorded at Rincon Hill during the Loma Prieta Earthquake

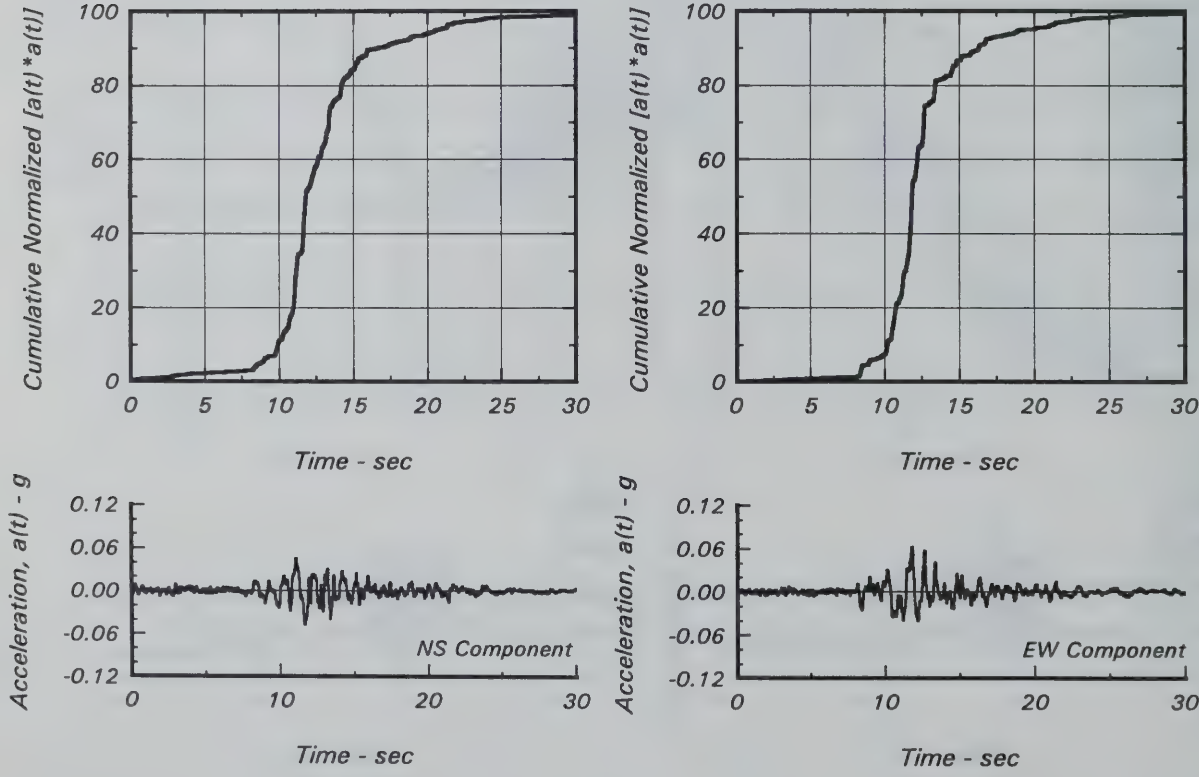

Fig. B-30 Husid Plots of Horizontal Components of Earthquake Ground Motions Recorded at Pacific Heights during the Loma Prieta Earthquake

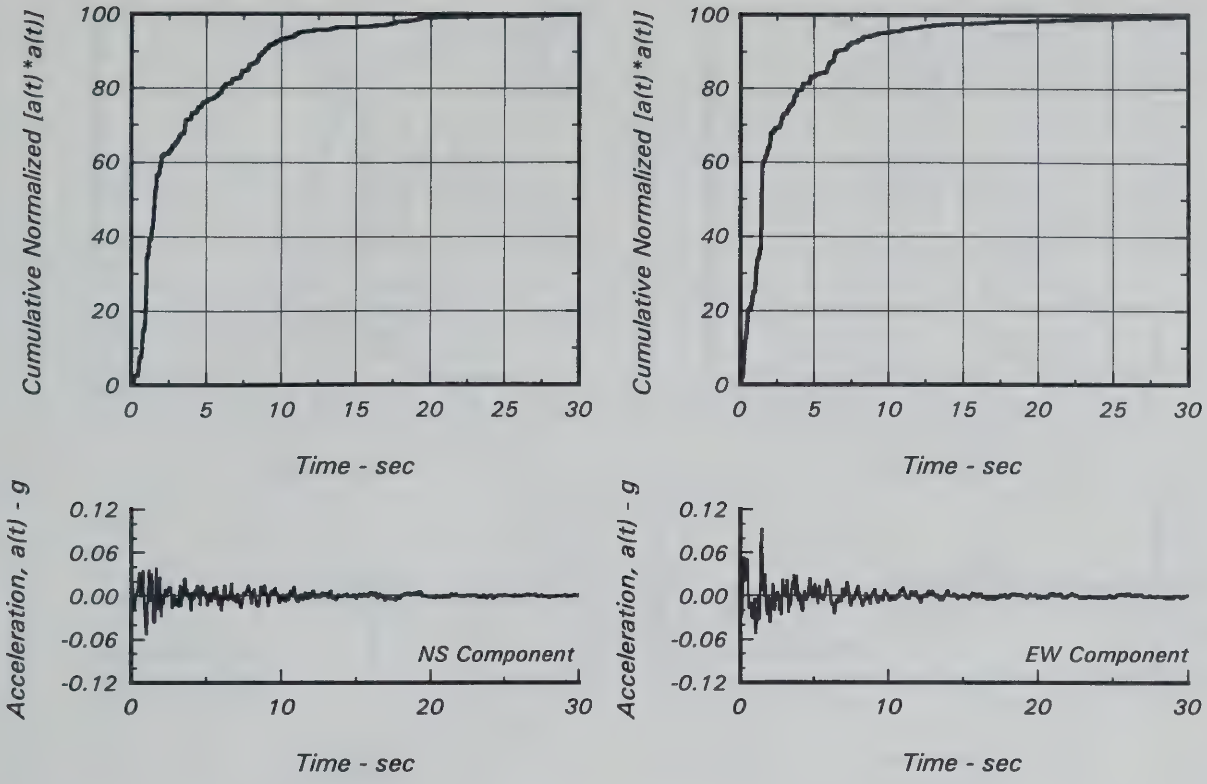

Fig. B-31 Husid Plots of Horizontal Components of Earthquake Ground Motions Recorded at Telegraph Hill during the Loma Prieta Earthquake

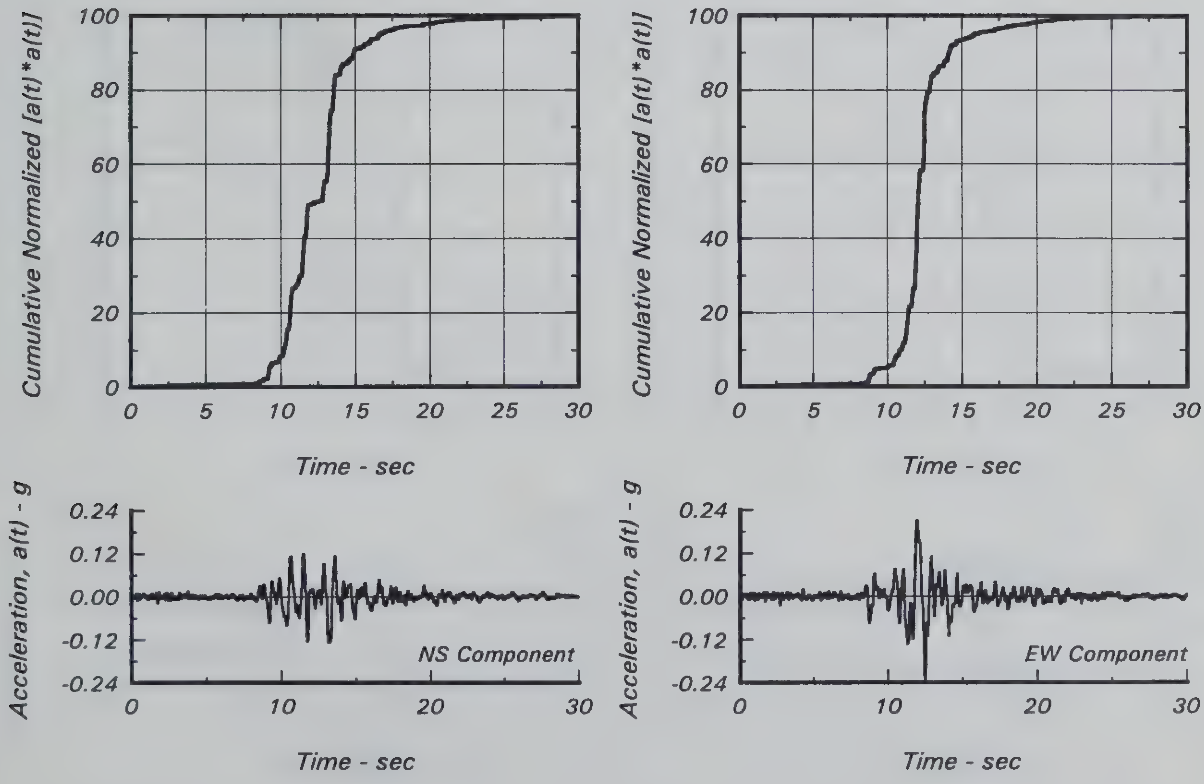

Fig. B-32 Husid Plots of Horizontal Components of Earthquake Ground Motions Recorded at Golden Gate during the Loma Prieta Earthquake

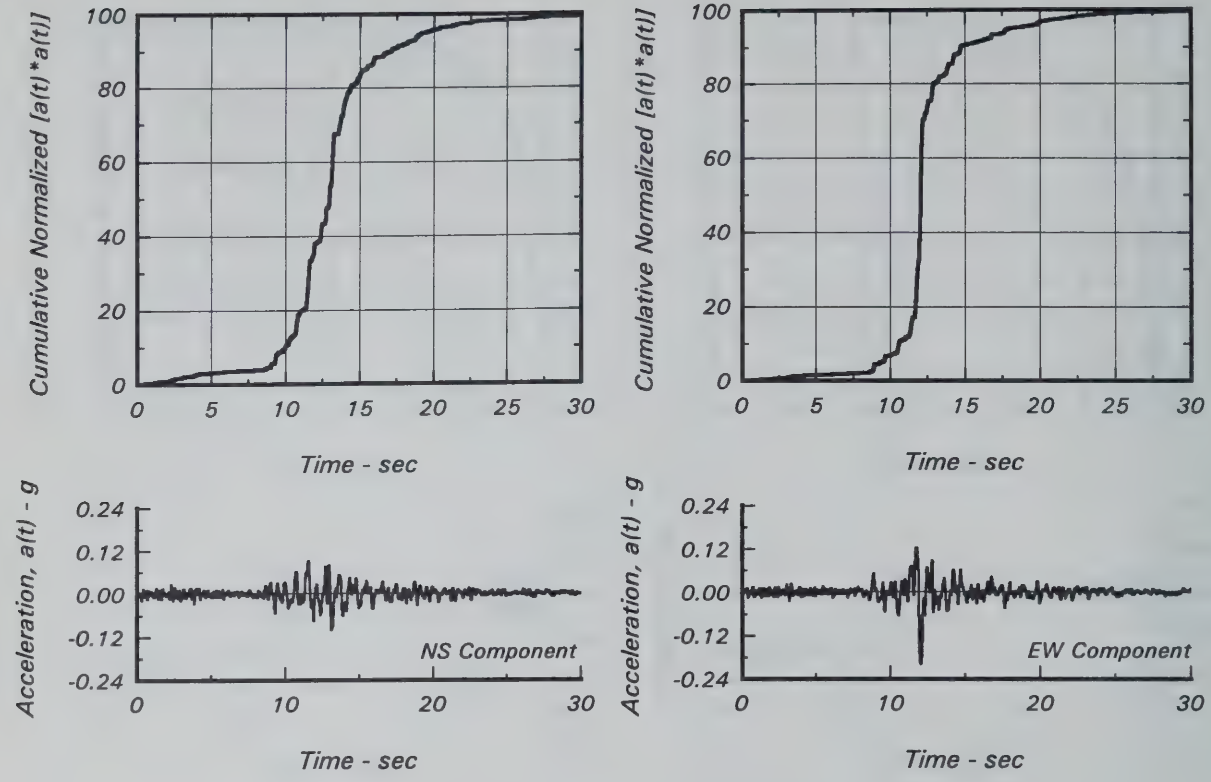

Fig. B-33 Husid Plots of Horizontal Components of Earthquake Ground Motions Recorded at the Presidio during the Loma Prieta Earthquake

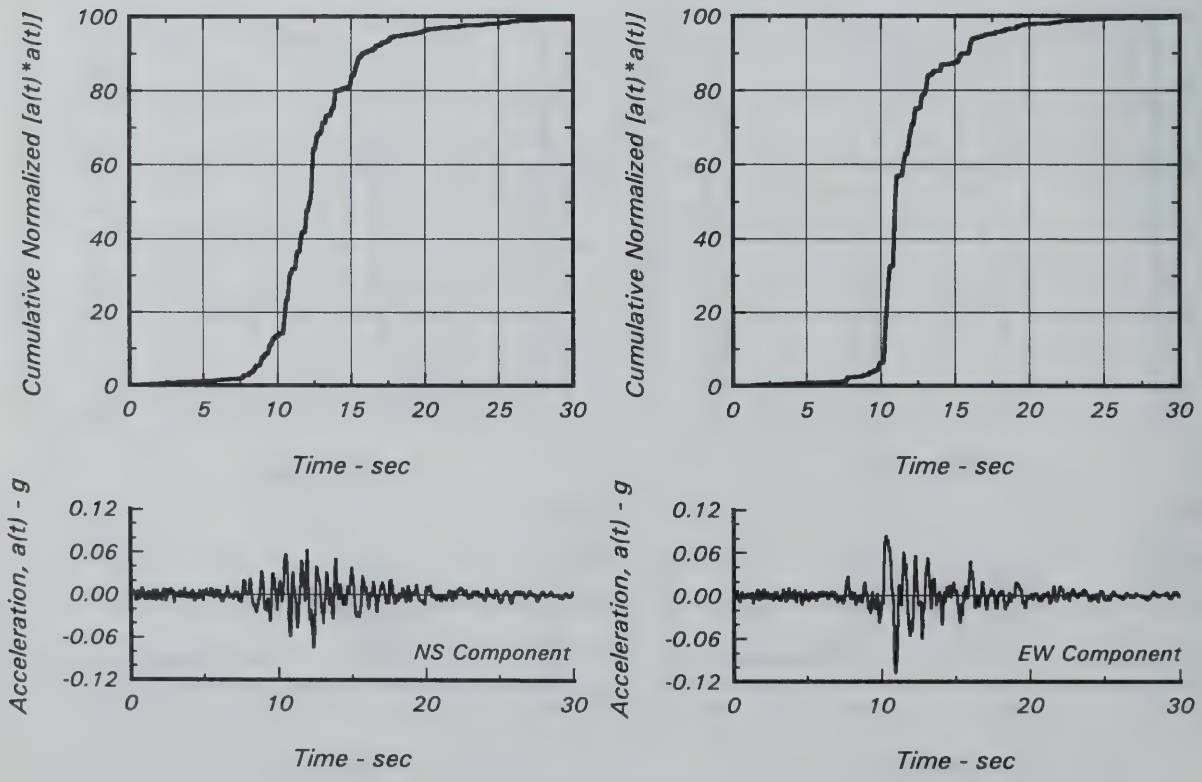

Fig. B-34 Husid Plots of Horizontal Components of Earthquake Ground Motions Recorded at the Cliff House during the Loma Prieta Earthquake

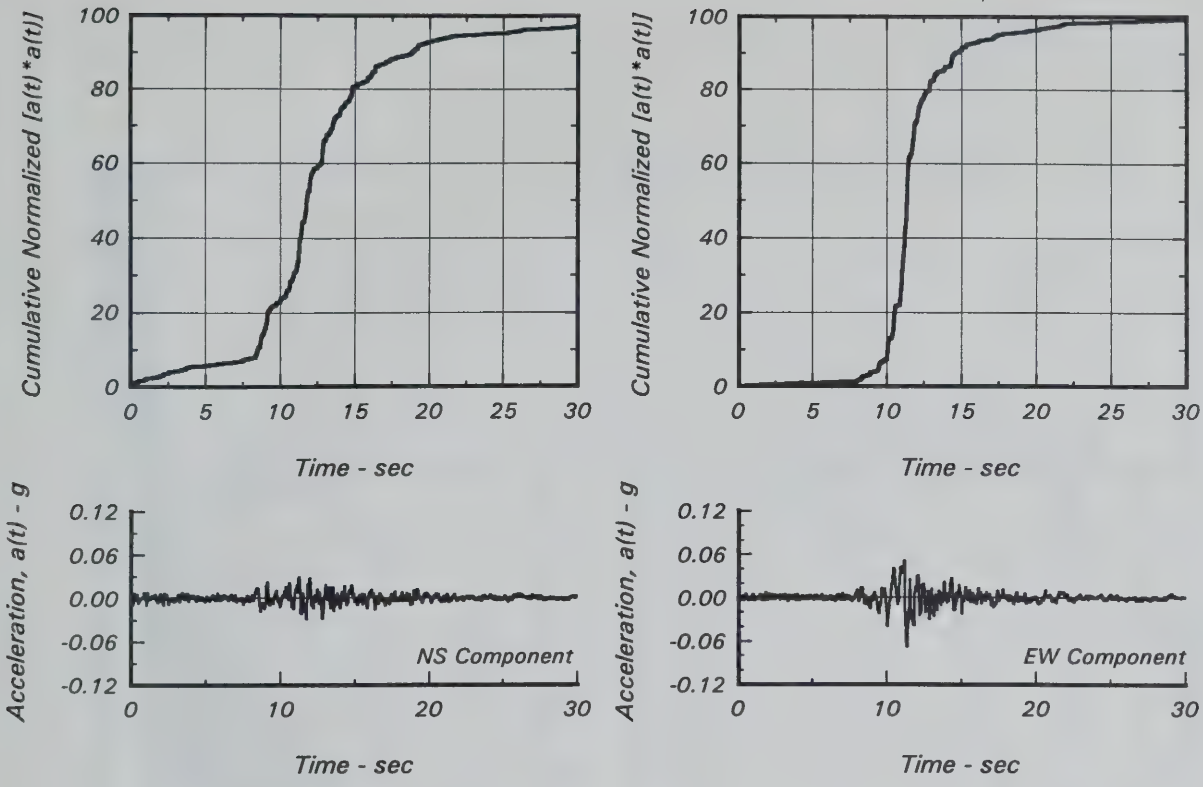

Fig. B-35 Husid Plots of Horizontal Components of Earthquake Ground Motions Recorded at Yerba Buena Island during the Loma Prieta Earthquake

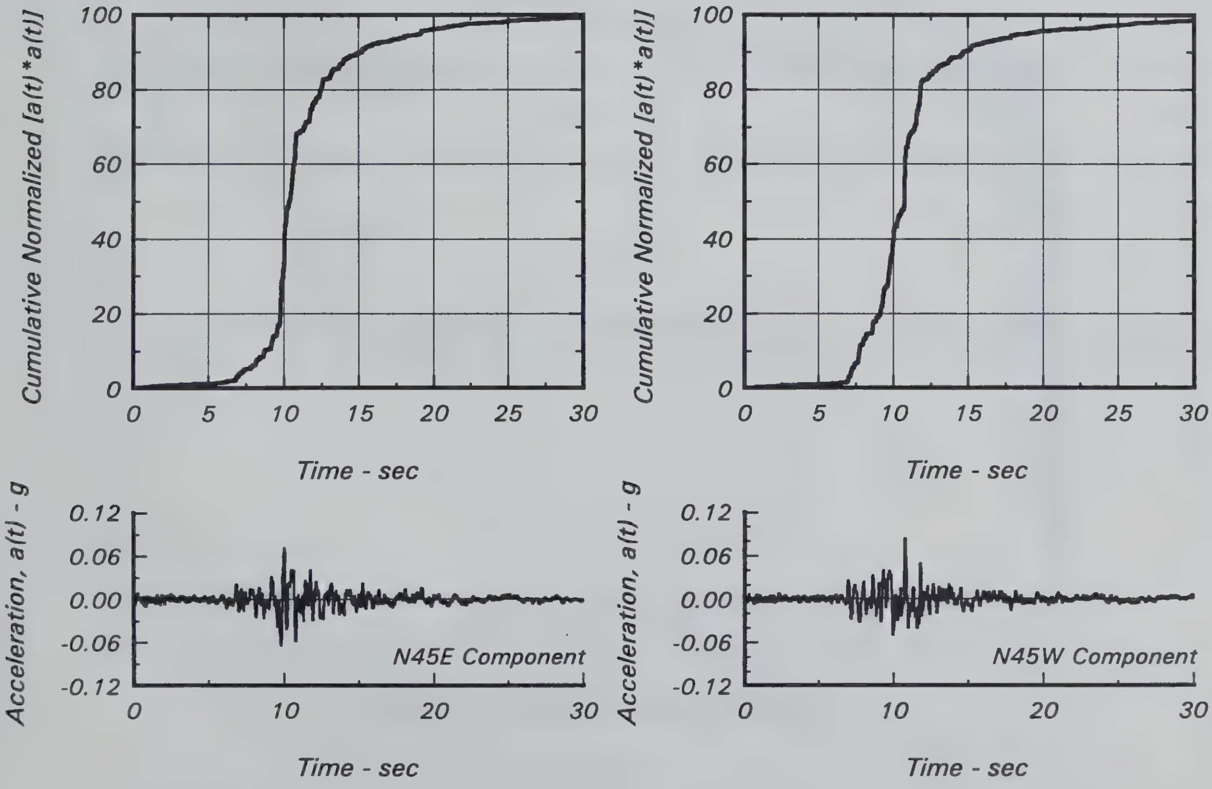

Fig. B-36 Husid Plots of Horizontal Components of Earthquake Ground Motions Recorded at Piedmont during the Loma Prieta Earthquake

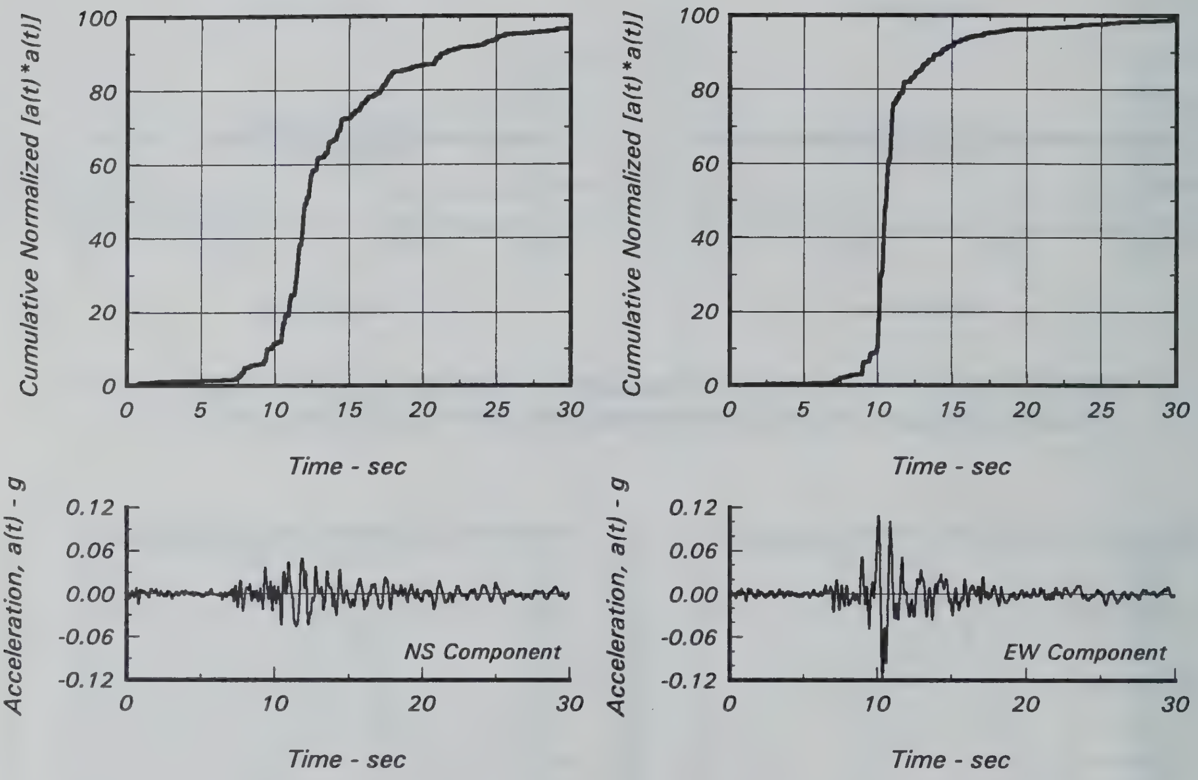

Fig. B-37 Husid Plots of Horizontal Components of Earthquake Ground Motions Recorded at Lawrence Berkeley Laboratory during the Loma Prieta Earthquake

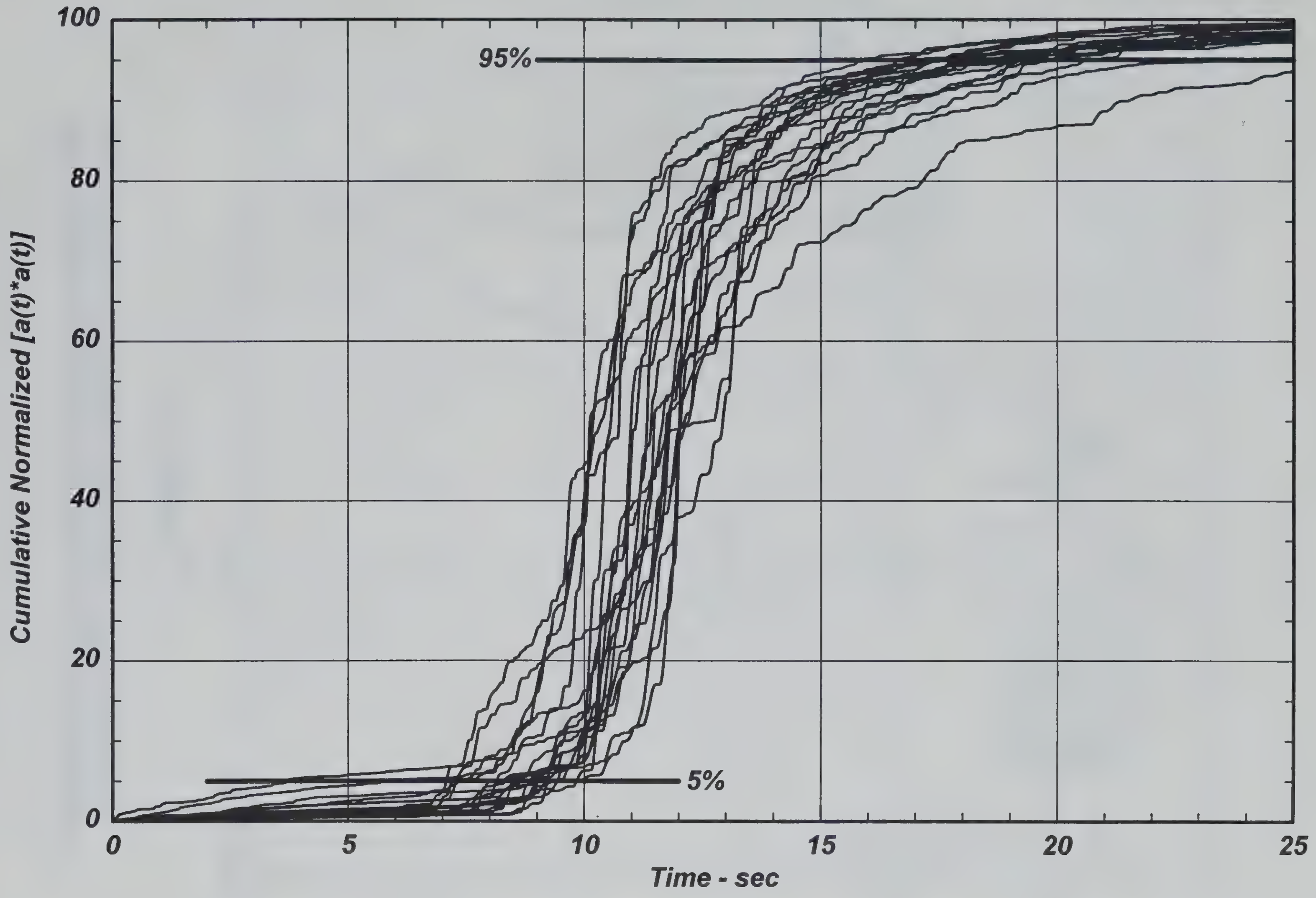

Fig. B-38 Husid Plots of Horizontal Components of Earthquake Ground Motions Recorded at Rock Sites in the San Francisco Bay Area During the Loma Prieta Earthquake

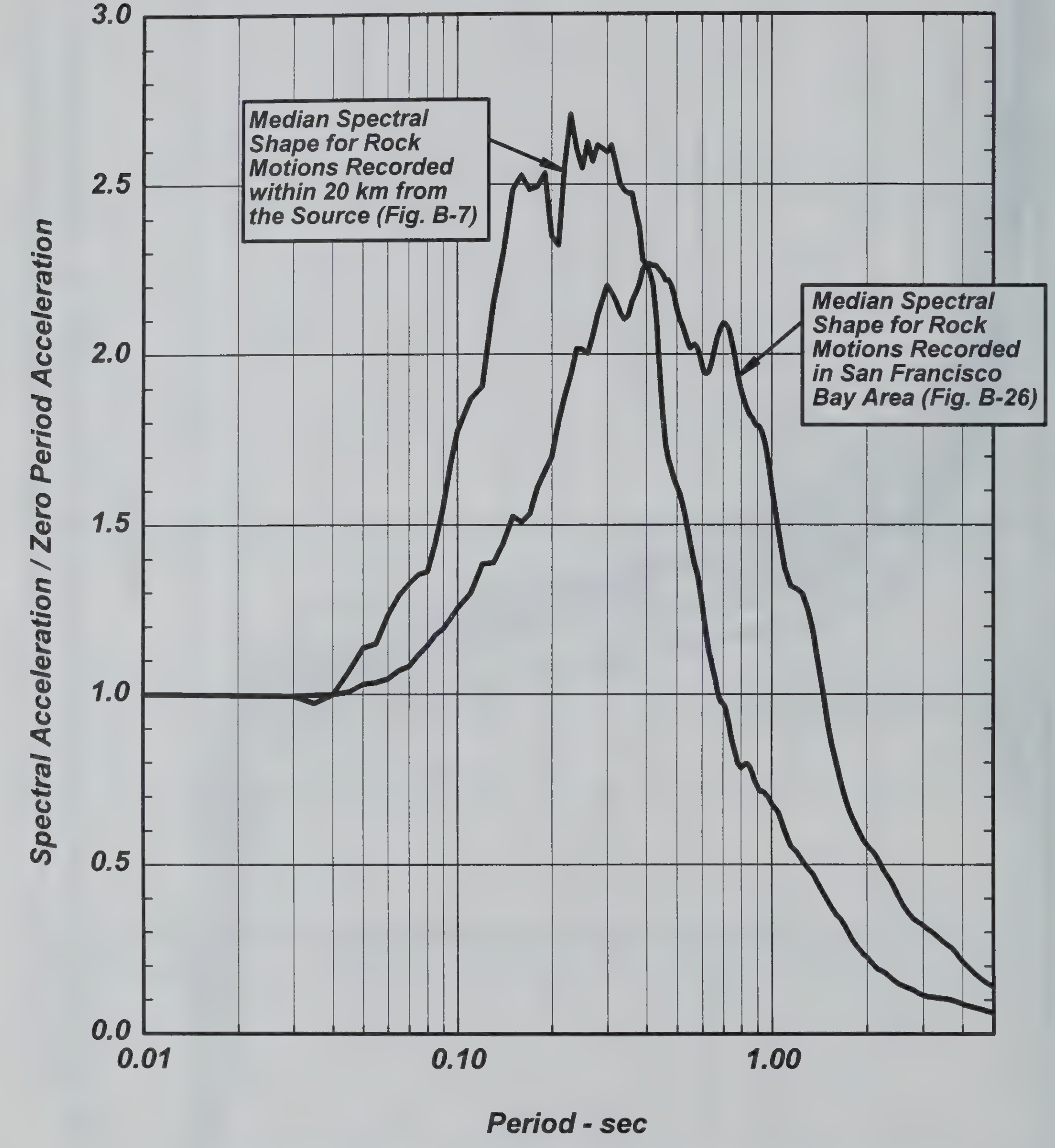

Fig. B-39 Median Normalized Spectral Shapes for Rock Motions Recorded During the Loma Prieta Earthquake

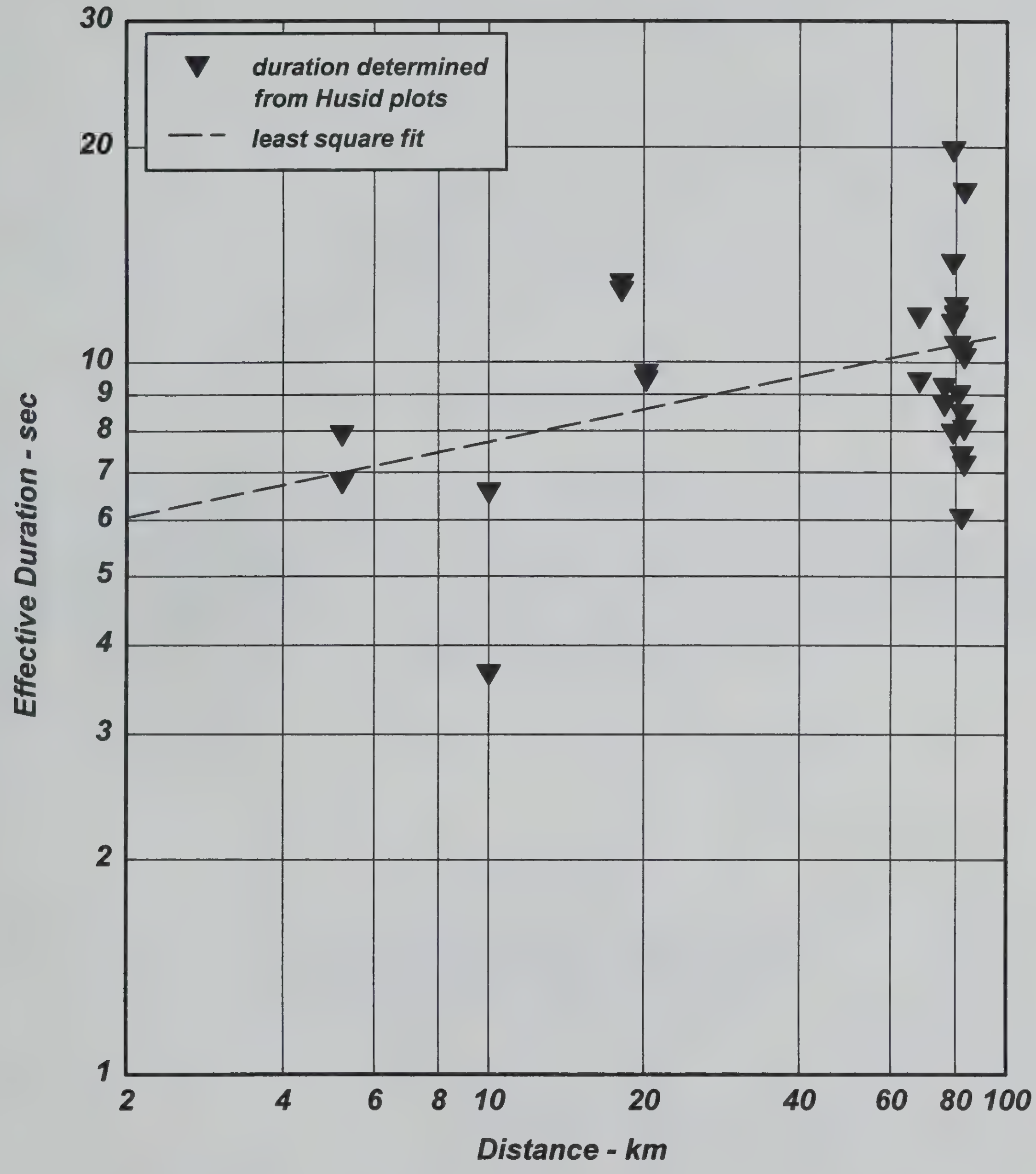

Fig. B-40 Effective Duration Obtained for Motions
Recorded at Rock Sites During the Loma Prieta Earthquake

APPENDIX C

CHARACTERISTICS OF THE HORIZONTAL EARTHQUAKE GROUND MOTIONS RECORDED AT SOFT SOIL SITES DURING THE 1989 LOMA PRIETA EARTHQUAKE

To Report on:

ASSESSMENT OF SITE RESPONSE ANALYSIS PROCEDURES

APPENDIX C

CHARACTERISTICS OF THE HORIZONTAL EARTHQUAKE GROUND MOTIONS RECORDED AT ROCK SITES DURING THE 1989 LOMA PRIETA EARTHQUAKE

C.1 INTRODUCTION

As described in Appendix A, nine of the 92 free field recordings obtained during Loma Prieta were at soft soil sites, all of which are in the San Francisco-Bay Area (see Fig. 1). The peak accelerations, peak velocities and peak displacements, spectral ordinates and effective duration (as defined from a Husid plot) of these rock motions are summarized in this Appendix.

C.2 CHARACTERISTICS OF HORIZONTAL MOTIONS RECORDED AT SOFT SOIL SITES

The characteristics of the horizontal earthquake ground motions recorded at these nine soft soil sites during the Loma Prieta earthquake are listed in Tables C-1 through C-3 and in Figs. C-1 through C-21 and are summarized below.

C.2.1 Peak Horizontal Accelerations, a, Velocities, v, and Displacements, d

The peak accelerations (Volume II), velocities and displacements of the earthquake ground motions recorded at these rock sites are listed in Table C-1.

C.2.2 Ratios v/a and ad/v^2

The ratios v/a and ad/v^2 for the twelve records listed in Table C-1 are listed in Table C-2. The average value of the ratio v/a for all the records listed in Table C-1 is about 147 cm/sec/g and the average value of the ratio ad/v^2 is about 1.6. Note that the recordings at Emeryville were not used to obtain the average values of v/a and ad/v^2; the effect of including the values for these recordings, however, is minimal.

C.2.3 Accelerograms and Spectral Accelerations

The accelerograms and the spectral accelerations (5 percent spectral damping) for these ground motions are presented in Figs. C-1 through C-9. The normalized spectra for all the recordings, except for those at Emeryville, are shown in Fig. C-10.

C.2.4 Husid Plots and Effective Duration

The Husid plots (using Eq. B-1 in Appendix B) for the horizontal accelerograms obtained at these soft soil sites in the San Francisco Bay Area are presented in Figs. C-11 through C-19 and the Husid plots for all the motions considered (except those at Emeryville) are shown in Fig. C-20.

The time at which $h(t) = 5$ percent and the time at which $h(t) = 95$ percent are listed in Table C-3 for each component included in Figs. C-11 through C-19. Also listed in Table C-3 are the values of effective duration as defined in Appendix B. The range in effective duration for the horizontal motions recorded at these soft soil sites is shown in Fig. C-21. Also shown in Fig. C-21 are the values of effective duration obtained for the rock sites included in Appendix B (see Fig. B-40) and the values obtained using the equation relating effective duration at rock sites and distance (Eq. B-2). As can be noted, Eq. B-2 appears to provide reasonable best estimates of duration for either site condition.

Table C - 1
Peak Accelerations, Velocities and Displacements of Horizontal Earthquake Ground Motions Recorded at Soft Soil Sites during the Loma Prieta Earthquake

Station	Distance km	Component	Peak Acceleration g	Peak Velocity cm/sec	Peak Displacement cm
APEEL No. 2	46.8	N43W	0.277	53.1	10.4
		S43W	0.227	35.9	5.68
Foster City	48.3	EW	0.283	45.4	14.7
		NS	0.257	31.8	6.28
San Francisco Airport	63.5	EW	0.332	29.3	5.92
		NS	0.235	26.5	5.05
Alameda Naval Station	76.0	EW	0.209	42.6	14.1
		NS	0.268	22.2	4.65
Outer Harbor Wharf	76.4	N55E	0.271	42.3	9.17
		N35W	0.287	40.8	9.88
Emeryville	81.0	EW	0.260	41.1	8.21
		NS	0.214	21.5	3.75
Treasure Island	81.6	EW	0.159	33.4	12.2
		NS	0.100	15.6	4.48
Richmond City Hall - Parking Lot	85.0	N80E	0.106	14.7	2.60
		S10E	0.125	17.1	2.79
Larkspur Ferry Terminal	99.0	EW	0.137	20.3	5.14
		NS	0.096	13.8	3.64

Note: peak accelerations listed in this table are "Volume II" accelerations.

Table C - 2

Values of v/a and ad/v^2 of Horizontal Earthquake Ground Motions Recorded at Soft Soil Sites during the Loma Prieta Earthquake

Station	Distance km	Component	v/a cm/sec/g	ad/v^2
APEEL No. 2	46.8	N43W	192	1.00
		S43W	158	0.98
Foster City	48.3	EW	160	1.98
		NS	124	1.57
San Francisco Airport	63.5	EW	88.3	2.25
		NS	113	1.66
Alameda Naval Station	76.0	EW	204	1.59
		NS	82.8	2.48
Outer Harbor Wharf	76.4	N55E	156	1.36
		N35W	142	1.67
Emeryville	81.0	EW	158	1.24
		NS	101	1.70
Treasure Island	81.6	EW	210	1.71
		NS	156	1.81
Richmond City Hall - Parking Lot	85.0	N80E	139	1.25
		S10E	137	1.17
Larkspur Ferry Terminal	99.0	EW	148	1.68
		NS	144	1.80

Table C - 3
Effective Duration Determined from Husid Plots of Horizontal Earthquake Ground Motions Recorded at Soft Soil Sites during the Loma Prieta Earthquake

Station	Distance km	Component	Time at 5% seconds	Time at 95% seconds	Effective Duration seconds
APEEL No. 2	46.8	N43W	4.80	13.08	8.28
		S43W	5.46	17.01	11.55
Foster City	48.3	EW	8.22	19.91	11.69
		NS	7.27	24.43	17.16
San Francisco Airport	63.5	EW	8.65	19.95	11.30
		NS	8.73	19.54	10.81
Alameda Naval Station	76.0	EW	9.51	15.03	5.52
		NS	10.80	17.81	7.01
Outer Harbor Wharf	76.4	N55E	10.80	17.81	7.01
		N35W	10.15	18.83	8.68
Emeryville	81.0	EW	11.15	20.02	8.87
		NS	10.22	25.07	14.85
Treasure Island	81.6	EW	11.09	15.57	4.48
		NS	8.78	14.82	6.04
Richmond City Hall -	85.0	N80E	10.81	24.78	13.97
		S10E	10.73	22.78	12.05
Larkspur Ferry Terminal	99.0	EW	11.76	20.89	9.13
		NS	11.22	23.33	12.12

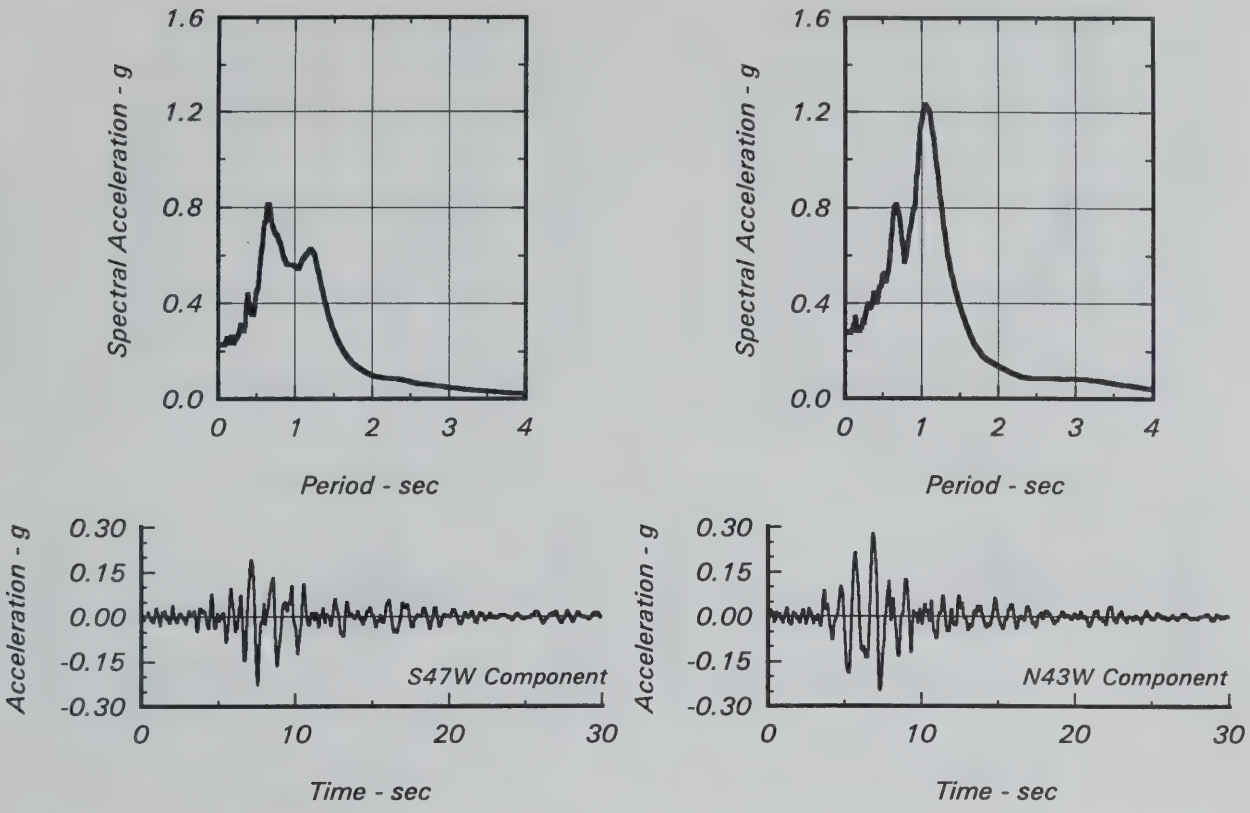

Fig. C-1 Accelerograms and Spectral Ordinates of the Horizontal Components of Earthquake Ground Motions Recorded at APEEL No. 2 during the Loma Prieta Earthquake

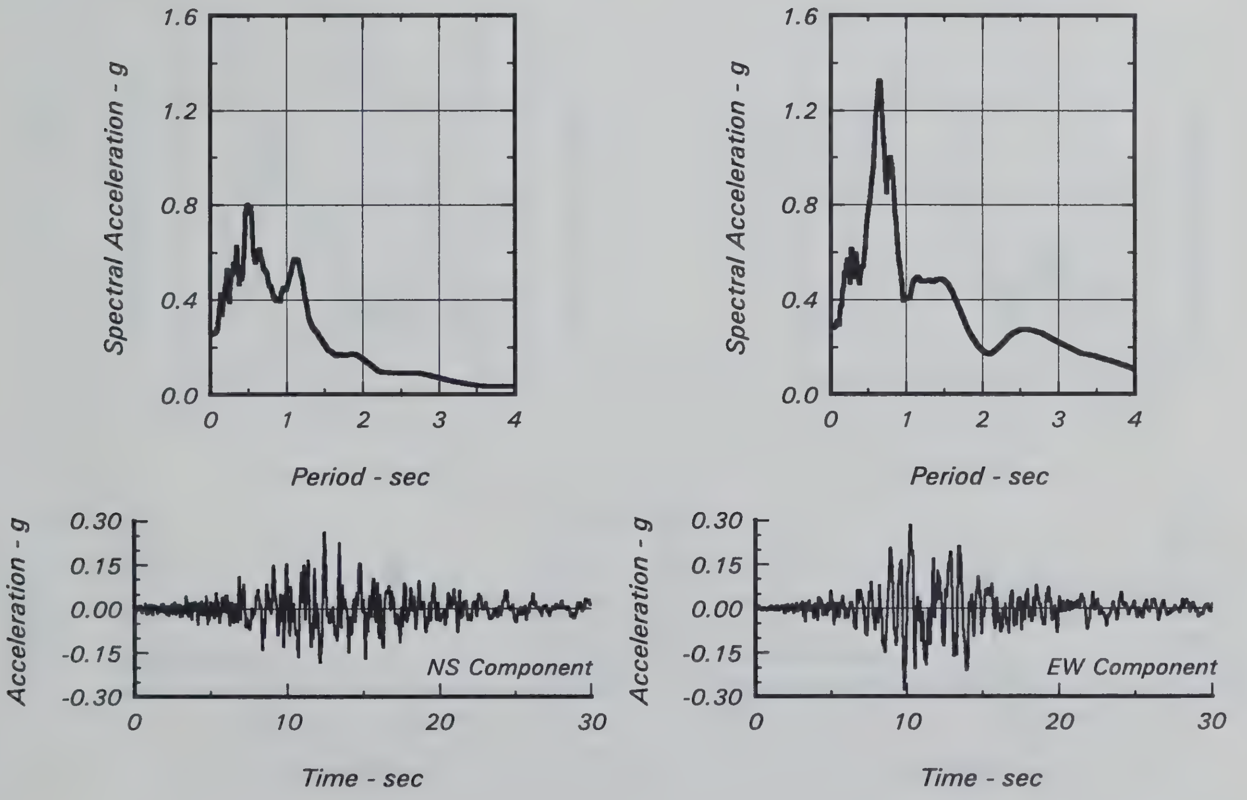

Fig. C-2 Accelerograms and Spectral Ordinates of the Horizontal Components of Earthquake Ground Motions Recorded at Foster City during the Loma Prieta Earthquake

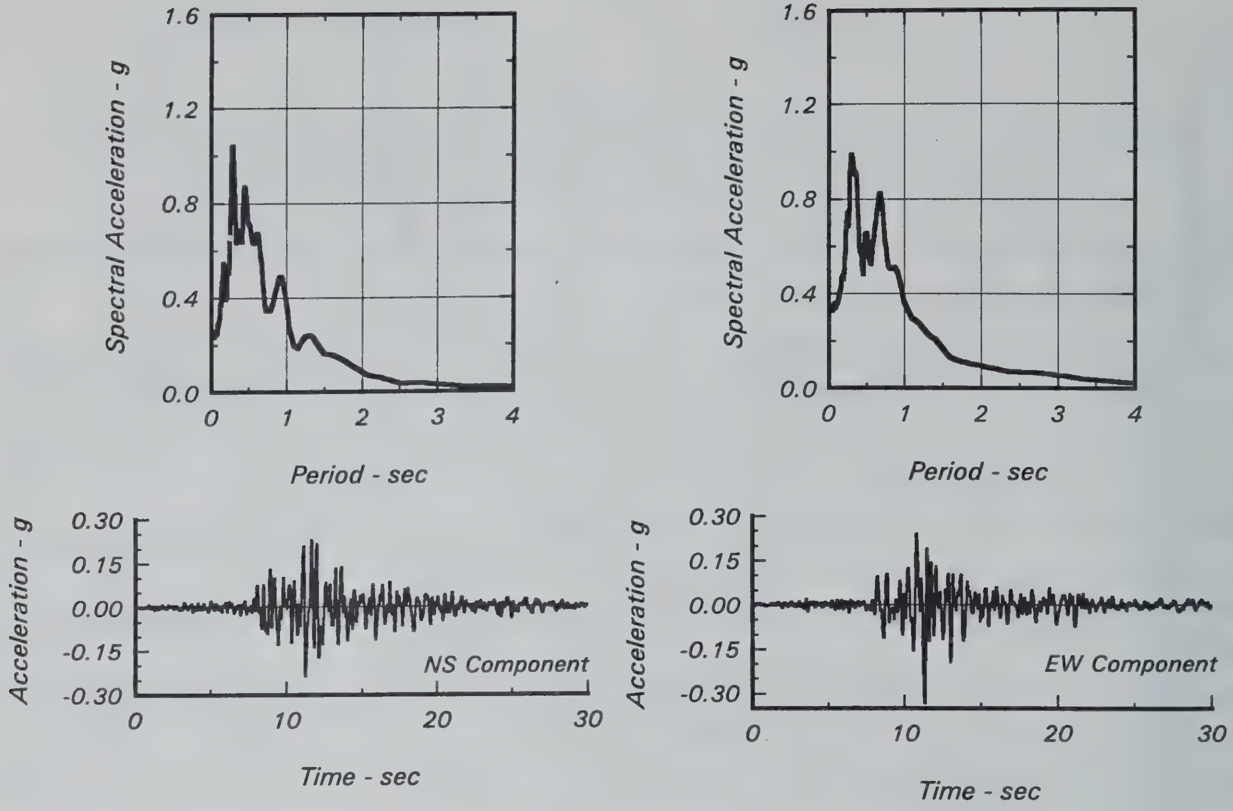

Fig. C-3 Accelerograms and Spectral Ordinates of the Horizontal Components of Earthquake Ground Motions Recorded at San Francisco Airport during the Loma Prieta Earthquake

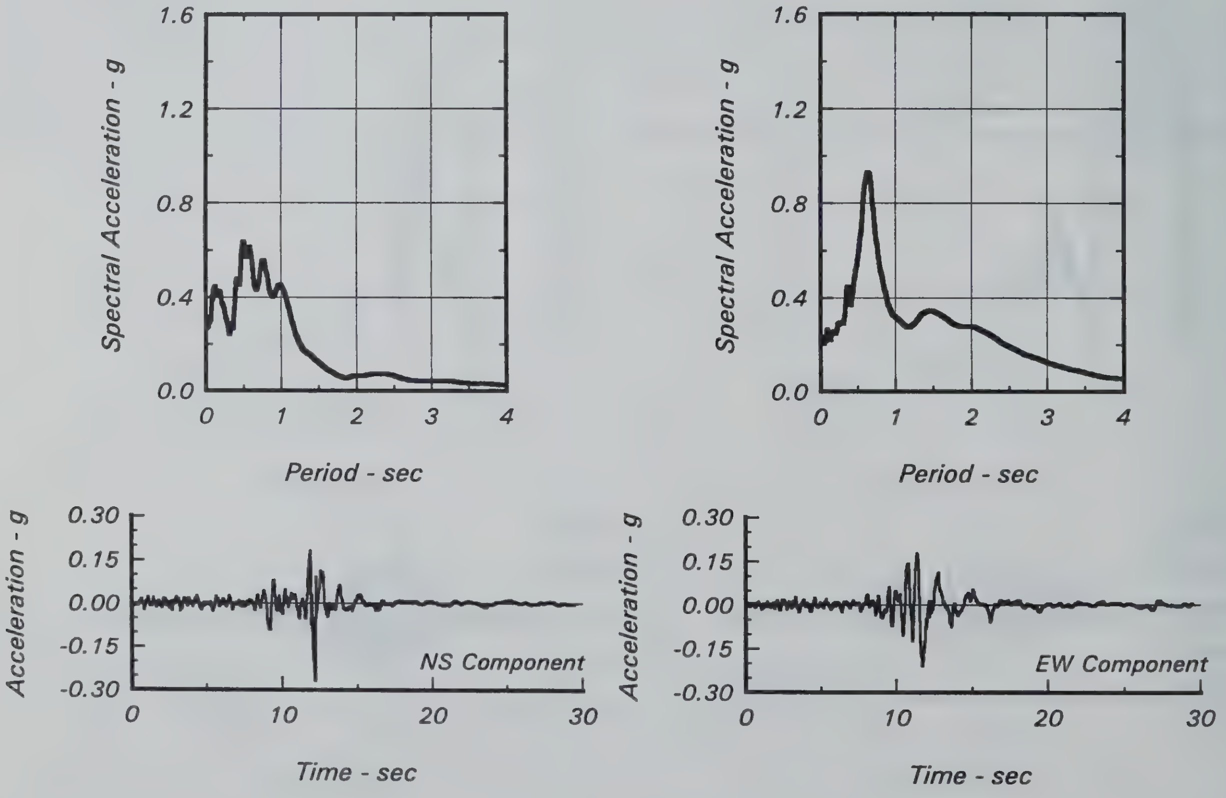

Fig. C-4 Accelerograms and Spectral Ordinates of the Horizontal Components of Earthquake Ground Motions Recorded at Alameda Naval Station during the Loma Prieta Earthquake

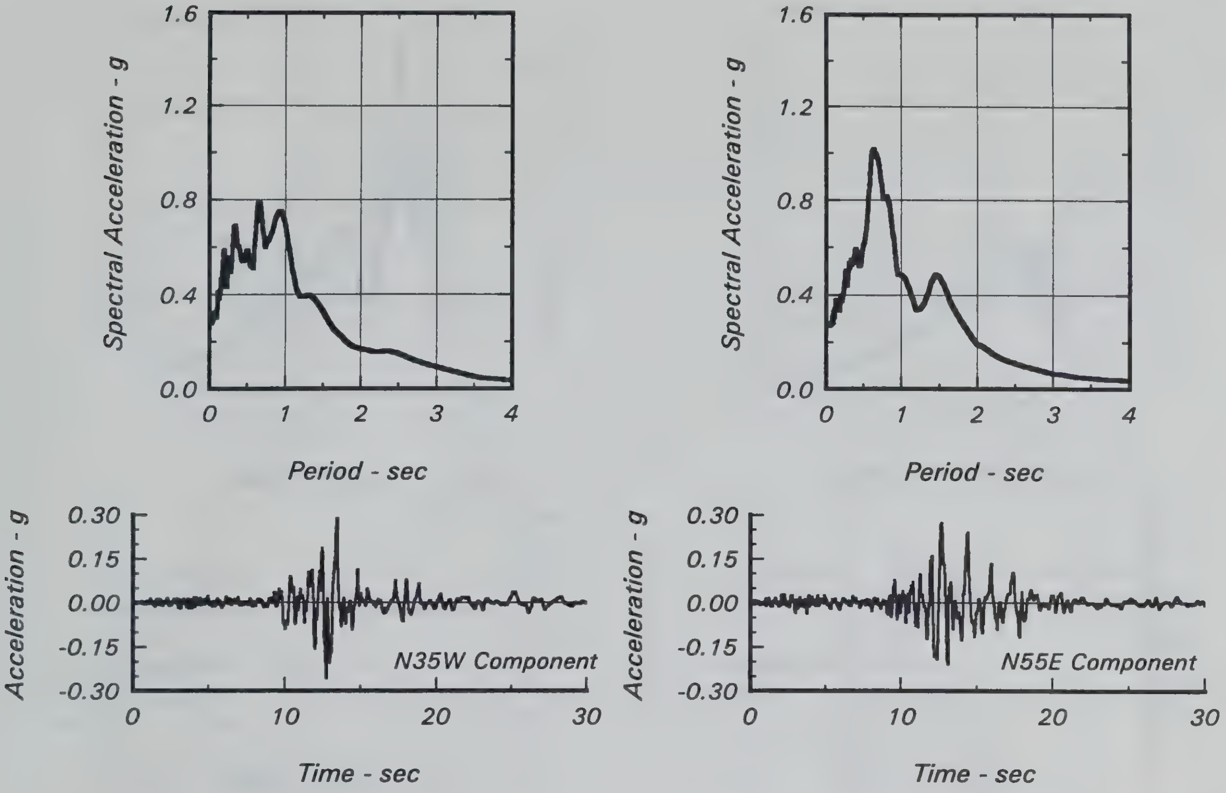

Fig. C-5 Accelerograms and Spectral Ordinates of the Horizontal Components of Earthquake Ground Motions Recorded at Outer Harbor Wharf during the Loma Prieta Earthquake

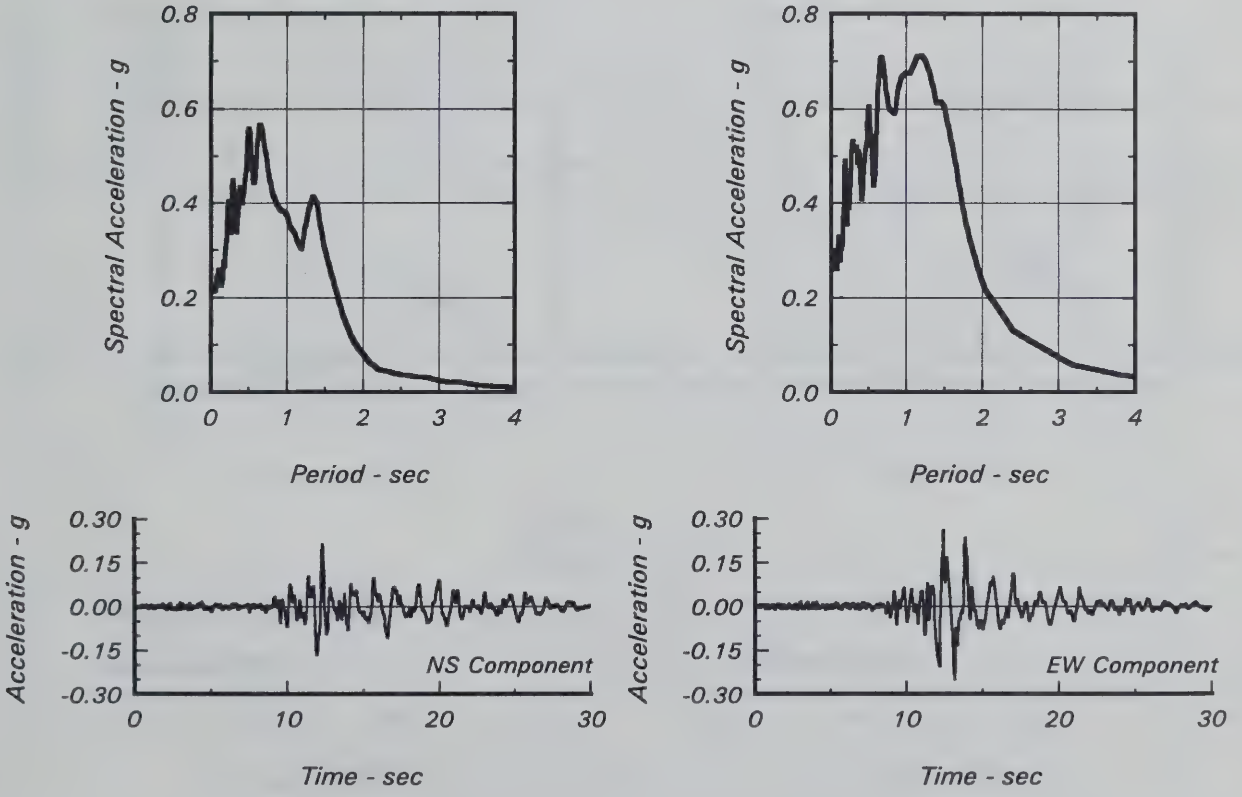

Fig. C-6 Accelerograms and Spectral Ordinates of the Horizontal Components of Earthquake Ground Motions Recorded at Emeryville during the Loma Prieta Earthquake

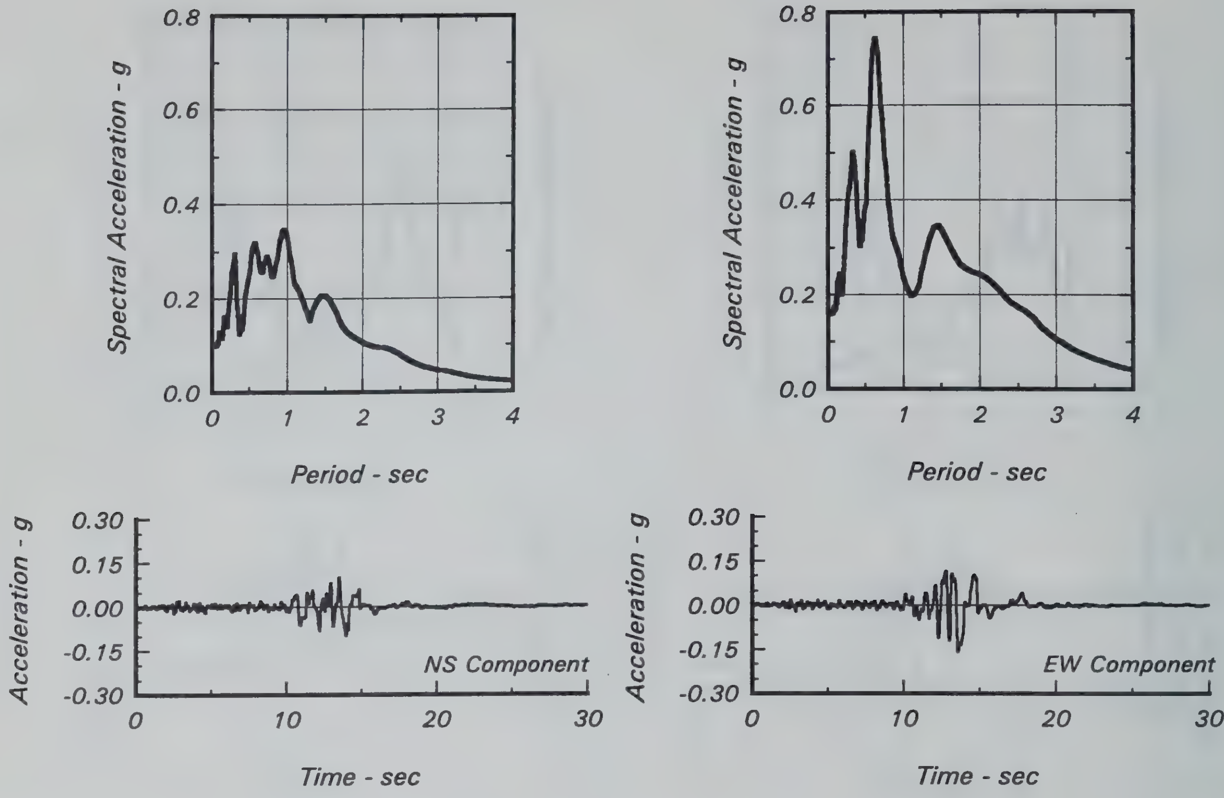

Fig. C-7 Accelerograms and Spectral Ordinates of the Horizontal Components of Earthquake Ground Motions Recorded at Treasure Island during the Loma Prieta Earthquake

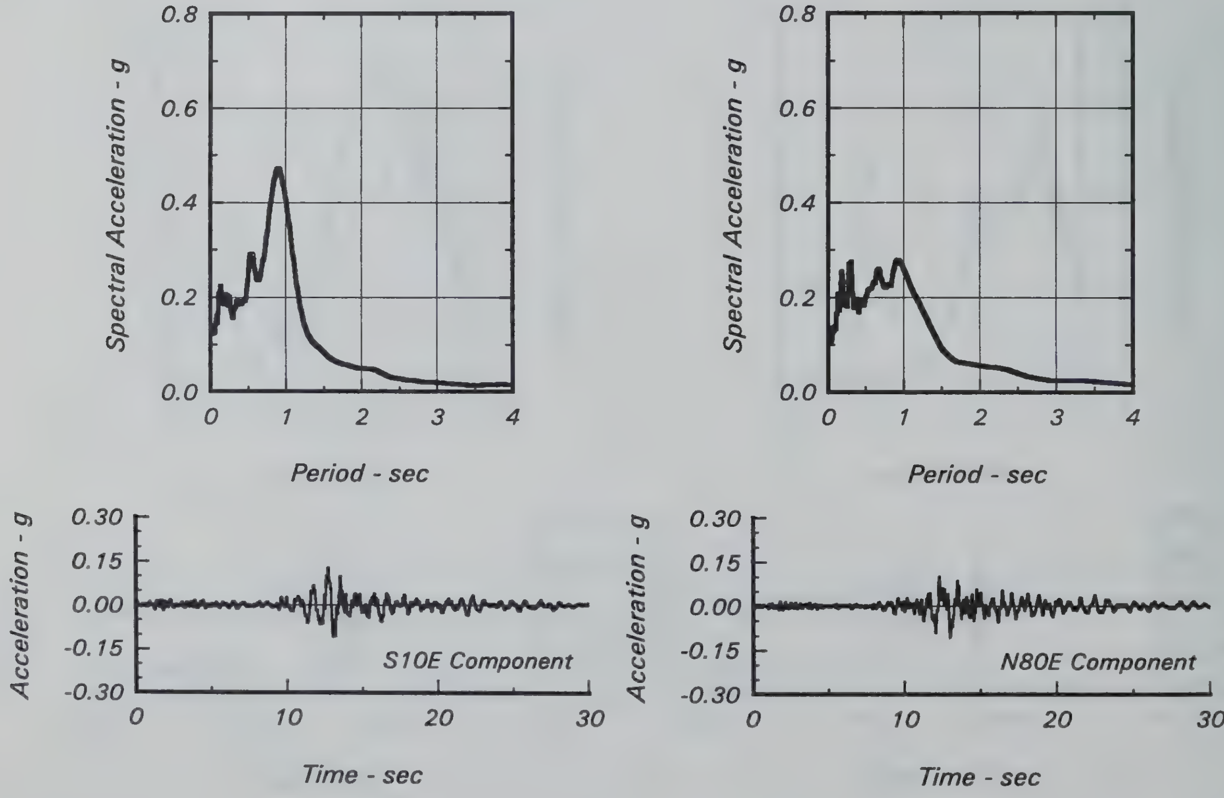

Fig. C-8 Accelerograms and Spectral Ordinates of the Horizontal Components of Earthquake Ground Motions Recorded at Richmond during the Loma Prieta Earthquake

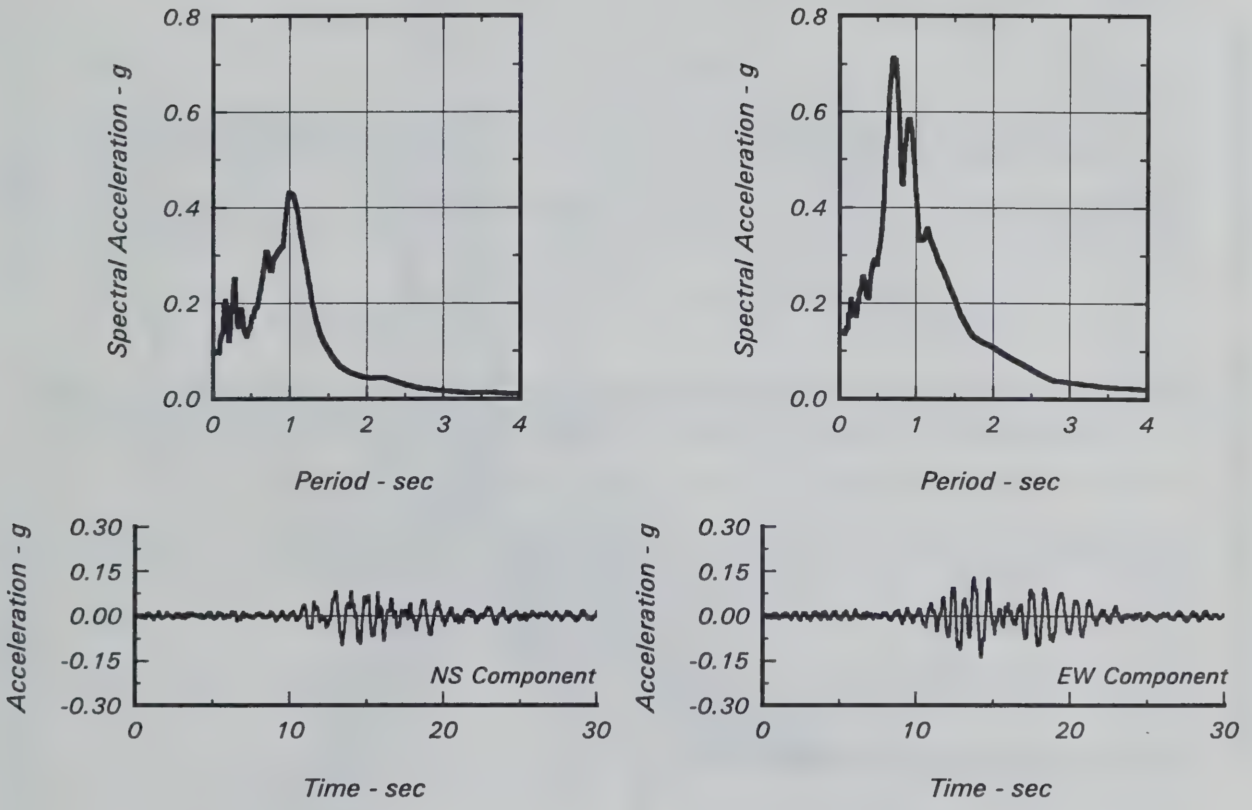

Fig. C-9 Accelerograms and Spectral Ordinates of the Horizontal Components of Earthquake Ground Motions Recorded at Larkspur during the Loma Prieta Earthquake

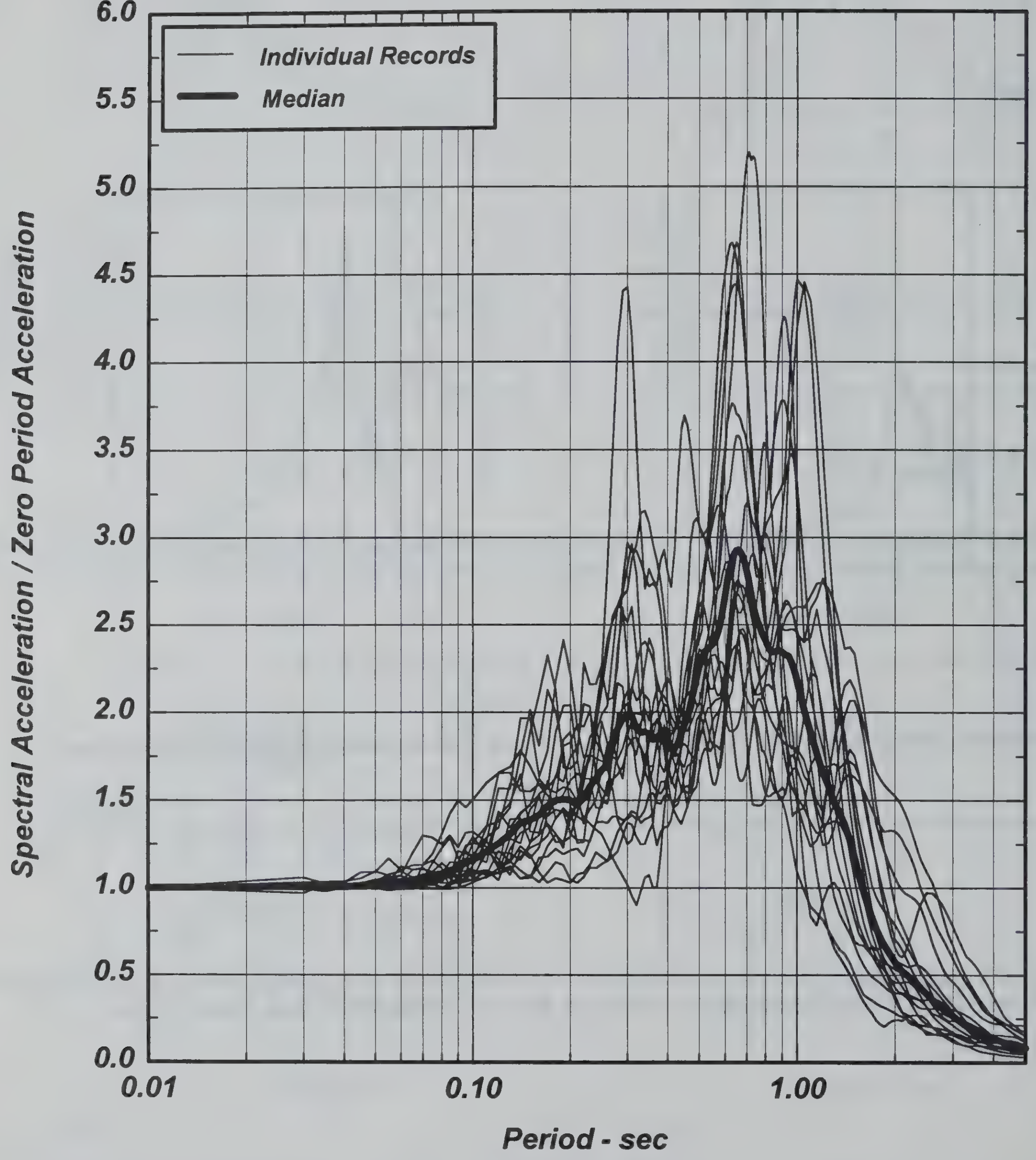

Fig. C-10 Normalized Spectra of Horizontal Motions Recorded at Soft Soil Sites in San Francisco Bay Area During the Loma Prieta Earthquake

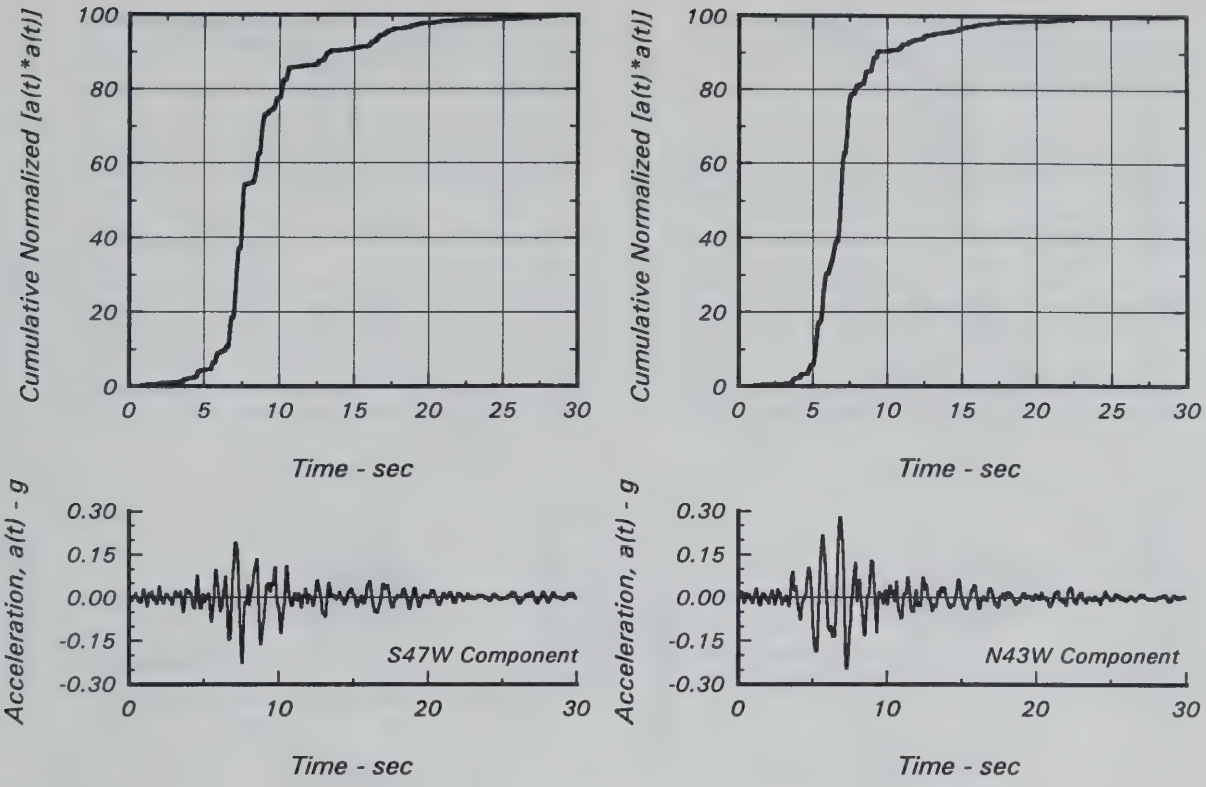

Fig. C-11 Accelerograms and Husid Plots of the Horizontal Components of Earthquake Ground Motions Recorded at APEEL No. 2 during the Loma Prieta Earthquake

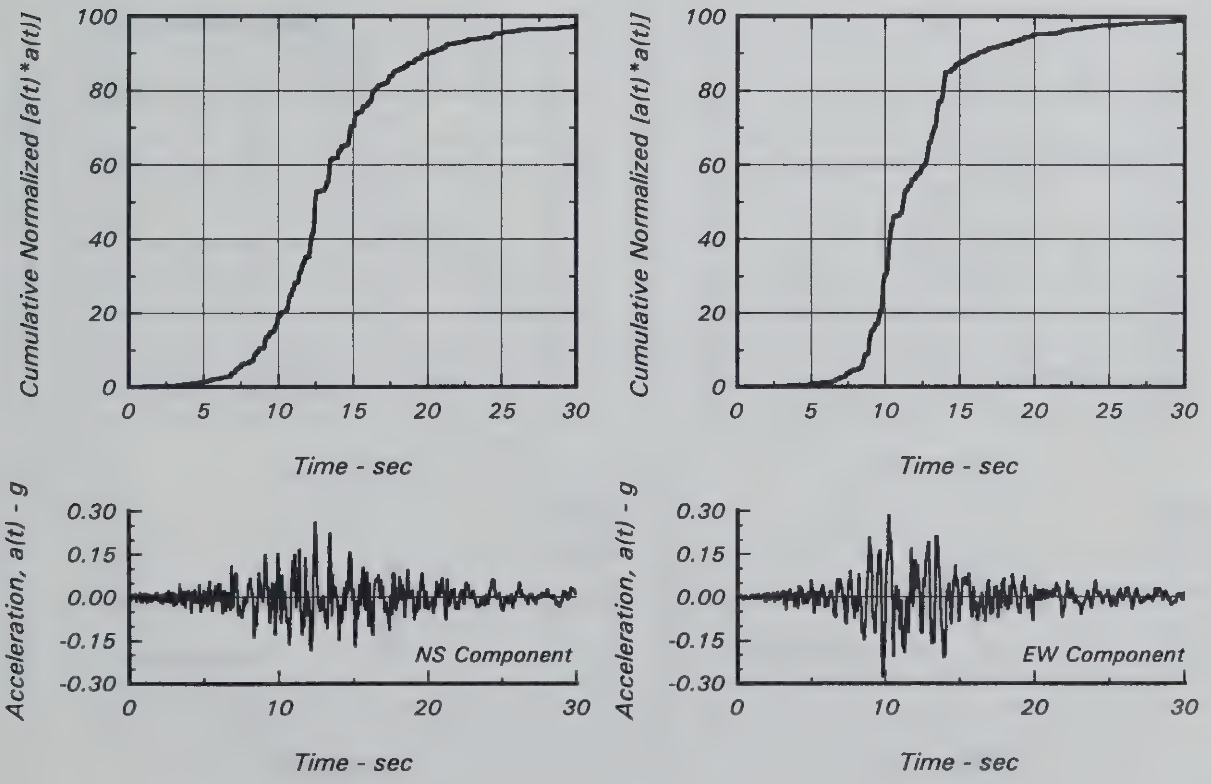

Fig. C-12 Accelerograms and Husid Plots of the Horizontal Components of Earthquake Ground Motions Recorded at Foster City during the Loma Prieta Earthquake

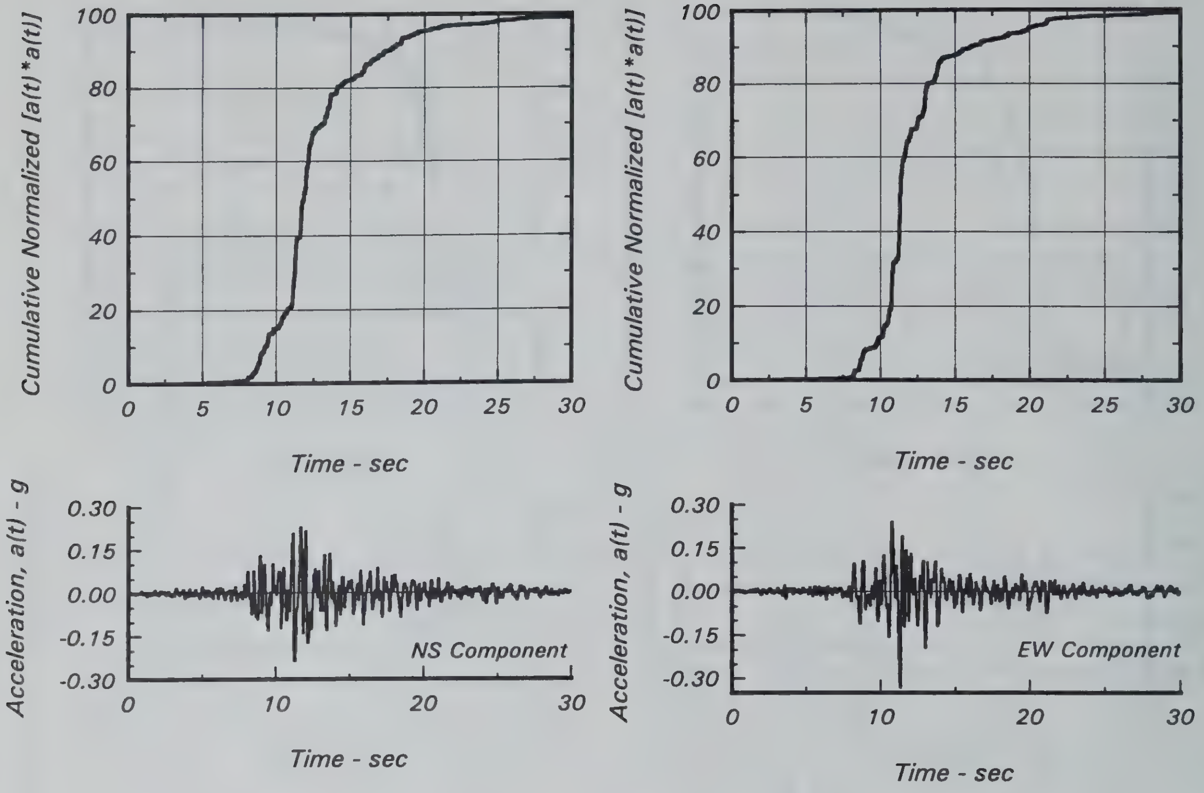

Fig. C-13 Accelerograms and Husid Plots of the Horizontal Components of Earthquake Ground Motions Recorded at San Francisco Airport during the Loma Prieta Earthquake

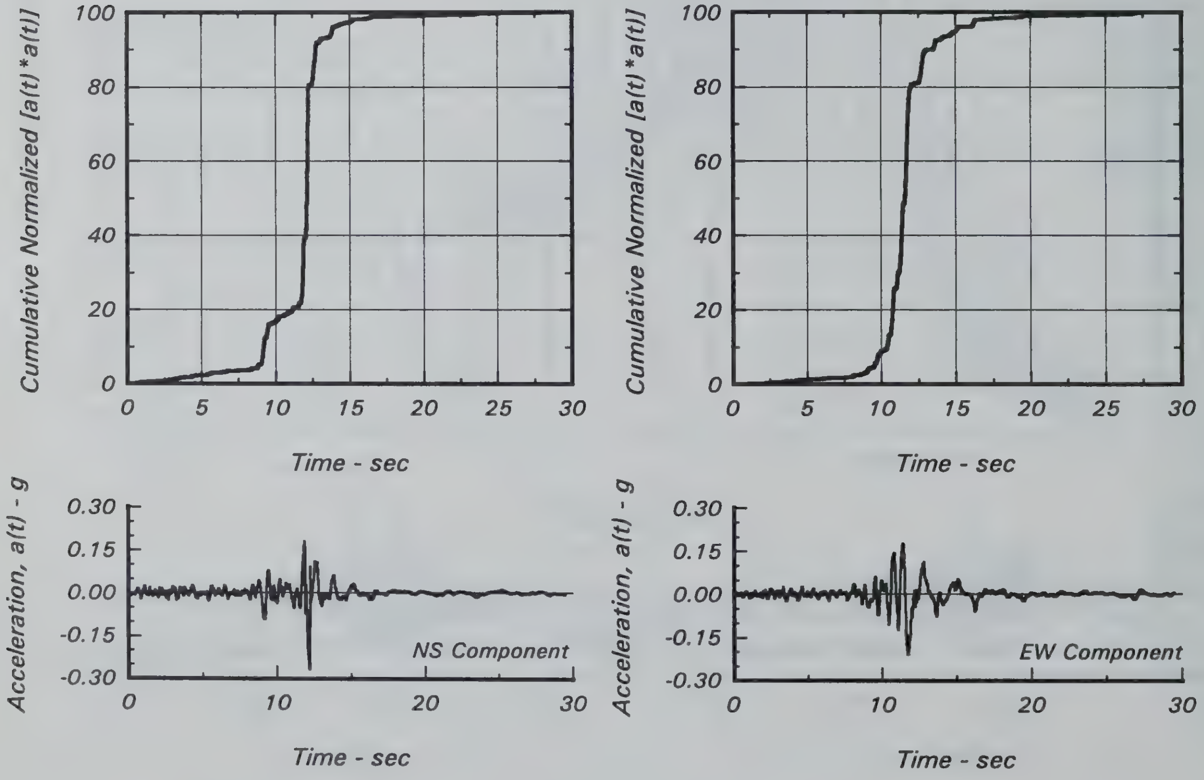

Fig. C-14 Accelerograms and Husid Plots of the Horizontal Components of Earthquake Ground Motions Recorded at Alameda Naval Station during the Loma Prieta Earthquake

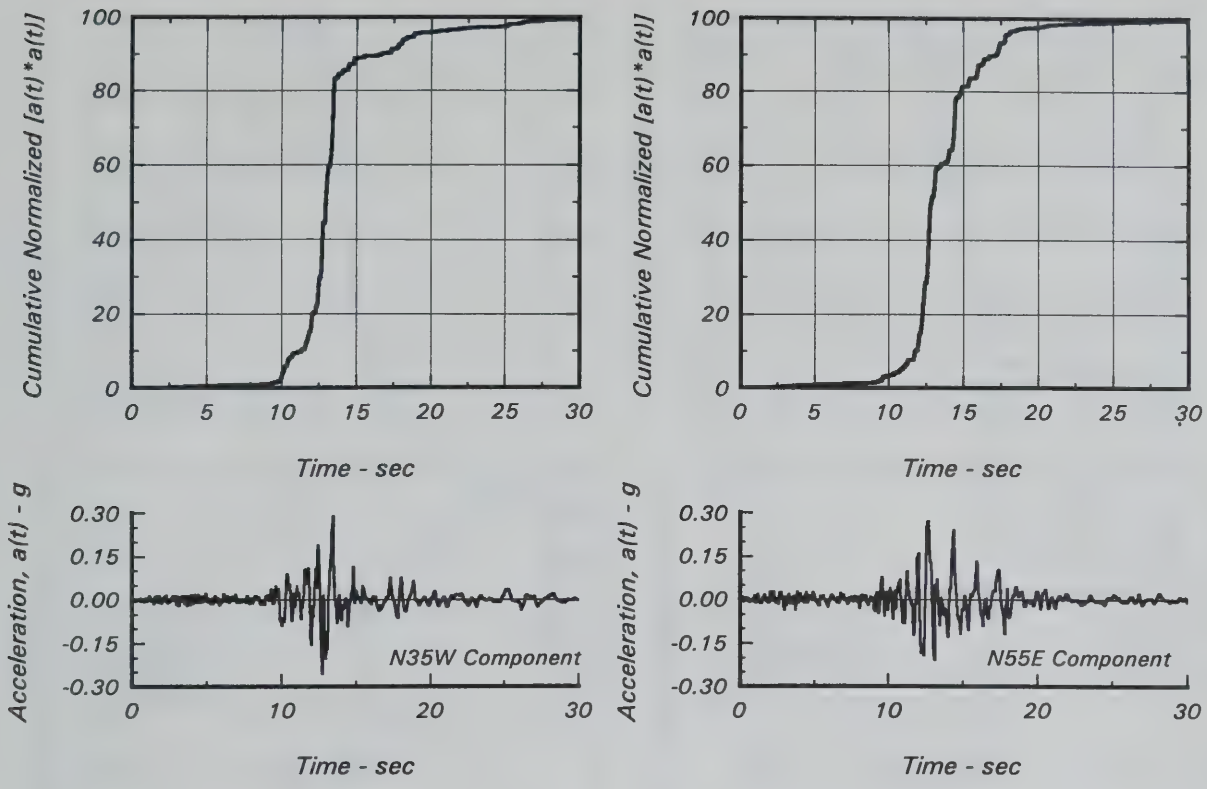

Fig. C-15 Accelerograms and Husid Plots of the Horizontal Components of Earthquake Ground Motions Recorded at Outer Harbor Wharf during the Loma Prieta Earthquake

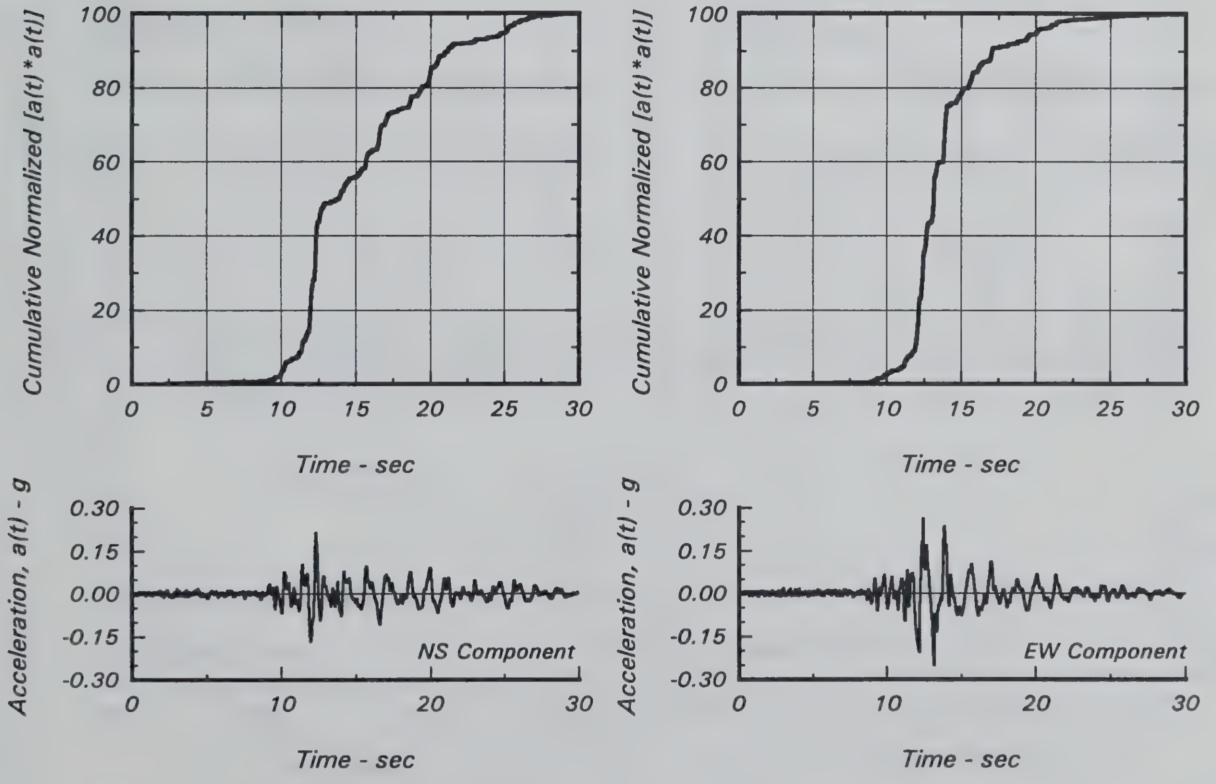

Fig. C-16 Accelerograms and Husid Plots of the Horizontal Components of Earthquake Ground Motions Recorded at Emeryville during the Loma Prieta Earthquake

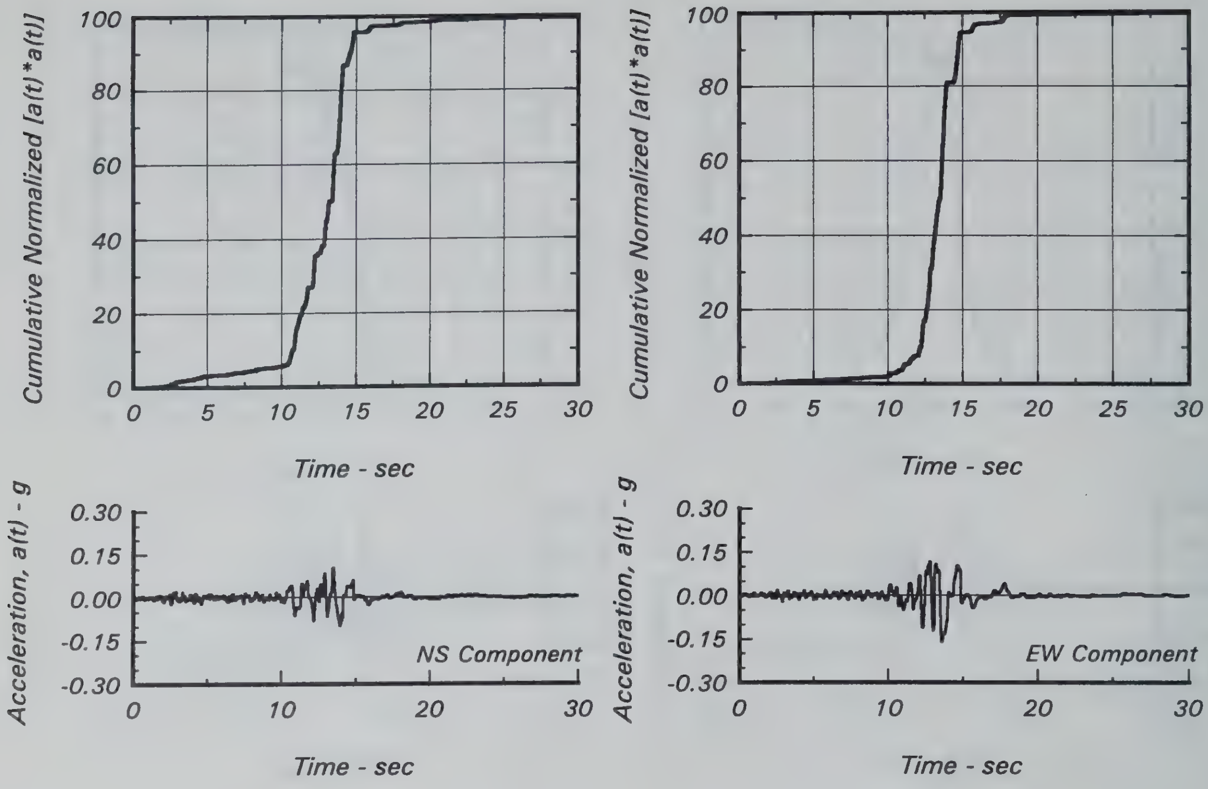

Fig. C-17 Accelerograms and Husid Plots of the Horizontal Components of Earthquake Ground Motions Recorded at Treasure Island during the Loma Prieta Earthquake

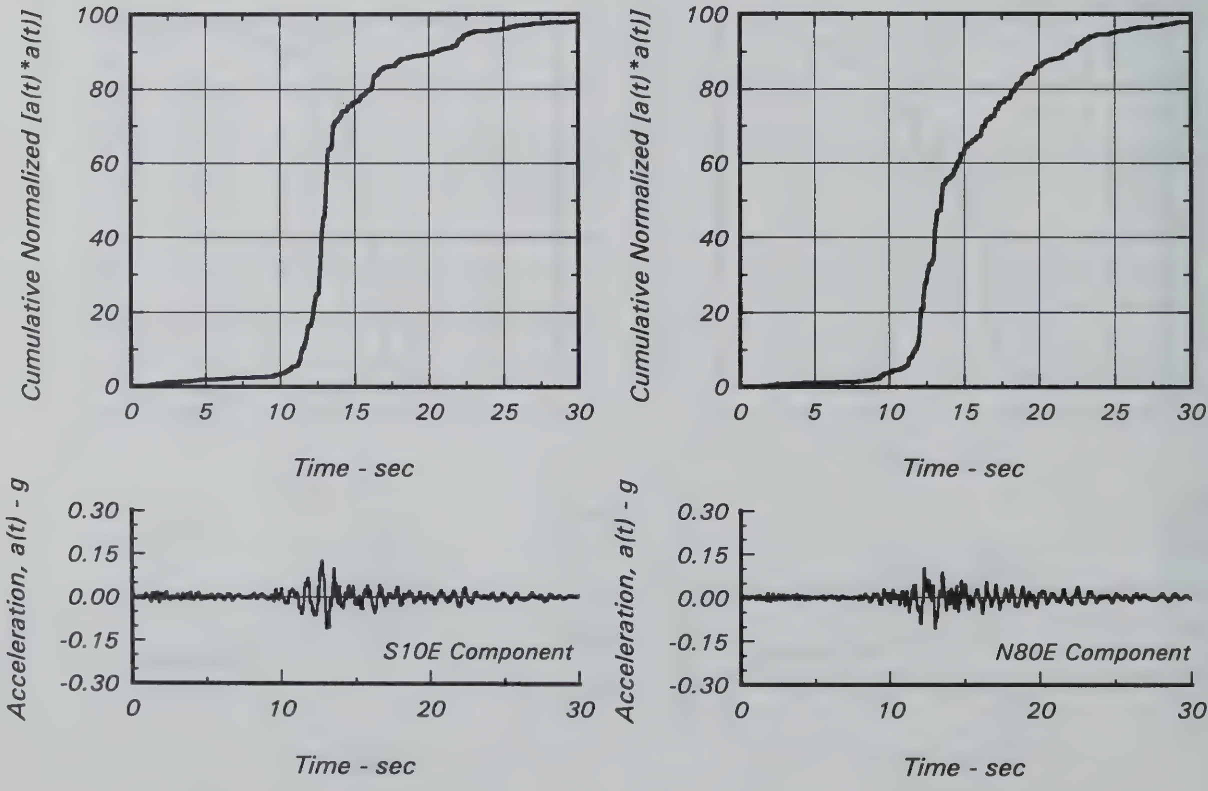

Fig. C-18 Accelerograms and Husid Plots of the Horizontal Components of Earthquake Ground Motions Recorded at Richmond during the Loma Prieta Earthquake

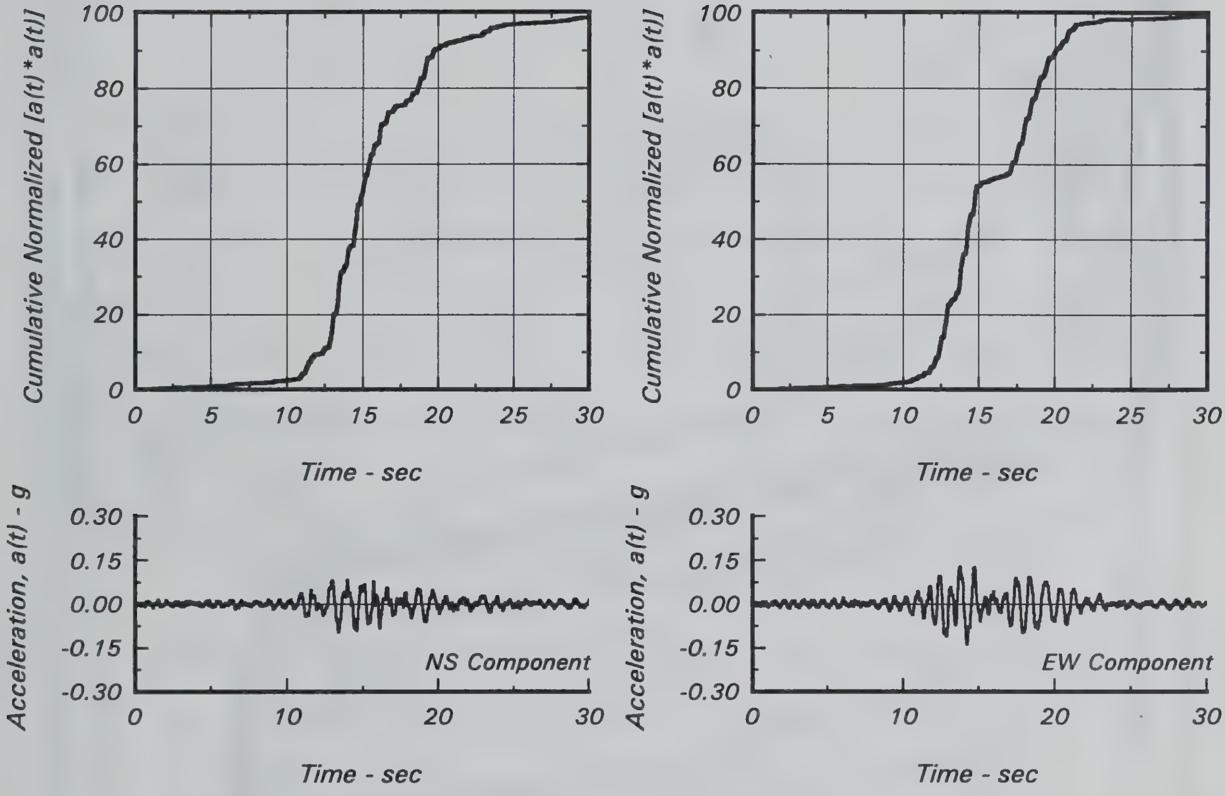

Fig. C-19 Accelerograms and Husid Plots of the Horizontal Components of Earthquake Ground Motions Recorded at Larkspur during the Loma Prieta Earthquake

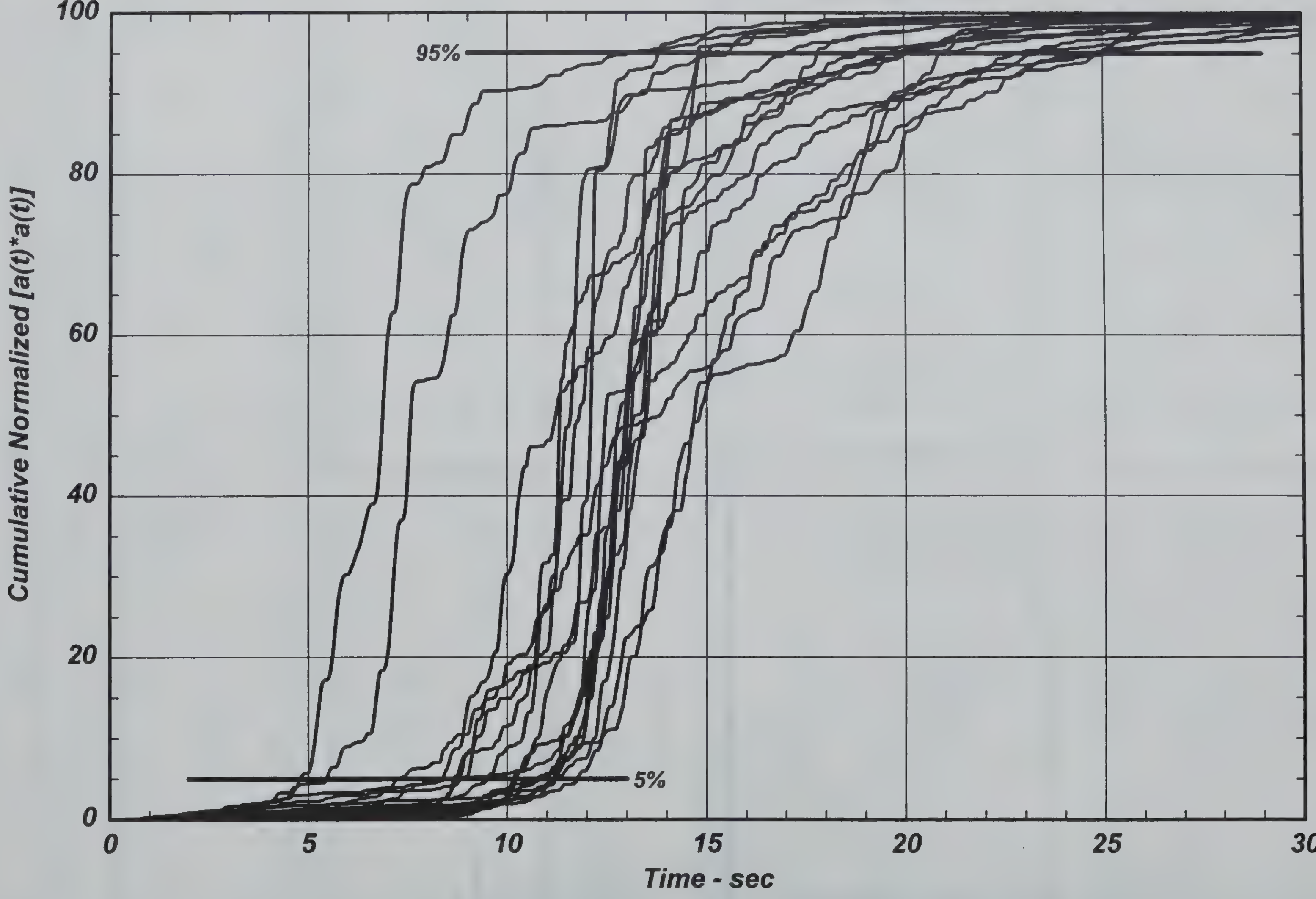

Fig. C-20 Husid Plots of Horizontal Components of Earthquake Ground Motions Recorded at Soft Soil Sites in the San Francisco Bay Area During the Loma Prieta Earthquake

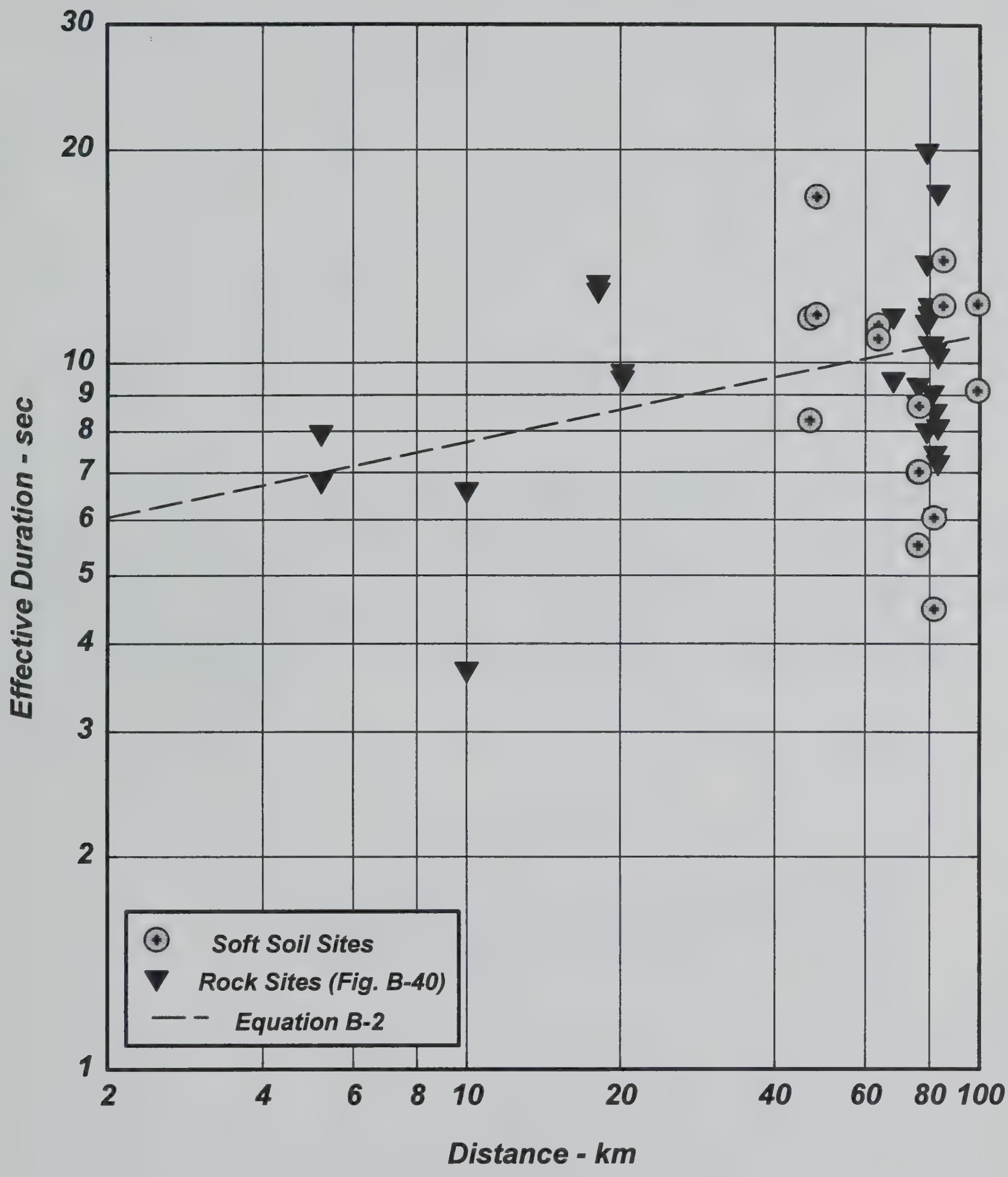

Fig. C-21 Effective Duration for Horizontal Motions Recorded at Soft Soil Sites and at Rock Sites During the Loma Prieta Earthquake

APPENDIX D

INPUT DATA FOR EQUIVALENT LINEAR ANALYSES AT THE TREASURE ISLAND SITE AND AT THE SAN FRANCISCO AIRPORT SITE BASED ON BEST ESTIMATE SHEAR WAVE VELOCITIES

To Report on:

ASSESSMENT OF SITE RESPONSE ANALYSIS PROCEDURES

APPENDIX D

INPUT DATA FOR EQUIVALENT LINEAR ANALYSES AT THE TREASURE ISLAND SITE AND AT THE SAN FRANCISCO AIRPORT SITE BASED ON BEST ESTIMATE SHEAR WAVE VELOCITIES

D.1 INTRODUCTION

The input data used for the equivalent linear analyses at the Treasure Island Site are listed in Section D.2 and those at the San Francisco Site are provided in Section D.3 of this appendix. These input data were used with computer program SHAKE91; the listings provided in this appendix follow the format specified in the user's manual for SHAKE91 (Idriss and Sun, 1992). Note that each sublayer thickness is given in feet, total unit weight is given in kip per cubic foot and shear wave velocity in feet per second. Thickness and shear wave velocity can be converted to meters and to meters per second by dividing the values given below by 3.28. Total unit weights can be converted to kN/m^3 by multiplying the unit weights given below by 157.2.

D.2 INPUT DATA FOR THE TREASURE ISLAND SITE

```
Option 1 -- dynamic soil properties - (max is thirteen):
    1
    3
   11     #1 modulus for clay (seed & sun 1989) upper range
0.0001    0.0003    0.001     0.003     0.01      0.03      0.1       0.3
1.        3.        10.
1.000     1.000     1.000     0.981     0.941     0.847     0.656     0.438
0.238     0.144     0.110
   11     damping for clay (Idriss 1990) - (about Lower Range from SI, 1970 for sand)
0.0001    0.0003    0.001     0.003     0.01      0.03      0.1       0.3
1.        3.16      10.
0.24      0.42      0.8       1.4       2.8        5.1       9.8       15.5
21.       25.       28.
   11     #2 modulus for sand (seed & idriss 1970) - upper Range
0.0001    0.0003    0.001     0.003     0.01      0.03      0.1       0.3
1.        3.        10.
1.000     1.000     0.990     0.960     0.850     0.640     0.370     0.180
0.080     0.050     0.035
   11     damping for clay (Idriss 1990) - (about Lower Range from SI, 1970 for sand)
0.0001    0.0003    0.001     0.003     0.01      0.03      0.1       0.3
1.        3.        10.
0.24      0.42      0.8       1.4       2.8        5.1       9.8       15.5
21.       25.       28.
    8     #3 modulus reduction for rock (Schnabel et al, 1972)
 .0001    0.0003    0.001       0.003     0.01      0.03       0.1      1.0
 1.000    1.000     0.9875    0.9525    0.900     0.810     0.725     0.550
    5     DAMPING IN ROCK   AVERAGE  9/4
 .0001    0.001     0.01        0.1       1.
  0.4     0.8       1.5         3.0       4.6
    3    1    2    3
```

```
Option 2 -- Soil Profile
    2
    1   36      TI - Best Estimate Shear Wave Velocities
    1    2           3.00                .050      .120      800.
    2    2           3.00                .050      .120      800.
    3    2           4.00                .050      .120      800.
    4    2           5.00                .050      .125      500.
    5    2           5.00                .050      .125      500.
    6    2           5.00                .050      .125      525.
    7    2           5.00                .050      .125      525.
    8    2           5.00                .050      .125      550.
    9    2           5.00                .050      .125      550.
   10    1           5.00                .050      .100      600.
   11    1           5.00                .050      .100      600.
   12    1           5.00                .050      .100      700.
   13    1           5.00                .050      .100      700.
   14    1           5.00                .050      .100      700.
   15    1           5.00                .050      .100      700.
   16    1           5.00                .050      .100      600.
   17    1           5.00                .050      .100      600.
   18    1           5.00                .050      .100      600.
   19    1           5.00                .050      .100      600.
   20    2           5.00                .050      .100      600.
   21    2          10.00                .050      .130     1000.
   22    2          10.00                .050      .130     1000.
   23    2          10.00                .050      .130     1000.
   24    2          10.00                .050      .130     1000.
   25    1          10.00                .050      .130      900.
   26    1          10.00                .050      .130      900.
   27    1          10.00                .050      .130      900.
   28    1          10.00                .050      .130      900.
   29    1          10.00                .050      .130      900.
   30    1          10.00                .050      .130      900.
   31    1          10.00                .050      .130      900.
   32    1          15.00                .050      .130      900.
   33    1          20.00                .050      .130      900.
   34    1          25.00                .050      .130     1250.
   35    1          25.00                .050      .130     1250.
   36    3                               .010      .140     4000.
Option 3 -- input motion:
    3
 1900 2048   .02    yb_90.acc                     (8f10.6)
             .0671    20.         3    8
Option 4 -- sublayer for input motion {within (1) or outcropping (0):
    4
   36    0
Option 5 -- number of iterations & ratio of avg. strain to max strain
    5
    0    7    0.5
Option 6 -- sublayers for which accn time histories are computed & saved:
    6
    1    2    3    4    5    6    7    8    9   10   11   12   13   14   15
    1    1    1    1    1    1    1    1    1    1    1    1    1    1    1
    1    0    0    0    0    0    0    0    0    0    0    0    0    0    0
Option 6 -- sublayers for which accn time histories are computed & saved:
    6
   16   17   18   19   20   21   22   23   24   25   26   27   28   29
    1    1    1    1    1    1    1    1    1    1    1    1    1    1
    0    0    0    0    0    0    0    0    0    0    0    0    0    0
```

```
Option 6 -- sublayers for which accn time histories are computed & saved:
    6
   30   31   32   33   34   36
    1    1    1    1    1    1
    0    0    0    0    0    0
execution will stop when program encounters 0:
    0
```

D.3 INPUT DATA FOR THE SAN FRANCISCO AIRPORT SITE

```
Option 1 -- dynamic soil properties - (max is thirteen):
    1
    3
   11     #1 modulus for clay (seed & sun 1989) upper range
0.0001    0.0003    0.001     0.003     0.01      0.03      0.1       0.3
1.        3.        10.
1.000     1.000     1.000     0.981     0.941     0.847     0.656     0.438
0.238     0.144     0.110
   11     damping for clay (Idriss 1990) - (about Lower Range from SI, 1970 for sand)
0.0001    0.0003    0.001     0.003     0.01      0.03      0.1       0.3
1.        3.16      10.
0.24      0.42      0.8       1.4       2.8        5.1        9.8      15.5
21.       25.       28.
   11     #2 modulus for sand (seed & idriss 1970) - upper Range
0.0001    0.0003    0.001     0.003     0.01      0.03      0.1       0.3
1.        3.        10.
1.000     1.000     0.990     0.960     0.850     0.640     0.370     0.180
0.080     0.050     0.035
   11     damping for clay (Idriss 1990) - (about Lower Range from SI, 1970 for sand)
0.0001    0.0003    0.001     0.003     0.01      0.03      0.1       0.3
1.        3.        10.
0.24      0.42      0.8       1.4       2.8        5.1        9.8      15.5
21.       25.       28.
    8     #3 modulus reduction for rock (Schnable et al, 1972)
 .0001    0.0003    0.001       0.003     0.01      0.03       0.1     1.0
 1.000    1.000     0.9875    0.9525    0.900     0.810     0.725     0.550
    5     DAMPING IN ROCK   AVERAGE  9/4
 .0001    0.001     0.01        0.1       1.
  0.4     0.8       1.5         3.0       4.6
    3    1    2    3
Option 2 -- Soil Profile
    2
    1   36      SFO - Best Estimate Shear Wave Velocities
    1    2          5.00                .050      .130     1260.
    2    1          5.00                .050      .105      290.
    3    1          5.00                .050      .105      290.
    4    1          5.00                .050      .105      290.
    5    2          6.00                .050      .120      500.
    6    2          6.00                .050      .120      500.
    7    2          8.00                .050      .120     1080.
    8    2          8.00                .050      .120     1080.
    9    2          8.00                .050      .120     1080.
   10    1          6.00                .050      .105      500.
   11    1          8.00                .050      .125     1215.
   12    1         10.00                .050      .125     1215.
   13    1         10.00                .050      .125     1215.
   14    1         10.00                .050      .125     1215.
   15    1         10.00                .050      .125     1215.
   16    1          10.00                .050      .125     1215.
   17    1          10.00                .050      .125     1215.
   18    1          15.00                .050      .130     1680.
   19    1          15.00                .050      .130     1680.
   20    1          15.00                .050      .130     1450.
   21    1          15.00                .050      .130     1450.
   22    1          20.00                .050      .130     1950.
   23    1          20.00                .050      .130     1950.
   24    1          20.00                .050      .130     1950.
   25    1          20.00                .050      .130     2040.
   26    1          20.00                .050      .130     2040.
   27    1          20.00                .050      .130     2040.
   28    1          20.00                .050      .130     2040.
   29    1          20.00                .050      .130     2040.
   30    1          20.00                .050      .130     2040.
   31    1          20.00                .050      .130     2040.
   32    1          20.00                .050      .130     2040.
   33    1          20.00                .050      .130     2040.
   34    1          20.00                .050      .130     2040.
   35    1          20.00                .050      .130     2040.
   36    3                               .010      .140     4000.
Option 3 -- input motion:
    3
 1900 2048   .02      ssf.acc                      (8f10.6)
             .1047    20.         3    8
Option 4 -- sublayer for input motion {within (1) or outcropping (0):
    4
   36    0
Option 5 -- number of iterations & ratio of avg. strain to max strain
    5
    0    8    0.5
Option 6 -- sublayers for which accn time histories are computed & saved:
    6
    1    2    3    4    5    6    7    8    9   10   11   12   13   14   15
    1    1    1    1    1    1    1    1    1    1    1    1    1    1    1
    1    0    0    0    0    0    0    0    0    0    0    0    0    0    0
Option 6 -- sublayers for which accn time histories are computed & saved:
    6
   16   17   18   19   20   21   22   23   24   25   26   27   28   29
    1    1    1    1    1    1    1    1    1    1    1    1    1    1
    0    0    0    0    0    0    0    0    0    0    0    0    0    0
Option 6 -- sublayers for which accn time histories are computed & saved:
    6
   30   31   32   33   34   35   36
    1    1    1    1    1    1    1
    0    0    0    0    0    0    0
execution will stop when program encounters 0:
    0
```